

## **Copyright Warning & Restrictions**

The copyright law of the United States (Title 17, United States Code) governs the making of photocopies or other reproductions of copyrighted material.

Under certain conditions specified in the law, libraries and archives are authorized to furnish a photocopy or other reproduction. One of these specified conditions is that the photocopy or reproduction is not to be “used for any purpose other than private study, scholarship, or research.” If a user makes a request for, or later uses, a photocopy or reproduction for purposes in excess of “fair use” that user may be liable for copyright infringement,

This institution reserves the right to refuse to accept a copying order if, in its judgment, fulfillment of the order would involve violation of copyright law.

**Please Note: The author retains the copyright while the New Jersey Institute of Technology reserves the right to distribute this thesis or dissertation**

Printing note: If you do not wish to print this page, then select “Pages from: first page # to: last page #” on the print dialog screen

The Van Houten library has removed some of the personal information and all signatures from the approval page and biographical sketches of theses and dissertations in order to protect the identity of NJIT graduates and faculty.

## **ABSTRACT**

### **VOLUME CHANGE BEHAVIOR OF CLAY SOILS AND THE EFFECT ON DISCRETE FRACTURES**

**By Heather Ann Hall**

This study examines the behavior of subsurface fractures in fine-grained soils such as clays in response to changing environmental conditions. Fractures serve as conduits for moisture transfer, which can lead to substantial shrinking and swelling of the surrounding fracture boundary soils. These volume changes, in turn, affect fracture geometry and moisture transmission rates. A new predictive model, termed the 'Fracture Volume Change Model' (FVC Model), has been developed to relate moisture transfer, soil volume change and associated changes in fracture aperture. The model assumes a discrete horizontal fracture in a laterally-infinite, saturated, expansive clay with rigid, outer no-flow boundaries and an inner flexible yielding boundary along the fracture. The FVC Model is based on the one-dimensional diffusion equation, which is solved analytically for both constant moisture and constant flux fracture boundary conditions. Changes in fracture aperture are predicted assuming normal shrinkage and either isotropic or anisotropic volume change. The model is expandable to bulk scale analysis of geologic formations with multiple stacked fractures.

The model was validated and calibrated in the laboratory using a custom-fabricated horizontal infiltrometer device. Tests were conducted on a

problematic clay soil from Fairfax County, Virginia, belonging to the southern montmorillonite facies of the Potomac Formation. Moisture content was varied from 17% to 33% by forcing air through an artificially created discrete fracture. Moisture changes in the fracture boundary soils caused the effective fracture aperture to fluctuate from near closure to 0.031 in. (0.79 mm). Upon application of excess moisture, it was not possible to effect full closure of the fracture. Moisture values predicted with the FVC Model demonstrated good agreement with the laboratory data, deviating 6% on average. Predictions of fracture aperture were generally overestimated. The model confirmed the dominance of internal hydraulic properties of the soil matrix over evaporation or infiltration mechanisms. The model was also used to predict soil desiccation rates for an environmental remediation project in an expansive clay in Santa Clara, California. Model application to agriculture, geotechnical engineering, and resource geology is also described.



**VOLUME CHANGE BEHAVIOR OF CLAY SOILS  
AND THE EFFECT ON DISCRETE FRACTURES**

**by  
Heather Ann Hall**

**A Dissertation  
Submitted to the Faculty of  
New Jersey Institute of Technology  
in Partial Fulfillment of the Requirements for the Degree of  
Doctorate of Philosophy in Environmental Science**

**Department of Chemical Engineering, Chemistry, and Environmental Science**

**May 2001**

**APPROVAL PAGE**

**VOLUME CHANGE BEHAVIOR OF CLAY SOILS  
AND THE EFFECT ON DISCRETE FRACTURES**

**Heather Ann Hall**

---

Dr. John R. Schuring, Committee Chair Chair and Professor of Civil and Environmental Engineering, NJIT	Date
---	------

---

Dr. John R. Dolan, Committee Member Adjunct Professor of Environmental Science, NJIT	Date
---	------

---

Dr. Dorairaja Raghu, Committee Member Professor of Civil and Environmental Engineering, NJIT	Date
---	------

---

Dr. Henry Shaw, Committee Member Professor of Chemical Engineering, NJIT	Date
---	------

---

Dr. Richard Trattner, Committee Member Associate Chairman and Professor of Chemistry and Environmental Science, NJIT	Date
--	------

Copyright © 2001 by Heather Ann Hall

ALL RIGHTS RESERVED

## BIOGRAPHICAL SKETCH

**Author:** Heather Ann Hall  
**Degree:** Doctorate of Philosophy  
**Date:** May 2001

### **Undergraduate and Graduate Education:**

- Doctorate of Philosophy in Environmental Science  
New Jersey Institute of Technology  
Newark, New Jersey, 2001
- Master of Science in Environmental Science  
New Jersey Institute of Technology  
Newark, New Jersey, 1995
- Bachelor of Arts in Geology-Biology  
Colby College  
Waterville, Maine, 1990

**Major:** Environmental Science

### **Publications:**

- Hall, H.A. 1995. "Investigation into Fracture Behavior and Longevity of Pneumatically Fractured Fine-Grained Formations," M.S. Thesis, New Jersey Institute of Technology, Newark, NJ.
- Hall, H.A. and R.E. Nelson. 1990. "Paleoenvironmental Analysis of Subfossil Coleoptera (Beetles) from Sandy River Terrace Sediments in Starks, Maine," *Maine Geologist*, 16(2): 5.

To my beloved family

## ACKNOWLEDGMENTS

Pursuit of my doctorate at New Jersey Institute of Technology (NJIT) has been an experience unequaled by any other in my lifetime. I wish to offer acknowledgments to those that supported my efforts. First, I am grateful to NJIT for awarding me a Presidential Fellowship that allowed me to pursue my studies on a full-time basis. The institution was also especially flexible in allowing me to have an advisor outside my primary department. Dr. John R. Schuring, from the Department of Civil and Environmental Engineering, played a significant role in incorporating an engineering element into my professional training, which had previously been in science. He is a truly gifted mentor whose creativity, dedication, and encouragement have been an immense source of inspiration. I feel extremely privileged to have worked with such an outstanding educator and a kind soul. I will always be indebted. I thank my other committee members, Dr. John Dobi, Dr. Dorairaja Raghu, Dr. Henry Shaw, and Dr. Richard Trattner, for their careful review of this project at various stages. I also want to thank Dr. Ronald Kane, Annette Damiano, Gayle Katz, and Clarisa Gonzalez-Lenahan in graduate studies for their help over the years.

The experimental portion of this project would not have been possible without the assistance of many people. Willy Woode of the Northern Virginia Soil and Water Conservation District, Ray Rainwater of Rainwater Landfill, Jeffrey Hall of J. Hall Homes, Michael Galbraith of NJIT, and various citizens of

Fairfax County, VA, helped to identify, locate and harvest the expansive soil for this work. Dr. Daniel Giménez of Environmental Science, Dr. Gene Giacomelli of Bioresource Engineering, and Dr. George Nieswand of Ecology, Evolution, and Natural Resources, all faculty of Rutgers University, generously offered use of their pressure plate apparatuses. Dr. Giménez, in particular, provided valuable soil physics technical oversight. I am also grateful for the help of his students, Cris San Miguel and Janice Karmon. Steve Harrold from Servi-Tech Laboratories developed the special soil analysis methods I requested, and Frank Johansson, Clint Brockway and Larisa Krishtopa provided crucial NJIT laboratory support. Finally, Michael Thompson and John Griscavage supervised the improvement of the environmental chamber for the horizontal infiltrometer tests.

Various colleagues have offered invaluable support over the course of this study. Special thanks go to Thomas Boland and Jannina Alvarez. Thomas Boland, our Pneumatic Fracturing (P.F.) Development Engineer, generously offered his resources and design expertise. Jannina Alvarez, an undergraduate member of the P.F. team, not only acted as a research assistant, but also offered her friendship and compassion beyond all others. Steven Arturo, a fellow NJIT graduate student, helped develop the mathematical solutions, and a former PF team member, Trevor King, provided the data for field validation. In addition, Michael Galbraith, Brian Sielski, Michael Canino, Jenny Lin Nassimi, Sean McGonigal, Deborah Schnell, Chad Sheng, Peniel Ortega, Hugo Fernandez, Minhaz Bootwala, and Navneet Kumar have been great colleagues.

Pursuing a doctorate has presented many personal challenges. I acknowledge Tanja von Ahnen, Kate Dannan, Michele Flynn, Kristin Hanson, Julie Hynes, Irina Kats, Laura Monteleone, Andrés Rodríguez, Kelly Barton Rogers, Sara December Rouland, and Diane Wisbeck. These special people have provided much needed balance in my life, unconditional love, and tremendous understanding, especially through the anti-social, hermit stages of this work. For important support at a critical juncture, I am deeply grateful to the City of Newark, NJ and to Saul Fenster, Eida Berrio, Laura Monteleone, Deborah Schnell, John Schuring, Michael Galbraith, Ronald Kane, Magaly Castro, Clifford Kuhn, and Marie Feuer. Also, Janet Maldonado, who entered my life in the latter stages of this project, has enlightened my life in ways I never thought possible.

Finally, I wish to offer the utmost of appreciation to my family, particularly my parents Martin and Janet Hall, my siblings and their spouses Jennifer and Lane Hall-Witt and Jeffrey and Michelle Hall, my grandparents Ernest LeRoy Hall, and the late Katherine Fuller Hall and Susan Wiles Steele, and Theresa and Michael DiCicco. I am blessed with a family who holds strong convictions and demonstrates, as role models, a true love of learning and an unparalleled passion for following their dreams.

I would like to close with a quote that has offered daily spiritual insight on many levels. Engraved on a plaque on my office wall, it reads, "In the middle of every difficulty, lies opportunity." *Albert Einstein*



## TABLE OF CONTENTS

Chapter	Page
1 INTRODUCTION .....	1
1.1 Overview .....	1
1.2 Objectives and General Approach .....	3
2 BACKGROUND.....	7
2.1 Previous Related Studies by the Investigator.....	7
2.2 Conceptual Framework for the Current Study .....	9
2.2.1 Volume Change in Fine-Grained Soil.....	9
2.2.2 Soil Fracture Genesis and Characterization.....	10
2.2.3 Interrelationship Between Volume Change and Fractures .....	15
2.2.3.1 Active Zones .....	15
2.2.3.2 Fracture Closure and Permanence .....	19
2.3 Mathematical Framework for the Current Study .....	21
2.3.1 Consolidation Theory for Saturated Domain.....	21
2.3.2 Unsaturated Domain Theory .....	25
2.3.3 Other Stress State Variables .....	28
2.3.4 Evaporation Theory .....	30
2.4 Industrial Applications.....	33
2.5 Previous Modeling Approaches.....	37
2.5.1 General Volume Change Modeling Approach .....	38

# TABLE OF CONTENTS

## (Continued)

Chapter	Page
2.5.2 Specific Models Incorporating Changes in Fracture Geometry .....	41
2.5.3 Relevance to the Current Study.....	43
3 EXPERIMENTAL STUDIES .....	47
3.1 Procedures.....	47
3.1.1 Soil Collection, Testing, and Preparation.....	47
3.1.2 Horizontal Infiltrometer Testing.....	52
3.1.2.1 Overview .....	52
3.1.2.2 Apparatus Setup .....	54
3.1.2.3 Operation .....	59
3.1.3 Material Parameter Testing.....	60
3.1.3.1 Consolidation Testing .....	61
3.1.3.2 Pressure Plate Soil Equilibration.....	61
3.1.3.3 Suction Testing .....	63
3.1.3.4 Water Retention Testing .....	65
3.1.3.5 Swell Testing.....	66
3.2 Results and Discussion .....	66
3.2.1 Soil Properties .....	66
3.2.1.1 Geology of the Potomac Formation .....	67
3.2.1.2 Physical and Chemical Testing .....	70

## TABLE OF CONTENTS (Continued)

Chapter	Page
3.2.1.3 Expansivity Characterization.....	78
3.2.2 Horizontal Infiltrometer Testing.....	83
3.2.2.1 Flow Results.....	83
3.2.2.2 Stages of Flow Behavior.....	87
3.2.2.3 Fracture Aperture Calculations .....	92
3.2.2.4 Moisture Characterization.....	98
3.2.2.5 Summary of Horizontal Infiltrometer Testing Results.....	107
3.2.3 Consolidation Testing.....	109
3.2.4 Water Retention Testing.....	115
3.2.5 Swell Testing .....	120
4 THEORETICAL MODELING .....	124
4.1 General Model Approach.....	124
4.1.1 Physical Concept.....	124
4.1.2 Assumptions.....	131
4.1.3 Mathematical Approach.....	136
4.2 Model Development .....	144
4.2.1 Specific Boundary and Initial Conditions.....	144
4.2.2 Mathematical Solutions .....	147
4.2.2.1 Fracture Volume Change (FVC) Model Solution.....	148

## TABLE OF CONTENTS (Continued)

Chapter	Page
4.2.2.2 Supporting Evaporation Rate Calculations.....	151
4.3 Model Suggestions for Other Conditions .....	153
4.3.1 Unsaturated Conditions .....	153
4.3.2 First Stage Evaporative Conditions .....	155
5 MODEL VALIDATION AND CALIBRATION.....	157
5.1 Objective .....	157
5.2 Laboratory Horizontal Inifltrometer Study .....	157
5.2.1 Validity of Model Assumptions .....	158
5.2.2 FVC Model Predictions for HI Drying Tests .....	160
5.2.2.1 Model Input Parameters .....	160
5.2.2.2 Case 1 Predictions .....	161
5.2.2.3 Case 2 Predictions .....	163
5.2.2.4 Implications of Case 1 and Case 2 Model Results .....	166
5.2.2.5 Fracture Aperture Predictions.....	167
5.3 Field Case Study .....	170
5.3.1 Overview of the Pneumatic Fracturing Process.....	170
5.3.2 Santa Clara Site Description.....	172
5.3.3 Pilot Study Test Data.....	174
5.3.4 FVC Model Predictions.....	176

## TABLE OF CONTENTS (Continued)

Chapter	Page
6 FVC MODEL APPLICATION PROCEDURES.....	182
6.1 Introduction.....	182
6.2 Procedural Guide to FVC Model.....	183
6.3 Functional Relationships .....	186
6.3.1 Moisture Content-Time Relationship .....	186
6.3.2 Fracture Aperture-Moisture Content Relationship .....	190
6.3.3 Fluid Flow-Moisture Content Relationship .....	190
6.4 Example Application .....	192
6.5 Data Requirements for Continued Model Calibration .....	199
7 CONCLUSIONS AND RECOMMENDATIONS .....	201
7.1 Conclusions .....	201
7.2 Recommendations for Future Work .....	205
APPENDIX A PHOTOGRAPHS.....	207
APPENDIX B HORIZONTAL INFILTRMETER FLOW DATA .....	217
APPENDIX C RAW HORIZONTAL INFILTRMETER MOISTURE DATA ..	225
APPENDIX D CONSOLIDATION TEST DATA .....	240
APPENDIX E SWELL TEST DATA .....	251
APPENDIX F SOLUTION DERIVATIONS.....	260

**TABLE OF CONTENTS**  
**(Continued)**

<b>Chapter</b>	<b>Page</b>
APPENDIX G SIGNIFICANCE OF THE COMPONENTS OF TOTAL SOIL WATER POTENTIAL .....	272
APPENDIX H SAMPLE CALCULATIONS .....	276
REFERENCES.....	287

## LIST OF TABLES

Table	Page
2.1 Terms Used to Characterize Rock Fractures .....	14
2.2 Measurement Techniques for Soil Fracture Classification.....	14
3.1 Laboratory Testing for Soil Characterization.....	51
3.2 Summary of Pressure Plate Samples .....	64
3.3 Comparison of Potomac Formation Physical Properties .....	71
3.4 Effect of Soil Reduction Method on Atterberg Limits .....	74
3.5 Results of Chemical Analyses on Potomac Formation.....	75
3.6 Comparison of Empirical Volume Change Ratings by Various Investigators For Potomac Formation Clays.....	84
3.7 Summary of Consolidation Test Coefficients .....	110
3.8 Empirical Relationships for Consolidation and Swell Indices .....	111
3.9 Summary of Suction Testing Results .....	119
3.10 Depths Associated with Overburden Pressures.....	122
3.11 Coefficients of Volume Change for Monotonic Wetting at Various Overburden Pressures.....	123
5.1 Model Input Parameters for HI Tests .....	161
5.2 Comparison of Predicted and Actual Final Fracture Apertures for HI Drying Tests .....	168
5.3 Santa Clara Site Soil Properties at 10.5 ft bgs.....	173
5.4 Summary of Post-Fracture SVE and HAI Testing.....	177
5.5 Model Input Parameters for Field Case Study .....	177

**LIST OF TABLES**  
**(Continued)**

<b>Table</b>	<b>Page</b>
C.1 Raw Moisture Data For Horizontal Infiltrometer Tests .....	226
D.1 Summary of Consolidation Test Data .....	241
E.1 Summary of Swell Test Data .....	252
H.1 Saturation Vapor Pressures of Water for Various Temperatures .....	282



## LIST OF FIGURES

Figure	Page
1.1 Overview of the Study Approach.....	5
2.1 Qualitative Design Model for Fractures in Fine-Grained Soils .....	8
2.2 Conditions for Volume Change .....	11
2.3 Sources of Fractures in Fine-Grained Geologic Formations .....	13
2.4 Concept of Active and Secondary Active Zones .....	16
2.5 Saturated Clay Layer Undergoing Consolidation.....	23
2.6 Constitutive Surface for the Unsaturated Soil Domain.....	26
2.7 Industrial Significance of Soil-Fracture Interactions.....	34
2.8 Typical Shrinkage Curve Showing Four Shrinkage Zones.....	38
2.9 Schematic Representation of the AHF Model.....	40
2.10 Changes in Fracture Volume for an Illite-Montmorillonite Clay Soil .....	42
3.1 Location of Soil Collection .....	48
3.2 Conceptual Schematic of the Horizontal Infiltrometer (HI) Test System...	52
3.3 Construction Details for the Horizontal Infiltrometer Apparatus.....	56
3.4 Experimental Setup of the Horizontal Infiltrometer System.....	57
3.5 Clay Mineral Facies in Potomac Formation Outcrop Belt from Virginia to New Jersey .....	68
3.6 Distribution of Localized Potomac Formation Deposits in Fairfax County and Vicinity .....	69
3.7 Grain Size Distribution for Potomac Formation Clays.....	73
3.8 Expansivity of Potomac Formation Clay Based on Hall (1995) Method.....	79

## LIST OF FIGURES (Continued)

Figure	Page
3.9 Raw Flow-Time Data and Standard Errors: Example HI Test 8C .....	86
3.10 Average Flow-Time-Pressure Data: Example HI Test 8C.....	86
3.11 Illustration of the Five Stages of Flow Behavior: Example Test 10C.....	88
3.12 Apertures and Reynolds Numbers for HI Tests 5C-11C.....	94
3.13 Soil Moisture Characteristics of HI Tests 5C-11C.....	99
3.14 Cross Sections of the Soil Block Length after Drying and Wetting .....	104
3.15 Consolidation Test e-log p Plot for Remolded Potomac Clay .....	110
3.16 Effects of Void Ratio on a) Coefficient of Consolidation; b) Coefficient of Volume Compressibility; and c) Hydraulic Conductivity .....	113
3.17 Shrinkage Curve for Remolded Potomac Clay.....	116
3.18 Desorption Water Retention Curve for Remolded Potomac Clay .....	117
3.19 Swell Test Curves for Remolded Potomac Clay .....	121
4.1 Physical Mechanisms For Changes in Horizontal Fracture Geometry .....	125
4.2 Representative Elemental Volume (REV) for the Current Study .....	127
4.3 Conditions for Volume Change in the REV (Case of Desiccation) .....	129
4.4 Boundary Constraints on the REV .....	132
4.5 Representation of the REV Half-Space .....	137
4.6 General Boundary and Initial Conditions on the REV Half-Space.....	138
4.7 Graphical Representation of Potential Initial Conditions .....	139

## LIST OF FIGURES (Continued)

Figure	Page
4.8 Horizontal Layering of the REV Half-Space .....	140
4.9 Change in Fracture Aperture and Stacking of Adjacent REVs .....	144
4.10 Groundwater Divide Present Between Adjacent REVs.....	146
4.11 General Form of the Case 1 and Case 2 FVC Model Functions (Case of Drying) .....	150
5.1 Comparison of HI Experimental Data with Case 1 Moisture Predictions.....	162
5.2 Comparison of HI Experimental Data with Case 2 Moisture Predictions using $E_{af}$ Evaporation Rates .....	164
5.3 Comparison of HI Experimental Data with Case 2 Moisture Predictions using Various Evaporation Rates .....	165
5.4 Aperture Corrections for Experimental Scaling Effects .....	169
5.5 Permeability Enhancement by Pneumatic Fracturing.....	171
5.6 Santa Clara Site Plan Layout .....	175
5.7 Comparison of Field Case Study Data with Case 1 FVC Model Moisture Predictions .....	180
6.1 Theoretical Moisture Content-Time Relationship.....	188
6.2 Theoretical Moisture Content-Fracture Aperture Relationship.....	191
6.3 Relationship between Fluid Flow and Moisture Content.....	192
6.4 Example Determination of Change in Moisture Content .....	195
6.5 Example Determination of Change in Fracture Aperture .....	197

# **LIST OF FIGURES** (Continued)

Figure	Page
B.1    Raw Flow-Time Data for Various HI Tests .....	218
B.2    Average Flow-Time-Pressure Data for Various HI Tests .....	222
C.1    Vertical Cross-Sections of the Soil Block at the Fracture Showing Moisture Data .....	233
D.1    Consolidation Time-Deformation Plots for Potomac Clay .....	242
E.1    Swell Test Time-Deformation Plots for Potomac Clay .....	253

## LIST OF SYMBOLS

Legend: F Force ; L Length; M Mass;  $\theta$  Temperature; T Time

$a_v$	=	coefficient of compressibility ( $L^2/F$ , $LT^2/M$ )
$A$	=	area ( $L^2$ ), FVC Model solution constant (L)
$b$	=	fracture aperture (L)
$b_e$	=	effective fracture aperture (L)
$b_{ef}$	=	final effective fracture aperture (L)
$B$	=	FVC Model solution constant (L)
$c$	=	constant moisture content ( $(FT^2/L)/(FT^2/L)$ , M/M, dimensionless)
$c_v$	=	coefficient of consolidation ( $L^2/T$ )
$C_c$	=	compression index (dimensionless)
$C_r$	=	recompression index (dimensionless)
$C_s$	=	swell index (dimensionless)
$C_w$	=	water capacity function ( $(L^3/L^3)/(F/L^2)$ , $L^2/F$ , $LT^2/M$ )
$D$	=	diffusivity ( $F/LT$ , $M/T^3$ )
$e$	=	void ratio ( $L^3/L^3$ , dimensionless)
$e_d$	=	mean vapor pressure in air at height of interest above water ( $F/L^2$ , $M/LT^2$ )
$e_o$	=	mean vapor pressure at water surface ( $F/L^2$ , $M/LT^2$ )
$e_2$	=	saturation vapor pressure at dewpoint ( $F/L^2$ , $M/LT^2$ )

## LIST OF SYMBOLS (Continued)

$e_0^0$	= saturated vapor pressure (F/L <sup>2</sup> , M/LT <sup>2</sup> )
$e_2^0$	= saturated vapor pressure at mean temperature in fracture (F/L <sup>2</sup> , M/LT <sup>2</sup> )
$E$	= evaporation rate (L/T)
$E_a$	= aerodynamic evaporation rate (L/T)
$E_{af}$	= aerodynamic evaporation rate in fracture (L/T)
$g$	= acceleration due to gravity (L/T <sup>2</sup> )
$G_s$	= specific gravity ((FT <sup>2</sup> /L <sup>4</sup> )/(FT <sup>2</sup> /L <sup>4</sup> ), (M/L <sup>3</sup> )/(M/L <sup>3</sup> ), dimensionless)
$h$	= height of soil in layer $j$ (L)
$h_{ave}$	= average vertical soil deformation (L)
$h_{min}$	= minimum vertical soil deformation (L)
$h_{max}$	= maximum vertical soil deformation (L)
$h_r$	= relative humidity ((FT <sup>2</sup> /L <sup>4</sup> )/(FT <sup>2</sup> /L <sup>4</sup> ), (M/L <sup>3</sup> )/(M/L <sup>3</sup> ), dimensionless)
$H$	= thickness of soil layer (L)
$H_f$	= final thickness of soil layer (L)
$H_i$	= initial thickness of soil layer (L)
$j$	= number of layers in REV Half-Space (L)
$K$	= hydraulic conductivity (L/T)

## LIST OF SYMBOLS (Continued)

$K_{vs}$	= vertical saturated hydraulic conductivity (L/T)
$L_1, L_2$	= linear distance from extraction point, $L_2 > L_1$ (L)
$m$	= number of intervals (L), moisture flux (L/T)
$m_1$	= net normal stress path
$m_2$	= matric suction stress path
$m_{sv}$	= saturated coefficient of volume change ( $L^2/F$ , $LT^2/M$ )
$m_{uv}$	= unsaturated coefficient of volume change ( $L^2/F$ , $LT^2/M$ )
$M$	= pressure ratio (dimensionless)
$n$	= aperture exponent, $b''$ (dimensionless), number of coordinates (L)
$P_0$	= external load at ground surface, units of head (L)
$P_1, P_2$	= absolute air pressure head at distance from extraction point, where $P_2 > P_1$ (L)
$P_{abs}$	= absolute pressure head (L)
$P_g$	= gauge pressure head (L)
$P_o$	= operating pressure head (L)
$P_s$	= standard pressure head (L)
$Q$	= flow rate ( $L^3/T$ )
$Q_o$	= operating flow rate ( $L^3/T$ )
$Q_s$	= flow rate under STP conditions ( $L^3/T$ )

## LIST OF SYMBOLS (Continued)

$r$	= fracture radius (L)
$r_s$	= geometric factor of volume change (dimensionless)
$R_1, R_2$	= radial distances from extraction point, where $R_2 > R_1$ (L)
$S$	= eigenfunction
$t$	= time
$T$	= FVC Model solution intermediate
$T_o$	= operating temperature ( $\theta$ )
$T_s$	= standard temperature ( $\theta$ )
$U$	= wind velocity (L/T), spacer variable for $u_w$ (F/L <sup>2</sup> , M/LT <sup>2</sup> ) or $w$ ((FT <sup>2</sup> /L)/(FT <sup>2</sup> /L), M/M, dimensionless)
$u_a$	= pore-air pressure (F/L <sup>2</sup> , M/LT <sup>2</sup> )
$u_w$	= pore-water pressure (F/L <sup>2</sup> , M/LT <sup>2</sup> )
$u_{w1}, u_{w2}$	= pore-water pressure at first and second boundaries, respectively (F/L <sup>2</sup> , M/LT <sup>2</sup> )
$u_{wi}$	= initial pore-water pressure (F/L <sup>2</sup> , M/LT <sup>2</sup> )
$v_j$	= volume of each unit interval $j$ (L <sup>3</sup> )
$V$	= unit volume of the REV Half-Space (L <sup>3</sup> ), air velocity (L/T)
$V_f$	= fracture volume (L <sup>3</sup> )
$V_t$	= total volume of soil mass (L <sup>3</sup> )



## LIST OF SYMBOLS (Continued)

$x$	=	space coordinate, lateral direction (L)
$w$	=	gravimetric water content $((\text{FT}^2/\text{L})/(\text{FT}^2/\text{L}), \text{M}/\text{M}, \text{dimensionless})$
$w_1, w_2$	=	gravimetric water content at first and second boundaries, respectively $((\text{FT}^2/\text{L})/(\text{FT}^2/\text{L}), \text{M}/\text{M}, \text{dimensionless})$
$w_e$	=	equilibrium gravimetric water content $((\text{FT}^2/\text{L})/(\text{FT}^2/\text{L}), \text{M}/\text{M},$ dimensionless)
$w_i$	=	initial gravimetric water content $((\text{FT}^2/\text{L})/(\text{FT}^2/\text{L}), \text{M}/\text{M},$ dimensionless)
$W$	=	fracture width (L)
$y$	=	space coordinate, horizontal direction (L)
$z$	=	space coordinate, vertical direction (L)
$\alpha_1, \alpha_2, \alpha_3$	=	solution constants (various dimensions)
$\beta$	=	arbitrary constant (L)
$\varepsilon$	=	volumetric strain $(\text{L}^3/\text{L}^3, \text{dimensionless})$
$\varepsilon_z$	=	strain in vertical direction (L/L, dimensionless)
$\gamma$	=	apparent specific gravity (dimensionless)
$\gamma_a$	=	unit weight of air $(\text{FT}^2/\text{L}^4, \text{M}/\text{L}^3)$
$\gamma_w$	=	unit weight of water $(\text{FT}^2/\text{L}^4, \text{M}/\text{L}^3)$
$\lambda$	=	eigenvalue

## LIST OF SYMBOLS (Continued)

$\mu$	=	matric suction ( $F/L^2$ , $M/LT^2$ ), Poisson's ratio (dimensionless)
$\nu$	=	kinematic viscosity of fluid ( $L^2/T$ ), spacer variable for moisture content in FVC Model solution derivation ( $(FT^2/L)/(FT^2/L)$ , $M/M$ , dimensionless)
$\pi$	=	osmotic suction ( $F/L^2$ , $M/LT^2$ )
$\theta$	=	volumetric moisture content ( $L^3/L^3$ , dimensionless)
$\rho_d$	=	dry soil density ( $FT^2/L^4$ , $M/L^3$ )
$\rho_w$	=	density of water ( $FT^2/L^4$ , $M/L^3$ )
$\sigma$	=	total (normal) stress ( $F/L^2$ , $M/LT^2$ ), FVC Model solution intermediate
$\sigma'_s$	=	saturated effective stress ( $F/L^2$ , $M/LT^2$ )
$\sigma'_{II}$	=	unsaturated effective stress ( $F/L^2$ , $M/LT^2$ )
$\nu$	=	moisture ratio (dimensionless)
$\Omega$	=	overburden potential ( $F/L^2$ , $M/LT^2$ )
$\psi$	=	total suction ( $F/L^2$ , $M/LT^2$ )
$\psi_g$	=	gravitational potential ( $F/L^2$ , $M/LT^2$ )

# CHAPTER 1

## INTRODUCTION

### 1.1 Overview

Volume change phenomena in fine-grained geologic formations is of critical importance in a number of scientific and engineering problems. An example is the effect of volume change in clay on contaminant transport at industrial waste sites. This is of particular significance from a perspective of contaminant mobilization and encapsulation processes (Suter et al., 1993; Hall, 1995). In addition, expansive soils are a major source of damage to structures and pavements (Jones and Holtz, 1973; Gillott, 1986); cracking clay soils make it nearly impossible to properly manage crops (Coulombe et al., 1996); and the oil and gas production industry is perpetually plagued with extraction difficulties related to formation swell (Krueger, 1986; Porter, 1989).

Recent approaches to solving these industrial problems are based on the prediction of soil volume change behavior. However, the complexity of the volume change phenomena has largely prevented success in solving these problems, as evidenced by the persistent financial losses over a widespread range of industries. Volume change is a result of many physical, chemical and mineralogical processes, many of which are not well understood. One area of particular interest is the interrelationship between volume change and fractures, which is the subject of this dissertation.

Fractures are generated in a clay matrix whenever the applied tensile or shear stresses exceed the natural strength of the material (Dexter, 1988). The geologic formation may be subjected to these stresses either naturally (e.g., desiccation, overburden removal, root growth, glacial movement) or artificially (e.g., tillage and vehicular traffic, remolding and compaction, subsurface fracturing). The presence of such fractures significantly influences the behavioral properties of the formation, especially with regard to fluid flow and strength.

In particular, fractured, fine-grained formations undergo large alterations in permeability as a result of small changes in the fracture aperture (i.e., width of the fracture opening). Through a series of experiments, Hall (1995) demonstrated the interdependence of fracture aperture and permeability through cyclic wetting and drying of a clay soil. Aperture changes were attributed to volume changes in the soil medium as the clay absorbed or released moisture. Flow and transport rates were found to be especially sensitive to a change in aperture on account of the dependence on the Cubic Law (i.e., flow rates in open fractures are proportional to the cube of the aperture). It was also concluded that this phenomenon has a potentially profound effect on environmental site modeling and remediation.

Another area of major concern involves heaving of foundations and pavements located on expansive clays. Since fractures are open spaces in the geologic formation, they can absorb some portion of the volume change. They also act as conduits for entry of moisture into the formation. A better

understanding of fracture behavior can improve heave predictions in swelling clays, allowing for more successful prevention and mitigation of damage to overlying engineering structures.

The industrial significance of the presence of fractures in clay soil has been widely recognized (Rowe and Booker, 1991; Saada et al., 1994; Jarvis and Leeds-Harrison, 1990; Liu and Civan, 1995). Previous studies on volume change and fractures have generally been focused at the microscopic (i.e., clay mineral) and megascopic (i.e., bulk matrix) levels. It is the intent of this research to expand upon the current body of knowledge and detail this interrelationship at the intermediate, or fracture macroscopic level.

## **1.2 Objectives and General Approach**

In order to address more effectively the industrial problems associated with expansive clay, an improved understanding of soil behavior is needed. Specifically, this research is designed to investigate soil volume change and its interrelationship with fracture geometry in clay soils. The specific objectives of this research study are to:

- (1) Experimentally examine the behavior of a horizontal, discrete fracture in expansive soil when fracture boundary soils are subject to moisture fluctuation. The major focus of this investigation is to

determine the potential for fracture dilation, closure, and cyclic reopening as a function of soil volume change.

- (2) Formulate a mathematical model to predict changes in fracture aperture in clay soils from soil moisture changes.
- (3) Validate and calibrate the mathematical model with data from laboratory experiments and a field case study.

The general approach used to accomplish the study objectives is summarized in Figure 1.1. The first step was problem formulation to establish a conceptual framework for the study. Problem formulation also included a review of available literature to identify industrial applications and previous mathematical modeling approaches. A summary of this review is presented in Chapter 2.

The laboratory studies centered around a bench-scale horizontal infiltrometer (HI) that was custom designed for this study to examine fracture aperture changes induced by moisture fluctuations in a horizontal discrete fracture. The laboratory portion of the study also involved locating, collecting and characterizing a suitable expansive clay soil for the HI tests. Tests were performed on this soil to identify parameters for eventual input in the mathematical model (e.g., stress-strain properties, water retention

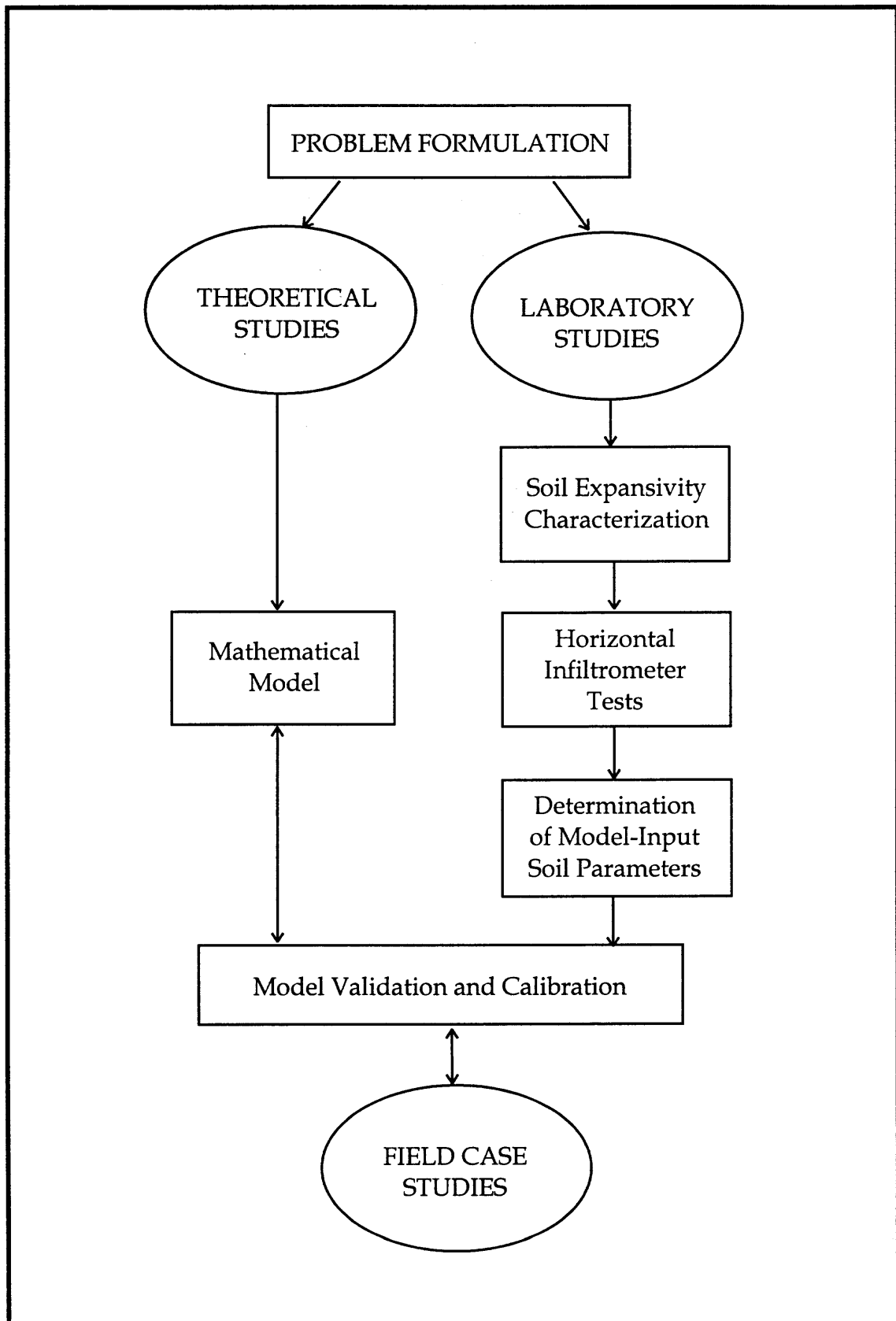


**Figure 1.1** Overview of the Study Approach

characteristics). Chapter 3 summarizes the laboratory experiments performed as part of this study.

The mathematical model was developed in parallel with the experimental work. The model uses consolidation theory coupled with strain calculations to predict fracture aperture. Chapter 4 presents the approach and development of the mathematical model. The model is then validated and calibrated with HI laboratory data and field pneumatic fracturing data in Chapter 5. The conclusions of the study are presented in Chapter 6 along with recommendations for future work.



## CHAPTER 2

### BACKGROUND

#### 2.1 Previous Related Studies by the Investigator

A preliminary study on the behavior of soil fractures was performed at New Jersey Institute of Technology (Hall, 1995). The work examined the impact of volume change on a discrete fracture in a natural, remolded clay soil. This section summarizes the results of this previous work.

The experimental portion of the study involved development of a new laboratory device for investigation of air flow through a discrete soil fracture. The device, termed a 'horizontal infiltrometer,' allowed quantitative testing of the effect of moisture fluctuation on fracture aperture. Fluctuations in air flow through an artificial discrete fracture in clay were attributed to changes to the fracture aperture, which were manifested as swelling and shrinking of the fracture boundary soils.

A new concept termed the 'secondary active zone' was introduced as part of this research to describe the susceptibility of soils adjacent to the fracture to volume change. It was developed in concert with the 'active zone analogy' commonly used to describe shrinking and swelling in surface soils. In essence, the concept postulates that fractured geologic formations may experience volume changes significantly deeper than non-fractured formations.

A qualitative design model, shown in Figure 2.1, was developed as part of the previous investigation. The model predicts the propensity of a formation for

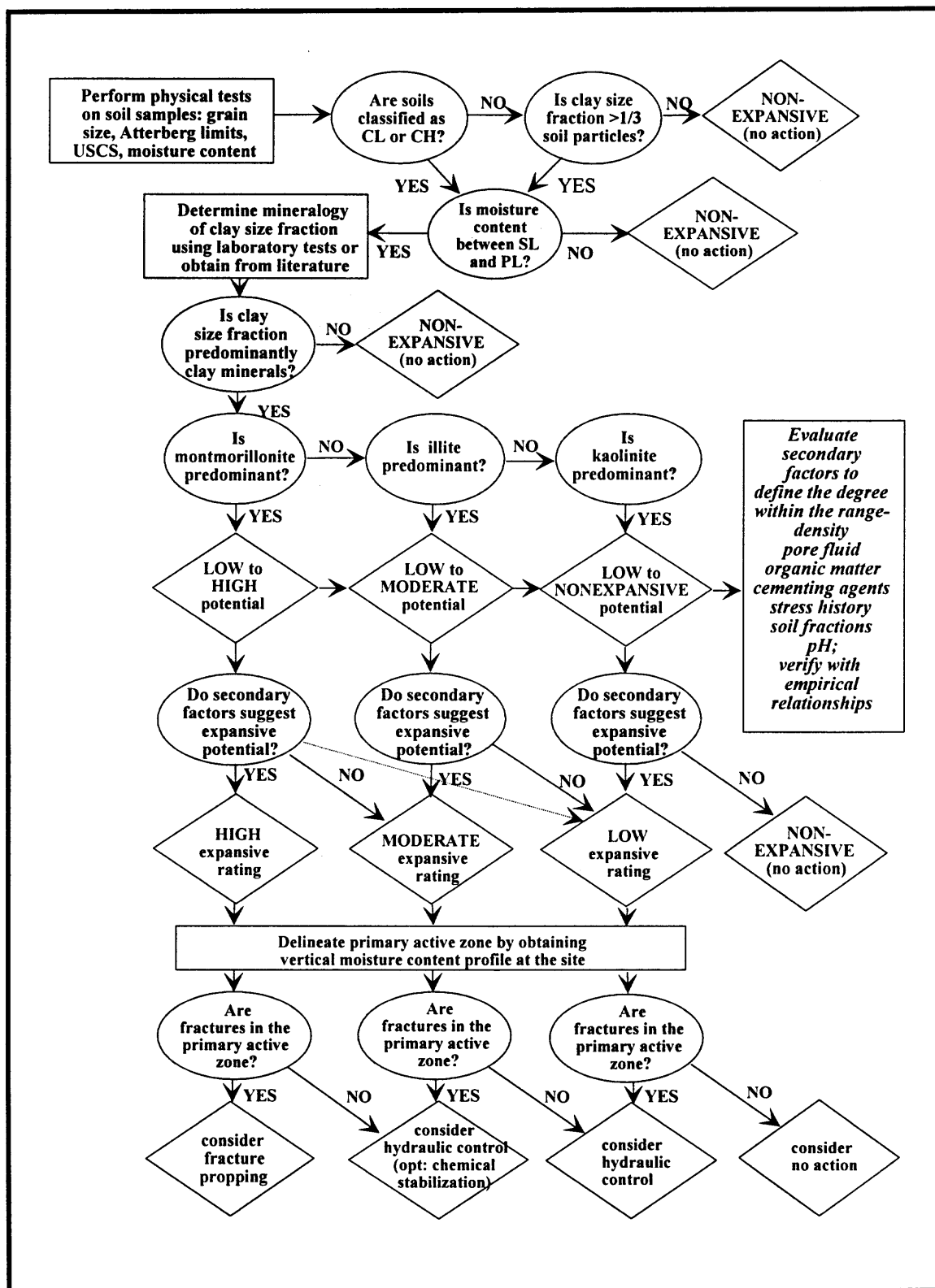


Figure 2.1 Qualitative Design Model for Fractures in Fine-Grained Soils (Hall, 1995)

volume change and recommends treatment alternatives. Expansivity ratings are used to describe the cumulative impact of formation properties and environmental conditions on volume change. The treatment alternatives are directed towards controlling volume changes by altering these parameters.

The current study expands upon results of this previous study, focusing on quantitative evaluation of the interaction between fractures and volume change, particularly with respect to related industrial problems.

## **2.2 Conceptual Framework for the Current Study**

This section develops the conceptual basis for the approach to investigating the geometry of soil fractures over time. Volume change and soil fractures are first addressed separately, followed by a discussion of their functional interrelationship. Included is a review of the active zone concept and current theories on fracture closure and permanence.

### **2.2.1 Volume Change in Fine-Grained Soil**

Fine-grained soils are the focus of this work because they are particularly susceptible to volume change, i.e., shrink-swell phenomena. Clay structure allows for both intra- and interlayer expansion, with the amount dependent on the soil mineralogy, particle size, density, reactivity, stress history, fabric, pH, and the presence or absence of organic matter and irreversible cementing agents. Soil activity is initiated by a shift in ambient environmental conditions such as

moisture, pressure, temperature, and pore fluid fluctuations. Resulting adjustments in the soil structure are manifested as volume change. Thus, the formation properties define the range of possible volume change, and the environmental conditions dictate the degree of expression. Figure 2.2 summarizes the conditions for volume change.

Formations notorious for volume change are designated as expansive, swelling, and cracking soils (e.g., soil taxonomy group Vertisols). These soils comprise 20-30% of the land area in the United States (Krohn and Slosson, 1980; Olive et al., 1989), with Texas carrying the bulk of the Vertisols (USDA-SCS, 1994). Expansive soils are also widely distributed in India, Australia, Sudan, and South Africa (Dudal and Eswaran, 1988; Wilding and Coulombe, 1996). The reader is referred to Hall (1995) for further discussion on the occurrence and extent of expansive soils.

## **2.2.2 Soil Fracture Genesis and Characterization**

The term fracture, in the context of this research, is used to describe discontinuities in the soil matrix which act as preferential flow conduits. This includes such popularly used terms as cracks, joints, fissures, and channels. Thus, fractures can range from a planar macroporosity with a micron-size aperture to a discrete fracture with a millimeter-size aperture.

The ubiquitous nature of fractures in fine-grained soils, particularly overconsolidated formations, is evidenced by the variety of sources from which

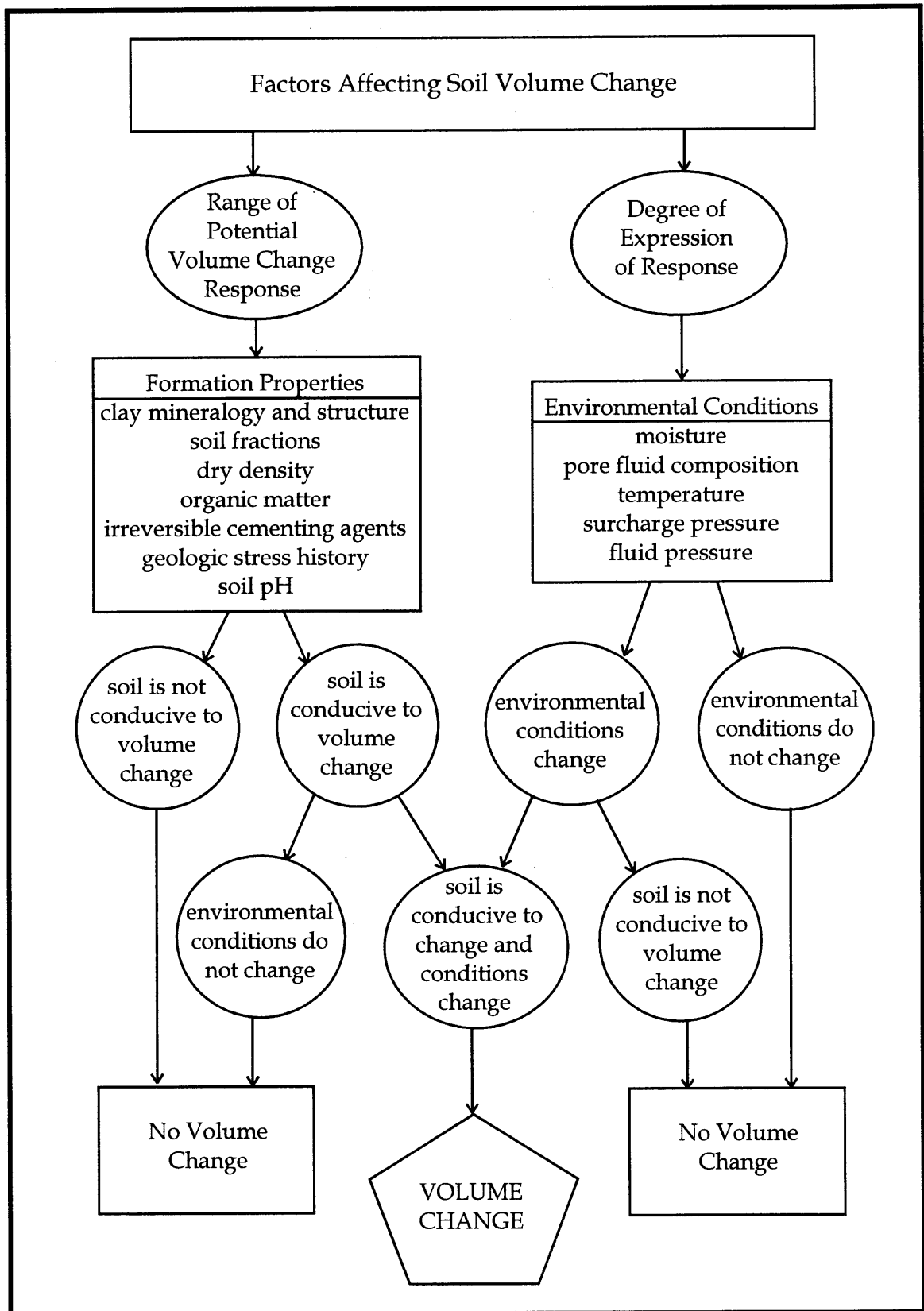


Figure 2.2 Conditions for Volume Change (Modified from Hall, 1995)

they are created. Figure 2.3 lists these sources, which may be natural or anthropogenic (i.e., generated by human influence), assembled from various references and this investigator's own experiences. Most natural sources such as desiccation, unloading, and bioturbation affect surficial soils, while fractures at depth are often a result of anthropogenic influence. Fractures are sometimes deliberately induced (e.g., pneumatic fracturing), while others are purely side effects (e.g., heated basements). Of significance to the environmental field is syneresis, where fractures develop as the pore water is replaced with a fluid of lower dielectric constant or higher salinity (Brown and Anderson, 1983).

Fractures in geologic formations are classified according to a set of geometric characteristics. Those characteristics used to classify rock fractures are shown in Table 2.1. While these may also theoretically apply to soils, their use is generally impractical since it is impossible to obtain undisturbed samples. Methods such as image analysis, numerical density techniques and surface topography analysis, which rely on soil samples, are thus capable of producing only semi-quantitative data at best. *In situ* techniques are limited to crude forms of measurement (e.g., steel rod to measure depth), or evaluation of properties indirectly related to fracture geometry (e.g., heave, flow). Table 2.2 summarizes the available methods for classifying soil fracture geometries. The lack of accurate, quantitative methods makes the macroscopic analysis of fractures a difficult task, and partly explains the absence of related work in the literature.

### NATURAL SOURCES

- Desiccation: Evaporation (climatic)  
 Transpiration (root uptake)  
 Water Migration (consolidation, ice crystallization nuclei)
- Unloading: Glacial Recession  
 Erosion of Overlying Sediment  
 Snow Melting
- Tectonics: Glaciotectonism (shear stress due to ice movement)  
 Orogenic (folding, faulting) or epeirogenic processes  
 Intrusions and diapirs (localized fractures)
- Other: Bioturbation (roots and root casts, burrowing)  
 Growth of ice lenses (freezing phenomena)  
 Chemical weathering (oxidation, release of K)  
 Secondary compression (plastic adjustment of soil fabric)  
 Syneresis (clay flocculation by e.g., microorganisms)  
 Swelling (change in environmental conditions)  
 Water pressure (natural hydraulic fracturing)  
 Inheritance from parent material (residual soils)  
 Shock (blowout from air compression on rapid water intake, especially dry, crusted saline soils)

### ARTIFICIAL SOURCES

- Fluid Pressure: Fracturing technologies  
 (hydraulic, pneumatic, explosive)
- Desiccation: *In situ* heat source (boiler, industrial processes)  
 Extraction of water (pumping, soil vapor extraction)
- Other: Swelling (irrigation, removal of surcharge pressure)  
 Tillage, vehicular traffic, machine vibration  
 Remolding and compaction (construction)  
 Differential settlement  
 Syneresis (due to inflow of a non-polar organic compound)

**Figure 2.3** Sources of Fractures in Fine-Grained Geologic Formations

**Table 2.1** Terms Used to Characterize Rock Fractures

TERM	DEFINITION
Persistence	the aerial extent of a discontinuity
Aperture	the perpendicular distance separating discontinuity walls
Orientation	the attitude of the discontinuity in space (i.e., strike and dip)
Wall	the waviness and surface unevenness relative to the mean
Roughness	plane of the discontinuity
Asperities or Filling	Localized points of contact or deposition between upper and lower fracture surfaces
Frequency	the quantitative distribution of discontinuities
Spacing	the perpendicular distance between adjacent discontinuities
Connectivity	the amount of intersection between discontinuities

Modified from Bates and Jackson (1984) and Barton (1987)

**Table 2.2** Measurement Techniques for Soil Fracture Classification

PARAMETER	SOIL	MEASUREMENT	REFERENCE
Volume	natural surficial fractures	Hand measurements of length, width, and depth; Infilling with sand	Dasog and Shashidhara (1993)
Length/Size	compacted clay liner	Photographs of fractured soil treated with dye	Elsbury et al. (1988)
Aerial Extent	Pneumatically fractured clay	Surface heave (rods, tiltmeters, levels, linear variable displacement transducers)	Venkatraman et al. (1995)
Orientation	laboratory soil samples	Impregnation with resin and image analysis	Bui and Mermut (1988)
Connectivity	Impregnated field samples	Numerical density techniques	Scott et al. (1988)
Roughness	soil fractured in hand	Surface topography analysis	Grant et al. (1990)
Aperture	Pneumatically fractured soil	<i>In situ</i> borehole video analysis	HSMRC et al. (1994)
	natural, fractured till	Cubic law analysis of <i>in situ</i> hydraulic flow	McKay et al. (1993)
Permeability (indicator parameter)	Pneumatically fractured soil	<i>In situ</i> packer air flow tests	Schuring and Chan (1992)
	natural, fractured till	<i>In situ</i> isolated-interval flow tests	McKay et al. (1993)
	agricultural, surface soil samples	Air permeability tests controlling matric suction	Blackwell et al. (1990); Roseberg and McCoy (1992)



### 2.2.3 Interrelationship Between Volume Change and Fractures

*Fractures provide an efficient pathway for changing environmental conditions, but are also significantly affected by the very volume changes which they create.* This interrelationship, which drives the current study, is discussed in this section with respect to active zones and fracture closure and permanence.

**2.2.3.1 Active Zones.** The term active zone is generally used to describe that portion of the surface soil profile that is subject to the greatest shrinking and swelling (Nelson and Miller, 1992). Volume change in the active zone results mainly from fluctuations in moisture due to varying infiltration, evaporation, and transpiration rates. Soil zones displaying the most activity occur in geographic locations where there are large cyclic, often semi-annual, changes in atmospheric conditions (e.g., dry seasons followed by wet seasons). The depth at which the water content becomes nearly constant defines the lower limit of the active zone, which generally extends a few to several meters into a fine-grained soil formation. Soils beneath surface coverings, such as pavements and foundations, will retain moisture to a greater degree than soils open to the atmosphere. Figure 2.4 illustrates this concept and that of a secondary active zone, which is explained later in this section.

Given a soil with a natural propensity for volume change, the thickness of an active zone depends on the capacity for environmental changes to penetrate the soil profile. An active zone is therefore a function the soil's ability to conduct

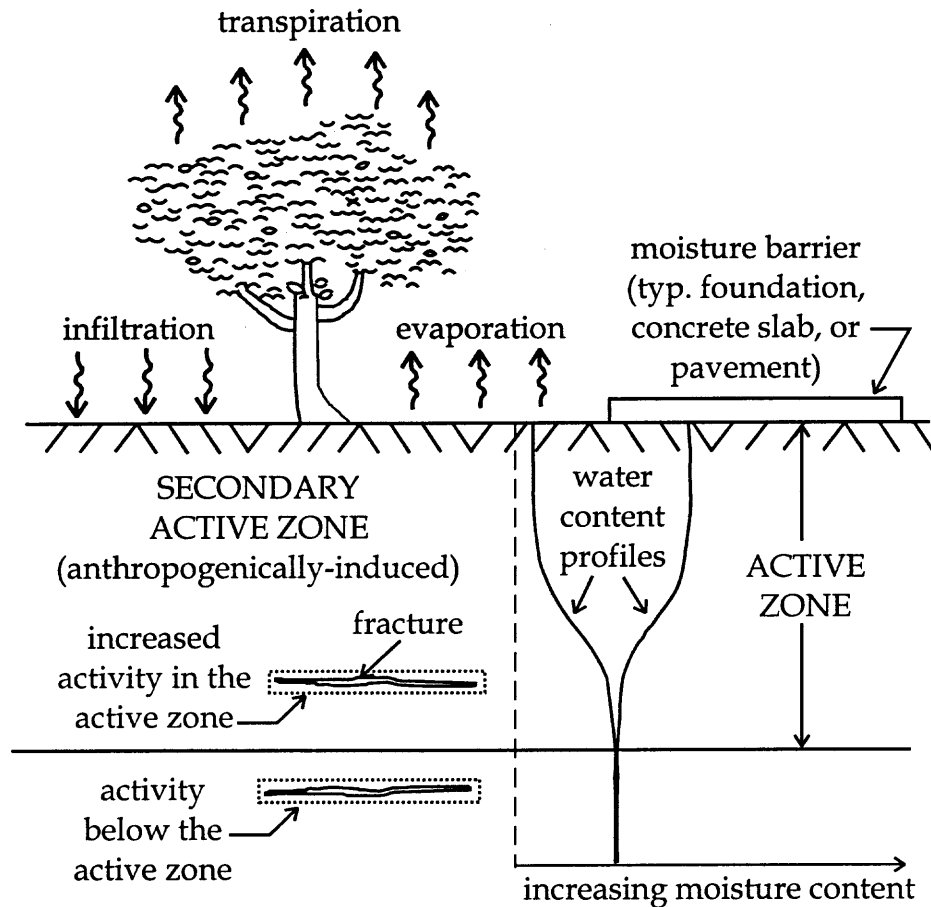


**Figure 2.4** Concept of Active and Secondary Active Zones  
(Modified from Hall, 1995)

fluid, which serves to transfer these changes from one location to another. In fine-grained soils, fluid conductivity is the combined result of flow through the porous media matrix and the fracture network. The contribution by fractures is particularly prevalent in near-surface soils characterizing the active zone. This concept is known as 'dual porosity' and can be used to express the relative contribution of each mechanism to total flow. While fracture flow is an

exponential function of aperture (i.e.,  $Q \propto b^n$ , where  $1 < n < 3$ ), porous media flow is a linear function of hydraulic conductivity (i.e.,  $Q \propto K$ ). This suggests that fractures are the major pathway for distribution of environmental changes in fine-grained soils.

Not only does soil permeability affect volume change, but volume change will in turn affect soil permeability. Once an environmental change enters the fracture, a gradient is established (e.g., mechanical, thermal, or chemical) and flow is induced in the adjacent porous matrix. As the fracture boundary soils adjust to the new stress state, increases or decreases in fracture aperture may occur from the resulting volume change. Shrinking will increase flow and accelerate the rate of change, while swelling will reduce both flow and change rates. In other words, there is an important balance between flow, which distributes environmental changes, and volume change, which controls the rate of exposure of soil to those changes.

Figure 2.4 also presents the idea of a 'secondary active zone,' which was introduced by Hall (1995). This is a non-naturally occurring active zone produced as a secondary effect of anthropogenic influence. Directly or indirectly, man's activities may create new fractures and/or subject the formation to increased exposure to environmental changes. Soils in the active zone may become more active, and volume change activity in previously inactive soils may now be initiated. Three general conditions that lead to the development of secondary active zones are conceptualized as follows:

Condition 1: Anthropogenic fractures in an expansive soil formation are subject to natural or induced environmental changes. The following are examples:

- Indoor heat creates fractures at the base of a building, which then contact the atmosphere by a shrinkage path that runs the length of the foundation.
- Air is extracted through pneumatically-induced fractures.

Condition 2: Natural fractures in an expansive soil formation are subject to induced environmental changes. An example is as follows:

- Soil vapor extraction is applied to a naturally fractured expansive soil in a geographic location with relatively minor atmospheric changes.

Condition 3: Natural or anthropogenic fractures in an engineered clay are subject to natural or induced environmental changes. The following are examples:

- Leachate enters compaction-induced fractures in a clay landfill liner.
- Fractures developed from burrowing animals in a remediation cap are subject to changing atmospheric conditions.

Active zones are thus a result of the interaction between volume change and soil fractures. A better understanding of this relationship will help to predict and control soil behavior in fine-grained geologic formations.

**2.2.3.2 Fracture Closure and Permanence.** The potential for fracture closure with time has major ramifications for active zones, since the exposure pathway for environmental changes is severely affected. Thus, a review of the theories surrounding fracture permanence and closure is appropriate for the study.

The closing of soil fractures, particularly as a result of the swelling of soil on rewetting, has been documented by Kays (1977), Fickies et al. (1979), Boyton and Daniel (1985), Dudal and Eswaran (1988), and Bouma and Loveday (1988). These same investigators found, however, that after apparent fracture closure, flow still exceeded that of the bulk matrix rather than returning to its pre-fracture state. The following theories have been used to explain this behavior:

(1) Fractures become permanent nucleation sites. Once fractures are formed they persist as planes of weakness or nucleation sites which act as locations of stress concentration within the soil matrix (Kuipers, 1984). Fractures will reopen when a critical tensile stress is applied under brittle conditions (Braunack et al., 1979). Under this view, fractures never permanently close.

(2) Weathering induces a structural change in fracture boundary soils.

Intensive weathering and the reorganization of clay minerals occurs along

fracture surfaces during cyclic wetting and drying. This is believed to inhibit the soil formation from ever returning to its initial state (van de Graaff, 1971). Weathering may also increase the resistance of particles to breakdown and displacement through preconsolidation of fracture boundary soils. This suggests that the longer the fractures remain open the more resistant they become to closure.

(3) Differential volume change occurs along the fracture. Differential volume change has been used to explain why fractures that appear to be closed do not behave in an unfractured state. For example, Dudal and Eswaran (1988) showed that slight, successive rain showers on a Vertisol may initiate fracture closure at ground surface, sealing the soil from additional moisture influx. Fractures, a short distance below the surface, however, remain open. Dasog and Shashidhara (1993) confirmed this by noting that apparent fracture closure at the surface does not greatly reduce infiltration.

(4) A reduced-density fracture filling occurs as a result of self-mulching. Self-mulching refers to higher elevation soil dropping into the base of a vertical, surficial soil fracture as boundary soils undergo volume change. This behavior is attributed particularly to gilgaied Vertisols. The reduced density or higher permeability of this fracture 'filling' was used by Bouma and Loveday (1988) to explain why water flowed in 'closed' fractures at rates higher than flow through the surrounding matrix.

It is clear that quantitative data are needed to back up the speculation regarding fracture permanence. The mathematical basis for studying changes in fracture geometry is now presented.

### 2.3 Mathematical Framework for the Current Study

This section presents the mathematical basis for the FVC Model (Chapter 4). First, the concepts and equations governing transient flow in the saturated and unsaturated domains are reviewed. This is followed by a discussion on additional stress state variables requiring consideration. The section concludes with an overview of evaporation theory.

#### 2.3.1 Consolidation Theory for Saturated Domain

In 1943, Terzaghi defined consolidation as the “decrease of the water content of a saturated soil without replacement of the water by air.” He recognized that this process is a function of the state of stress in the soil body which he described using the concept of effective stress. Terzaghi (1925) defined effective stress for the saturated soil system,  $\sigma_s'$ , as

$$\sigma_s' = \sigma - u_w \quad (\text{Eq. 2.1})$$

where  $\sigma$  is the total (normal) stress and  $u_w$  is the pore-water pressure. The mathematical theory he developed to describe the dissipation of pore-water pressure over time and space, and the associated deformation of the soil, is called

consolidation theory. The traditional application of the theory is expressed physically in the following example.

Consider a saturated clay layer undergoing consolidation as shown in Figure 2.5(a). The clay of thickness  $H$  is confined between two layers of sand. An instantaneous increase in total (normal) stress of  $\Delta\sigma$  is applied at ground surface. At time  $t = 0$ , the stress increase,  $\Delta\sigma$ , induces an equal increase in the pore-water pressure at all depths (i.e.,  $\Delta\sigma = \Delta u_w$ ). At some later time  $t$  ( $0 < t < \infty$ ), the water in the void spaces drains into the sand layers to dissipate the excess pore-water pressure.

By this process, the excess pore-water pressure at any depth in the clay layer will gradually decrease, and the stress carried by the soil solids (effective stress) will increase. However, the magnitudes of  $\Delta\sigma_s'$  and  $\Delta u_w$  at various depths will change since the flow is controlled by the permeability of the clay and the length of the drainage path. At time  $t = \infty$ , the entire excess pore-water pressure is dissipated (i.e.,  $\Delta u_w = 0$ ) and the total stress increase is carried by the soil structure. Figure 2.5(b) graphically illustrates the variations in total stress, pore-water pressure, and effective stress during these time periods. This gradual increase in effective stress and decrease in the moisture content results in a time-dependent decrease in thickness,  $H$ , of the clay layer; the clay layer is undergoing consolidation.



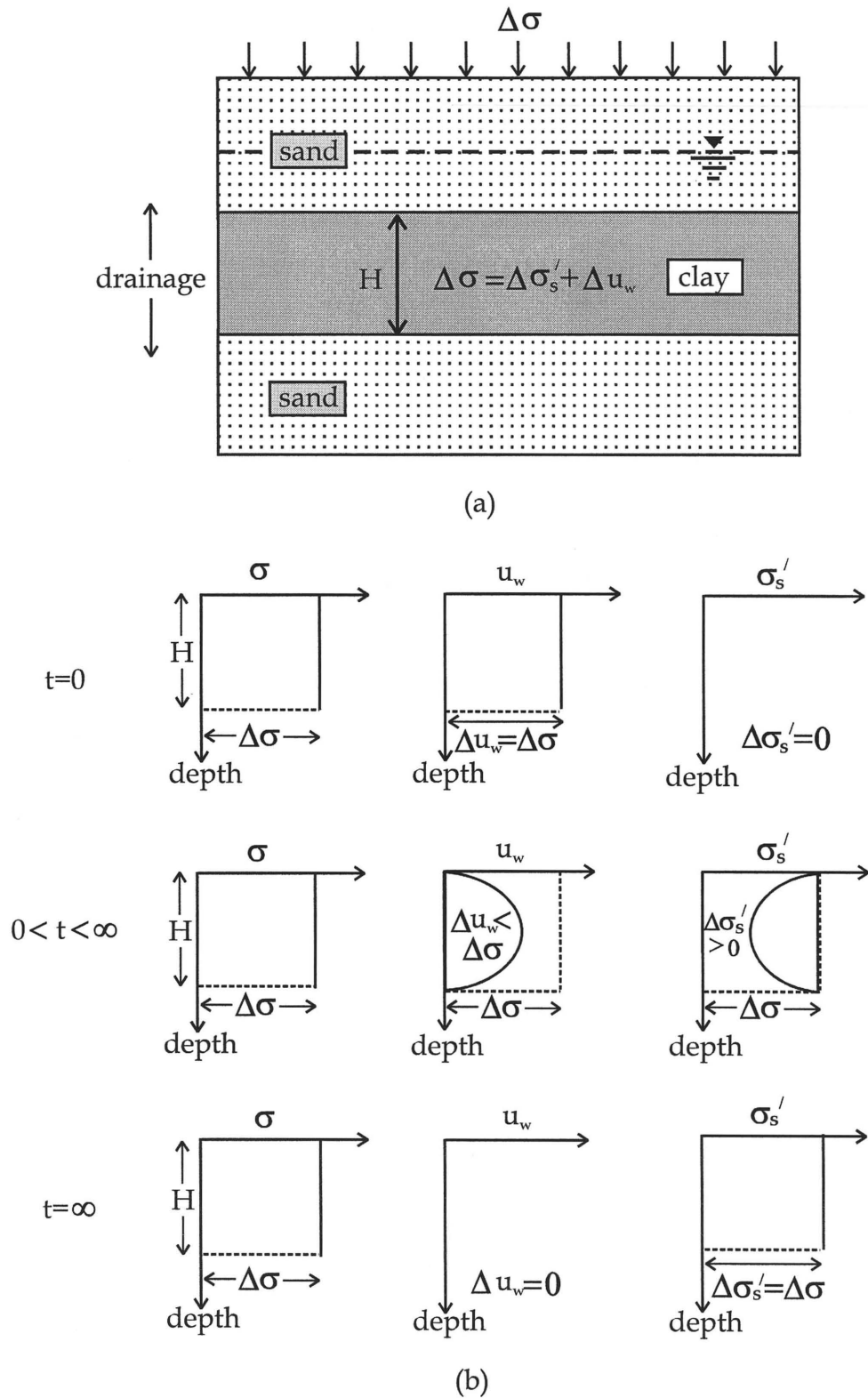


**Figure 2.5** Saturated Clay Layer Undergoing Consolidation  
 (a) Physical Illustration; (b) Variation of Total Stress, Pore-Water Pressure and Effective Stress (after Das, 1994)

Equivalently, if the load  $\Delta\sigma$  is removed, an excess negative pore-water pressure would be induced. As the pore-water pressure dissipates, there is an accompanying decrease in effective stress. The clay layer would subsequently increase in volume, or swell, a process typically referred to as 'reverse consolidation.' In the remainder of this document, the term consolidation will be used to refer to both 'forward' and 'reverse' consolidation processes unless otherwise specified.

Terzaghi (1943) coupled the equations that describe flow through porous media with the stress-strain constitutive equations to express this phenomenon mathematically. By limiting flow and strain to the vertical direction,  $z$ , he derived the one-dimensional consolidation equation:

$$\frac{\partial u_w}{\partial t} = c_v \frac{\partial^2 u_w}{\partial z^2} \quad (\text{Eq. 2.2})$$

This equation describes the dissipation of pore-water pressure,  $u_w$ , in time,  $t$ , and space,  $z$ , for saturated soils. It is noted that Eq. 2.2 is a form of the familiar heat-diffusion equation, which was the basis for Terzaghi's derivation. The coefficient in this equation,  $c_v$ , is called the coefficient of consolidation. It is a laboratory-determined soil material parameter expressed as,

$$c_v = \frac{K(1+e)}{\gamma_w a_v} \quad (\text{Eq. 2.3})$$

where  $K$  is the hydraulic conductivity of the soil,  $e$  is the void ratio,  $\gamma_w$  is the unit weight of water, and  $a_v$  is the coefficient of compressibility ( $\partial e / \partial u_w$ ). Terzaghi recognized the applicability of this theory to modeling volume change in expansive soils, but did not pursue the subject in any detail. Although the saturated domain has its place in certain volume change applications, unsaturated conditions may also be of interest.

### 2.3.2 Unsaturated Domain Theory

Fredlund and Morgenstern (1977) succeeded in extending the concept of effective stress to unsaturated soils without the use of an empirical component. Unsaturated soils are those where the soil has two fluid phases in the pores: pore water and pore air. Using pore-air pressure,  $u_a$ , as a reference pressure, the unsaturated effective stress variable,  $\sigma_u'$ , was defined as a composite function of two independent components,

$$\sigma_u' = f[(\sigma - u_a), (u_a - u_w)] \quad (\text{Eq. 2.4})$$

The stress state variable  $\sigma - u_a$  is termed the net normal stress and is used to represent changes in geostatic or mechanical loading. The other stress state variable is termed the matric suction and is denoted as,

$$\mu = u_a - u_w \quad (\text{Eq. 2.5})$$

Matric suction may be conceptualized as the pressure differential at the air-water interface that is balanced by surface tension forces.

Note that the expression for effective stress in the unsaturated domain is not single-valued like that of the saturated domain. The use of two independent stress state variables is required because the function is stress-path dependent. This behavior is illustrated in Figure 2.6, which depicts the constitutive relation between the stress state and deformation state variables.

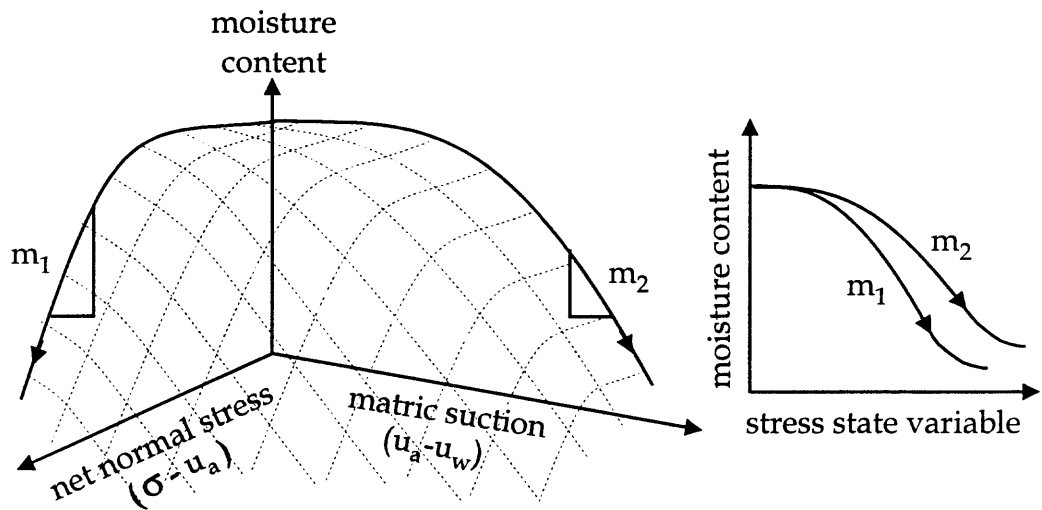


**Figure 2.6** Constitutive Surface for the Unsaturated Soil Domain  
(after Fredlund and Rahardjo, 1993)

The constitutive surface clearly shows hysteretic behavior with changes in unsaturated moisture content. This path dependency is apparent by the differences in slope between the net normal stress path ( $m_1$ ) and the matric suction stress path ( $m_2$ ).

With the unsaturated stress state variables defined, a theory to describe transient changes in effective stress was then extended to the unsaturated domain. Fredlund and Rahardjo (1993a) proposed a rigorous method involving the use of independently represented air and water phases. This method is limited in that the required model parameters are not industrially available.

An alternative approach, developed by soil physicists, uses model parameters that are more closely related to available field-measured parameters. This method assumes, however, that the net normal stress is constant. This method is based on a form of the Richards' (1931) equation that describes the matric potential in soil during transient flow (Rees and Thomas, 1993). The equation is as follows:

$$K(\theta)_z \frac{\partial^2 \mu}{\partial z^2} + \frac{\partial K(\theta)_z}{\partial z} = \frac{\partial \theta}{\partial \mu} \frac{\partial \mu}{\partial t} \quad (\text{Eq. 2.6})$$

where  $\mu$  is the matric suction, and  $\theta$  is the volumetric moisture content. The term  $\partial \theta / \partial \mu$  is the specific moisture capacity, or the water capacity function ( $C_w(\theta)$ ), determined from laboratory testing. The term diffusivity,  $D$ , is often used to express a combination of  $K(\theta)$  and  $\partial \theta / \partial \mu$  into one variable where  $D = K(\theta) / C_w(\theta)$ . Equation 2.6 is derived by relating the Buckingham-Darcy flux equation with the continuity equation.

Equation 2.6 is differentiated from the saturated consolidation equation by the fact that  $\mu$  is the environmental variable and  $K$  is a function of  $\theta$ . The

hydraulic conductivity,  $K$ , is significantly affected by the combined changes in void ratio and degree of saturation. As a soil becomes unsaturated, air replaces water in the pore space and  $K$  decreases rapidly as the space available for water flow reduces. Note, however, that the Richards' equation for the unsaturated domain (Eq. 2.6) reduces to Terzaghi's equation (Eq. 2.2) under saturated conditions.

### 2.3.3 Other Stress State Variables

Other state variables that apply to consolidation are osmotic suction and overburden potential. While not considered in traditional uses of consolidation theory, these variables may have significance for certain soil types.

A diffuse layer of ions, known as the diffuse double layer (Gouy, 1910; Chapman, 1913), emanates from the surface of clay minerals on account of negative surface charges from isomorphic substitution. An osmotic gradient is established because the ion concentrations at the clay mineral surface are high relative to that in the surrounding pore water. The pressure differential associated with this gradient is the osmotic suction. Changes in osmotic suction are thus associated with adjustments to the diffuse double layer, which is manifested as soil volume change.

In most field situations, the osmotic suction is constant and is thus considered a minor factor of volume change. It may be significant only for isolated environmental applications that experience large anthropogenically-

induced temperature and pore fluid changes that include cation type and concentration and relative permittivity (i.e., dielectric constant) of the pore fluid.

The combination of matric and osmotic suctions is referred to as total suction (or soil suction),  $\psi$ , which is often considered to be the total free energy of the soil water:

$$\psi = f(\mu, \pi) \quad (\text{Eq. 2.7})$$

Although sometimes written as a sum, the  $\mu$  and  $\pi$  components are not necessarily additive (Nelson and Miller, 1992). Total suction replaces the matric suction term where the effects of both  $\mu$  and  $\pi$  are important. Osmotic suction would be significant relative to matric suction in very dry soils where there is incomplete cation hydration or the bound water is supersaturated.

The overburden potential ( $\Omega$ ), or the envelope pressure, is a parameter considered by soil physicists as a descriptor of stress state, particularly for swelling soils (Iwata et al., 1988; Jury et al., 1991). The overburden potential is given by,

$$\Omega = \left( P_0 + \int_0^z \gamma dz \right) \frac{de}{dv} \quad (\text{Eq. 2.8})$$

where  $z$  is the depth to the point of interest,  $P_0$  is the external load at ground surface (i.e.,  $z = 0$ ), and  $e$  is the void ratio (Philip, 1969). The terms  $v$  and  $\gamma$  are the moisture ratio and the apparent wet specific gravity defined, respectively, as,

$$v = \theta (1 + e) \quad (\text{Eq. 2.9})$$

$$\gamma = \frac{v + G_s}{1 + e} \quad (\text{Eq. 2.10})$$

where  $G_s$  is the specific gravity of the soil particles (Philip, 1969). The overburden potential is the pressure imposed on the soil water by the weight of the overburden. This is significant for swelling soils where interparticle contacts are inhibited by double layer water (i.e., water associated with the diffuse layer of ions emanating from the permanent charge clay mineral surface).

#### 2.3.4 Evaporation Theory

The rate of moisture evaporation from a soil surface is dependent on a driving force and a resistance. Three distinct stages of evaporation are evident depending on the force that predominates. In the first stage, the water loss is a function of external meteorological factors such as wind speed, relative humidity, and flux of radiant energy to the surface (Penman, 1948). In other words, the soil is able to provide water at a rate that approaches the evaporative demand, and as such, there is a constant rate of evaporation. This corresponds to the drying of a relatively wet soil.

As the soil dries further, the matric suction increases and the soil resists the removal of additional water. With a concurrent reduction in hydraulic conductivity, the water transmission properties of the soil begin to control the rate of evaporation. At this point, the soil transitions to the second stage of



evaporation, where the evaporation rate is less than the evaporative demand. The rate decreases to 30% to 40% of the initial rate and eventually becomes independent of the evaporative potential (Ghildyal and Tripathi, 1987).

The point of transition between the first two stages is termed the critical time,  $t_c$ . The critical time has been shown to vary from two to fourteen days for agricultural soils at ground surface during summer and winter drying, respectively (Shouse et al., 1982; Idso et al., 1974).

The soil enters the third stage of evaporation when the water content of the soil surface reduces to the air dry value (Kimbal and Jackson, 1971). Water movement at such a low water content is influenced by hydration forces which take place in the first two molecular layers around the soil particles (Ghildyal and Tripathi, 1987). Evaporation occurs, then, when the kinetic energy of the molecules in this layer exceed the adsorptive forces. Thus, unless the soil is exposed to a large quantity of evaporative energy, little to no evaporation will occur in expansive clay soils because of their high suctions. A method for computing the evaporative demand on a soil surface is now presented.

For first stage evaporation, the soil mimics the characteristics of free water since there is no resistance to water flow. In 1802, Dalton expressed the fundamental law of evaporation from a free water surface (Ghildyal and Tripathi, 1987), as,

$$E = (e_o - e_d) \cdot f(U) \quad (\text{Eq. 2.11})$$

where  $e_o$  is the mean vapor pressure at the water surface,  $e_d$  is the mean vapor pressure in the air at some observational height above the water surface, and  $f(U)$  is a function dependent on the horizontal wind velocity. The function  $f(U)$  has been expanded with the use of empirical relations by Penman (1956). The new equation, which represents the aerodynamic evaporation,  $E_a$ , is,

$$E_a = 0.35 \cdot (e_2^0 - e_2) \cdot \left[ 0.5 + \frac{U_2}{100} \right] \quad (\text{Eq. 2.12})$$

where  $e_2^0$  is the saturation vapor pressure at the mean air temperature in mm Hg;  $e_2$  is the saturation vapor pressure at the dewpoint in mm Hg; and  $U_2$  is the mean wind speed (horizontal) at 2 m height above the ground in miles/day. The equation yields of  $E_a$  in mm/day.

The saturation vapor pressure at the dewpoint,  $e_2$ , is further defined as,

$$e_2 = \frac{\bar{h}_r}{100} \cdot e_o^0 \quad (\text{Eq. 2.13})$$

where  $\bar{h}_r$  is the average relative humidity and  $e_o^0$  is the saturated vapor pressure at the water surface at temperature  $T_o$  in mm Hg (Penman, 1956).

Evaporation theory will be used in Section 4.0 to support the theoretical modeling for the current study. The next section presents a summary of the industrial applications that are of interest for the current study.

## 2.4 Industrial Applications

The behavior of fractures in fine-grained soil formations is of significant interest in several scientific and engineering fields. This section summarizes the various industrial applications associated with fractures and volume change. Hall (1998) provides an extended discussion of these applications.

The disciplines most affected include the environmental, civil/geotechnical engineering, agricultural, and the field of resource geology. Figure 2.7 summarizes various areas within each discipline where the presence of fractures may be either advantageous to disadvantageous, depending on the particular application. In all cases, it is either the fluid flow or shear strength properties of the bulk soil that are affected by the fractures. A generalized summary of each of the major disciplines follows:

Environmental: Fractures significantly impact flow and contaminant transport rates through fine-grained soil formations that are naturally low in primary permeability. Thus, changes in secondary permeability, due to the effect of soil volume change on fracture apertures, have major implications for a variety of environmental applications. For example, fluid flow and contaminant transport modeling of advective and diffusive soil processes rely on the hydraulic properties of a formation, which are a function of the interrelationship between fractures and volume change. In practice, however, hydraulic properties are usually determined from physical data such as grain size (Vukovic and Soro,

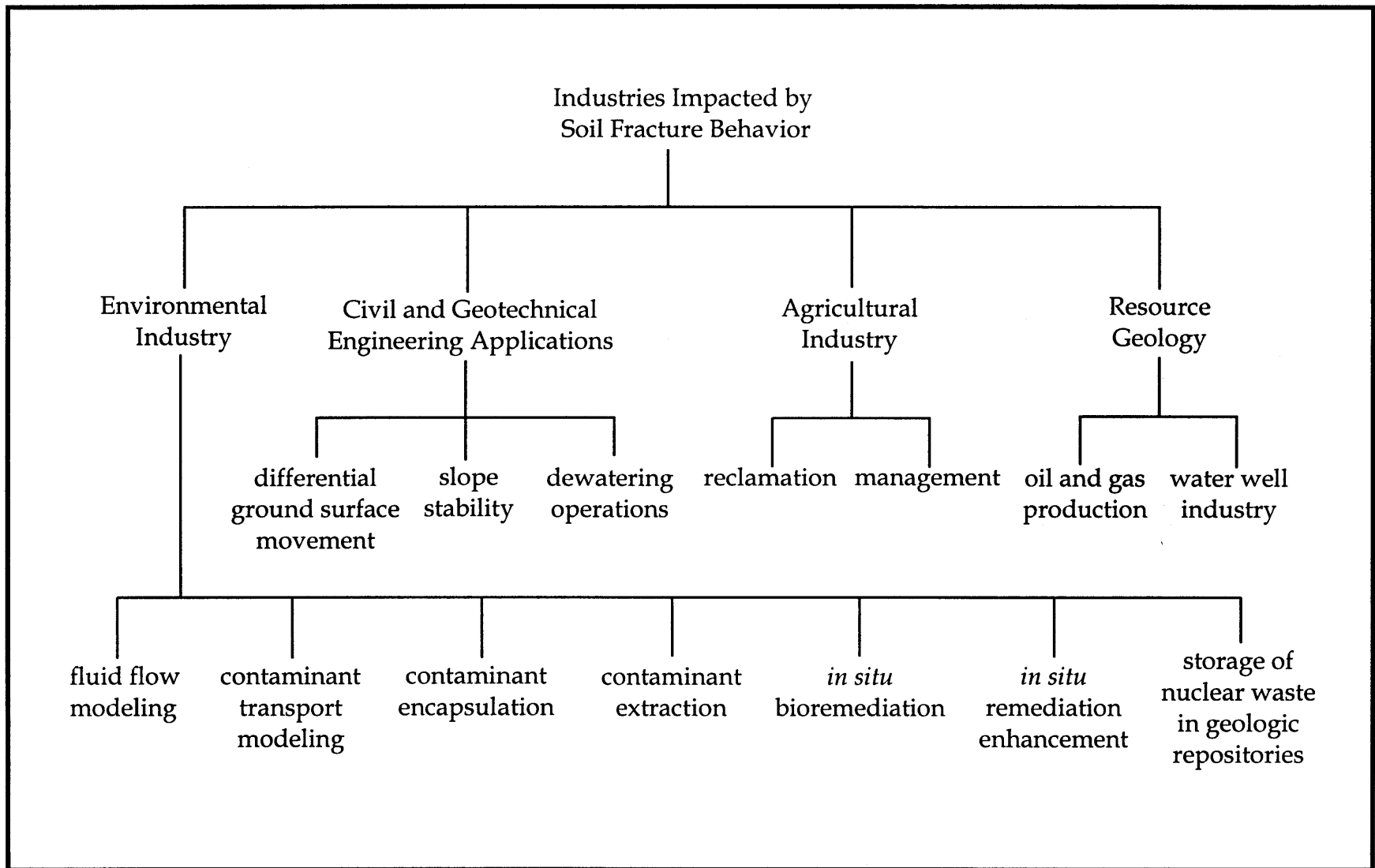


### Figure 2.7 Industrial Significance of Soil-Fracture Interactions

1992) that neglect fractures effects altogether, or from *in situ* flow tests (Dawson and Istok, 1991; Johnson et al., 1990) that give only an instantaneous view of fracture effects.

The remediation industry, which often relies on the results of model analysis, is also affected. In fine-grained soils, the effectiveness of primary remediation technologies, such as soil vapor extraction, groundwater pump and treat and *in situ* bioremediation, largely depends on the extent to which the geologic formation is fractured. The greater the degree of fracturing, the more rapid the remediation. In contrast, the presence of fractures often compromises the integrity of containment when clay is used as an encapsulating material. This is true for near-surface containment of environmental contaminants as well as for long-term storage of nuclear waste in deep geologic repositories.

A third important environmental application is the use of *in situ* enhancement technologies that can be coupled with the primary remedial process. An example is pneumatic fracturing, a technology with which the investigator is associated. The process involves the creation of artificial fractures by the injection of pressurized gases that act as preferential flow pathways and enhance the rate and extent of contaminant removal. The field case study selected to validate the new theoretical model will be a pneumatic fracturing project (Section 4.3.3). Other enhancement technologies affected by fractures include hydraulic fracturing and air sparging.

Civil and geotechnical engineering: Differential ground surface movement due to the shrink-swell processes of clay soils is a source of major damage to structures, pavements, and utilities. Fractures play an important role in this process since they distribute moisture, which induces soil volume change. The fractures may also absorb some portion of the volume change.

Fractures may also act as stress concentrators which lead to shear band formation and subsequent slope failures (Vallejo, 1993; Saada et al., 1994). The influence of fracture dilation and closure on shear strength, while not considered in the current study, warrants additional research.

Finally, it is often necessary to remove groundwater from clay soils during excavation or construction to improve soil strength. The efficiency of such dewatering is largely controlled by soil fractures.

Agricultural: Clay soils are important agricultural resources, due in part to their ability to retain moisture and nutrients. Fractures play a major role in soil aeration, drainage, and nutrient distribution. Understanding the interactions between volume change and fractures will aid in maximizing the productivity and sustainability of arable land through proper management strategies. It will also provide insight into the complex structural properties of shrink-swell clays, which will encourage the reclamation of fertile soils that remain uncultivated.

Resource geology: Certain industries rely on fractures in clay-rich formations for the removal of natural resources, such as oil and gas for the petroleum industry

and water for the water well industry. Leakoff of liquids from either hydraulic fracturing or groundwater extraction causes swelling of clay minerals that results in the reduction of primary and secondary permeability. This is referred to as 'formation damage,' and it has severe economic implications since extraction rates may be temporarily or even permanently affected.

In the majority of related industrial applications, moisture content changes appear to be the most significant environmental condition influencing volume change. The exception is nuclear waste storage where moisture is second to temperature effects. This investigator has therefore chosen to focus on the effects of moisture fluctuation. A review of past approaches used to model the interaction between volume change and fracture geometry is now presented.

## **2.5 Previous Modeling Approaches**

The functional relationship between volume change and fractures has long been recognized to affect soil behavior. The traditional focus has been on predicting changes in fluid conductivity as an indicator of fracture dilation and closure. Only recently have quantitative models begun to appear in the literature that directly evaluate changes in fracture geometry. The agricultural field has taken the lead by developing several water balance models with fracture geometry components. This section reviews the general approach to volume change modeling and how it has been applied to simulate changes in fracture volume.

### 2.5.1 General Volume Change Modeling Approach

Soil scientists have adopted an approach to modeling soil volume change which differs from that of the civil and geotechnical engineering disciplines (Section 2.3). Volume change is predicted directly from soil moisture content changes through use of a shrinkage curve and geometric considerations.

A 'shrinkage curve' relates volume change and moisture content for unconfined soil clods dried from an initially wet state. Figure 2.8 shows the four shrinkage zones on a typical shrinkage curve: structural, normal, residual, and zero.

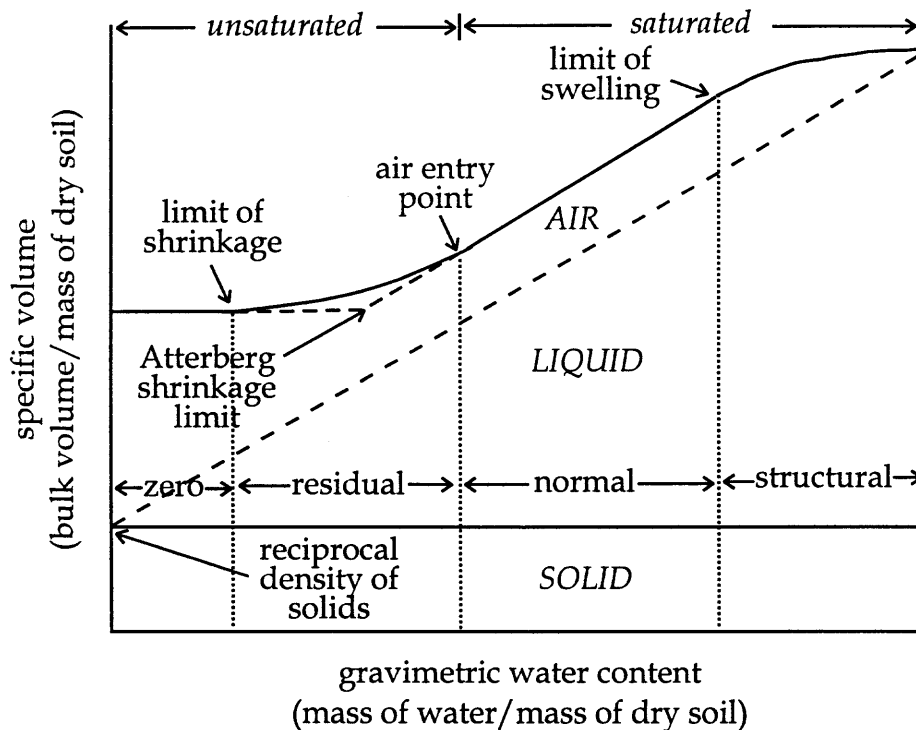


**Figure 2.8** Typical Shrinkage Curve Showing Four Shrinkage Zones (Modified from Giraldez et al., 1983; Tariq and Durnford, 1993; Ghildyal and Tripathi, 1987)



Structural shrinkage occurs at the wettest part of the moisture range where volume change is less than the volume of water removed. In the normal range, the volumetric change equals the volume of water loss. The soil becomes unsaturated in the residual zone and the water loss exceeds the soil volume change. In the zero shrinkage range, the soil has reached its densest configuration with no further decrease in volume with moisture loss. Extended normal shrinkage zones may be present in expansive soils (Bronswijk, 1988; Tariq and Durnford, 1993). Also, note that the Atterberg shrinkage limit ( $SL$ ) is defined as the intersection of the slopes of normal and zero shrinkage.

Various investigators have attempted to model the relationships implicit in the shrinkage curve. Theoretical functions have been fit to experimental data to generate empirically based equations for each shrinkage zone (Giraldez et al., 1983; McGarry and Malafant, 1987; and Tariq and Durnford, 1993). With these equations, volume changes are mathematically attributed to moisture changes.

For field applications, it is necessary to know the relative intensity of volume change in the vertical and horizontal directions. Aitchison and Holmes (1953) and Fox (1964) independently developed a model, called the AHF model, which distinguishes between one- and three-dimensional swelling of soil at ground surface. A schematic representation of the AHF model is shown in Figure 2.9. In this model, the initial soil volume is depicted as a cube devoid of fractures (Fig. 2.9a). When no air is present in the system and the soil is laterally confined, the only way for the soil to expand is to heave one-dimensionally (Fig.

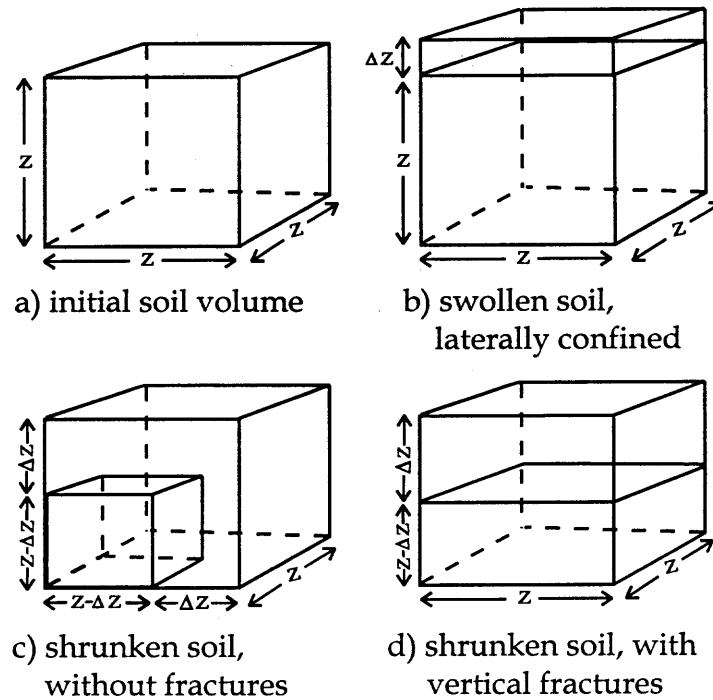


**Figure 2.9** Schematic Representation of the AHF Model  
(Modified from Giraldez et al., 1983)

2.9b). However, as the soil shrinks, air begins to enter the soil and volume change is considered three-dimensional (Fig. 2.9c). Thus, in the unsaturated state, soil can swell or shrink in all directions. If soil fractures develop, they are expected to predominate in the vertical direction. The volume is therefore spaced laterally and shrinkage occurs in the vertical direction (Fig. 2.9d). The AHF model assumes uniform volume change in each direction in the soil body. Voltz and Cabidoche (1995) extended this model to non-uniform volume change.

The next section presents specific models that use the shrinkage curve and the principles of the AHF model to predict changes in fracture geometry from soil volume change.

### 2.5.2 Specific Models Incorporating Changes in Fracture Geometry

Bronswijk (1986) was the first to account for the impact of fracture geometry on soil behavior by simulating changes in fracture volume from moisture fluctuations. Slightly modifying the AHF model, Bronswijk considered the initial soil element to contain regularly spaced, vertical fractures. The soil is broken up into compartments with cubic geometries of length  $z$ . Water is assumed to infiltrate into the soil matrix at ground surface, and as runoff and rainfall into the vertical fractures that run directly to drains or the water table. One-dimensional moisture flow is predicted with the unsaturated flow equation (Eq. 2.6), and is converted to volume change using the shrinkage curve and a geometric characteristic,  $r_s$ , where  $r_s = 3$  for three-dimensional isotropic shrinkage and  $r_s = 1$  for one-dimensional subsidence. The change in  $z$  is given as,

$$\Delta z = z - z \left( \frac{V_i - \Delta V_i}{V_i} \right)^{\frac{1}{r_s}} \quad (\text{Eq. 2.14})$$

where  $V_i$  is the total volume of the soil mass and  $\Delta V_i$  is the change in that volume due to shrinking and swelling. These values are then converted into a change in fracture volume ( $\Delta V_f$ ) by,

$$\Delta V_f = \Delta V_i - z^2 \Delta z \quad (\text{Eq. 2.15})$$

The total fracture volume is then calculated by adding up the changes in the fracture volumes of the individual compartments. Under the assumption that all

vertical soil movements lead to changes in soil layer thickness, horizontal fractures must be either absent or stable.

Bronswijk (1988) integrated this approach into an existing flow model called FLOWEX (Wind and Van Doorne, 1975; Buitenkijk, 1984), and termed the improved model FLOCR, from FLOW in CRacking Soils. Bronswijk (1988, 1989) simulated changes in fracture volume with FLOCR in a mixed illite-montmorillonite Dutch field soil using thirty-year daily precipitation and potential evapotranspiration data. Actual changes in fracture volume were calculated as the difference between three-dimensional volume change and change in layer thickness. Disks were positioned at various levels in the field soil to measure vertical movements. Figure 2.10 shows results of the model simulation as compared to the 'actual' values.

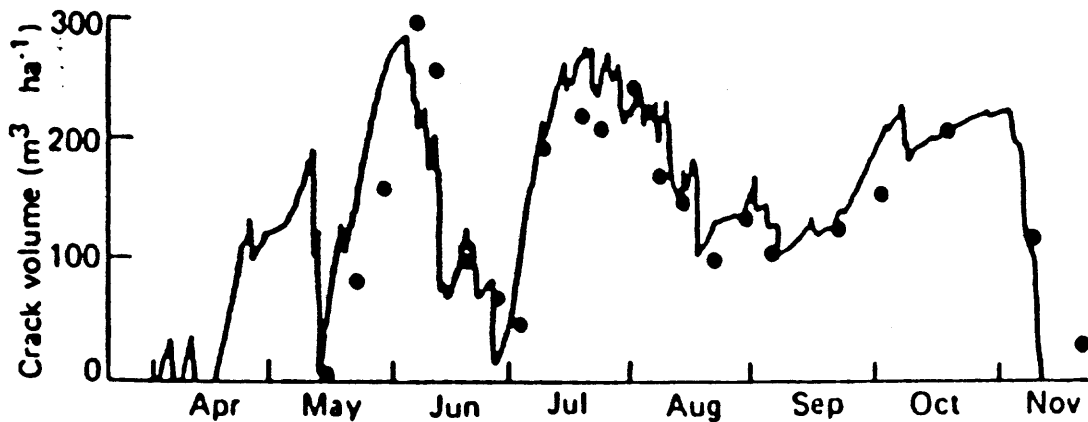


Figure 2.10 Changes in Fracture Volume for an Illite-Montmorillonite Clay Soil: • Measured, — Simulated (Bronswijk, 1988)

The fracture volume in the upper two feet of ground surface fluctuated from almost complete closure to 300 m<sup>3</sup>/ha during the 8-month test period. The model seemed to accurately simulate changes in fracture volume. Bronswijk (1991) used this method to determine soil moisture content changes by measuring vertical soil movements.

Oostindie and Bronswijk (1992) then integrated FLOCR with Groenendijk's and Kroes' (1997) solute transport model ANIMO. Bromide tracer and nitrogen transport were simulated with FLOCR/ANIMO in a cracked clay soil with moderate results (Hendriks et al., 1999).

Jarvis and Leeds-Harrison (1987) developed a water-balance model called CRACK that accounts for changes in water storage in the cracks and uptake rates into aggregate macropores. This expands on Bronswijk's model assumption that rain entering the cracks at the soil surface is immediately routed to the water table. Continuous exchange of water between the two domains (i.e., fracture and aggregate macropores) was added in a second version of CRACK (Jarvis, 1989). The model calculates crack width from crack porosity, given as a function of the bulk soil water status, the slope of the shrinkage curve, and aggregate size. Jarvis and Leeds-Harrison (1990) successfully applied CRACK to simulate water content changes in a heavy clay soil in southern England.

### **2.5.3 Relevance to the Current Study**

The objective of the previous model studies was similar to that of the current

study, i.e., to predict changes in fracture geometry from moisture flow and associated soil volume changes. However, there are several distinct differences that set the current study apart from past approaches. These distinctions are briefly summarized below, and they are further explained in Chapter 4, which describes the model approach.

Depth and dominant fracture orientation: The previous models were developed for near-surface agricultural soils where vertical fractures predominate. The current study extends the analysis of fracture geometry to deeper soils, where horizontal fractures predominate.

Fracture orientation is typically a function of the state of stress in the soil body. Fractures tend to propagate in the direction normal to the least principal stress in the formation (Hubbert and Willis, 1957). Since most soils are overconsolidated due to past geologic events (e.g., overburden stress relief, desiccation, tectonic forces), the least principal stress is in the vertical direction, and fractures propagate horizontally.

In near-surface soils (e.g., 0 to 1 m below grade), vertical fractures predominate. The vertical orientation is attributable to: (1) disturbances in near-surface soil, which cause the soil to behave in a normally consolidated manner; and (2) strain effects, which are caused because the shallow active zone is very thin in comparison to its areal extent. It is noted that even in near-surface soils, horizontal fracture frequency increases with depth (Bui and Mermut, 1988).

Site of exposure to environmental changes: In the agricultural models, the soil is exposed to environmental changes through fluctuations in atmospheric conditions at ground surface. Since flow is modeled in one-dimension vertically, the impact of volume change in fracture boundary soils from changing conditions in the fracture is neglected. The current study recognizes that the fracture is the principal conduit for the environmental fluctuations which affect fracture boundary soils.

Soil structure: Agricultural use of expansive clay soils often requires either deep ripping (i.e., disturbing the soil below the normal cultivation layer without inverting) or moling (i.e., creation of fine, subsurface, unlined soil drains). These techniques increase drainage which is needed to avoid the waterlogging of surface soils. These forms of tillage, along with other near-surface processes such as frost action, create coarsely structured soil. In addition, biotic activity in near-surface soil results in secondary permeability features such as root and worm holes. The presence of macropores created by these processes dictate modeling in the unsaturated domain. The clay peds thus contribute little to the overall flow.

The deeper expansive soils modeled in the current study are typically not subjected to these disturbances. The soils are denser and have much lower hydraulic conductivity. In this case, flow occurs predominantly through the clay peds. Because the peds in expansive soil exhibit an extended normal shrinkage

range, the soil is most appropriately modeled in the saturated domain.

Bulk network versus discrete modeling approach. The agricultural modeling approach focuses on large network flow systems, where columns of soil are separated by open vertical fractures. The fractures function primarily as sources of bypass flow to installed drainage systems and to the phreatic water surface. Fracture volumes are calculated in bulk over an area of agricultural interest (i.e., at the megascopic scale).

The current study uses a discrete fracture approach, where volume changes of individual fractures can be determined. A field-scale system is simulated by the stacking of multiple discrete fracture units. Thus, the new model approach allows for predictions on both the macroscopic and megascopic scales.



## **CHAPTER 3**

### **EXPERIMENTAL STUDIES**

#### **3.1 Procedures**

This section reviews the procedures for the laboratory studies that were performed in conjunction with the modeling effort. These included soil collection, testing and preparation; horizontal infiltrometer testing; and material parameter testing.

##### **3.1.1 Soil Collection, Testing, and Preparation**

A natural clay soil with a moderate to high propensity for volume change was chosen for use in the experimental portion of the study. The soil was obtained from a construction debris landfill in Lorton, VA (Rainwater Landfill), located in the southeastern portion of Fairfax County on the northwestern edge of the Mason Neck (Figure 3.1). The formation appears to be an isolated montmorillonite deposit, uncharacteristic of the soils along the eastern seaboard. The general location was identified by literature documenting residential housing damage resulting from differential ground surface heave (ENR, 1992). The location was sited using local geologic maps (Seiders and Mixon, 1981; Froelich, 1985) and Fairfax County soil survey and urban development maps (Fairfax County Soil Science Office, 1993).

The unvegetated hill from which the soil was collected had eroded into large gullies (Appendix A, Photo A-1). Large shrinkage cracks up to 2 in. (5 cm)

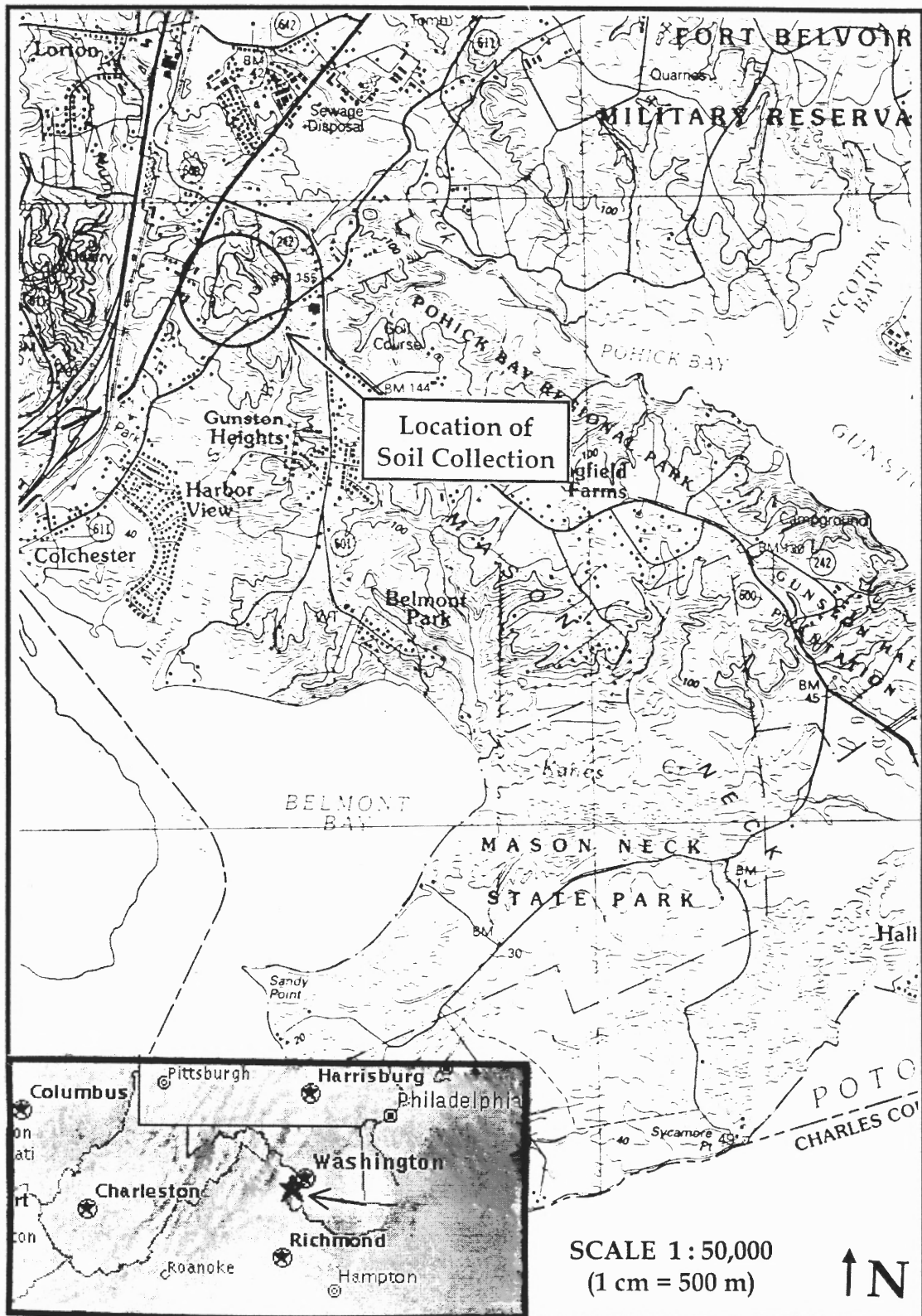


Figure 3.1 Location of Soil Collection.

in width were apparent at the surface and extended to approximately 10 in. (25 cm) below ground surface (Photo A-2). A highly plastic deposit of unweathered clay, approximately 5 ft (1.5 m) below ground surface, was chosen for collection. The deposit was so stiff that it could not be excavated with hand tools, except where weathered near ground surface. Thus, a bulldozer was used to excavate the clay, which maintained itself as large blocks (Photos A-3 and A-4). The clay ranged in color from blue to red, with the majority of the soil being a mixture of the two. Approximately 1000 lbs. (450 kg) of soil was sealed in airtight bags and transported to NJIT.

A series of laboratory tests was performed on the soil to determine its physical, chemical, and mineralogical characteristics. Physical property testing was performed at NJIT and included Atterberg limits, grain size, specific gravity, classification by Unified Soil Classification System (USCS), and organic matter content. Natural moisture content samples were also obtained from the center of the soil blocks immediately upon arrival at NJIT.

Servi-Tech Laboratories in Dodge City, KS, performed a soil salinity appraisal. Testing included saturation water content, exchangeable cations (Ca, Mg, K, Na), cation exchange capacity (CEC) by summation, extractable (water-soluble) ions (Ca, Mg, Na, K, B,  $\text{HCO}_3^-$ ,  $\text{Cl}^-$ ,  $\text{SO}_4^-$ ), pH, and electrical conductivity (extractable and soluble salts). In addition, data useful for inferring mineralogical composition were requested using methods of Tan (1996). These included total CEC ( $\text{CEC}_t$ ), representing both variable and permanent charges of

clay minerals, permanent charge CEC ( $CEC_p$ ), and exchangeable  $H^+$  and Al. Table 3.1 summarizes the types of physical and chemical testing that were performed. Results, discussion and expansivity characterization based on these tests are presented in Section 3.2.1.

To prepare the soil for the experimental work, both manual labor and size reduction equipment were required to reduce the large, hard clay blocks to clod-size format. The soil blocks were first broken up manually with a sledgehammer and chisel into fist-size pieces. The soil was then placed into a rotary shredder, Model FB12 Flake Breaker, manufactured by Jacobson, Inc. (Minneapolis, MN). The shredded soil fell by gravity through a 0.4 in. (1 cm) diameter screen. The soil was then sprayed with distilled water to a uniform moisture content of 31 to 32 wt%, homogenized, and placed in airtight plastic bags. An environmental chamber (Environmental Growth Chambers, Inc., Chagrin Falls, OH) was used to store the soil at a temperature and humidity characteristic of subsurface conditions, approximately 54-57°F (12-14°C) and 75-85% relative humidity (RH). The soil was allowed to equilibrate for at least three weeks prior to HI testing.

Atterberg limits were compared before and after shredder reduction. This was done to ensure that the mechanical action of the equipment would not cause excessive breakage of the clay minerals, thus affecting the shrink-swell properties. In addition, since some of the soil was broken down by hand (i.e., before the shredder was available), Atterberg limits on soils reduced by hand were compared to those reduced by the shredder.

**Table 3.1** Laboratory Testing for Soil Characterization

Property	Number	Description	Reference
<b>Physical Tests (NJIT)</b>			
Atterberg Liquid and Plastic Limits	D 2217-85 D 4318-98	Wet preparation method Standard LL, PL methods	ASTM (2000f,k)
Atterberg Shrinkage Limit	D 4943-95	Wax method	ASTM (2000m)
Grain size analysis	D 2217-85 D 1140-97 D 422-63	Wet preparation (coarse) Wet sieve procedure (fine) Mechanical and hydrometer method	ASTM (2000f,d,a)
Specific gravity	D 854-98	Pycnometer method	ASTM (2000c)
USCS classification	D 2487-98	Standard method	ASTM (2000i)
Organic matter	D 2974-87	Combustion (440°C)	ASTM (2000j)
Moisture content	D 2216-98	Drying (105°C)	ASTM (2000e)
<b>Physical and Chemical Tests (Servi-Tech Laboratories)</b>			
Saturation paste/percentage	S-1.00	Water mixed with soil to saturation	Gavlak et al. (1994)
Saturation paste soil pH	S-1.10	pH meter on saturation extract	Gavlak et al. (1994)
1:1 soil pH	--	pH meter on soil-water (1:1) slurry	Eckert (1988)
Electrical conductivity	S-1.20	Conductance meter on extract (exchangable and soluble salts)	Gavlak et al. (1994)
Soluble bicarbonate	S-1.30	Titration with HCl	Gavlak et al. (1994)
Soluble chloride	S-1.40	Flow injection analysis on saturation paste extract	Gavlak et al. (1994)
Soluble boron	S-1.50	ICP analysis on saturation paste extract	Gavlak et al. (1994)
Soluble Ca, Mg, Na	S-1.60		
Soluble sulfate	S-1.70		
Exchangeable Ca, Mg, K, Na	--	ICP analysis on ammonium acetate extract at pH 7.0	Brown and Warncke (1988)
Cation exchange capacity (CEC)	--	Summation method	Brown and Warncke (1988)
Total CEC (CEC <sub>t</sub> )	--	BaCl <sub>2</sub> -TEA at pH 8.2, CaCl <sub>2</sub> replacement, AAS analysis	Tan (1996)
Permanent charge CEC (CEC <sub>p</sub> )	--	BaCl <sub>2</sub> at acid pH, CaCl <sub>2</sub> replacement, AAS analysis	Tan (1996)
Exchangeable H <sup>+</sup> and Al	--	KCl-titration method	Tan (1996)

-- not applicable; USCS = Unified Soil Classification System; ICP = inductively coupled plasma; TEA = triethanolamine; AAS = atomic adsorption spectrometry

### 3.1.2 Horizontal Infiltrrometer Testing

A horizontal infiltrrometer (HI) test system, modified from Hall (1995), was used to conduct bench scale laboratory experiments for the current study. The overall purpose of the tests was to examine changes in fracture aperture in fine-grained soil due to fluctuations in moisture content. Specifically, the HI tests were designed to: (1) gather additional insight into the physical behavior of fractures and fracture boundary soils; and (2) obtain data for calibration and validation of the 'Fracture Volume Change Model.'

**3.1.2.1 Overview.** The horizontal infiltrrometer system was designed to mimic flow through a discrete fracture in a natural clay soil. Figure 3.2 shows the concept of the test system.

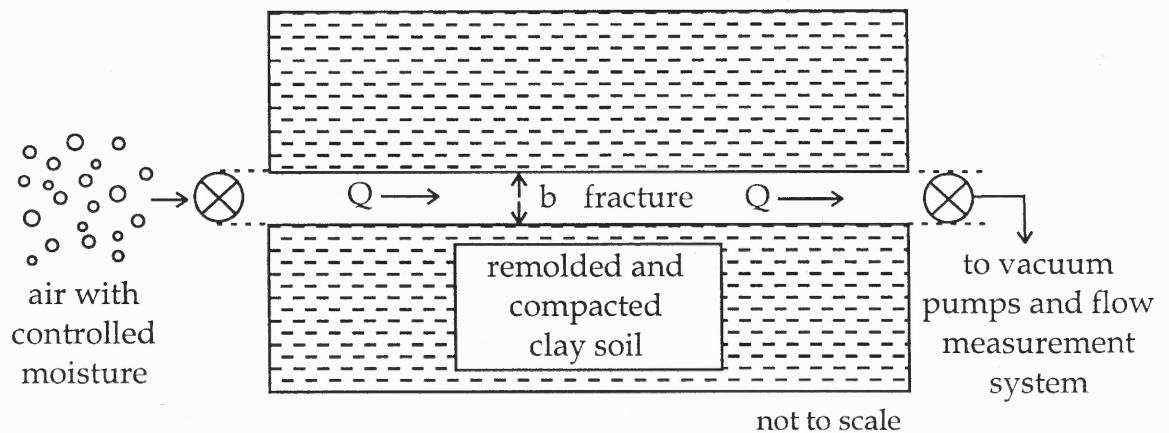


**Figure 3.2** Conceptual Schematic of the Horizontal Infiltrrometer (HI) Test System

The general function of the horizontal infiltrometer may be described as follows. First, a horizontal fracture is created in a block of clay soil that has a known density and moisture content. Next, air is pulled through the fracture to induce environmental changes in the fracture boundary soils. The moisture content of the influent air is varied to cause either hydration or dehydration. This causes the soils to swell or shrink and the aperture of the fracture to either dilate or contract, depending on the moisture content trend.

Three main variables are controlled during operation of the HI test. They are as follows:

Fluid Flow. Fluid flow in the artificial fracture is monitored continuously throughout each test. Changes in fluid flow are directly related to fracture dilation or closure, as described by the Cubic Law (Appendix F).

Moisture Content. Each HI experiment begins with the soil block at a known constant moisture content. At the completion of the test, the final moisture content profile of the soil block is determined to quantify soil moisture change.

Time: The HI tests were run for various time durations to examine the impact of environmental rate change on the fracture boundary soils.

The horizontal infiltrometer tests were run within a range of stress states. The moisture contents of interest were those between the shrinkage limit and the

liquid limit, with the majority performed at a moisture near the plastic limit. The design of the device precluded testing of soils outside this range on account of either soil collapse or energy restrictions (Hall, 1995). The effects of monotonic wetting and drying, as well as cyclic moisture events, were examined.

**3.1.2.2 Apparatus Setup.** The horizontal infiltrometer apparatus consists of an open rectangular metal box, measuring 16 in. (41 cm) I.D. in length, 7.25 in. (18 cm) I.D. in width, and 5 in. (13 cm) in height, into which the remolded test soil was compacted at a known moisture content. Compaction was accomplished with the standard Proctor rammer (ASTM 2000b) to attain uniform, consistent packing between tests. The fracture was created by placing a thin metal strip spacer, measuring 2.5 in. (6.4 cm) in width and 0.029 in. (0.074 cm) in thickness, in the center of the soil block and compacting the soil around it. Copper pipe sections, sharpened on one end, were driven into the soil around each end of the metal strip for connection to a flow manifold. The discrete, artificial fracture was created by pulling the metal strip out of one end of the soil block. Spacers placed inside the metal box allowed for easy removal of lateral confinement at the termination of each test. A series of photographs detailing the setup and compaction of the HI tests are shown in Photos A-5 through A-9.

The initial moisture content of the soil was maintained at 31 to 32 wt% for the HI tests. Therefore, compaction occurred wet of the optimum since Byle and Davit (1992) report that the optimum moisture for Potomac Formation clay



ranges from 20 to 27 wt%. Dry densities for the HI tests varied from 91 to 92 lb/ft<sup>3</sup> (1.46 to 1.47 g/cm<sup>3</sup>), which is in the range of maximum dry densities of 88 to 96 lb/ft<sup>3</sup> (1.41 to 1.54 g/cm<sup>3</sup>) reported by Byle and Davit (1992).

Once packed, the apparatus was sealed in plastic and allowed to sit overnight in the environmental chamber. This allowed dissipation of excess pressures (resulting from compaction), and equilibration to ground-surface temperature. A series of fittings was attached to the copper pipe sections at each end of the soil block including valves for vacuum tightness checks, quick disconnect fittings to allow for the addition of moisture, and fittings to attach Magnehelic® vacuum pressure gauges. A schematic of the HI soil block unit is shown in Figure 3.3.

The horizontal infiltrometer apparatus was connected by a vacuum hose to a flow measurement system and two vacuum pumps arranged in series (Figure 3.4). The flow measurement system was comprised of three flow measurement devices: a mass flowmeter, a pitot tube and a rotameter. Triple redundancy was used for all flow measurements on account of the importance of this experimental parameter. The specifications for each of the flow systems are described below:

- Electronic mass flowmeter: Model 565, manufactured by Kurz Instruments (Monterey, CA), measures mass flow from 0 to 50 ft<sup>3</sup>/min (0 to 1.42 m<sup>3</sup>/min) with an accuracy of  $\pm 2\%$  of the flow reading plus  $\frac{1}{2}\%$  of the full

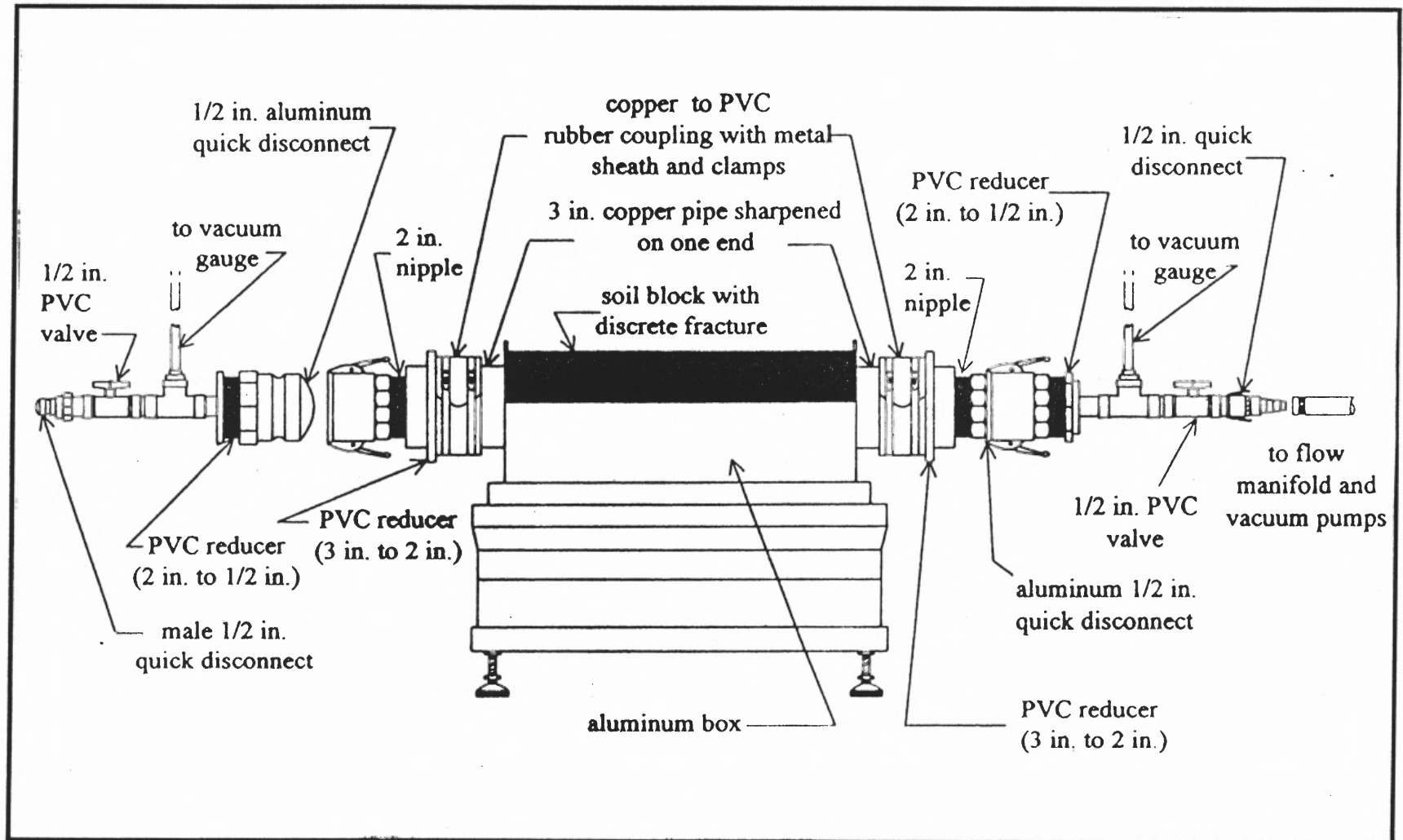


Figure 3.3 Construction Details for the Horizontal Infiltrometer Apparatus (Hall, 1995)

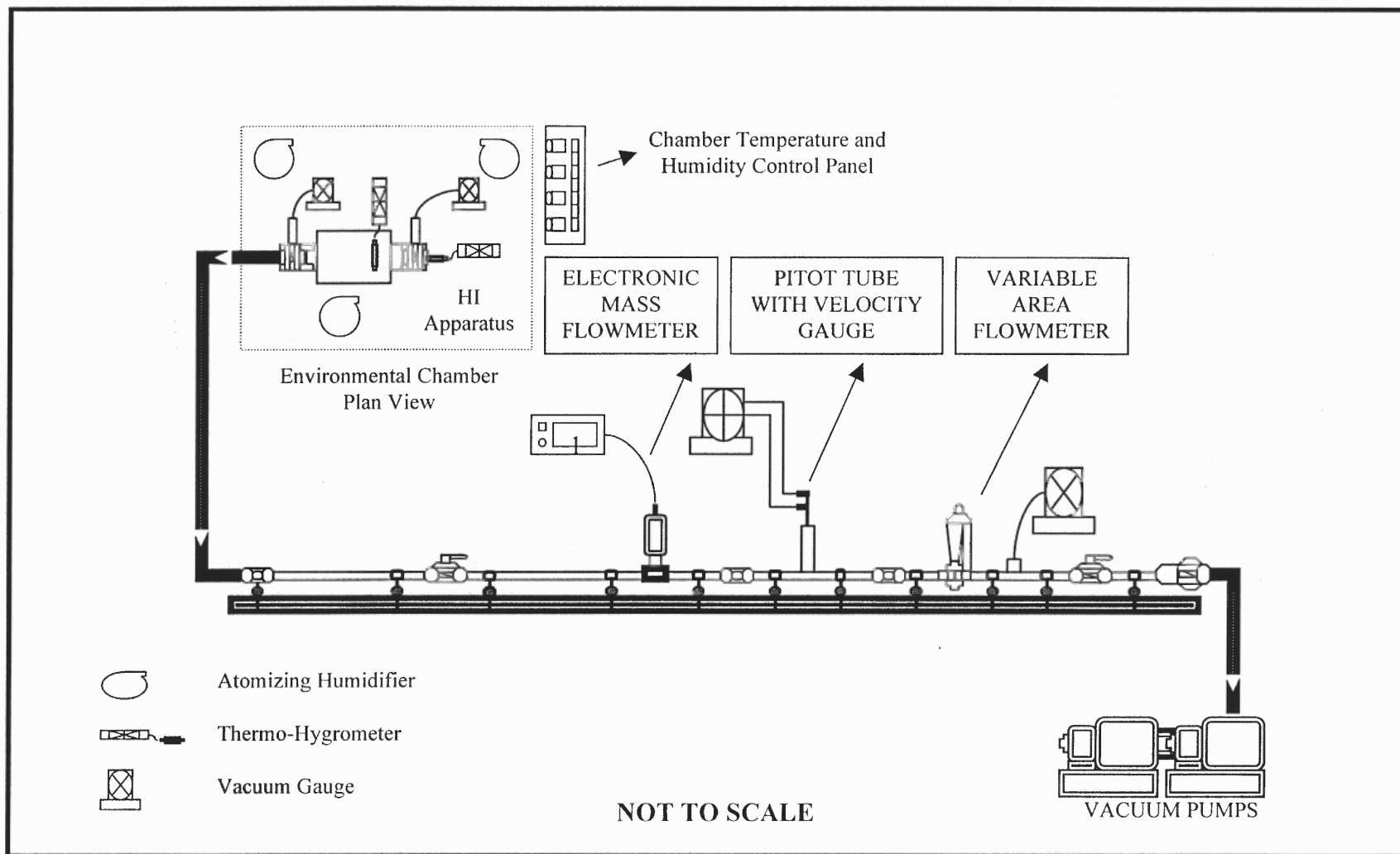


Figure 3.4 Experimental Setup of the Horizontal Infiltrometer System

scale. It is equipped with a thermocouple for internal correction to standard temperature conditions. The manufacturer calibrated the flowmeter prior to the experimental portion of this study.

- Pitot tube with Magnehelic® velocity gauge: Models 167 and 2000-00 AV, manufactured by Dwyer Instruments (Michigan City, IN), measure velocity pressure from 300 to 2,000 ft/min (91 to 610 m/min). For the 1 in. (2.54 cm) pipe diameter used for testing, accuracy of the pitot tube is estimated to be  $\pm 5\%$ , down from the literature-stated value of  $\pm 2\%$  accuracy for a 4 in. (10.2 cm) pipe diameter (personal communication-Dwyer).
- Variable area flowmeter (rotameter): The Ratosight™ flow indicator (Model 10A2235A) measures flow from 1 to 14 ft<sup>3</sup>/min (0.03 to 0.4 m<sup>3</sup>/min). The meter was designed by Bailey, Fischer, and Porter and manufactured by ABB Instrumentation (Warminster, PA). The indicator is used in the horizontal flow mode and has a pressure drop of 4.5 in. (11.4 cm) water and an accuracy of  $\pm 5\%$ .

The entire flow measurement system was connected with 1 in. (2.54 cm) diameter soldered copper tubing (Type M). The system contains ball valves on either end for pressure testing, and a Magnehelic® pressure gauge with a range of 0 to 100 in. water (0 to 254 cm) (Model 2100, Dwyer Instruments). All devices were calibrated to standard pressure and temperature of 14.7 lb/in<sup>2</sup> and 70°F

(101 kPa and 21°C). The flow measurement system was pressure tested periodically to ensure that it was airtight.

**3.1.2.3 Operation.** The HI tests were performed in an environmental chamber (Environmental Growth Chambers, Inc., Chagrin Falls, OH) at typical subsurface temperatures of 54 to 57°F (12 to 14°C). Existing humidity in the chamber was generally sufficient, although on occasion moisture was added with two atomizing humidifiers that were part of the chamber control system. The tests were run under a passive inlet condition, i.e., the inlet end was open to the atmosphere. The differential pressure of the vacuum pumps pulled a continuous flow of air through the fracture.

Soils were hydrated through use of three atomizing humidifiers located throughout the chamber. This method allowed for sufficient hydration, yet retarded the rate enough to observe the progress of volume change. Dehydration was induced by pulling dry air through the fracture.

Two portable thermo-hygrometers (Model HI8564, Hanna Instruments, Woonsocket, RI) were used to measure humidity and temperature during testing. One was located at the inlet and the other measured ambient conditions just above the soil block. LiCl and NaCl salts were used to calibrate the meters prior to use. The readable ranges of relative humidity and temperature were 10.0% to 95.0% and 0 to 140°F (0 to 60°C), respectively, with accuracies of  $\pm 5\%$  and  $\pm 0.7^\circ\text{F}$  ( $0.4^\circ\text{C}$ ), respectively. Atmospheric pressure was also monitored to

allow for the adjustment of data to standard pressure.

Upon completion of the test, the fracture apertures at the inlet and outlet were measured with metal strips of differing thicknesses (i.e., feeler gauge). Then, the soil block was excavated from the top down. Ninety-seven soil moisture content samples were taken from ten horizontal and eight vertical layers. Sampling frequency was increased around the fracture, with fewer samples towards the top and bottom of the soil block. The sample locations were standardized to ensure consistency between tests. Photographs of this process are shown in Appendix A (Photos A-9 to A-11). Each test was documented photographically with particular emphasis on fracture geometry, soil morphology, and shrinkage cracking of the fracture boundary soils.

It should also be noted that a series of experimental runs were performed with earlier versions of the horizontal infiltrometer device, flow system, and thermo-hygrometers. Details of the previous system are provided in Hall (1995). Data generated during these earlier experiments were used by applying correction factors that reflected improvements to the flow system and humidity measurements.

### **3.1.3 Material Parameter Testing**

Several additional tests were performed on the clay test soil to better define its physical properties and to aid in identification of input parameters for the FVC Model. This section describes these tests, which included consolidation testing,

pressure plate soil equilibration, suction testing, water retention testing, and swell testing.

**3.1.3.1 Consolidation Testing.** Consolidation tests were performed at NJIT on Potomac Formation remolded clay samples according to ASTM (2000h) Method D2435-96. The soil was compacted at 50 wt% moisture (to ensure saturation) into a Proctor mold (ASTM, 2000b). The soil was extruded, sliced, and cut into a 2.813 in. (7.145 cm) ring. The ring was then placed into a fixed ring consolidation cell, and the specimen was subjected to incremental loading while the sample was given free access to distilled water. Unloading, reloading, and reuniting cycles followed. Each load was allowed to act for 24 hours to define the end-of-primary (EOP) void ratio. Rigid porous stones on the top and bottom faces of the specimen allowed for drainage.

**3.1.3.2 Pressure Plate Soil Equilibration.** Pressure plate equilibration was performed according to ASTM Method D 2325-68 (ASTM, 2000g) in order to: (1) determine the relationship between soil matric suction and water content; and (2) prepare soils of different suctions for swell testing. Pressure membrane devices would have been more appropriate given the fine-grained, shrink-swell properties of the soil; however, these devices were not available.

The soil was compacted at 31 to 32 wt% moisture into a Proctor mold (ASTM, 2000b). The soil block was then extruded from the mold, sliced, and cut

into a ring. Rubber rings that conform to the specifications of ASTM (2000g) were used for the water retention tests. Specially designed steel rings were used for the swell tests. The height was chosen to be as small as possible to allow for adequate equilibration, and large enough to meet size requirements for ASTM (2000l) specifications for swell tests. Shrinkage of the soil specimen during equilibration was also taken into account. The rings measured 3.625 in. (9.208 cm) in diameter (I.D.), 0.6 in. (1.5 cm) in height for the 0.3 and 1.0 bar (30 and 100 kPa) samples, and 0.7 in. (1.8 cm) in height for the 5.0 and 15.0 bar (500 and 1500 kPa) samples.

Once the soil was inserted in the rings, it was allowed to sit in a water bath for several weeks to saturate fully. Just prior to testing, the soil was cut to the dimensions of the ring, since saturation had increased the volume of soil from the pre-saturated state. The samples were then taken to Rutgers University in New Brunswick, NJ, for testing. The moisture-capillary tests were performed at the Soil Science Laboratory in the Environmental Science Department, and the swell tests were done at the Bioenvironmental Engineering Laboratory located in the Department of Bioresource Engineering. All tests were run with equipment manufactured by Soilmoisture Equipment Corporation (Goleta, CA), using Laboratory Setup 023. This included 5-bar (500 kPa) and 15-bar (1500 kPa) pressure plate extractors (Models 1600 and 1500, respectively), a compressor (Model 500), and a pressure regulation manifold (Model 700CG23). The equipment allowed for equilibration in the 0 to 15 bar (0 to 1500 kPa) suction



range.

For testing, the samples were placed on a porous (high air-entry) ceramic pressure plate within the pressure vessel. Using the axis-translation technique (Hilf, 1956), air pressure above atmospheric was applied to the soil specimens and the water pressure was kept at atmospheric through a connection on the rubber membrane at the lower end of the plate. The samples were allowed to rest as water was forced out of the sample. The matric potential is the difference between air and water pressures.

The samples were allowed to remain in the pressure plate extractors for as long as possible, given the availability of the equipment. The plate with the highest air-entry value for a given suction was chosen to minimize equilibration time. The test conditions and retention times are presented in Table 3.2.

**3.1.3.3 Suction Testing.** Two types of suction tests were performed including thermocouple psychrometer testing and filter paper suction testing. One or more of these methods were applied to both water retention and swell samples.

Tru Psi (Model SC10X), manufactured by Decagon (Pullman, WA), was the thermocouple psychrometer device used to measure suction at the completion of each test. The Peltier thermocouple used in this instrument is accurate over a range of -3 to -35 bars (-300 to -3500 kPa). Thus, only soils equilibrated at suctions greater than -3 bars (-300 kPa) could be tested. This measurement was only a general indication of whether the soils had reached

**Table 3.2** Summary of Pressure Plate Samples

<b>Equilibration Suction (bars)</b>	<b>Pressure Plate (bars)</b>	<b>No. of Samples</b>	<b>Retention Time (days)</b>
<b>Water Retention Samples</b>			
0.1	0.5	3	6
0.2	0.5	3	8
0.3	0.5	6	6
0.5	1.0	9	9
1.0	3.0	9	12
2.0	3.0	9	16
5.0	15.0	3	17
15.0	15.0	9	24
<b>Swell Test Samples</b>			
0.3	0.5	5	21
1.0	3.0	5	41
5.0	15.0	5	33
15.0	15.0	5	54

equilibrium, as the device is calibrated to -22.9 bars (2290 kPa) and measures total rather than matric suction. Ten samples at a time were equilibrated in the unit for at least 20 minutes prior to each run. A calibration check using 0.5 molal KCl was performed before and after each set of 10 samples. The accuracy of the instrument in the lower suction range is expected to be  $\pm 0.5$  bar (50 kPa) (personal communication with Decagon).

Filter paper suction tests were performed on three of the water retention samples to verify suction according to ASTM (2000n). Both total and matric

suction testing were performed by equilibrating Whatman® No. 42 filter paper with the soil samples in sealed containers. Two papers were placed in direct contact with the soil, and a third was placed between them for measurement of matric suction. A filter paper, raised off the surface of the soil, collected ambient moisture in the jar for total suction measurement. Following the 10-day equilibration time, the moisture contents of the two filter papers were determined and the matric and total suctions determined from the ASTM (2000n) calibration curve.

**3.1.3.4 Water Retention Testing.** Water retention testing was performed on both the water retention samples and portions of selected swell samples after removal from the pressure plate extractors. The entire soil volume for each of the water retention specimens was tested. Because the swell samples were too large to be tested directly, portions were removed for testing. For the 0.3 bar (30 kPa) and 5.0 bar (500 kPa) swell samples, one and four samples, respectively, were cutout using 1 in. (2.54 cm) and 1.25 in. (3.2 cm) diameter cutting rings.

Samples were measured to the nearest 0.001g for moisture content determination. They were then coated in low temperature paraffin wax and the volumetric water content determined using the relationship between weight in water and weight in air (ASTM, 2000m). Following volume determination, the wax was peeled off and the soil sample was placed in the oven. The mass of dry soil was used to calculate gravimetric and volumetric moisture contents.

**3.1.3.5 Swell Testing.** One-dimensional swell tests were performed according to ASTM (2000I) Method D 4546-96 (Method B). Soil samples, previously equilibrated in the pressure plate extractor to suctions of 0.3, 1.0, 5.0 and 15.0 bars (30, 100, 500 and 1500 kPa), were placed in the oedometer apparatus. For each suction, both free swell at 0.01 bar (1 kPa) and overburden pressures of 0.12, 0.49, and 1.25 bars (12, 49, and 125 kPa) were tested. One-dimensional swell was measured as the sample was given free access to distilled water. The tests were run for 10 to 15 days, which was sufficient to define primary and secondary swell trends.

## **3.2 Results and Discussion**

In this section, the results of the physical and chemical soil testing, horizontal infiltrometer experiments, and the material parameter testing are presented. Results of the pressure plate soil equilibration and suction testing are incorporated into the respective sections on water retention testing and swell testing.

### **3.2.1 Soil Properties**

The intent of this section is to describe the physical, chemical, and mineralogical properties of the test soil and how each influences volume change potential (i.e., expansivity). The results of testing are integrated with published information on the Potomac Formation.

**3.2.1.1 Geology of the Potomac Formation.** The Potomac Formation forms the basal unit of much of the Atlantic Coastal Plain Physiographic Province. Figure 3.5 shows its outcrop region as a belt that runs through large metropolitan areas from Virginia to New Jersey just east of the Piedmont Province. In general, the Potomac Formation is a variable combination of interbedded sequences of gravel, sand, silt, and clay, with often large and abrupt variations in lithology (Obermeier et al., 1984). The soil colors range from bluish grey to red and yellow. Demarcated into two sedimentary facies, there is a northern kaolinite-illite sequence and a southern montmorillonite sequence (Figure 3.5). Different source provenances are believed to account for the mineralogical patterns (Glaser, 1969). It is the montmorillonite facies of the Potomac Formation that is of interest to this study.

The term 'marine clay' has gained wide local usage in Virginia to describe the fine-grained montmorillonite sequence (Johnson, 1990). However, deposition is believed to have occurred in fresh or brackish water rather than in a true marine (ocean) environment (Johnson, 1990). These Lower Cretaceous-age sediments are actually fluvial (river) and possibly deltaic deposits of the ancestral Potomac River, which today lies to the east of the southern clay facies (Obermeier et al., 1984). The fine-grained sediments of the Potomac Formation were apparently deposited as overbank flood-plain deposits or as fillings in abandoned meanders. Figure 3.6 shows the local depositional features of the Potomac Formation in Fairfax County, VA and vicinity.

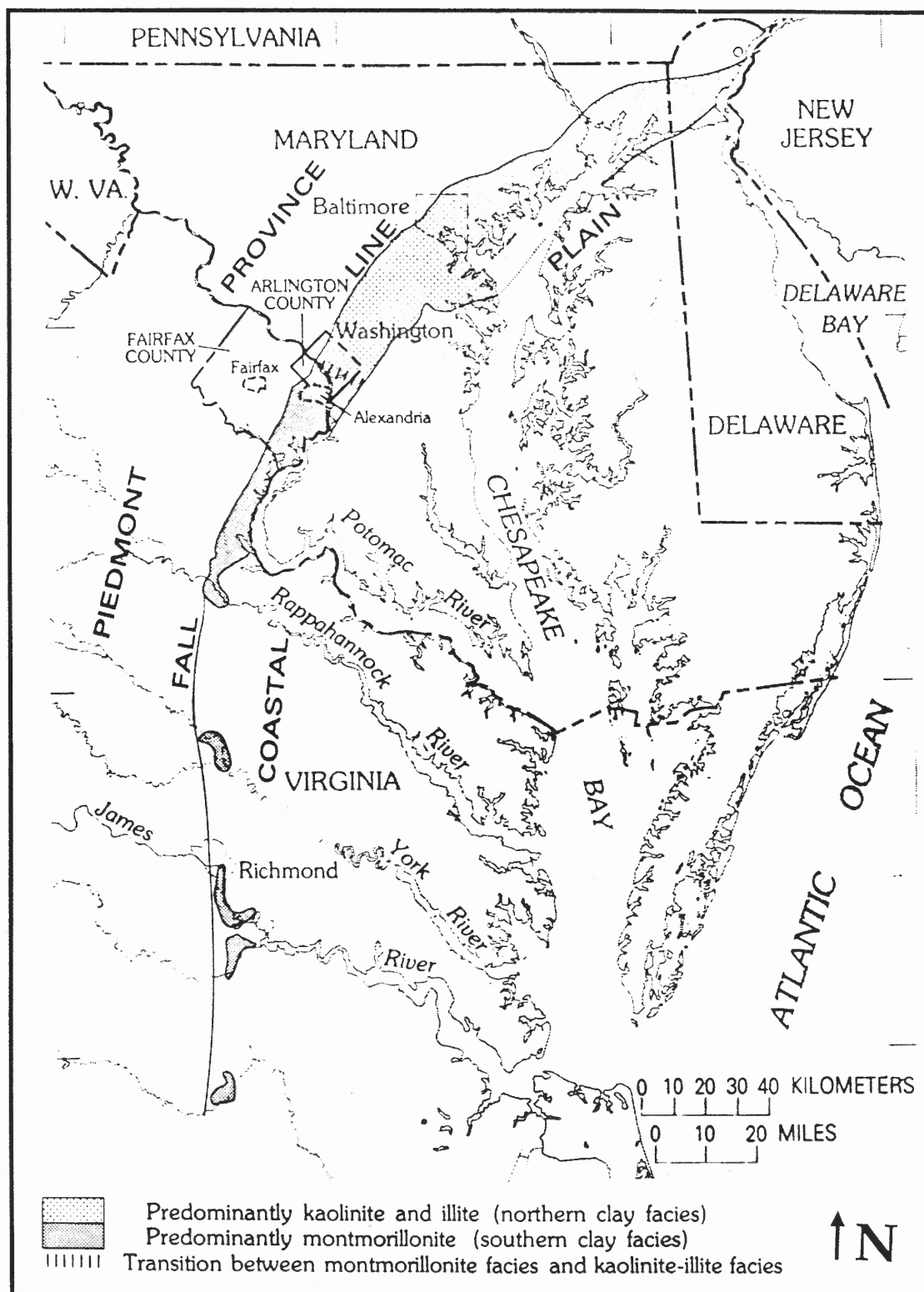
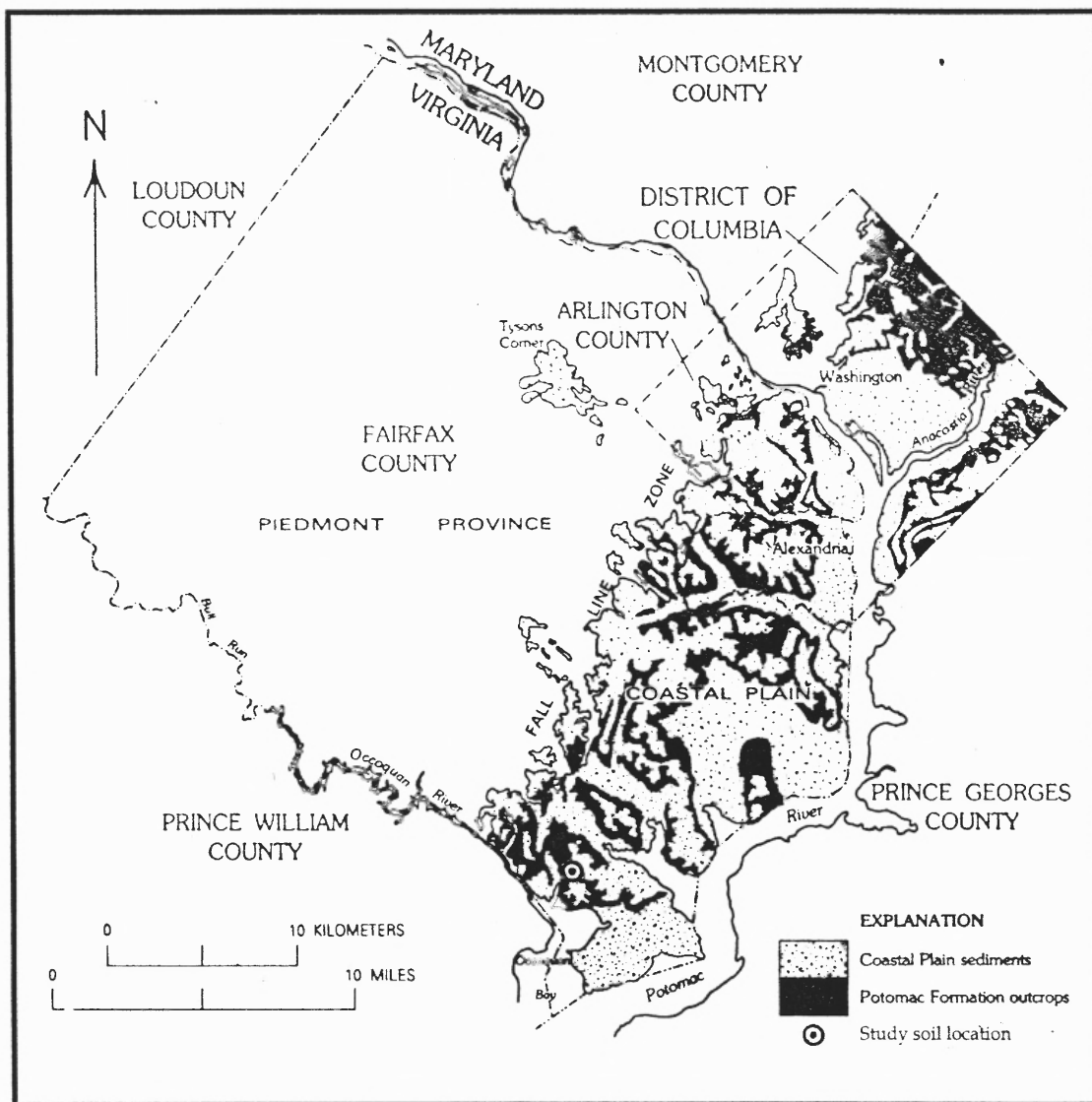


Figure 3.5 Clay Mineral Facies in Potomac Formation Outcrop Belt from Virginia to New Jersey (after Force and Moncure, 1978).



**Figure 3.6** Distribution of Localized Potomac Formation Deposits in Fairfax County and Vicinity (after Obermeier et al., 1984).

On a widespread scale, the Potomac Formation ranges up to 1200 ft (366 m) in thickness (Obermeier, 1984). In the Fairfax County vicinity, it ranges from 1 ft (0.3 m) to greater than 160 ft (50 m) thick, with an areal extent of up to hundreds of meters (Obermeier and Langer, 1986). Where unweathered, the clay and silt are highly overconsolidated and very stiff, and the montmorillonite facies is moderately to highly susceptible to shrinking and swelling (Obermeier, 1979). The soils are also characterized as having high erosion potential at the surface (i.e., weathered soils), particularly where unvegetated, and they have extremely low internal drainage (Fairfax County Soil Science Office, 1983).

**3.2.1.2 Physical and Chemical Testing.** This section presents results of the physical and chemical testing performed on the Potomac Formation clay, using the methods previously described in Section 3.1.1. Discussion of the significance of these characteristics on the shrink-swell properties of the soil is reserved for Section 3.2.1.3.

The physical testing results of the aggregate field sample are summarized in Table 3.3. Based on visual inspection, the sample was divided into two predominant components, which consisted of relatively highly plastic red and blue clays. A less plastic blue clay was isolated as a third minor constituent. As indicated, the test soil is primarily a high plasticity clay (*CH*) and also contains a small quantity of high plasticity silt (*MH*). All three samples contained over 99% fines, with 36% to 39% of fines in the clay size fraction ( $<2\ \mu\text{m}$ ). The high



**Table 3.3.** Comparison of Potomac Formation Physical Properties

Test Parameter	Red Clay	Blue Clay	Blue Clay (Less Plastic)
Grain Size (%)			
Sand (fine)	1	2	2
Fines	99	98	98
Silt	60	60	62
Clay (<2 $\mu$ m)	39	38	36
Clay (<1 $\mu$ m)	22	24	30
Atterberg Limits			
Liquid Limit ( <i>LL</i> )	68	66	56
Plastic Limit ( <i>PL</i> )	27	26	30
Shrinkage Limit ( <i>SL</i> )	16, 13	11, 10	14
Plasticity Index ( <i>PI</i> )	41	40	26
Shrinkage Index ( <i>SI</i> )	11, 14	15, 16	16
Miscellaneous			
Natural Moisture Content (wt%)	29.1, 28.6, 30.2	29.3, 28.7, 28.8	--
Specific Gravity ( <i>G<sub>s</sub></i> )	2.77	2.75	--
Organic Matter (wt%)	2.6	2.6	--
USCS Classification	<i>CH</i>	<i>CH</i>	<i>MH</i>

-- not performed

concentration of clay <1  $\mu$ m (22 to 30%) combined with the high plasticity and shrinkage indices suggests the presence of montmorillonite as the dominant clay mineral. The Atterberg results for the test soil showed good correlation with published values for Potomac Formation clays. For example, Obermeier et al. (1984) report average *LL*s of 60 to 70, with exceedences of 100, and average *PL*s in the high 20s and 30s, with lower values occasionally observed. Byle and Davit (1992) report *LL*s of 74 to 85 and *PL*s of 23 to 68.

The less plastic blue clay is believed to contain a greater percentage of minerals other than montmorillonite since the grain size distribution of the three

samples is relatively uniform (Figure 3.7). The USCS *MH* classification suggests that these particles may be finely divided, primary rock-forming minerals rather than clay minerals. This seems to affect only the range over which the soil is plastic (i.e., 15% *PI* decrease); the shrinkage index (*SI*) appeared consistent with the more plastic samples. A homogenous test soil was created by mixing all clay soils together.

The natural water content of the test soils averaged 29.1 wt%, with a range of 28.7 to 30.2 wt%. This is consistent with literature values of 26 to 36 wt% determined by Byle and Davit (1992). Note that the natural water content slightly exceeds the *PL* at this depth. Obermeier et al. (1984) found that the natural water content is normally less than the plastic limit at depths greater than 20 to 30 ft (6 to 9 m), and he showed that it exceeded the *PL* by as much as 10% in shallower, weathered zones.

The specific gravity averaged 2.76, which is in the typical range for quartz and feldspar-based inorganic clays such as the Potomac Formation. The SCS (1971) classifications put the Potomac Formation into a class of 'medium' (*MM*) with regard to organic matter (2.6 wt%). The organic matter will account for a small percentage of the ion exchange sites.

It should be noted that the clay did not break down easily during remolding, so a comparative study was performed to investigate whether breakage may have artificially elevated the Atterberg limits. Table 3.4 presents the results of Atterberg limit data measured after reduction by hand as compared

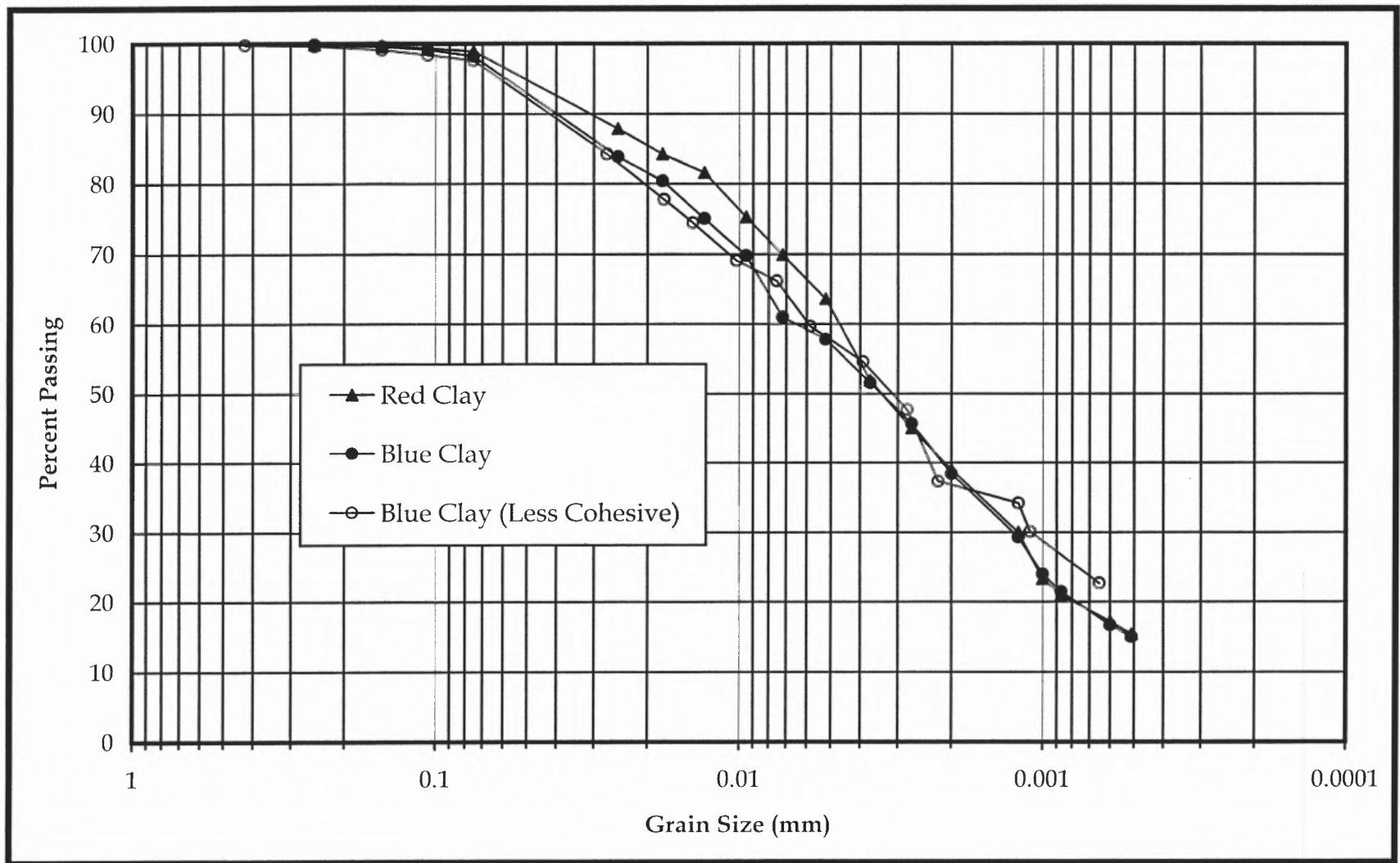


Figure 3.7 Grain Size Distribution for Potomac Formation Clay

**Table 3.4** Effect of Soil Reduction Method on Atterberg Limits

Atterberg Limits	Mixed Soil (Reduced By Hand)		Mixed Soil (Reduced By Shredder)	
	Sample A	Sample B	Sample A	Sample B
Liquid Limit ( <i>LL</i> )	61	62	67	65
Plastic Limit ( <i>PL</i> )	27	--	28	--
Shrinkage Limit ( <i>SL</i> )	13	--	12	--
Plasticity Index ( <i>PI</i> )	34	--	39	--
Shrinkage Index ( <i>SI</i> )	14	--	16	--

-- not performed

to reduction with the shredder (see Section 3.1.1). Note that there was a slight increase in the *LL* ranging from 3 to 6, suggesting minor mechanical alteration. The *PL* and *SL* did not seem to be affected, however. Note also that the Atterberg limit values of the soil before reduction are very similar to those after reduction. Thus, it was concluded that mechanical reduction of the soil did not significantly affect the physical properties of the soil.

Results of the chemical analyses on the Potomac Formation clay are presented in Table 3.5. The exchangeable ions represent the ions that are within the structure of the clay mineral primarily by isomorphous substitution. Thus, the quantity is indicative of the type of clay mineral, with montmorillonite possessing the greatest amount of isomorphous substitution. The exchange complex is quite substantial, and it is dominated by  $\text{Ca}^{+2}$  and  $\text{Mg}^{+2}$  with greatly subordinate  $\text{Na}^{+}$  and  $\text{K}^{+}$ . This is consistent with published values of exchangeable bases for unweathered clay-rich portions of the Potomac

Table 3.5 Results of Chemical Analyses on Potomac Formation

ANALYTE	TEST RESULT
<b>Exchangeable Ions (ppm):</b>	
Ca <sup>+2</sup>	4,016
Mg <sup>+2</sup>	2,288
Na <sup>+</sup>	31
K <sup>+</sup>	416
Al	<0.1 meq/100 g soil
H <sup>+</sup>	<0.1 meq/100 g soil
<b>Extractable Salts at 66-68% Water Saturation (ppm):</b>	
Ca <sup>+2</sup>	32.6
Mg <sup>+2</sup>	21.4
Na <sup>+</sup>	15.6
K <sup>+</sup>	19.1
S	60.7
B	0.03
Cl <sup>-</sup>	14.8
HCO <sub>3</sub> <sup>-</sup>	41
<b>Conductivity:</b>	
Electrical Conductivity (soil water extract)	0.4 mmho/cm
Soluble Salts (saturated paste)	0.81 mmho/cm
<b>Soil pH:</b>	
1:1 Soil-Water Ratio	6.4
Saturated Paste Water Content	6.1
<b>Cation Exchange Capacity:</b>	
Summation	40.3
Total (CEC <sub>t</sub> )	37.1
Permanent Charge (CEC <sub>p</sub> )	24.9
<b>Ratios:</b>	
Exchangeable Sodium Percentage (ESP)	0.0
Sodium Adsorption Ratio (SAR)	0.5
Cation:Anion Ratio	4.6/4.9
<b>Agricultural Soil Designations:</b>	
Non-Saline	
Non-Sodic	

Formation (Obermeier et al., 1984). Quantities of exchangeable aluminum and hydrogen are negligible.

The amount of water-soluble ions (i.e., extractable salts) in the soil solution is quite small relative to the amounts in the exchangeable forms. Note that the ratios of  $\text{Ca}^{+2}$  and  $\text{Mg}^{+2}$  to  $\text{Na}^{+}$  and  $\text{K}^{+}$  have greatly reduced, suggesting an affinity of the clay mineral structure for divalent cations. This is even more pronounced because of the low salt concentrations, where  $\text{Ca}^{+2}$  and  $\text{Mg}^{+2}$  become even more effective competitors for clay exchanges sites (McBride, 1994).

The low soluble salt concentrations are also reflected in the conductivity values. The Potomac Formation clays are within the 0 to 2 mmho/cm range for non-saline classification as defined by EPA's Environmental Sampling Expert System (ESES) (Cameron, 1991). Low osmotic potential is implied.

The low exchangeable sodium percentage (i.e.,  $<5$ ) reduces the potential for spontaneous clay dispersion, structural breakdown, and seal or crust formation (Tanji, 1990). This suggests that dislodgment of clay particles from the aggregate structure is not expected to be a significant phenomenon of fracture aperture changes during horizontal infiltrometer testing with Potomac Formation soils. Note also that the slightly higher sodium adsorption ratio (SAR) is a reflection of the higher ratio of  $\text{Na}^{+}$  to  $\text{Ca}^{+2}$  and  $\text{Mg}^{+2}$  in the soil solution as compared to that in the exchange complex.

The Soil Survey Staff (1993) defined 13 pH classes for soils in their “Examination and Description of Soils” Handbook. The Potomac Formation clay falls in the range of 6.1 to 6.5, and classifies as slightly acidic (SA).

The cation exchange capacity (CEC) is considered high according to EPA’s ESES (Cameron, 1991), which uses the following CEC classes (expressed as meq/100g soil): high (>20), medium (12-20), and low (<12). The CEC calculated as a summation of the  $\text{NH}_4^+$  exchangeable bases at pH 7 (i.e., 40.3 meq/100 g soil) is very similar to the CEC measured from the  $\text{Ba}^{+2}$  exchange at pH 8.2 (i.e., 37.1 meq/100 g soil).

Clay mineralogy may be inferred from CEC results, given quantitation of total and permanent charge components ( $\text{CEC}_t$  and  $\text{CEC}_p$ , respectively). The difference between the  $\text{CEC}_t$  and  $\text{CEC}_p$  yields the variable charge CEC ( $\text{CEC}_v$ ). The  $\text{CEC}_v$  is pH-dependent charge that occurs due to ‘dangling bonds’ on the edges of the silicate particles edges (McBride, 1994). The  $\text{CEC}_v$  is not a reflection of the CEC caused by isomorphous substitution from which clay mineralogy is inferred. It should also be noted that some of the cation exchange capacity is attributed to the organic matter, which typically has 2 to 20 times more CEC than soil clays (Conklin, 2000).

In this case, the  $\text{CEC}_p$  (i.e., 24.9 meq/100 g soil) exceeds the  $\text{CEC}_v$  (i.e., 12.2 meq/100 g soil), implying that the majority of the cation exchange is occurring within the structure. This is traced to the clay mineral montmorillonite. Force and Moncure (1978) and Glaser (1969) report that the clay soils in the

montmorillonite facies of the Potomac Formation are comprised predominately of montmorillonite-illite mixed-layer clay and relatively pure montmorillonite. Minor components are pure illite or clay mixtures of montmorillonite and illite, containing small amounts of vermiculite and kaolinite.

**3.2.1.3 Expansivity Characterization.** This section presents a discussion of the volume change potential of the Potomac Formation clay using Hall's (1995) classification model (Section 2.1). The analysis is based on the physical, chemical, and mineralogical properties described in the previous section (3.2.1.2), which dictate the range of potential volume change response. Secondly, the analysis is based on environmental conditions, which control the degree of expression of this response to both the natural and experimental conditions of this study. Only by collectively examining a soil's characteristics and conditions can expansivity be effectively evaluated. A schematic of the decision analysis for applying the classification model to the Potomac Formation clays is presented in Figure 3.8. Discussion is centered on the red and blue clay as the major soil components, with less emphasis on the minor, less plastic blue clay.

***Physical Properties:*** The general physical properties of the Potomac Formation were first used to determine that the soil is potentially expansive. These included a USCS classification of *CH* (i.e., clay of high plasticity) and a 39% clay size fraction ( $<2\ \mu\text{m}$ ). In addition, the moisture content for the horizontal



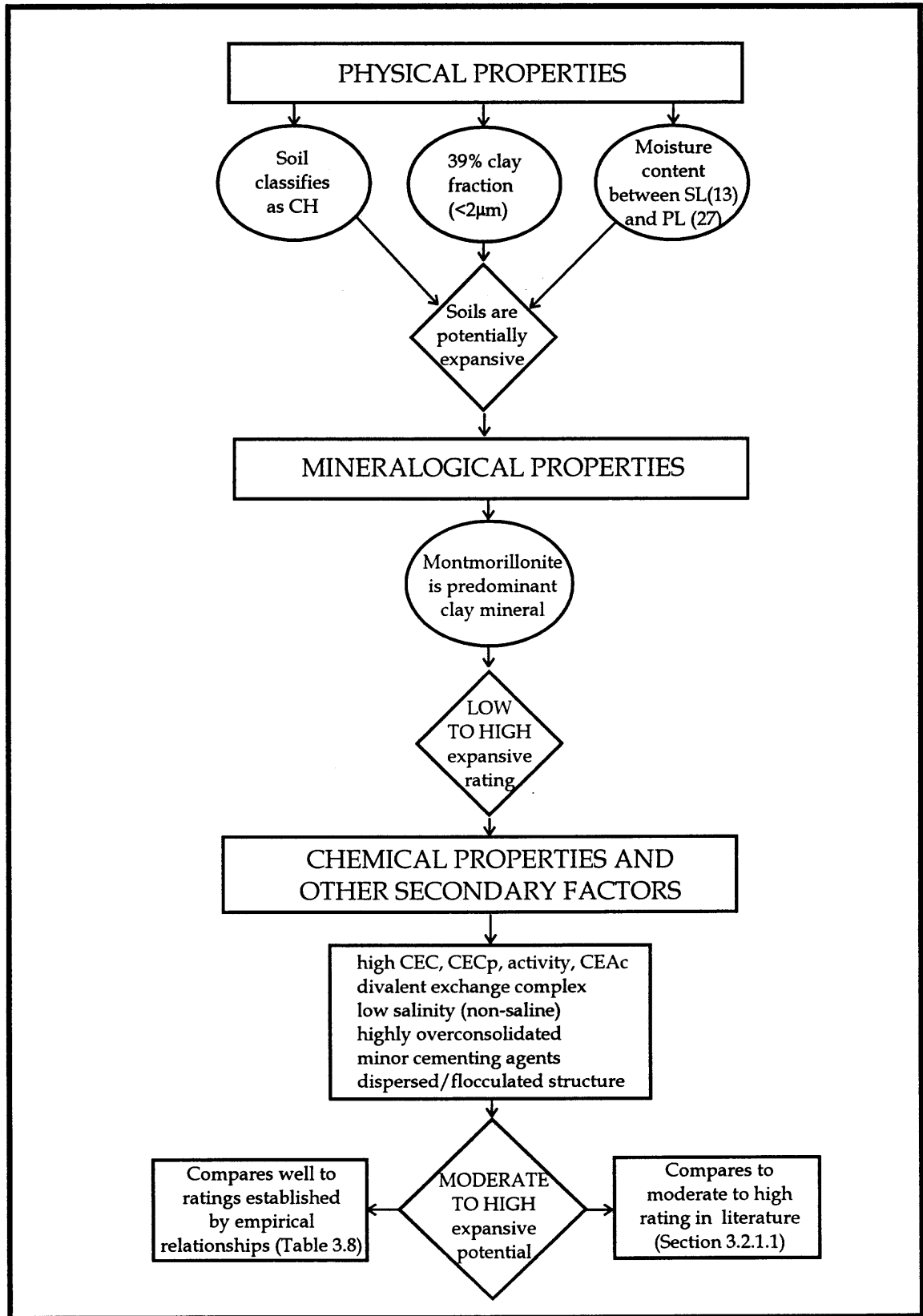


Figure 3.8 Expansivity of Potomac Formation Clay based on Hall (1995) Method

infiltrometer tests, as well as for typical field conditions, ranges between the *SL* (13) and the *PL* (27). It is noted that environmental changes for the horizontal infiltrometer test are restricted to moisture content fluctuations with minor influences of temperature and pressure. Surcharge pressure was held constant.

***Mineralogical Properties:*** An expansivity rating of low to high was then generated based on the predominance of montmorillonite in the sample. Montmorillonite is the most expansive clay mineral followed by mixed illite-montmorillonite, illite and kaolinite in decreasing order. The high cation exchange capacity (*CEC*), activity ( $PI/\%<2\ \mu\text{m}$ ), and cation exchange activity ( $CEC/\%<2\ \mu\text{m}$ ) also suggested that a significant portion of the clay fraction is composed of clay minerals. Soils with a high ratio of clay minerals to nonclay minerals, such as primary rock forming minerals (e.g., feldspars, quartz) and noncrystalline material (e.g., allophane), are most expansive.

The degree of expansivity within this range was then established by evaluating secondary factors of expansivity. A discussion of these factors follows.

***Chemical Properties and Other Secondary Factors:***

Chemical Properties: The soil contains an exchange complex comprised primarily of divalent exchange cations, namely  $\text{Ca}^{+2}$  and  $\text{Mg}^{+2}$ , rather than monovalent cations, such as  $\text{Na}^{+}$  and  $\text{K}^{+}$ . The divalent ions tend to counteract

the tendency toward swelling by forming electrostatic bridges between adjacent particles, creating larger particles as platelets stacked together into “quasi-crystals” (McBride, 1994). Thus, an expansivity of smaller magnitude is expected for the Potomac Formation clays as compared to a Na-based soil. This is also reflected in the low *ESP* ratio.

Soils in lower electrolyte solutions are more expansive with all other properties equal (McBride, 1994). The low salt concentration in the pore water of the Potomac clay thus increases the swelling potential. The use of distilled water in the preparation and saturation of soils for the horizontal infiltrometer tests is thus expected to slightly increase the expansive potential as compared to natural soils. Also, soils are more expansive where there is a greater ratio of lower valence (e.g.,  $\text{Na}^+$ ) to higher valence (e.g.,  $\text{Ca}^{+2}$ ) exchangeable cations in the pore water and the base saturation is relatively low. In this case, there is a ratio of approximately 1.5 in favor of higher valence ions, and base saturation is moderately high.

Other Secondary Factors: The stress history shows that the Potomac Formation clays are heavily overconsolidated (Obermeier and Langer, 1986). These soils are much more expansive than normally consolidated or underconsolidated formations under equal void ratios. Since the remolded clay was packed at a relatively high density for the horizontal infiltrometer tests (see Section 3.2.2), the expansivity potential was maintained.

Sedimentation of the Potomac Formation in fresh or brackish water tends to suggest that the clay structure is dispersed (i.e., more parallel particle orientation). However, the remolding of the clay for the experiments will cause the structure to behave more flocculated. Thus, the clay in the horizontal infiltrometer tests is expected to be slightly more expansive (isotropically) than soil under its natural conditions. The slightly higher *PL* values in the samples exposed to mechanical reduction equipment tended to confirm this.

Cementing agents are not expected to be significant in reducing the expansive potential in Potomac Formation clays. Carbonates (caliches), oxides and hydroxy-interlayering, typically by Al, Fe, or Mg, are expected to be minimal as evidenced by the low concentrations of  $\text{HCO}_3^{2-}$ , exchangeable Al, and soluble Mg. In addition, formation of hydroxy (Al, Fe) interlayering requires a  $\text{pH} < 6.0$ , while hydroxy (Mg) interlayering requires an alkaline pH. Some iron oxide cementation would be likely under oxidizing conditions although the test soils were largely unweathered.

The presence of a moderate amount of organic content is expected to have little influence on expansivity, since the majority is expected to occur as a humic fraction, and there are no observable organic fractions in the soil. Only soils with high nonhumic fractions are associated with high shrinkage.

In summary, the secondary factors show that the clay exhibits a great deal of expansivity, but soil properties and environmental conditions do not

maximize the expansivity. Thus, a moderate to high expansivity potential is assigned to the Potomac Formation clays. Empirical volume change relationships developed by other investigators (Table 3.6) suggest a similar result, as do expansivity descriptions in the literature (Section 3.2.1.1).

### **3.2.2 Horizontal Infiltrometer Testing**

This section presents the results of the horizontal infiltrometer bench-scale testing. This includes: (1) presentation of flow results; (2) discussion of the stages of flow behavior; (3) analysis of the changes in fracture aperture; and (4) soil moisture characterization. A summary of the horizontal infiltrometer testing concludes this section.

**3.2.2.1 Flow Results.** Eighteen horizontal infiltrometer (HI) runs were performed as part of this study. Data from Tests 5C through 11C have been chosen to represent typical HI test results. These runs are also considered the most accurate on account of progressive improvements to the flow, pressure, and humidity measurement systems.

All of the tests illustrate flow behavior under monotonic drying. An additional wetting cycle follows for Tests 6C, 7C, and 11C. Cyclic effects are illustrated in Test 10C, where soils were exposed to alternating episodes of drying and wetting.

**Table 3.6** Comparison of Empirical Volume Change Ratings by Various Investigators For Potomac Formation Clays

METHODS	SOIL PROPERTIES USED IN ANALYSIS				VOLUME CHANGE RATINGS		
	Property Evaluated	Red Clay	Blue Clay	Blue Clay (Less Plastic)	Red Clay	Blue Clay	Blue Clay (Less Plastic)
Altmeyer (1955)	SL	15	11	14	Low	Moderate	Low
Chen (1965)	% fines	99	98	98	Very High	Very High	High-Very High
	LL	68	66	56			
	SPR <sup>1</sup>	30-100	30-100	30-100			
Chen (1988)	PI	41	40	26	High-Very High	High-Very High	Moderate-High
Holtz and Gibbs (1956)	% <1 $\mu$ m	22	24	30	Moderate-High	High	Moderate-High
	PI	41	40	26			
	SL	15	11	14			
McKeen and Hamburg (1981); Hamburg (1985)	activity	1.1	1.1	0.72	High to Very High	High to Very High	High to Very High
	CEAc	0.99	1.0	1.1			
Raman (1967)	PI	41	40	26	Low-Very High	Moderate-Very High	Moderate-High
	SI	13	16	16			
Ranganatham and Satyanarayana (1965)	SI	13	16	16	Moderate	Moderate	Moderate
Skempton (1953)	activity	1.1	1.1	0.72	Moderate	Moderate	Low
Snethen et al. (1977)	LL	68	66	56	High	High	Moderate-High
	PI	41	40	26			
	$\mu_{nat}$ <sup>2</sup>	6	6	6			

SPR standard penetration resistance (blows/ft);  $\mu_{nat}$  suction at natural moisture content (tsf); CEAc cation exchange activity

<sup>1</sup> Data from Obermeier et al. (1984); <sup>2</sup> Estimated from water retention data of this study

The raw flow-time data for HI Tests 8C is presented in Figure 3.9, which is considered to be typical of the horizontal infiltrometer tests. The flow is represented by measurements of three instruments: a rotameter, a pitot tube, and a digital mass flow meter (See Section 3.1.2). The raw flow-time data for the other HI tests are contained in Appendix B. Since there are differences in the flow values among the three instruments, a statistical analysis was undertaken. Instrumental errors for the measured flows, plotted as error bars, are shown in Figure 3.9. Figure 3.9 also displays three representative standard deviations (STDEV) and maximum relative percent differences (RPD). Note that the flows are generally within the limits of instrumental error, as shown by overlapping of the error bars. The greatest deviation in flow measurements occurs at the low-end flows, as shown by the high RPD and STDEV values. Inaccuracies are normally expected at the lower ends of an instrument's measurement scale.

In general, the rotameter reported the highest flows and the digital meter the lowest, with a relatively constant rate of change. The lower-end pitot tube measurements tended to coincide with the digital flows, and the higher-end flows with the rotameter measurements. Note that the trends in data are similar between all three instruments and the error is generally reasonable. Since the true flow is not known, it was decided to use averaged data to represent flow for the HI experiments.

The average flow data were adjusted to standard conditions of 14.7 psi (101 kPa) and 70°F (21°C). Figure 3.10 shows the average flows under operating

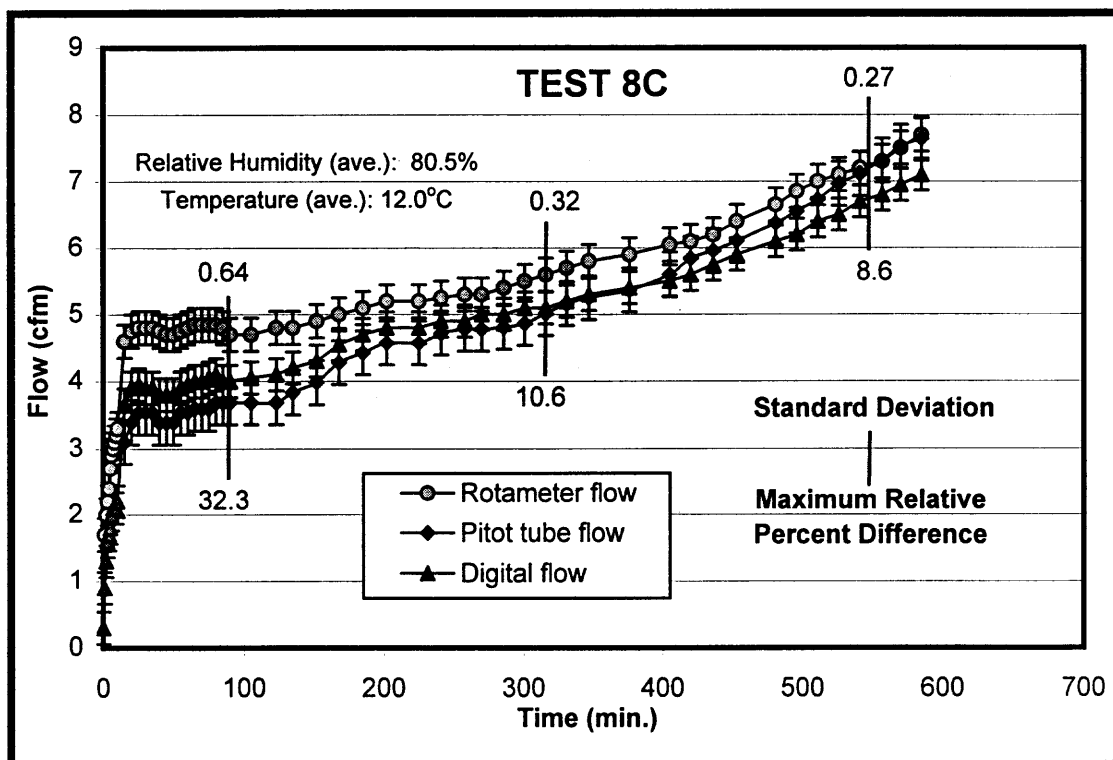


Figure 3.9 Raw Flow-Time Data and Standard Errors: Example HI Test 8C

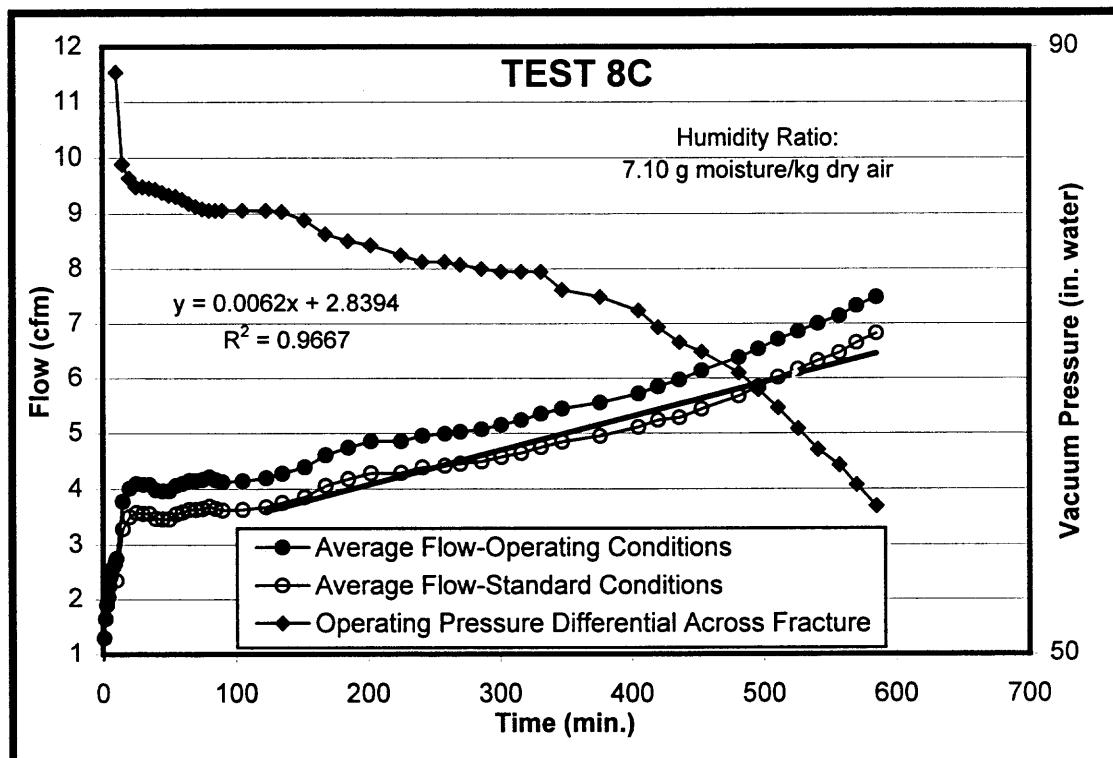


Figure 3.10 Average Flow-Time-Pressure Data: Example HI Test 8C



and standard conditions for the same test. Also included is the pressure differential across the fracture. Measured pressures were generally inversely proportional to flows, ranging from -96 to -45 in. water (-244 to -114 cm water). Associated data for the other HI tests are contained in Appendix B.

Absolute quantities of moisture were also calculated, using temperature and relative humidity data, using psychrometric charts published by the American Society of Heating Refrigerating and Air Conditioning Engineers, Inc. (ASHRAE). The data are reported as humidity ratios (Figure 3.10) in units of g moisture/kg dry air.

**3.2.2.2 Stages of Flow Behavior.** Test 10C will be used to illustrate the generalized flow behavior for the horizontal infiltrometer tests, which may be broken into five distinct stages. These stages are shown in Figure 3.11 as A, B, C, D, and E and are described in detail below.

**Initial Ramping Stage [A]:** The first stage is characterized by a rapid increase in the rate of flow that occurs within the first 10 minutes of the test. This stage is an effect of system operation rather than soil properties. The tests were run by ramping up the pressure (and flow) gradually at 10 in. water/min (25 cm water/min) until a pressure of -96 in. water (244 cm water) was reached. This was done to minimize dynamic contractions of the soil body, bringing the process to a more pseudostatic state.

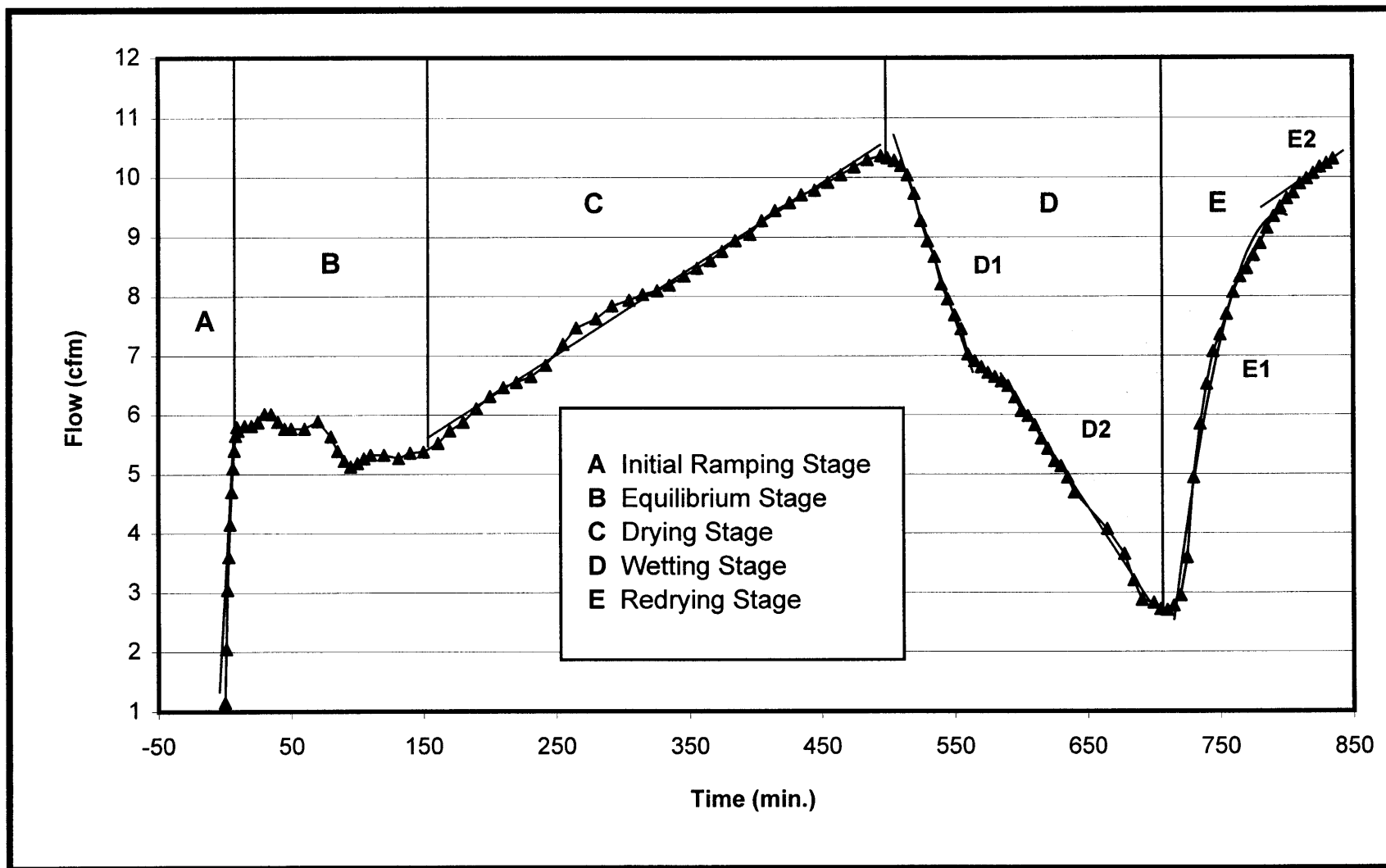


Figure 3.11 Illustration of the Five Stages of Flow Behavior: Example Test 10C

**Equilibrium Stage [B]:** This stage is characterized by alternating positive and negative fluctuations in the rate of change in flow. During this stage, the soil is apparently attempting to adjust to new stress states created from application of the vacuum, while simultaneously starting to shrink due to moisture evaporation. Although the duration of the equilibrium stage is slightly different for each test, the general flow behavior was similar. The various mechanisms believed to be occurring during in this stage will now be discussed.

When the vacuum is applied, the soil body compresses inward toward the fracture under the negative pressure. The inward deformations are likely to be both elastic and plastic (i.e., consolidation). Elastic effects will occur instantaneously, while consolidation, which occurs as swell in this case, will occur more slowly because of the low permeability of the clay. Simultaneous with the elastic-plastic contraction effects is soil drying, which will tend to consolidate or shrink the adjacent soil causing the aperture to increase.

In fact, the latter part of the equilibrium stage is probably characterized by competition between consolidation (swell) due to pressure influences, which decreases flow, and consolidation from drying, which increases flow. Eventually, the consolidation related to the pressure effects slows or stops, the drying effects dominate, and the flow behavior moves fully into stage C.

**Drying Stage [C]:** Stage C represents the flow behavior as water evaporates from the fracture boundary soils. The physical removal of water causes the soil

structure to collapse (or consolidate), the aperture to open, and the flow rate to increase. The increase in flow in this stage is generally a linear function of time. The upper limit of the drying cycle was chosen at just above 10 ft<sup>3</sup>/min (0.3 m<sup>3</sup>/min) to represent an order of magnitude increase in flow. If drying was to occur very much longer, shrinkage cracks would reach the soil block boundaries thereby creating bypass flow and causing an increase in the rate of change of drying.

Note that the rates of change in flow during the drying stage varied between tests. Variations in air temperature, relative humidity, and initial flow rate likely account for this behavior. Drying stage temperatures and relative humidities for Tests 5C through 11C varied from 54°F to 62°F (12°C to 16.4°C) and 78.7% to 82.0%, respectively. The resulting humidity ratios ranged from 7.10 to 9.23 g moisture/kg dry air. An analysis of these phenomena suggests that the rate of change in flow is a combined effect of all three parameters.

**Wetting Stage [D]:** Stage D shows the flow behavior when the soil is exposed to moist air, at a relative humidity of 95 to 100%. The moisture enters the soil, the structure swells, the aperture closes and the flow decreases. Note that the data show two different rates of change in flow, which are designated as Substages D1 and D2. The higher rate in the early portion of the wetting stage [D1] is characterized by an average drop of 0.07 ft<sup>3</sup>/min (0.002 m<sup>3</sup>/min) for Tests 6C, 7C, and 10C. Substage D1 is attributed to two major mechanisms. First, the aperture

is relatively large and thus the quantity of moisture entering the fracture is considerable. Second, the matric suctions are relatively high, so the entering moisture is absorbed quickly by the fracture boundary soils. This causes a sharp decrease in flow due to swelling at the inlet (See Section 3.2.2.4), which results in a rapid localized decrease in aperture. The rate of change in flow then decreases to an average of  $0.02 \text{ ft}^3/\text{min}$  ( $0.0006 \text{ m}^3/\text{min}$ ) as the aperture and matric suction decrease, which characterizes Substage D2.

Also, it is noted that during the wetting stage, the fracture flows were reduced by approximately half an order of magnitude to a point below the initial flow levels. Beyond this, the flows tended toward steady state (see Test 4, Appendix B). Apparently, complete fracture closure was not possible given conditions of the horizontal infiltrometer test. It is speculated that moisture stripping was occurring so rapidly that full closure was not possible. The high air velocities in the fracture, which averaged  $160 \text{ mi/hr}$  ( $260 \text{ km/hr}$ ), substantiate this. The fractures would be expected to more closely approach closure under low flow conditions. However, as previously discussed in Section 2.2.3.2, complete closure of the fracture would not be expected due to structural changes in the fracture boundary soils and effects of differential volume change.

**Redrying Stage [E]:** This stage represents the flow behavior when the soil is exposed to dry air following wetting. This stage may be represented by two substages. Substage E1 is characterized by a rapid, non-linear increase in flow.

Since the fracture constrictions were localized at the inlet, it was only necessary to remove a small amount of moisture to restore the fracture aperture. Thus, the aperture opens relatively quickly as compared to the 'drying stage' flow behavior. Eventually, the fracture opens enough to reach the maximum flow obtained in the drying cycle. From here, the rate of change in flow is representative of the drying stage, which defines Substage E2.

**3.2.2.3 Fracture Aperture Calculations.** Estimates of effective fracture aperture were computed from the horizontal infiltrometer flow and pressure data. Since actual apertures can vary along the length of the fracture, the effective aperture represents an averaging of the various aperture dimensions. Constricted portions will inhibit flow while more dilated portions will increase flow. It is expected that most experiments began with a constant aperture (i.e., the actual aperture equals the effective aperture). However, as the experiment progressed, the apertures likely varied considerably along the fracture length. Figure 3.12 shows the effective aperture variations with time for HI Tests 5C through 11C.

Effective apertures were calculated using the Cubic Law (Appendix F) with an exponent value of three (i.e.,  $n=3$ ) and included the effects of gas compressibility. Note that the effective aperture mimics the flow data, as the two are proportional to one another. The effective apertures for Tests 5C through 11C ranged from 0.014 to 0.031 in. (0.36 to 0.79 mm).

The Reynolds numbers were also calculated from the flow data, and these are also plotted on Figure 3.12. Calculated Reynolds numbers ranged from approximately 2,000 to 9,500, which suggests that the upper-level flows are bordering the turbulent regime. Since the Cubic Law exponent can reduce with increasing turbulence, it is possible that the apertures may be slightly overestimated.

The effective apertures at the end of the initial ramping stage vary from approximately 0.016 to 0.020 in. (0.41 to 0.53 mm), a relative percent difference of 22%. Note also that the apertures are smaller than the thickness of metal plate spacer (i.e., 0.029 in. (0.74 mm)). This difference is attributed to disturbance during the pull, effects of gravity on the upper fracture boundary soils, and compression due to the vacuum pressures.

The fracture apertures were also measured with a feeler gage at the inlet and outlet ends at the completion of each test. The inlet apertures could only be measured for the drying tests, as the fracture was nearly sealed after wetting. For the drying tests 5C, 8C, and 9C, the inlet apertures measured 0.035 in. (0.89 mm), 0.027 in. (0.69 mm), and 0.049 in. (1.2 mm), respectively, which compared to the calculated effective apertures of 0.025 in. (0.64 mm), 0.025 in. (0.64 mm), and 0.031 in. (0.79 mm), respectively. Thus, in general, the apertures at the ends were higher than the final calculated apertures, suggesting preferential drying at the ends. It was also interesting to note that the aperture at the outlet end did not vary between wetting and drying, averaging 0.050 in. (1.3 mm). This

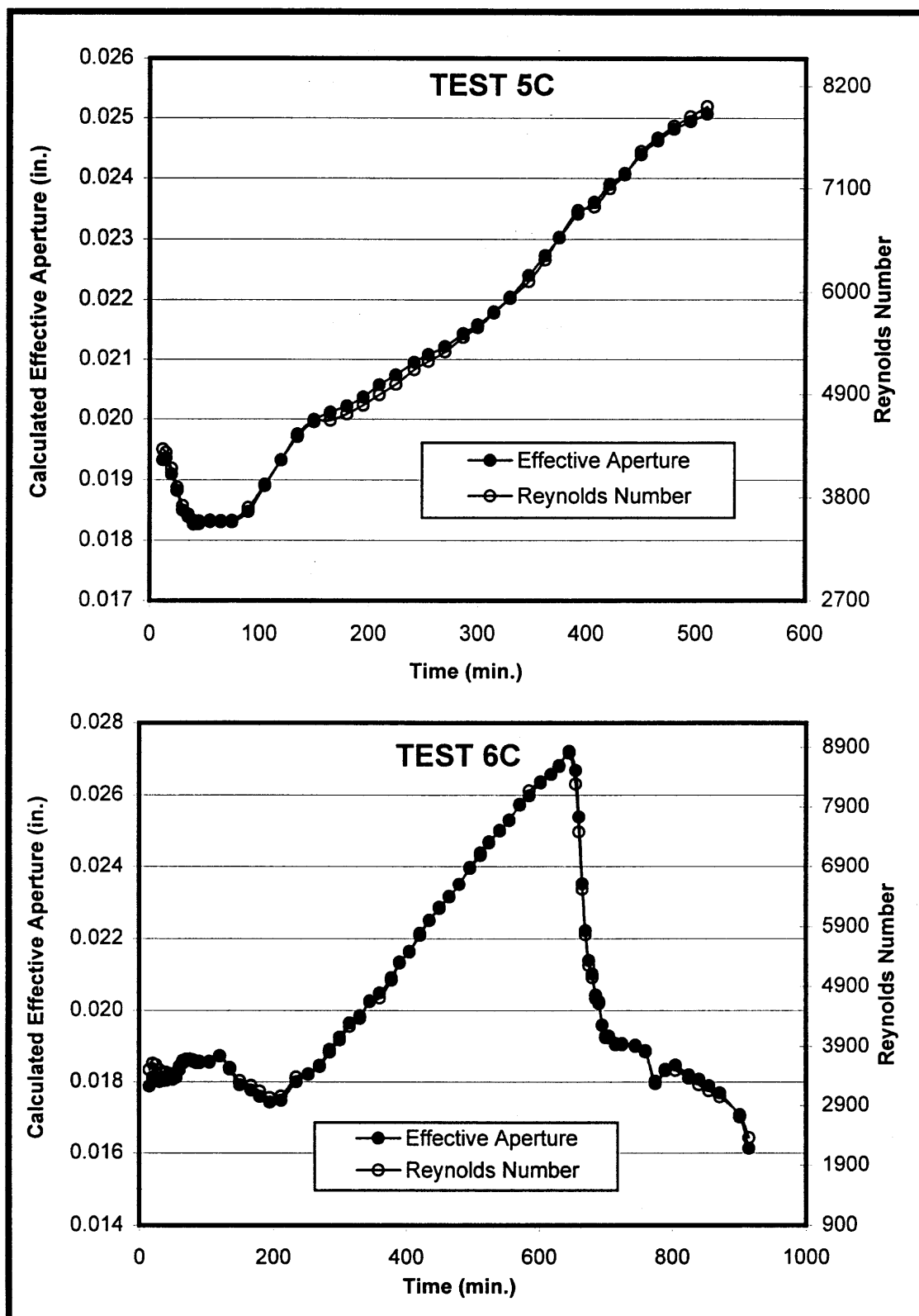


Figure 3.12 Apertures and Reynolds Numbers for HI Tests 5C-11C



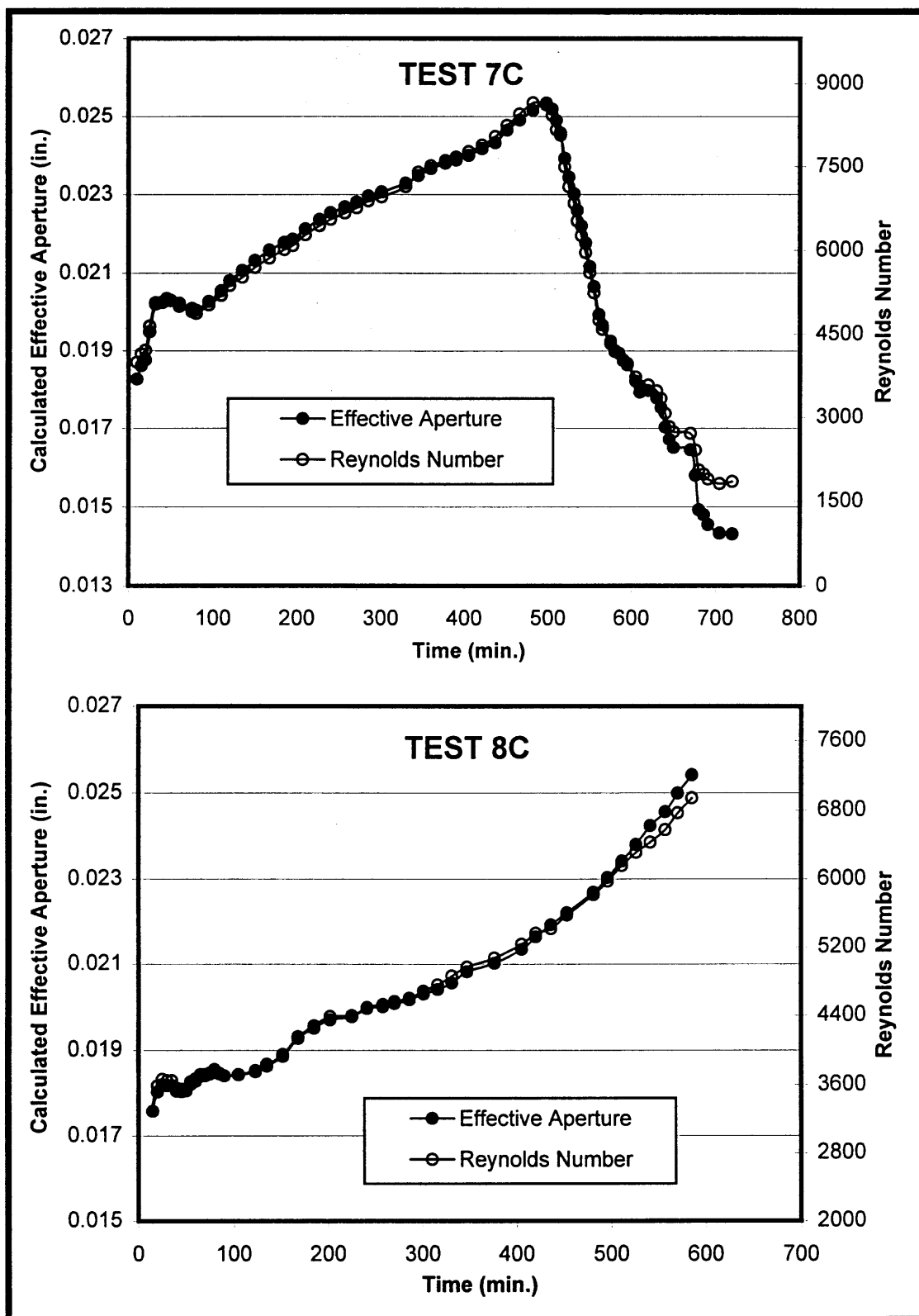


Figure 3.12 (cont'd.) Apertures and Reynolds Numbers for HI Tests 5C-11C

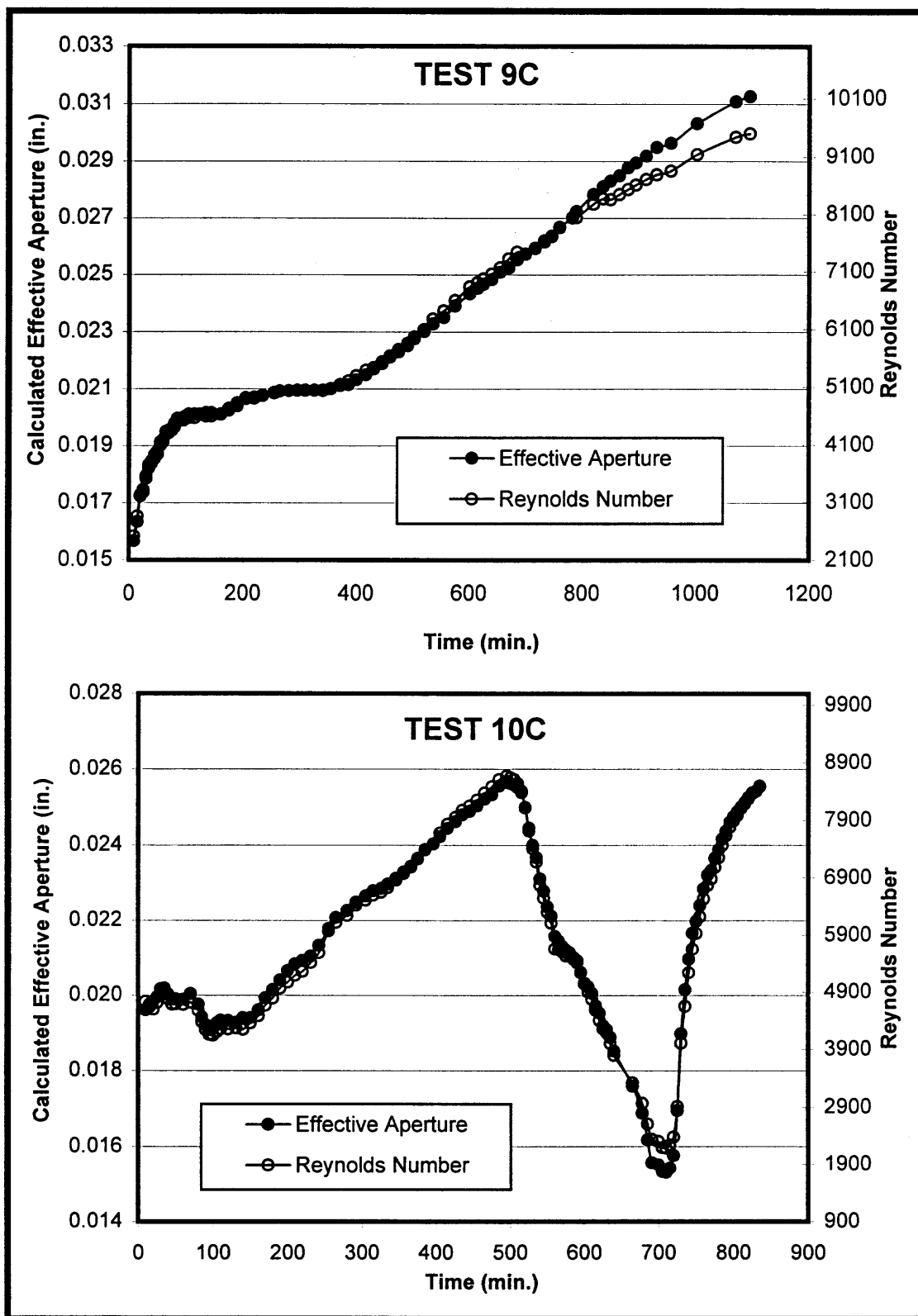


Figure 3.12 (cont'd.) Apertures and Reynolds Numbers for HI Tests 5C-11C

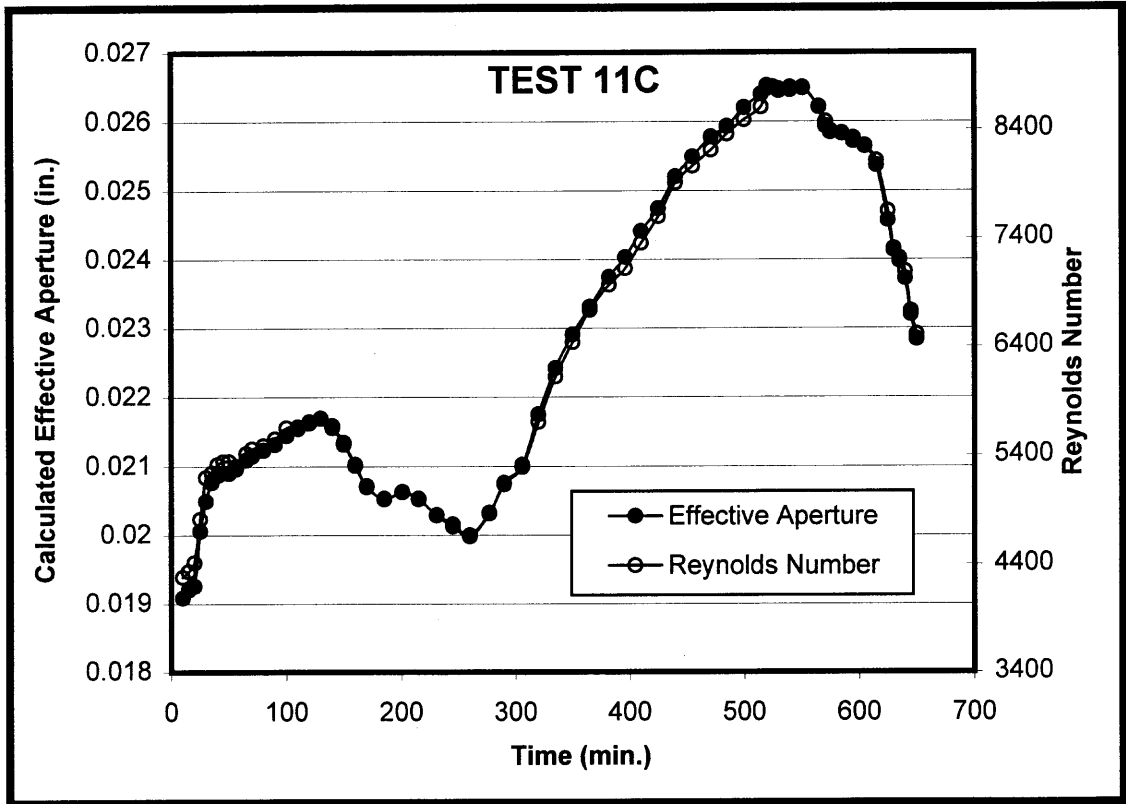


Figure 3.12 (cont'd.) Apertures and Reynolds Numbers for HI Tests 5C-11C

supports the notion that localized swelling occurred at the inlet. The reader is referred to Section 3.2.2.4 for a more detailed discussion of these phenomena.

**3.2.2.4 Moisture Characterization.** This section presents and discusses the results of moisture characterization of the soil block performed at the completion of each horizontal infiltrometer test. It includes modeling results of the moisture data, comparison of moisture properties with flow behavior, and observations during excavation of the block. The supporting raw moisture content data for Tests 5C through 11C are provided in Appendix C.

Modeling of the moisture content data was performed using Rockworks99<sup>®</sup> software, of Rockware, Inc., Golden, CO. The computational results were imported into the three-dimensional graphics software Slicer Dicer<sup>®</sup>, Version 3.03, of Visualogic, Inc., Bellevue, WA. Together, these software produce a solid-zoned model that aids in visualizing the results. A directionally-weighted algorithm was chosen from the Rockworks99<sup>®</sup> software that applied strong biasing along the width of the fracture. The declustering mechanism in the program was disabled because the moisture content data were not evenly distributed. Figure 3.13 presents the graphical output of the solid modeling effort for Tests 5C through 11C. The grading of color and form for a particular test is related to the nature and duration of the environmental change. The pinching off of the data just inside the inlet end is an interpolation anomaly that does not represent the raw data (See Appendix C).

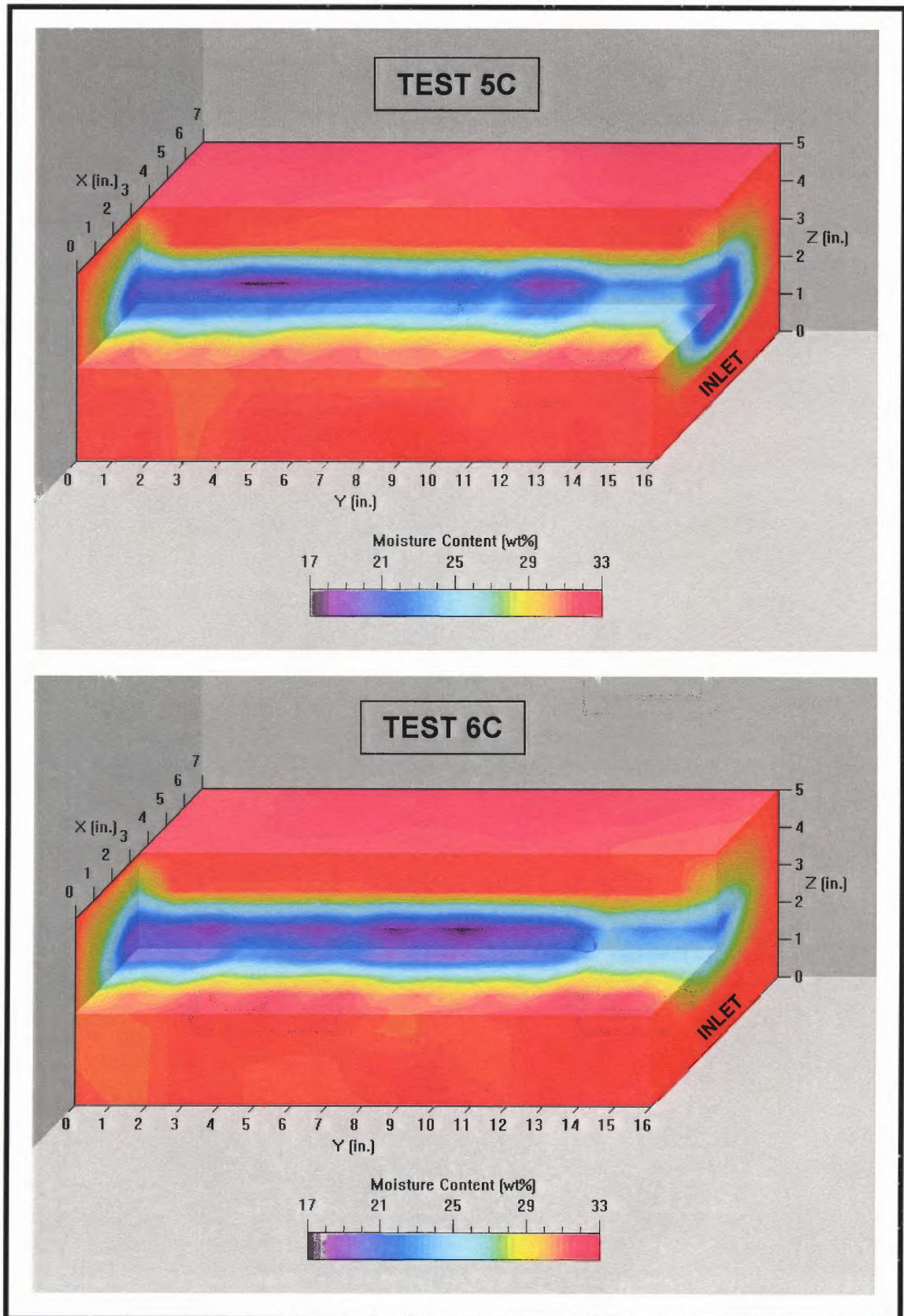


Figure 3.13 Soil Moisture Characteristics of HI Tests 5C-11C



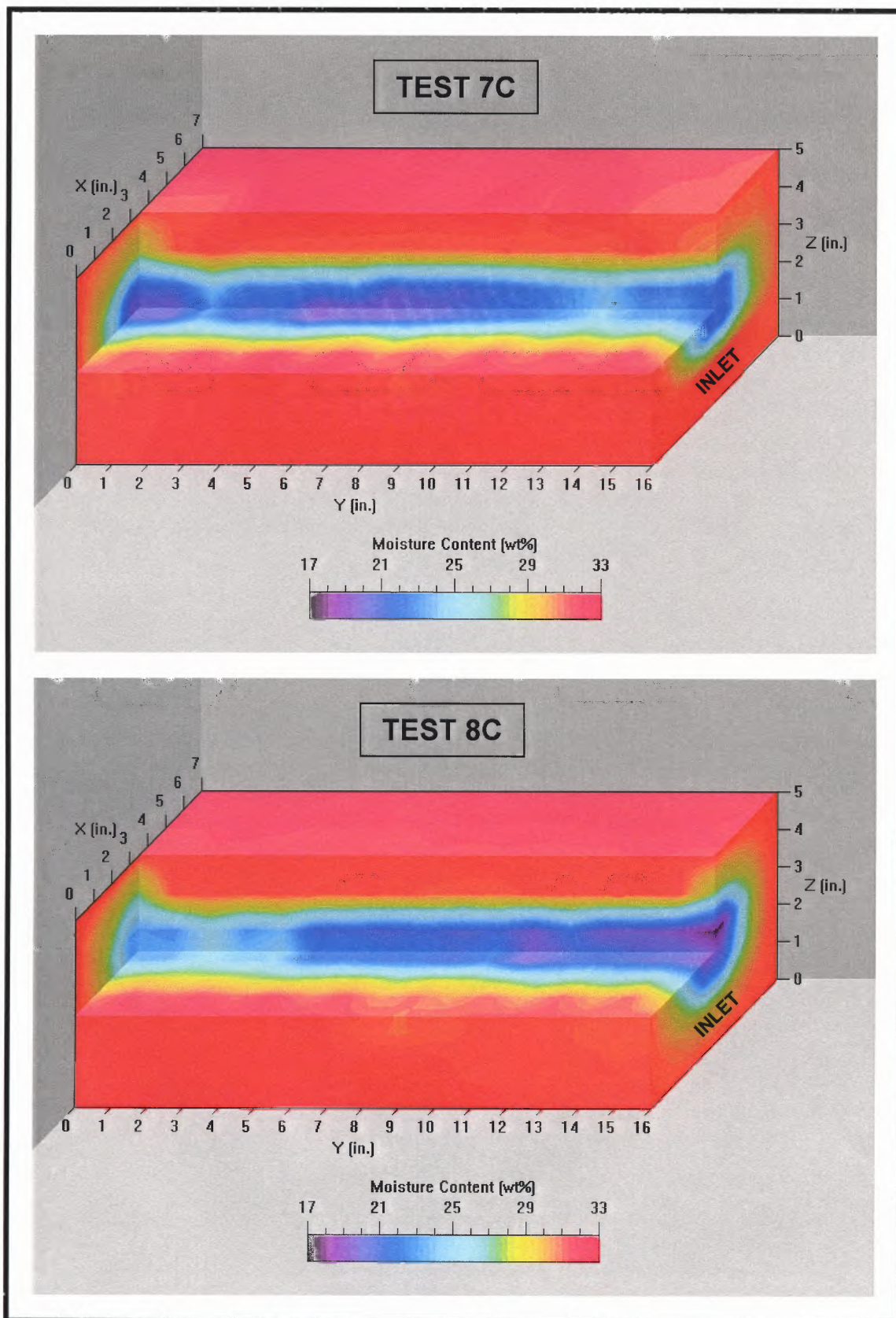


Figure 3.13 (cont'd.) Soil Moisture Characteristics of HI Tests 5C-11C

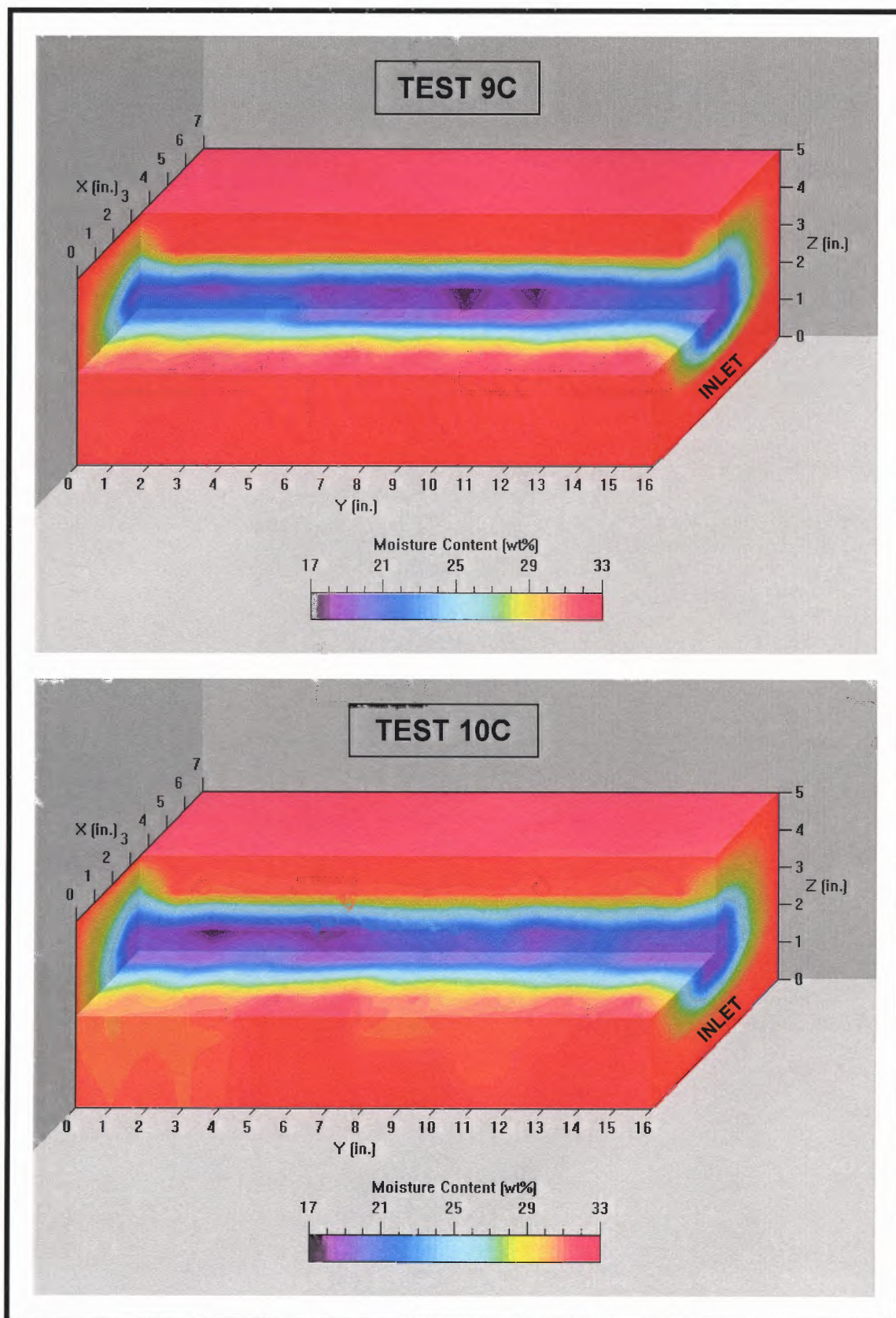


Figure 3.13 (cont'd.) Soil Moisture Characteristics of HI Tests 5C-11C



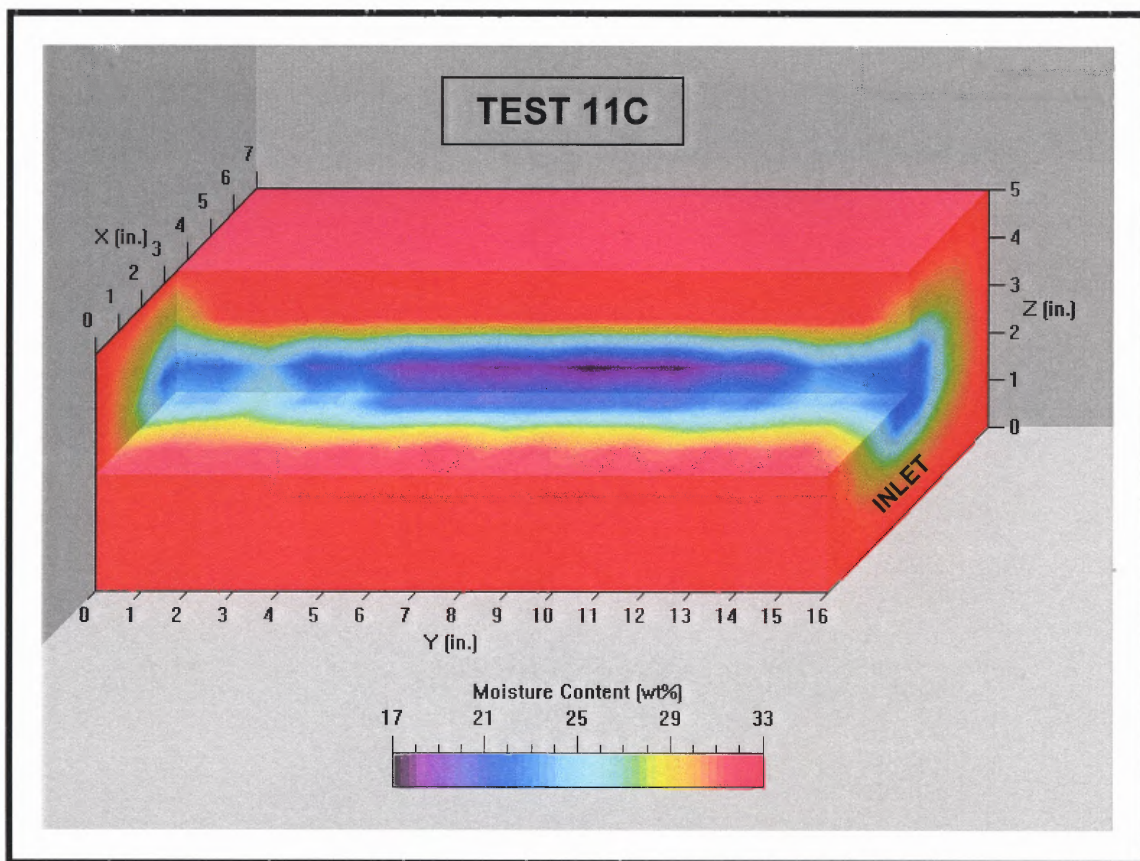


Figure 3.13 (cont'd.) Soil Moisture Characteristics of HI Tests 5C-11C



Vertical cross sections along the length of the soil block, presented in Figure 3.14, show the final moisture distributions above and below the fracture after drying (i.e., Tests 5C, 8C, and 9C), redrying (i.e., Test 10C), and wetting (i.e., Tests 6C, 7C, and 11C). The moisture content data are plotted at average distances from the fracture of zero to 0.25 in. (6.4 mm), 0.25 to 0.5 in. (6.4 to 13 mm), 0.5 to 1.0 in. (13 to 25 mm), 1.0 to 1.5 in. (25 to 38 mm) and 1.5 to 2.5 in. (38 to 64 mm) from the fracture. The moisture contents also represent data that have been averaged across the length of the fracture: the inner eight inches for drying and redrying, and the full length of the soil block for wetting. This is due to the extreme drying and localized wetting on the ends, which is described further in this section. Full cross-sections, from which the computations were performed, are provided in Appendix C. The observations and trends from moisture characterization are summarized below:

1. *Drying occurred as a progressive process outward from the fracture.* Moisture immediately adjacent to the fracture was removed first, followed by a drying front moving outward from the fracture. This is documented by the concentration of drier soils along the center of the soil block, colored in purple and blue (Figure 3.13). The cross-sectional data (Figure 3.14) show that the soils at the fracture decreased to 30 to 50% of the initial moisture content, with moisture contents increasing towards the outer soil boundaries.

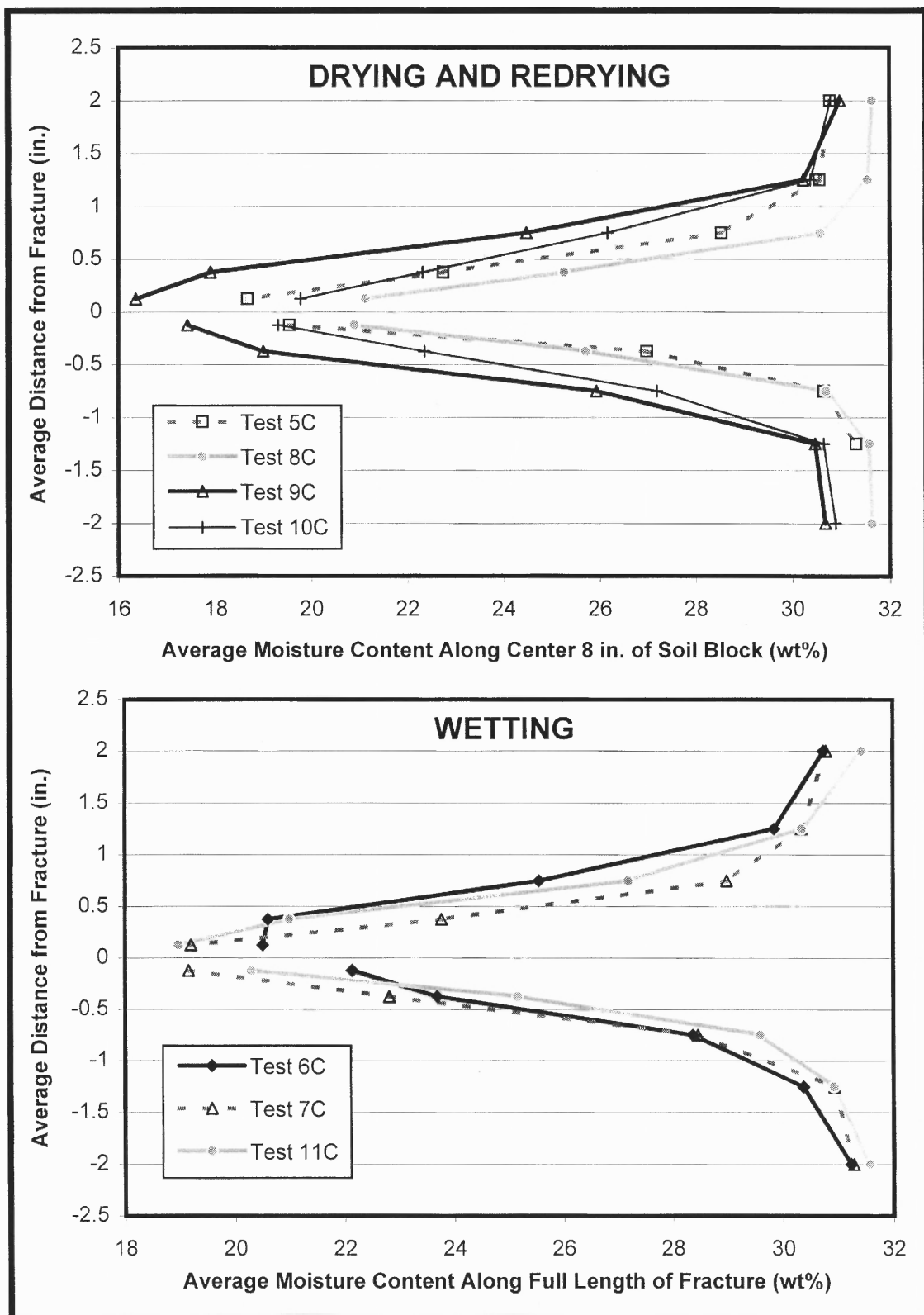


Figure 3.14 Cross-Sections of the Soil Block Length after Drying and Wetting

2. *The drying behavior at the ends was different than the mid-section of the block.* Figure 3.13 shows excessive drying occurred at the inlet, and to a lesser extent, at the outlet. This phenomenon is purely a manifestation of the experimental setup. The mid-sectional data show a more uniform moisture content change, and these data are expected to most closely represent one-dimensional behavior. Thus, moisture content data from the inner eight inches of the soil block along the length of the fracture will be used for calibration and validation of the theoretical model (Chapter 4).

3. *There was preferential drying of the upper fracture boundary soils relative to the lower fracture boundary soils.* Figure 3.14 shows differing moisture contents at equal distances above and below the fracture. This phenomenon is believed to be related to the compaction procedure for the test soil. Prior to placement of the sheet metal spacer, the lower fracture boundary soils were scraped to ensure proper spacer seating. It is believed that the resulting slickensided surface reduced the downward permeability, which retarded drying of the lower boundary soils.

4. *Shrinkage cracks developed vertically from the fracture during drying.* As the soil dried, vertical shrinkage cracks developed outward from the fracture. Upon excavation, the fracture surface showed roughly hexagonal blocks created from shrinkage, with average diameters of 1 in. (2.54 cm). The number of cracks did

not appear to increase with drying, but rather the cracks extended further into the boundary soils away from the fracture. The cracking pattern was similar among all the HI runs. Examples of the shrinkage cracks are shown in Appendix A (Photos A-12 through A-14).

Note that none of the cracks extended to the edge of the block. Thus, there was no flow bypassing the fracture, which was substantiated by pressure tests performed at the conclusion of HI testing. The spikes extending outward in Figure 3.13 are believed to be interpolation anomalies. Thus, it was concluded that all of the measured flow was attributed to fracture flow, since flow through pores of the fracture boundary soils is considered negligible (Section 3.2.3).

5. *Wetting was localized at the inlet end.* Figure 3.13 shows a higher concentration of moist soils at the inlet relative to the rest of the fracture. It is believed that soils at the inlet adsorbed the greatest quantity of moisture because of their proximity to the induced environmental changes. High matric suction values and fallout of moisture droplets from the air stream are two probable mechanisms.

This phenomenon is perhaps best illustrated in observations of the soil block upon completion of the test. The reader is referred to the photographs in Appendix A. Photo A-15 shows that the soils from Test 6C were very wet at the inlet as compared to other parts of the fracture. Wetting also caused the vertical shrinkage cracks to seal at the fracture level (Photo A-16).

Because wetting is localized at the inlet, the aperture constriction is also localized. The inlet end has swollen and almost completely sealed the fracture after wetting for Test 11C (Photo A-17). Having cleared out the entrance of the fracture with a feeler gauge, the constriction was shown to be superficial (Photo A-18). The fracture was wide open behind the entrance soils. This explains why the moisture contents along the fracture are more representative of drying conditions than wetting conditions, even though flows were reduced beyond initial levels. The slightly higher moisture contents of the wetted soils in Figure 3.14, relative to the dried soils, is an averaging effect of data along the full length of the fracture.

The localized inlet-end swelling also has important implications for the redrying behavior. The localized aperture constriction allows for a relatively quick recovery of the fracture aperture when redrying. This is consistent with the flow data that showed a rapid increase in aperture compared with initial drying. The cross-sectional moisture content data for Test 10C also showed that the fracture boundary soils after redrying were similar to those after initial drying.

**3.2.2.5 Summary of Horizontal Infiltrometer Testing Results.** The horizontal infiltrometer tests provided important qualitative and quantitative data related to the hypotheses and objectives of this study. The following is a list of the key results:

- The HI tests verified the concept of a secondary active zone (Section 2.2.3.1).  
The fracture is indeed a means of exposing the soil to environmental changes, which was manifested as drying and wetting progressing outward from the fracture.
- One-dimensional drying was observed near the center of the soil block. Moisture content data in the central zone are considered to be most appropriate for validation and calibration of the theoretical model.
- Shrinkage of the soil occurred three dimensionally. Volume change in the vertical direction was manifested as fracture aperture change, and in the lateral directions as vertical shrinkage cracks.
- Wetting was localized at the inlet, thereby isolating the aperture constriction to the fracture entrance.
- Full closure of the fracture was not observed under the experimental conditions of the horizontal infiltrometer tests.
- During the second stage drying cycle, the fracture was restored to its original aperture. It is noteworthy that the rate of fracture reopening was considerably greater than for the initial drying cycle.

These concepts will be used in the development of the theoretical model presented in Chapter 4. A review of the material parameter tests performed to obtain model input parameters is now presented.

### **3.2.3 Consolidation Testing**

This section presents the results of consolidation tests performed on remolded Potomac Formation clay. A comparison of the computed indices and coefficients with standard correlations in the literature is also included.

The sequence for the consolidation test was an initial loading cycle, followed by unloading, reloading, and a final re-unloading. Figure 3.15 shows variations in the void ratio with each incremental change in pressure. The corrected void ratio represents properties of primary consolidation (i.e., the time-dependent compression or swell due to the dissipation of the excess pore-water pressure). The effects of primary compression and secondary consolidation have been excluded. Table 3.7 is a summary of the resulting calculated consolidation coefficients. The raw time-deformation curves for the various loads are presented in Appendix D.

The initial moisture content of the remolded Potomac clay for the consolidation test was 47.3 wt%, which corresponded to 96.4% saturation. The final moisture content at the conclusion of the test was 39.9 wt%, with an associated saturation of 99.0%. Therefore, for all practical purposes, the entire

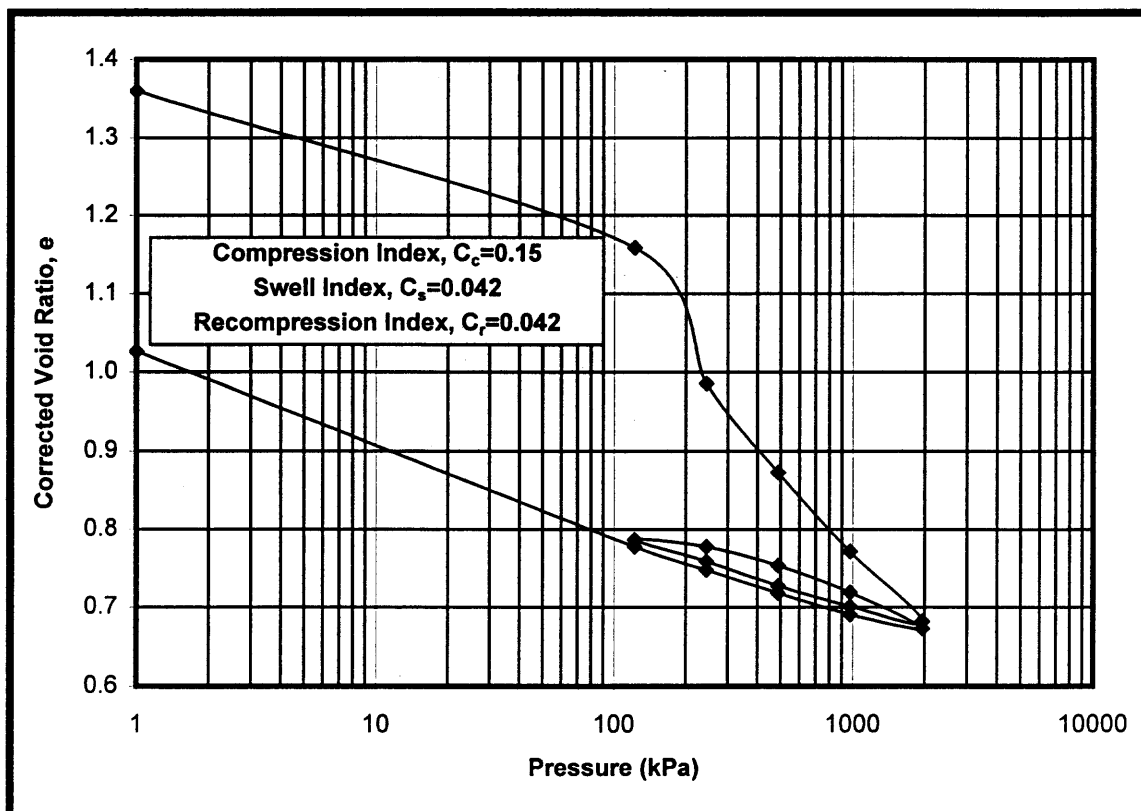


Figure 3.15 Consolidation Test e-log p Plot for Remolded Potomac Clay

Table 3.7 Summary of Consolidation Test Coefficients

Coefficients	Loading (average)	Unloading (average)	Reloading (average)	Reunloading (average)
Coefficient of Consolidation, $c_v$ (in <sup>2</sup> /min) (cm <sup>2</sup> /sec)	5.8 E-04 6.2 E-05	1.9 E-04 2.1 E-05	2.9 E-04 3.1 E-05	1.5 E-04 1.6 E-05
Coefficient of Volume Change, $m_{sv}$ (ft <sup>2</sup> /lb) (m <sup>2</sup> /MN)	1.7 E-05 0.36	3.0 E-06 0.06	2.0 E-06 0.04	1.3 E-05 0.28
Vertical Hydraulic Conductivity, $K_{vs}$ (ft/min) (cm/sec)	3.1 E-09 6.2 E-09	7.7 E-11 1.5 E-10	1.3 E-10 2.5 E-10	1.5 E-10 2.9 E-10



test was run under saturated conditions. Dry unit weight varied from an initial value of 73.1 lb/ft<sup>3</sup> (1.17 g/cm<sup>3</sup>) to a final value of 81.2 lb/ft<sup>3</sup> (1.30 g/cm<sup>3</sup>).

The compression index,  $C_c$ , for the Potomac clay was determined to be 0.15. This represents the change in void ratio over one log cycle of pressure change for the initial loading cycle (i.e., for a 10-fold pressure increase). The swelling index,  $C_s$ , which represents the slope of the unloading curve, was computed to be 0.042. An equivalent value of 0.042 characterized the Potomac clay recompression index. These results are compared with various standard published correlations for natural clays in Table 3.8.

**Table 3.8** Empirical Relationships for Consolidation and Swell Indices

Method	Relationship	Potomac Clay	
		Properties	Index
Terzaghi and Peck (1948)	$C_c' = 0.007 (LL - 10)$	$LL = 65$	0.4
Terzaghi and Peck (1948)	$C_c = 0.009 (LL - 10)$	$LL = 65$	0.5
NFEC (1986)	$C_c = 0.0054 (2.6w - 35)$	Ave. $w = 30\%$	0.2
NFEC (1986)	$C_c = 1.15 (e_o - 0.35)$	$E_o = 1.0$	0.7
Rendon-Herrero (1983)	$C_c = 0.141 G_s^{1.2} ((1+e_o)/G_s)$	$G_s = 2.76$ $e_o = 1.0$	0.3
Nagaraj and Murty (1985)	$C_c = 0.2343 (LL/100) G_s$	$LL = 65$ $G_s = 2.76$	0.4
Kulhawy and Mayne (1990)	$C_c = PI/74$	$PI = 38$	0.5
Nagaraj and Murty (1985)	$C_s = 0.0463 (LL/100) G_s$	$LL = 65$ $G_s = 2.76$	0.08

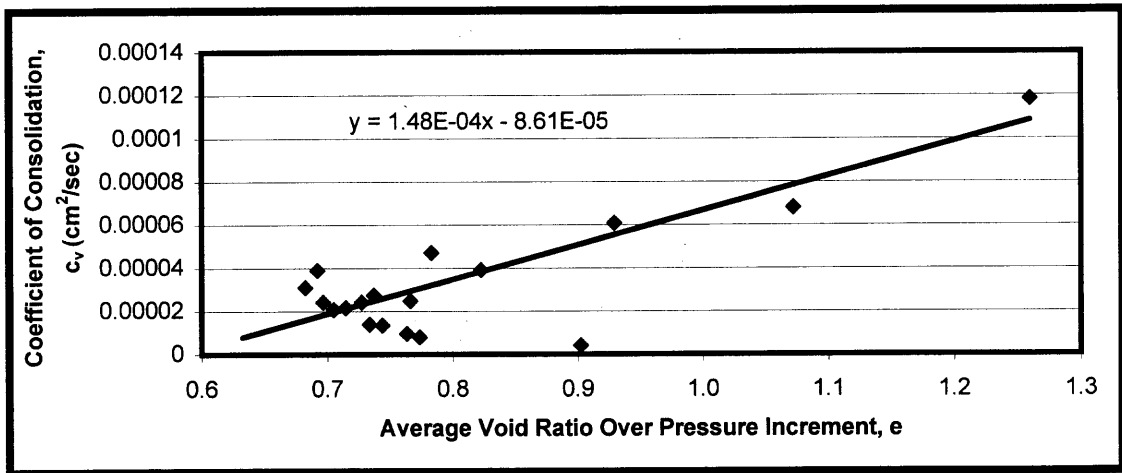
$C_c'$  Compression Index for remolded soil;  $C_c$  Compression Index for natural soils;  $LL$  liquid limit;  $w$  natural water content;  $e_o$  initial void ratio;  $G_s$  specific gravity;  $PI$  plasticity index;  $C_s$  Swell Index

In general, the values determined for the test soil tended towards the lower end of the range of published values. This is attributed to remolding, which typically reduces index values 25 to 50% compared with undisturbed soils (Lambe and Whitman, 1979).

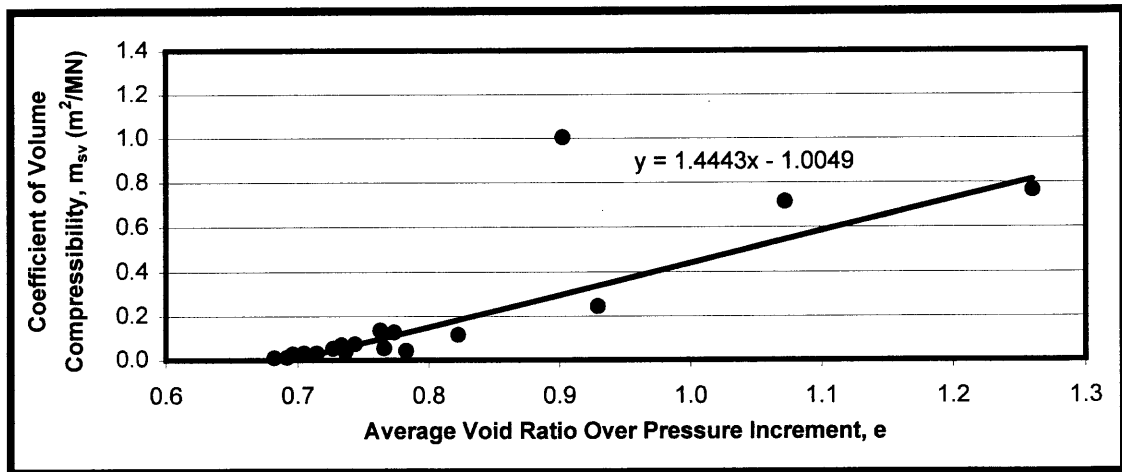
The coefficient of consolidation,  $c_v$ , from which the consolidation indices are computed, is important since it is an indicator of the rate of compression or swell under the load increment. The  $c_v$  values were calculated by the log fitting method and varied almost two orders of magnitude (Table 3.7). As expected, the coefficient of consolidation appears to be a linear function of void ratio, as shown in Figure 3.16.

An average  $c_v$  value of  $5.8 \times 10^{-4} \text{ in}^2/\text{min}$  ( $6.2 \times 10^{-5} \text{ cm}^2/\text{sec}$ ) characterizes the virgin compression curve, and a value approximately half of that, at  $2.4 \times 10^{-4} \text{ in}^2/\text{min}$  ( $2.6 \times 10^{-5} \text{ cm}^2/\text{sec}$ ), represents the reloading curve. Computed  $c_v$  values for the first and second unloading stages were similar, with average values  $1.7 \times 10^{-4} \text{ in}^2/\text{min}$  (of  $2.1 \times 10^{-5} \text{ cm}^2/\text{sec}$ ) and  $1.6 \times 10^{-4} \text{ in}^2/\text{min}$  ( $1.7 \times 10^{-5} \text{ cm}^2/\text{sec}$ ), respectively. Correlations between  $LL$  and  $c_v$ , presented by NFEC (1986), suggest that the results of the consolidation test performed as part of this study are representative of completely remolded samples. Note that the void ratio of disturbed samples under a particular effective stress is lower than the equivalent undisturbed sediments, particularly for sensitive soils (Mitchell, 1993).

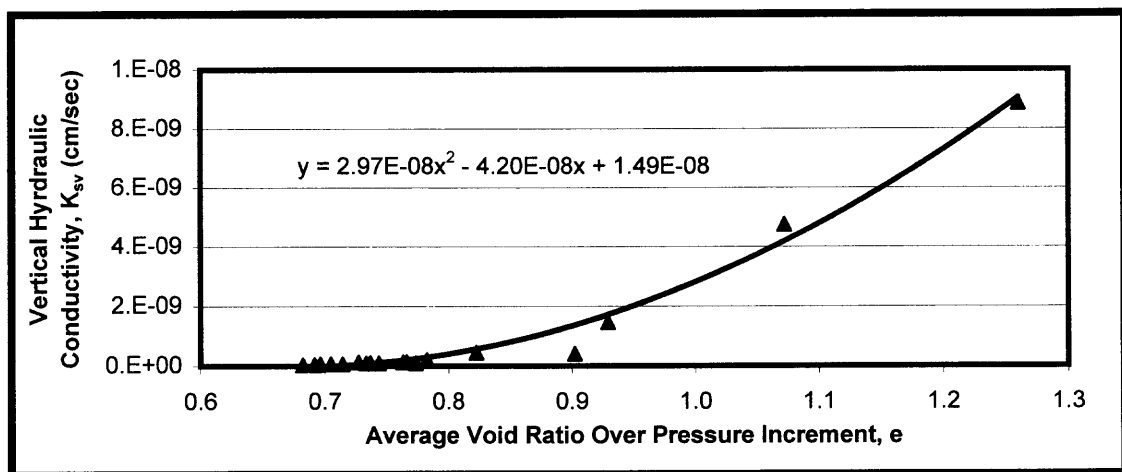
The saturated coefficient of volume change,  $m_{sv}$ , is the compression or swell of a soil layer per unit of original thickness due to a given unit increase in



a.



b.



c.

Figure 3.16 Effect of Void Ratio on a) Coefficient of Consolidation; b) Coefficient of Volume Compressibility; and c) Hydraulic Conductivity

pressure (i.e.,  $\partial \varepsilon_v / \partial \sigma_s$ ). It is also known as the coefficient of volume compressibility and the modulus of volume change. For the Potomac clay, the  $m_v$  varied from  $5 \times 10^{-7}$  to  $6 \times 10^{-5}$  ft<sup>2</sup>/lb (0.01 to 1.15 m<sup>2</sup>/MN). Averages values of  $2 \times 10^{-5}$ ,  $3 \times 10^{-6}$ ,  $2 \times 10^{-6}$ ,  $1 \times 10^{-5}$  ft<sup>2</sup>/lb (0.36, 0.06, 0.04, and 0.28 m<sup>2</sup>/MN) characterized the loading, unloading, reloading, and reuniting stages, respectively. The lower end compressibilities are expected to be most representative of the natural, undisturbed Potomac clay, as they are typical of heavily overconsolidated clay (Head, 1994). Figure 3.16 shows that the saturated coefficient of volume change is also a linear function of void ratio.

Saturated vertical hydraulic conductivities,  $K_{sv}$ , were computed directly from the consolidation test data at each void ratio. The values varied from  $10^{-11}$  to  $10^{-10}$  to  $10^{-8}$  ft/min ( $10^{-9}$  to cm/sec) and again showed a strong correlation to void ratio (see Figure 3.16). The very low conductivity is representative of unweathered marine clays, which have typical hydraulic conductivities of  $1.5 \times 10^{-10}$  to  $3.9 \times 10^{-7}$  ft/min ( $8 \times 10^{-11}$  to  $2 \times 10^{-7}$  cm/sec) (Domenico and Schwartz, 1990).

The preconsolidation pressure could not be determined since the samples were completely remolded. Obermeier et al. (1984), however, reported preconsolidation values of 20 to 40 ksf (10 to 20 kgf/cm<sup>2</sup>) in excess of existing overburden, even on hilltops. Preconsolidation values were shown to increase with depth by an amount approximately equal to the increased overburden stress. It was suggested that the high preconsolidation has been imparted

primarily by the weight of overlying sediments, which were later removed by erosion.

### **3.2.4 Water Retention Testing**

This section describes the results of the water retention and associated suction testing. The two major outcomes are descriptions of the moisture-volume and the moisture-suction relationships for the remolded Potomac clays. These are represented in Figures 3.17 and 3.18 as shrinkage and water retention (or characteristic) curves, respectively.

Results of the water retention tests suggest that there is a very large normal shrinkage range. A linear relationship is evident in Figure 3.17 between the specific volume and the moisture content. Thus, as moisture is removed, the soil structure collapses in volume equal to the volume of water removed. This implies that the soil is saturated throughout the linear portion of the shrinkage curve. For the Potomac clays, this behavior is expected through the entire range of both natural and anthropogenic moisture fluctuations. Thus, in a field situation, the volume reduction of the soil is manifested as cracking rather than pore desaturation.

Naturally occurring expansive soils are generally considered to be unsaturated in the literature. The results of this study show that these results must be qualified for the expansive soil types. The unsaturated component is comprised only of fracture (or crack) volume. Thus, the traditional methods for

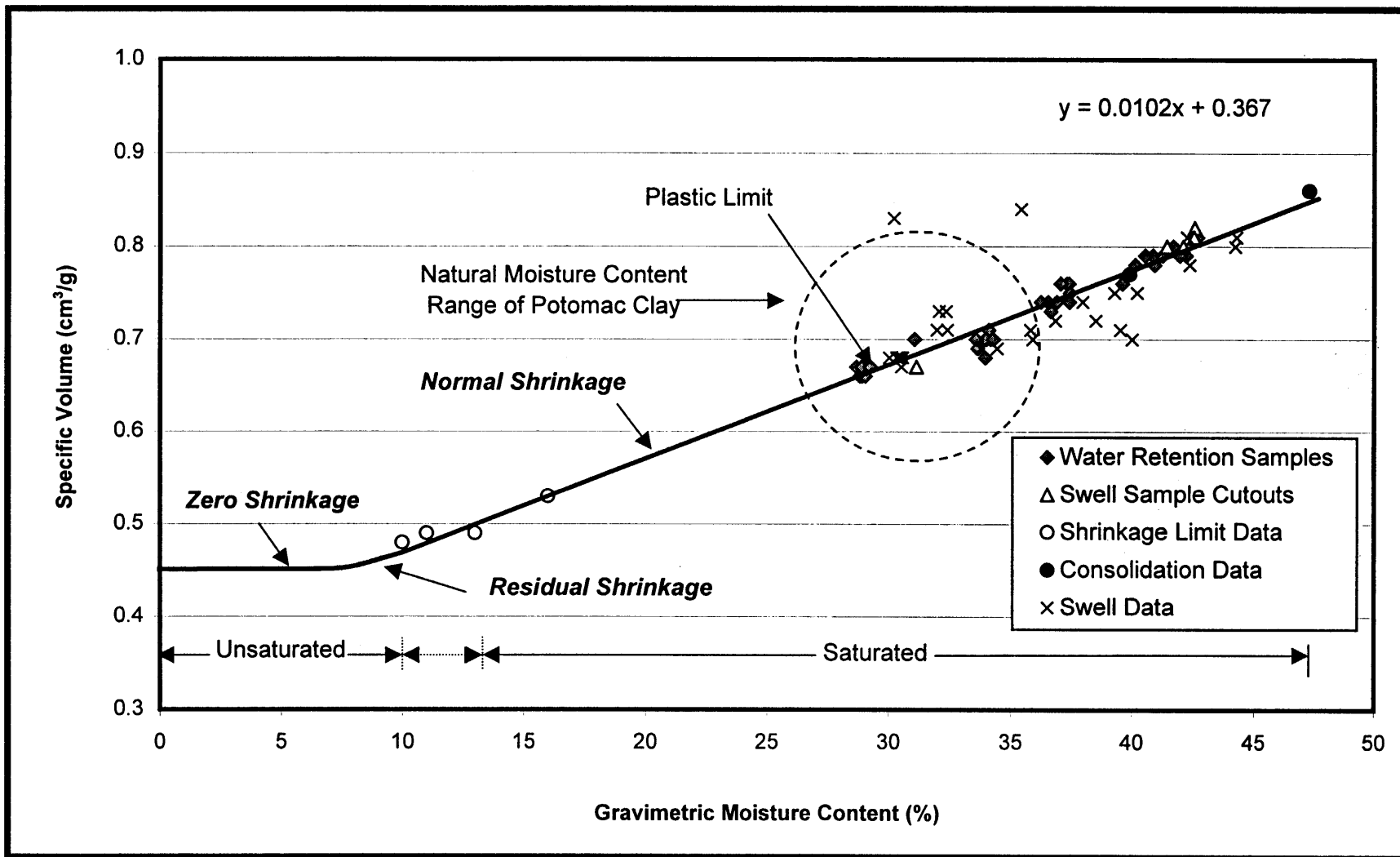


Figure 3.17 Shrinkage Curve for Remolded Potomac Clay

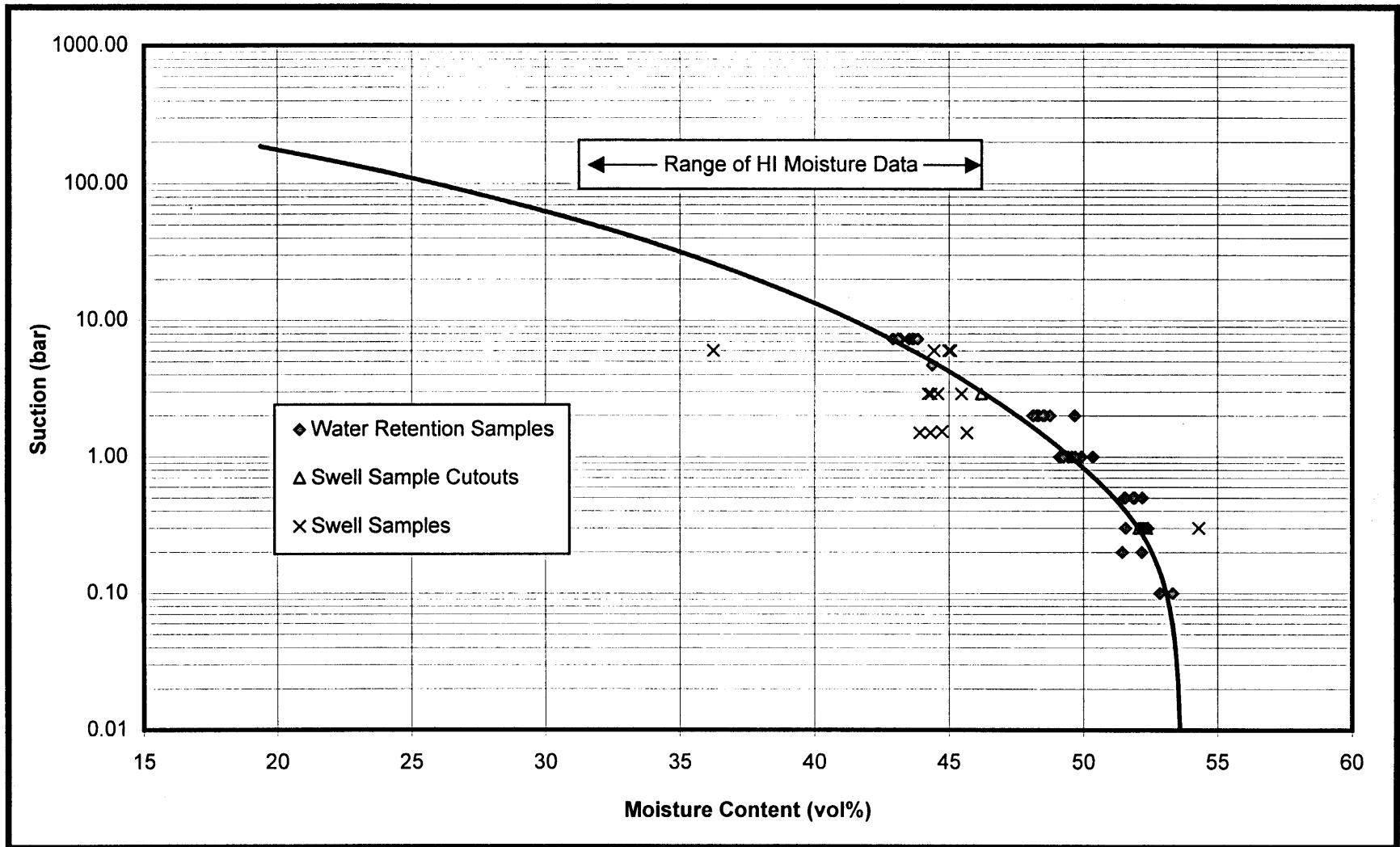


Figure 3.18 Desorption Water Retention Curve for Remolded Potomac Clay

describing unsaturated hydraulic conductivities, based on pore-size distribution models, may not be appropriate for modeling expansive soils.

Note that the data are most consistent where the volume was measured using the wax method (i.e., water retention samples, swell sample cutouts, and shrinkage limit data). The consolidation data also showed good agreement. The moisture-volume relationships for the swell samples are believed to be less accurate due to slight cracking from pressure plate equilibration and averaging effects of the height of the specimen after drying.

The shrinkage curve may also be used to determine the relationship between gravimetric and volumetric moisture contents, where  $\rho_w \theta = \rho_d w$ . Dry density may be computed from Figure 3.17 as the inverse of the specific volume. Note that the dry density of the soil varies from 75 to 131 lb/ft<sup>3</sup> (1.2 to 2.1 g/cm<sup>3</sup>) over a 37 wt% range in moisture. Thus, montmorillonite soils may be considered expansive at moisture contents from the *SL* to well beyond the *PL*.

Figure 3.18 shows the specific moisture capacity function,  $\theta(\mu)$ , for the remolded Potomac clays. The form of this function is typical of clays. The moisture content at which the suction drops sharply with very little additional water being added, 53.5 vol% (44 wt%) is the field capacity. This is the point at which additional water drains away rather than being absorbed into the soil. It is the maximum amount of water the soil can hold and thus represents a 'zero' suction.



At moisture contents below the field capacity, the soil is in a state of suction. This suggests that while the soil pedes are saturated, the pore-water pressures are negative, comparable to the capillary fringe in groundwater applications. Again, this suggests a unique property of expansive soils.

The shrinkage curve is considered estimated since matric suction was inferred primarily from equilibration suctions. Psychrometer and filter paper suction testing verified that the soils did not reach equilibrium, especially at the higher suctions (Table 3.9).

**Table 3.9** Summary of Suction Testing Results

<b>Equilibration Matric Suction (bars)</b>	<b>Total Suction: Thermocouple Psychrometer (bars)</b>	<b>Total Suction: Filter Paper (bars)</b>	<b>Matric Suction: Filter Paper (bars)</b>
<b>Water Retention Samples</b>			
0.1	--	--	--
0.2	--	--	--
0.3	--	--	--
0.5	--	--	--
1.0	--	--	--
2.0	--	--	--
5.0	4.7	--	--
15.0	7.3	--	--
<b>Swell Test Samples</b>			
0.3	--	0.6	0.3
1.0	--	9.3	6.0
5.0	2.9	--	--
15.0	2.1	2.0	1.5

-- Not tested

This was due to a reduced area of flow as the soil shrunk away from the ceramic plate, combined with the extremely low soil permeability ( $10^{-10}$  to  $10^{-8}$  to ft/min ( $10^{-11}$  to  $10^{-9}$  cm/sec)). The suctions for the swell test samples are expected to be underestimated on account of drying which is believed to have occurred between equilibration and swell testing. Despite the equilibration and suction measurement problems, the form of the curve is generally representative of field suctions. Nelson and Miller (1992) observed that expansive clay soils generally exhibit field suction between 1 and 100 atm (100 and 10,000 kPa), which is the general range for this data.

### 3.2.5 Swell Testing

The swell testing results for the Potomac remolded clay are presented in this section. A comparison to related literature results is also included. The reader is referred to Section 3.2.4 for a discussion of the suction testing results associated with the swell tests.

The final results of the swell testing are presented in Figure 3.19 as the relationship between primary swell and overburden pressure for a variety of soil suctions. This relationship was determined from individual time-deformation plots, which are provided in Appendix E.

The depths associated with the overburden pressures may be calculated for the Potomac clay by assuming a variation in dry density of 75 to 131 lb/ft<sup>3</sup> (1.2 to 2.1 g/cm<sup>3</sup>) from the shrinkage curve (Figure 3.17). Table 3.10 shows the

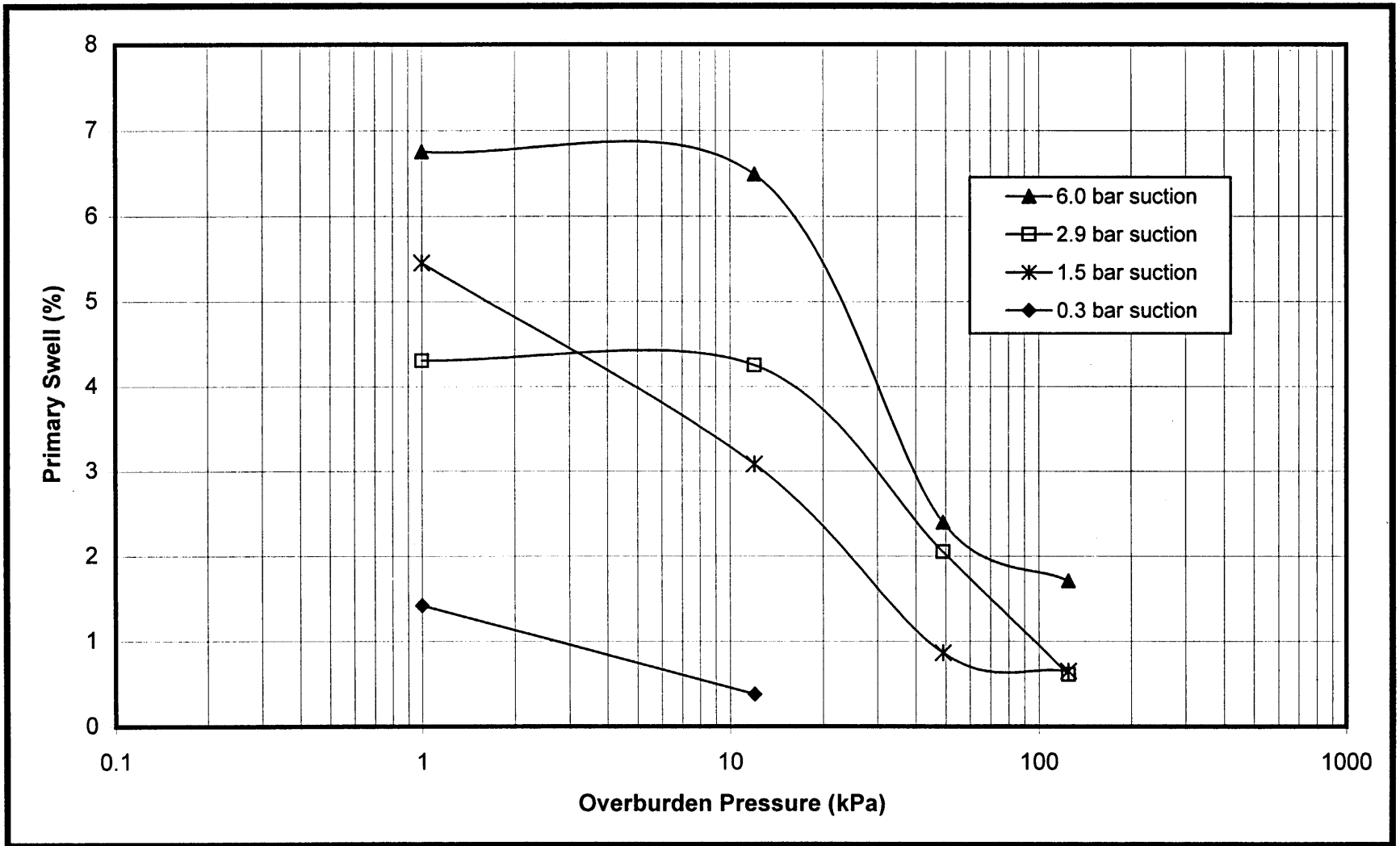


Figure 3.19 Swell Test Curves for Remolded Potomac Clay

overburden pressures used for swell testing and the corresponding depths below ground surface.

**Table 3.10** Depths Associated with Overburden Pressures

Overburden Pressure (kPa)	Depth Below Ground Surface*	
	(ft)	(m)
1	0.2 to 0.4	0.07 to 0.13
12	2 to 3	0.6 to 1.0
49	8 to 14	2 to 4
125	20 to 35	6 to 11

\*For a range of dry densities from 2.1 to 1.2 g/cm<sup>3</sup> (131 to 75 lb/ft<sup>3</sup>)

At a depth of approximately 0.3 ft (1 m) below ground surface, the Potomac clay exhibited a range of primary swell from 7% at 6 bar (600 kPa) suction (i.e., 44 vol% or 30 wt%) to 1.5% at 0.3 bar (30 kPa) suction (i.e., 53 vol% or 43 wt%). It is interesting to note that even soils 20 to 35 ft (6 to 11 m) below ground surface still exhibited swell from 0.5 to 1.8%. The percent swell is slightly higher than that reported in the literature. Byle and Davit (1992) reported magnitudes of 4.4% and 1.3% under vertical pressures of 50 and 300 lb/ft<sup>2</sup> (0.2 and 1.2 kPa) on remolded Potomac clay from south central Fairfax County.

The calculated coefficients of volume change ( $m_v$ ) for the remolded Potomac clay are shown in Table 3.11, representing the relationship between vertical strain and effective stress (i.e.,  $\partial \varepsilon_v / \partial \mu$ ).

**Table 3.11** Coefficients of Volume Change for Monotonic Wetting at Various Overburden Pressures

Overburden Pressure (kPa)	Average Void Ratio	Coefficient of Volume Change		
		bar <sup>-1</sup>	ft <sup>2</sup> /lb	m <sup>2</sup> /kN
1	1.0	0.0075	3.6 E-06	0.08
12	1.0	0.0099	4.7 E-06	0.10
49	1.1	0.0030	1.4 E-06	0.03
125	0.9	0.0026	1.2 E-06	0.03

The results range from 1.2 to 3.6 × 10<sup>-6</sup> ft<sup>2</sup>/lb (0.03 to 0.10 m<sup>2</sup>/kN), which are similar to the unloading cycle of the consolidation test, where the coefficient of volume change averaged 3.0 × 10<sup>-6</sup> ft<sup>2</sup>/lb (0.06 m<sup>2</sup>/kN). However, based on the expected underestimation of the suction values (see Section 3.2.4), the  $m_v$  coefficients calculated from the swell test results are believed to be overestimated. Appropriate adjustments must be made to account for the effect of void ratio on the  $m_v$  coefficient.

This concludes the chapter on the experimental portion of this study. The following chapter describes the theoretical modeling, which paralleled the experimental work.

## CHAPTER 4

### THEORETICAL MODELING

#### 4.1 General Model Approach

This section outlines the approach for development of the 'Fracture Volume Change Model' (FVC Model). The model is used to predict changes in fracture geometry resulting from volume change in expansive clay soils. While others have attempted similar models, the literature review suggests that this study is the first attempt to model: (1) discrete fractures; (2) horizontal fractures, (3) fractures at depth, and (4) volume changes induced from environmental conditions within the fracture. This section begins with a description of the physical concepts behind the model. Next, the assumptions and conditions are reviewed, followed by a description of the mathematical approach.

##### 4.1.1 Physical Concept

There are three basic physical mechanisms by which the geometry of a discrete fracture may change over time in a fine-grained soil. These are illustrated in Figure 4.1 and are briefly described below:

1. **Volume Change** (Fig. 4.1a). Volume change occurs in soil when there is a shift in environmental conditions such as moisture fluctuation. Affected soils will shrink or swell depending on the nature of the environmental change. If the soil formation contains fractures, then the volume change

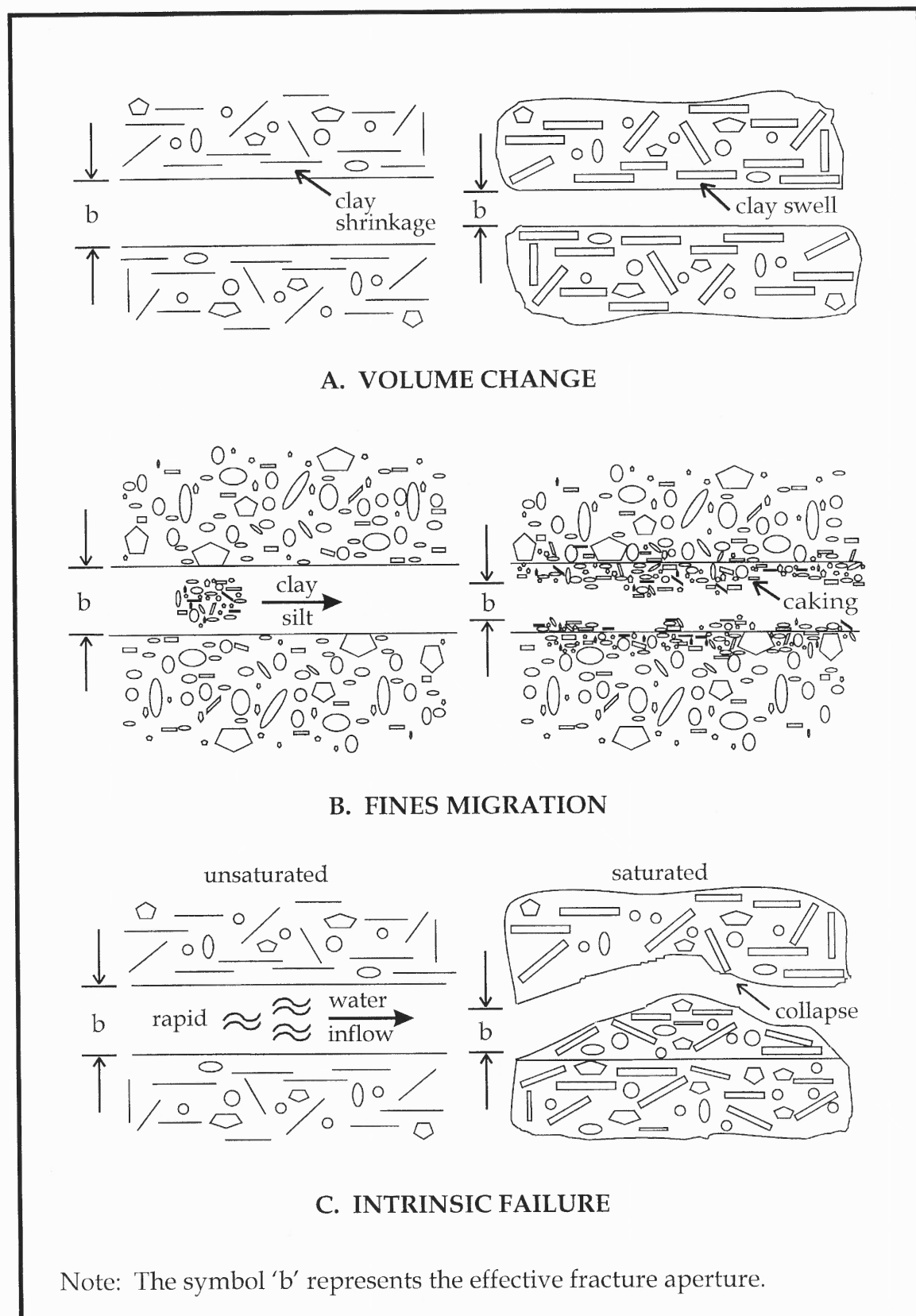


**Figure 4.1** Physical Mechanisms for Changes in Horizontal Fracture Geometry

will affect the geometry of the fracture, i.e., it causes the fracture to dilate or constrict. This behavior is most noticeable in clays, and it is strongly expressed in clays containing montmorillonite.

2. **Fines Migration** (Fig. 4.1b). In some soils, fine particles of clay or silt dislodge from the matrix, become suspended in the pore fluid, and are transported by advective flow. The deposition or removal of these particles from the fracture boundary results in a localized change in effective aperture. The accumulation of transported particles is known as 'caking,' which causes a reduction in primary permeability. The soil dispersivity determines the propensity for this behavior; non-saline soils with Na-based exchange complexes or illite dominance are particularly susceptible.
  
3. **Intrinsic Failure** (Fig. 4.1c). Intrinsic failure is the breaking of weak interparticle bonds as the swelling process pulls clay particles apart (Murray and Quirk, 1990). Large pressures induced from rapid wetting may lead to tensile failure and localized collapse of fracture boundary soils. Non-saline soils with Ca-based exchange complexes are prone to this behavior, especially those at high matric suction.

Among these, volume change is expected to have the greatest effect on fracture geometry, and it is thus the focus of this model. In order to investigate



this mechanism, a physical model of the soil system must first be established. Consider a hypothetical, idealized fracture, as portrayed in Figure 4.2, with its width, length, and height aligned along the  $x$ ,  $y$  and  $z$ -axes, respectively.

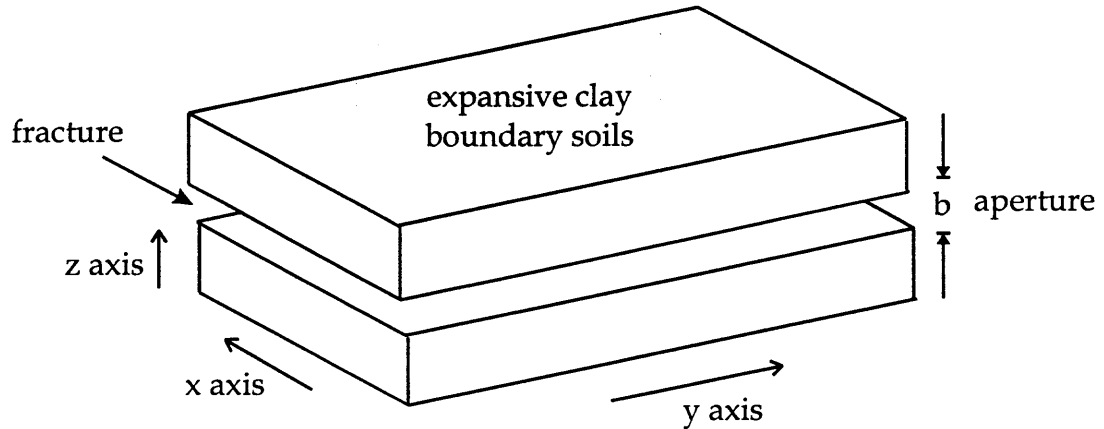


**Figure 4.2** Representative Elemental Volume (REV) for the Current Study

The walls of the fracture are parallel, and the distance between the walls is termed the fracture aperture, or  $b$ . The soils that bound the discrete fracture, termed 'fracture boundary soils,' are assumed to be expansive. This physical model will be retained as the representative elemental volume (REV) throughout the current study.

The means by which volume change affects the REV is next considered. Fluid moving through the REV, which may be in either a gaseous or liquid state, causes the soil to change from its equilibrium state on account of a shift in environmental conditions. The fracture boundary soils are most affected since

fluid flow in fine-grained formations occurs predominantly along the fracture. In response, the fracture boundary soils attempt to seek equilibrium with the new stress state. Dissipation of induced pressures (positive or negative) results in an adjustment to the soil structure. For expansive clay soils, the deformation is manifested in the form of either shrinking or swelling.

It is further hypothesized that the fracture aperture,  $b$ , will undergo significant changes due to the lack of restriction against movement into the open fracture. The degree of change in fracture aperture is a function of the conditions within the REV. There are three general conditions of saturation that may prevail in the REV that are described below. The effects of these conditions for the desiccation case are illustrated in Figure 4.3, although they apply to both shrinking and swelling.

**Condition 1:** *Water is removed from initially saturated fracture boundary soils and a saturated state prevails.* In this case, as water is removed, the soils are capable of adjusting their structure to accommodate the loss in volume. As a result, a saturated state is maintained. Volume change of the soil is proportional to the volume of water removed. For the swelling case, this would entail an increase in moisture content of already saturated soils. This condition is primarily a consequence of the expandable structure of montmorillonite clay minerals and correlates to the structural/normal shrinkage phases defined by the soil scientists (Section 2.5.1).

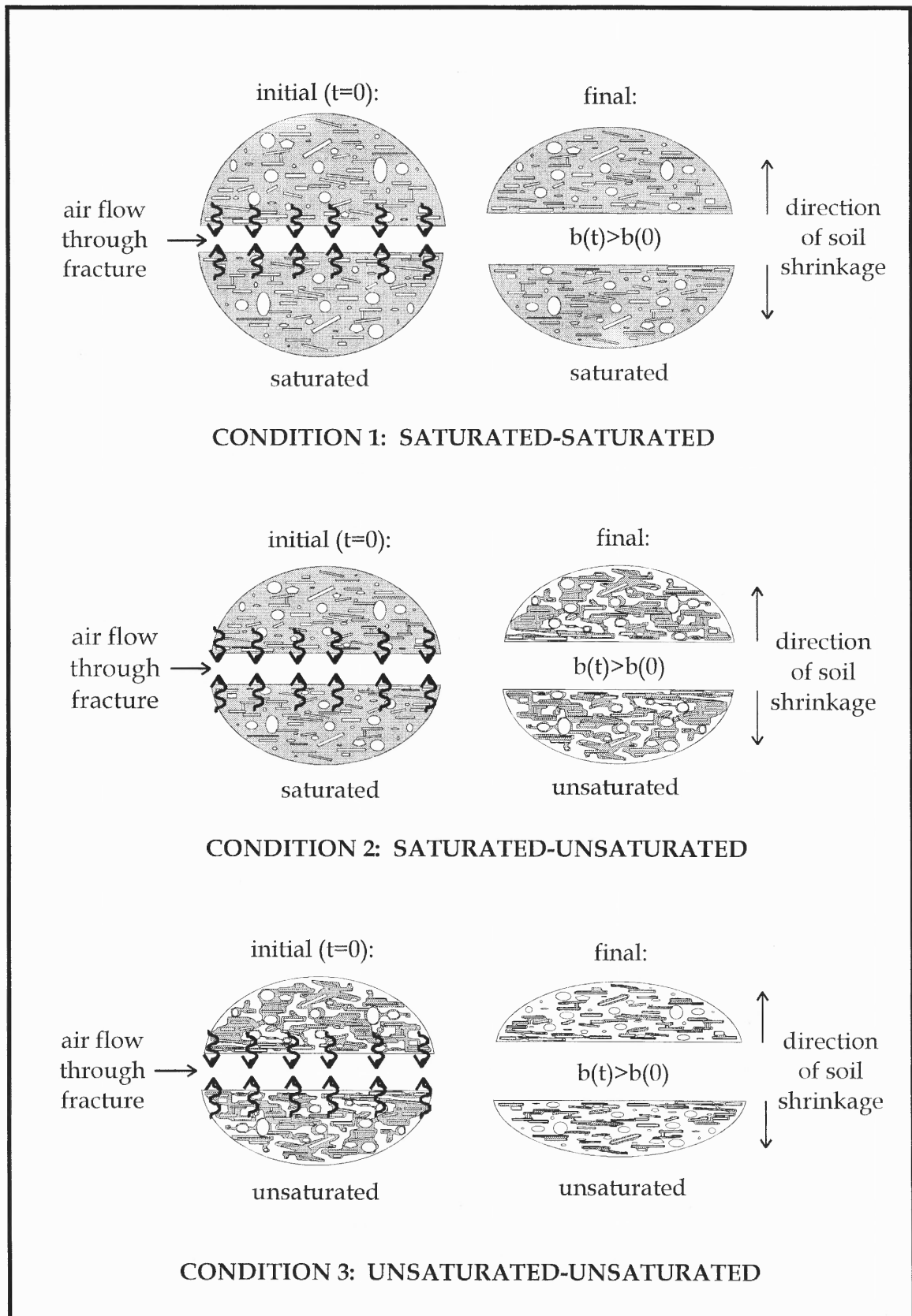


Figure 4.3 Conditions for Volume Change in the REV (Case of Desiccation)

**Condition 2:** *Water is removed from initially saturated fracture boundary soils and an unsaturated state prevails.* This condition represents the case where air replaces lost water in the soil pores as water is removed. The resultant volume change of the soil is less than the equivalent volume of soil water removed. For the swelling case, this condition represents water uptake by initially unsaturated soils. The supply of water is large enough that the soil subsequently becomes saturated. This condition correlates to the transition between the normal and residual shrinkage phases defined by the soil scientists (Section 2.5.1).

**Condition 3:** *Initially unsaturated fracture boundary soils are further reduced in moisture content.* In this case, unsaturated pores are further desaturated, with additional air entering the pores. For the swelling case, water displaces the air in the soil pores, yet the soil remains in an unsaturated state. This condition correlates to the residual shrinkage phase defined by the soil scientists (Section 2.5.1).

While a change in fracture aperture occurs for all three conditions, the relevance of each differs. In the current study, the saturated to saturated case (i.e., Condition 1) is most significant since expansive soils remain in the normal shrinkage state for the range of typical field moisture fluctuations. Also, this state exhibits the maximum amount of soil volume change for a given change in

moisture. Thus, the focus of the theoretical work is directed towards the saturated case.

#### 4.1.2 Assumptions

The analysis of volume change is complex as it involves the coupling of phenomena from the fields of fluid mechanics, soil mechanics, soil physics, and thermodynamics. To solve a problem of this complexity, a basic set of assumptions must be established. These assumptions may not be strictly satisfied in reality, but they are necessary in order to arrive at a solution. The assumptions, which are presented below, apply to the physical model presented in Figure 4.2. A justification of each assumption is provided along with implications for model applications.

1. **The soil is assumed to be homogeneous.** The physical, chemical, and mineralogical properties of the soil are assumed to be constant and equal along all axes at any time,  $t$ .

***Justification:*** This is a necessary assumption for mathematical simplicity, and it is common to most geotechnical and hydrogeological models.

***Implications:*** In reality, all soil formations are heterogeneous to some degree. The model is expected to provide a reasonable approximation for field conditions.

2. The REV is structured with outer rigid, no-flow boundaries, inner flexible yielding boundaries, and infinite lateral boundaries. It is assumed that the upper and lower horizontal faces of the REV are rigid and unyielding. Thus, the only flexible, yielding boundary is located internally along the fracture, as illustrated in Figure 4.4. Both boundaries extend infinitely in the lateral direction. The rigid boundaries also act as no-flow boundaries for soil moisture.

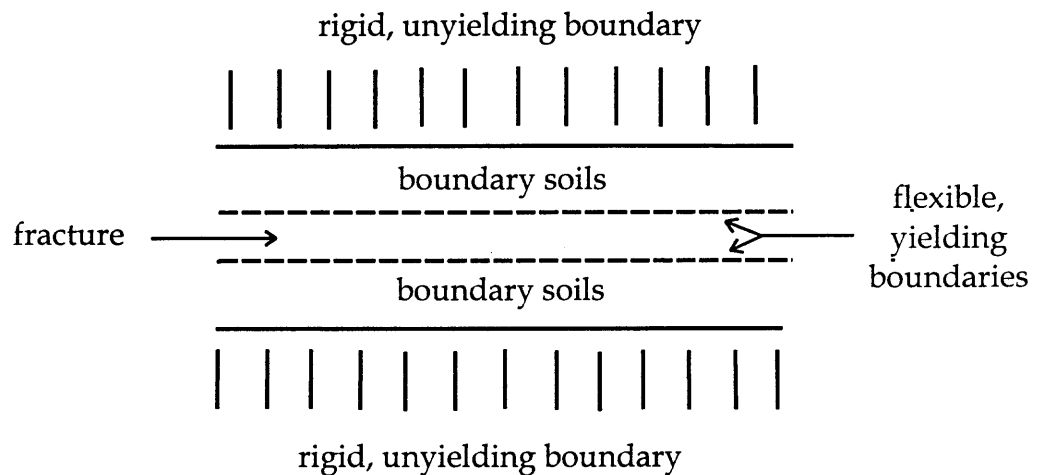


**Figure 4.4** Boundary Constraints on the REV

*Justification:* This assumption constrains the elemental volume with respect to strain and moisture flow. The outer rigid boundaries provide a stationary reference against which change in fracture aperture may be measured. The infinite lateral boundaries limit the strain of interest to a predominantly vertical direction. The no-flow boundaries isolate the REV and require that moisture transfer only occurs via the fracture. These constraints are justified by the fact

that at the field scale, the REV is surrounded by a soil mass, and the fracture is the principal conduit for environmental fluctuations.

*Implications:* This assumption permits expansion of the model from a single REV to a field-scale system where multiple 'stacked' fractures will likely be present. Thus, it allows the strains of each REV to be added to obtain bulk changes in fracture geometry. However, the assumption ignores potential interactions between adjacent REV's. Also, the assumption limits the model to subsurface fractures, since very shallow fractures will be affected by ground surface. This is because the ground surface acts as a flexible, yielding boundary.

3. Flow is assumed to occur in one-dimension in the direction normal to the fracture plane. The problem is constrained to the one-dimensional case, where flow occurs in the direction normal to the fracture plane, the  $z$  direction. For horizontal fractures, this is the vertical direction.

*Justification:* In fine-grained geologic formations advective fluid flow occurs predominantly through the fracture as opposed to flow through the soil pores. Thus, the most prominent gradient will be established in a plane normal to the fracture.

*Implications:* This assumption excludes application of the model to soils with a significant lateral component of flow, such as soils with high permeability and layered heterogeneous soils.

4. **The total (normal) stress is assumed to remain constant.** Externally applied stress and the thickness of the soil overburden are assumed to be constant.

*Justification:* This assumption allows for removal of the total (normal) stress component from the stress state descriptor.

*Implications:* The model will not apply to soils where effective stress changes occur as a result of changes in total normal stress, such as the addition or removal of an engineering structure, erosion or deposition. In addition, the effect of changes in moisture content inside the REV on the overburden potential is neglected.

5. **Soil conditions are assumed to be isothermal.** The temperature in the soil body is assumed to remain constant.

*Justification:* This assumption excludes the impact of a thermal gradient on volume change.

*Implications:* The model will not apply to heated soils, including areas adjacent to a subsurface boiler room, *in situ* hot gas injection for remediation purposes, and radioactive waste decay in subsurface geologic repositories. Frozen soils are also excluded on account of their unique behavior.

6. **The pore fluid is assumed to be isohaline and to have constant dielectric properties.** The pore fluid composition throughout the elemental volume is assumed to be constant. Chemical effects which control volume change at the



level of the diffuse double layer are neglected.

*Justification:* This assumption is necessary to isolate the mechanical component of volume change.

*Implications:* The model will not be applicable to soils with differential-concentration pore water. This would include cases such as salt water intrusion or environmental contamination by metals and organics. Changes in osmotic potential are thus neglected.

7. The moisture-transfer properties of the soil are assumed to be non-hysteretic. The rate of change of the state of the soil water is assumed to be constant for a specific moisture content, irrespective of sorption or desorption.

*Justification:* This is a necessary assumption for mathematical simplicity that is common to most physical models of soil behavior. The existence of these hysteretic effects in practice is not in question.

*Implications:* The model will provide only an approximation to recently deposited clay soils and those which have had little change in moisture content since deposition. Hysteretic behavior is expected to be a maximum for such soils. The importance of hysteresis is lessened in soils of older geologic age since they have been subjected to numerous cycles of wetting and drying.

These seven assumptions, as applied to the REV, govern the mathematical approach for modeling soil-fracture interactions, which will now be described.

### 4.1.3 Mathematical Approach

The general approach of the mathematical model is to link the volume change properties of the soil with the equations that predict changes in stress state. For saturated soils, changes in stress state can be determined with Terzaghi's (1943) consolidation equation. The equation describes changes in pore-water pressure,  $u_w$ , in space (i.e.,  $z$ , the vertical direction) and time,  $t$ , and is expressed as,

$$\frac{\partial u_w}{\partial t} = c_v \frac{\partial^2 u_w}{\partial z^2} \quad (\text{Eq. 4.1})$$

where  $c_v$  is the coefficient of consolidation. A second form of the equation may be envisioned as,

$$\frac{\partial w}{\partial t} = c_v \frac{\partial^2 w}{\partial z^2} \quad (\text{Eq. 4.2})$$

where the gravimetric moisture content,  $w$ , is the dependent variable. Gravimetric moisture content is substituted here for volumetric moisture content, which is directly proportional to the pore-water pressure. The substitution is valid because there is a linear relationship between specific volume and gravimetric moisture content for the saturated case. Eq. 4.1 should be used when available data are in the form of  $u_w$ , and Eq. 4.2 is appropriate when data for  $w$  are available.

The model approach using these equations, under the conditions and assumptions previously presented, is described as the following sequence of steps:

**Step 1-**Identify the initial stress state and boundary conditions

**Step 2-**Solve the flow equation and predict future stress state

**Step 3-**Relate the change in stress state to vertical soil deformation

**Step 4-**Relate soil deformation to changes in fracture aperture

Each of the steps is now described with respect to the REV under study.

### **STEP 1: Identify the Initial Stress State and Boundary Conditions**

To evaluate a potential change in the state of stress, it is first necessary to define the initial stress state and boundary conditions. To simplify the description of these properties with respect to the conceptual model, it is useful to split the REV into two halves. The geometric split is made along a horizontal plane centered in the fracture as shown in Figure 4.5.

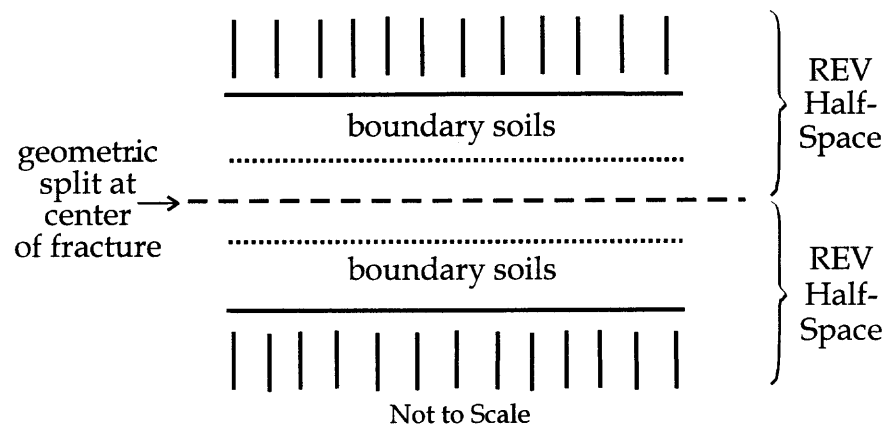


**Figure 4.5** Representation of the REV Half-Space

Under these geometric considerations, it is assumed that conditions on either side of the fracture are symmetric. This effectively limits analysis to an REV 'half-space.'

The governing equation (Eq. 4.1 or 4.2) requires two boundary conditions in terms of  $z$  (space) and an initial condition in terms of  $t$  (time). Figure 4.6 illustrates these conditions for the REV half-space.

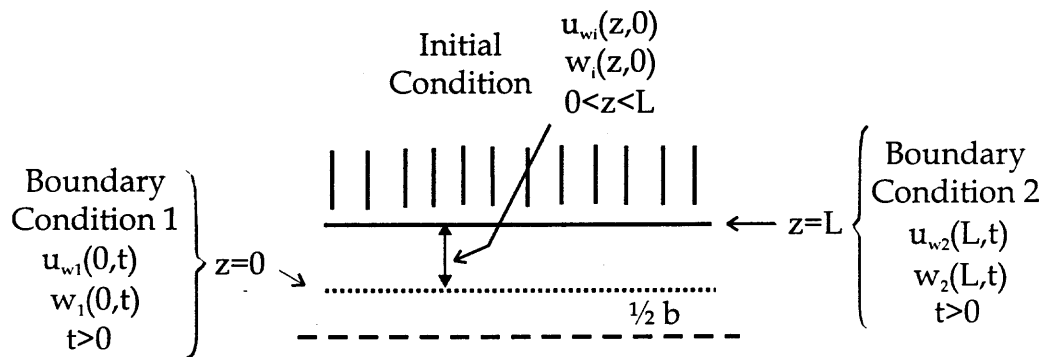


**Figure 4.6** Boundary and Initial Conditions on the REV Half-Space

The boundary conditions BC1 and BC2 define the pore-water pressure or gravimetric moisture content at the lower ( $z = 0$ ) and upper ( $z = L$ ) surfaces, respectively, for the REV half-space at any time,  $t$ , other than zero. The initial condition (IC) is a description of the distribution of pore-water pressure,  $u_{wi}$ , or moisture content,  $w_i$ , at time  $t = 0$  and at any distance,  $z$ , where  $0 \leq z \leq L$ . The time  $t = 0$  represents the instant after which environmental conditions initiate a change in stress state at the inner, flexible, yielding boundary. The IC is a function of depth, defined as  $u_{wi}(z,0) = f(z)$  or  $w_i(z,0) = f(z)$ , and it may be

represented as a gradient between the stress state on the upper and lower boundaries, where  $M = U_2 / U_1$  and  $U = u_w$  or  $w$ . Figure 4.7 shows five applicable initial conditions.

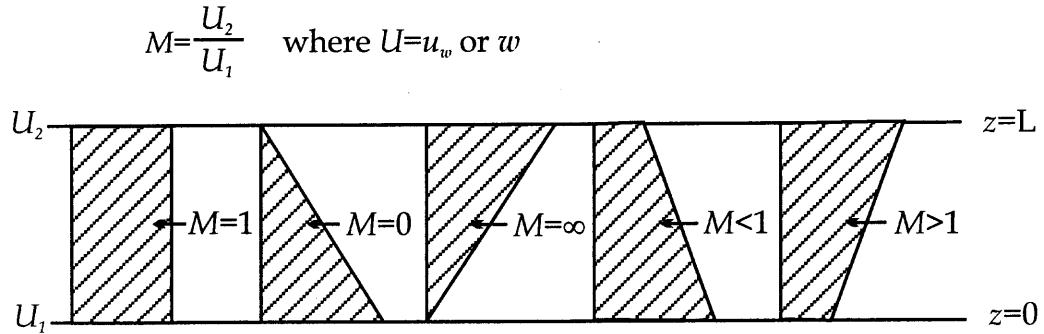


**Figure 4.7** Graphical Representation of Potential Initial Conditions

In the first condition the pore-water pressure or moisture content is constant with depth (i.e.,  $M = 1$ ). This represents the most commonly applied initial condition. Alternately, the parameter may vary linearly with depth. This may occur if either the upper or lower boundary tends toward zero (i.e.,  $M = 0$ ;  $M = \infty$ ) or if there is a non-zero, finite gradient between the upper and lower boundaries ( $M < 1$ ;  $M > 1$ ).

## STEP 2: Solve the Flow Equation and Predict Future Stress State

With these conditions identified, the next step is to solve the associated flow equation and predict the future stress state. Terzaghi's consolidation equation (Eq. 4.1) is a linear, homogeneous, second-order partial differential of parabolic

type and may be solved analytically in most cases. Once a solution is generated, it may be used to predict the future stress state using a set of input parameters.

### STEP 3: Relate Stress State Changes to Vertical Soil Deformation

The most direct method for relating stress state change to vertical soil deformation is through the use of moisture content. For saturated expansive soils, the change in moisture volume is assumed to be exactly equal to the change in soil volume. Thus, soil deformation is calculated by integrating the volumetric moisture change over the REV half-space. Here, the integration will be estimated using a discrete summation since the equation for the stress state function is typically unavailable. The summation is accomplished by first splitting the REV half-space of height  $H$  into a series of  $j$  horizontal layers of height  $h$ , as shown in Figure 4.8.

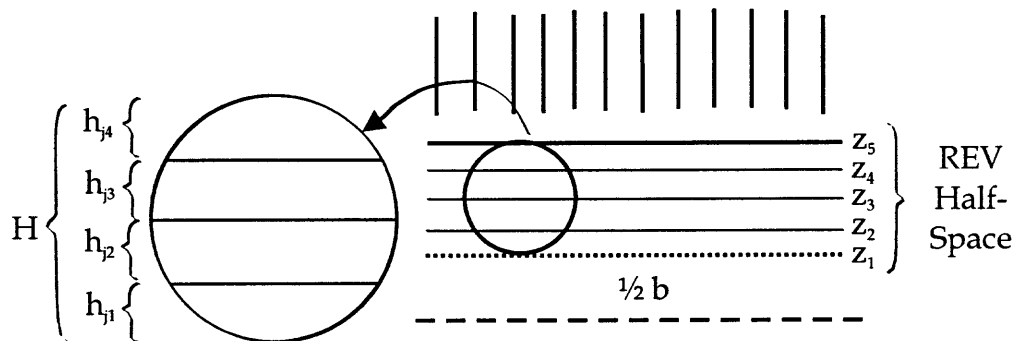


**Figure 4.8** Horizontal Layering of the REV Half-Space

The change in moisture content at each vertical space coordinate,  $z$ , is calculated as,

$$\Delta w_{(z_n)} = w_{i_{(z_n)}} - w_{f_{(z_n)}} \quad (\text{Eq. 4.3})$$

where  $w_i$  and  $w_f$  are the initial and final moisture contents, respectively, and  $n$  is the number of coordinates. The average moisture content change over each interval is then determined as,

$$\Delta w_{(j_m)} = \frac{\Delta w_{(z_n)} + \Delta w_{(z_{n+1})}}{2} \quad (\text{Eq. 4.4})$$

where  $m$  is the number of intervals. By summing the volumetric change of each interval,  $\Delta v_j$ , at any time,  $t$ , the volumetric change of the REV half-space,  $\Delta V$ , is obtained. This is shown mathematically as,

$$\Delta V = \sum_{j=1}^m \frac{\Delta w_{(j_m)} \cdot \bar{\rho}_{d_{(j_m)}} \cdot h_{(j_m)} \cdot A_{(j_m)}}{\rho_w} \quad (\text{Eq. 4.5})$$

where  $\bar{\rho}_d$  is the average dry density of the soil over the interval,  $\rho_w$  is the density of water, and  $A$  is the unit area of the interval taken as one square unit for simplification.

Once  $\Delta V$  is determined, it is necessary to relate this volume change to a vertical deformation. There are two possible approaches. The first is a one-dimensional approach where it is assumed that all of the deformation occurs in

the vertical direction. This might occur where soils are swelling under lateral constraint. The change in height of the REV half-space,  $\Delta H$ , therefore becomes,

$$\Delta H = \frac{\Delta V}{A} \quad (\text{Eq. 4.6})$$

where  $A$  is the unit area of the REV half-space, which is taken as unity.

The second case assumes that the deformation will occur in three dimensions. Here,  $\Delta H$  is computed by first calculating the final volume of the REV half-space,  $V_f$ , as,

$$V_f = (H_i \cdot A) - \Delta V \quad (\text{Eq. 4.7})$$

where  $H_i$  is the initial height of the REV half space. The value of  $V_f$  is then used to calculate final heights in each direction assuming isotropic strain behavior. The final heights are expressed as,

$$H_{fz} = H_i - (\% \varepsilon \cdot H_i) \quad (\text{Eq. 4.8})$$

$$H_{fy} = 1 - (\% \varepsilon \cdot 1) \quad (\text{Eq. 4.9})$$

$$H_{fx} = 1 - (\% \varepsilon \cdot 1) \quad (\text{Eq. 4.10})$$

where  $H_{fz}$ ,  $H_{fy}$ , and  $H_{fx}$  are the final heights in the vertical, horizontal and lateral directions, respectively, and  $\varepsilon$  is the volumetric strain. For three-dimensional volume change, then,  $\Delta H$  may be computed as,



$$\Delta H = H_i - H_{fz} \quad (\text{Eq. 4.11})$$

It is also possible to calculate deformation by relating stress state changes to volume change indices of the soil. For this method, the available data will be expressed as pore-water pressures and the one-dimensional change in height, may be computed by,

$$\Delta H = \sum_{j=1}^m \Delta u_{w(j_m)} \cdot m_{sv(j_m)} \cdot h_{(j_m)} \quad (\text{Eq. 4.12})$$

where  $m_{sv}$  is the saturated coefficient of volume change representing the relationship between vertical strain and pore-water pressure  $(\partial \varepsilon_z / \partial u_w)$ . The three-dimensional volume change is calculated in a manner similar to that described above.

#### STEP 4: Relate Soil Deformation to Changes in Fracture Aperture

The final step in the model approach is to relate the vertical deformation of the REV half-space,  $\Delta H$ , to a change in fracture aperture,  $\Delta b$  (Figure 4.9). Since the only flexible, yielding boundary is located at the fracture,  $\Delta b$  may be computed as,

$$\Delta b = 2 \cdot \Delta H \quad (\text{Eq. 4.13})$$

Figure 4.9 also illustrates how the model can be applied to a field-scale system consisting of a series of 'stacked' REV. Bulk changes in fracture volume may be

determined by summing the vertical strains of each REV.

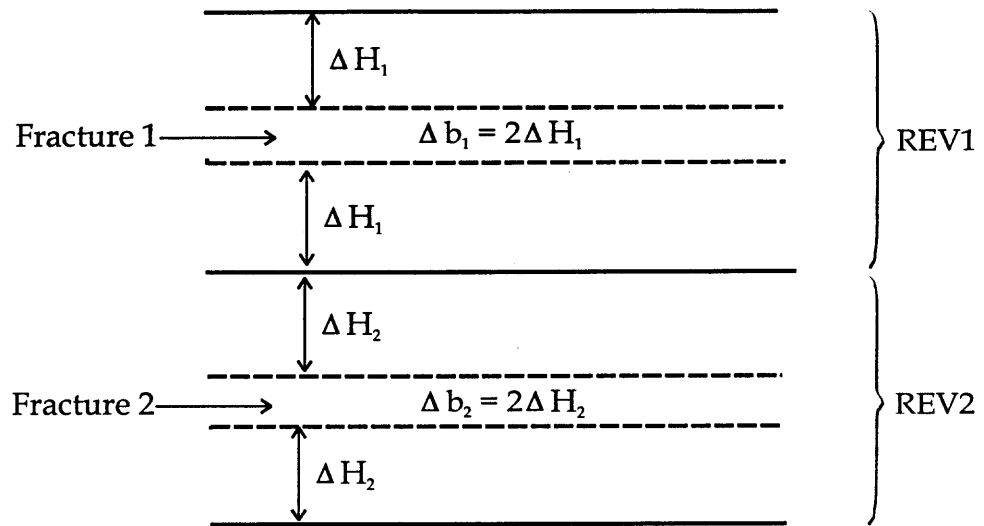


**Figure 4.9** Change in Fracture Aperture and Stacking of Adjacent REVs

## 4.2 Model Development

Now that the physical concept, general assumptions and mathematical approach for the model have been established, the final step is to solve the model. This section begins by defining the specific boundary and initial conditions. A presentation of the general analytical solution follows. The section concludes with a review of supporting evaporation rate calculations and suggestions for adapting the model approach to other conditions.

### 4.2.1 Specific Boundary and Initial Conditions

The specific boundary and initial conditions described in this section have been selected by assuming that the Representative Elemental Volume (REV) is

situated within an extended soil mass, and all environmental changes occur from within the fracture. This leads to the following conditions:

**Boundary Condition 1 [BC1].** Two different conditions may be envisioned along the fracture boundary. The first condition, termed 'Case 1,' sets the boundary along the fracture to a constant equilibrium moisture content,  $w_e$ . For drying, this is the moisture content below which virtually no evaporation occurs, signaling the start of third stage evaporation. It is a function of both soil type and meteorological conditions (i.e., geographic region). The  $w_e$  for drying may be estimated by the Atterberg shrinkage limit ( $SL$ ) for most expansive soils in temperate and semi-arid climates. Some adjustment may be appropriate in arid regions, where the  $SL$  would tend to overestimate the equilibrium moisture content.

If, on the other hand, the system is in a wetting mode, the equilibrium moisture content at the boundary may be approximated as the field capacity, also known as the soil water holding capacity. This represents an upper moisture content limit beyond which no absorption takes place. It is also the moisture content at 'zero' suction. Mathematically, the constant equilibrium moisture content for BC1 is expressed as  $w(0,t) = w_e$  for  $0 < t < \infty$ .

In the second approach, termed 'Case 2,' the fracture boundary is represented by a constant flux, the magnitude of which is controlled by an interrelationship between the hydraulic properties of the soil and the

environmental conditions in the fracture. BC1 is defined mathematically for this study as  $w(0,t) = m + w_i$  for  $0 < t < \infty$ , where  $m$  is a rate of evaporation or infiltration, and  $w_i$  is the initial moisture content.

**Boundary Condition 2 [BC2].** Since two REV's abut one another in the field-scale, this boundary is most appropriately considered as a groundwater divide. This concept is illustrated in Figure 4.10. Line A-B represents a divide across which no flow takes place. BC2 is therefore expressed as a constant flux boundary as  $\partial w(L,t)/\partial z = 0$  for  $0 < t < \infty$ . The REV half-space is said to be 'half-closed' because one boundary is freely draining while the other is at no-flow conditions.

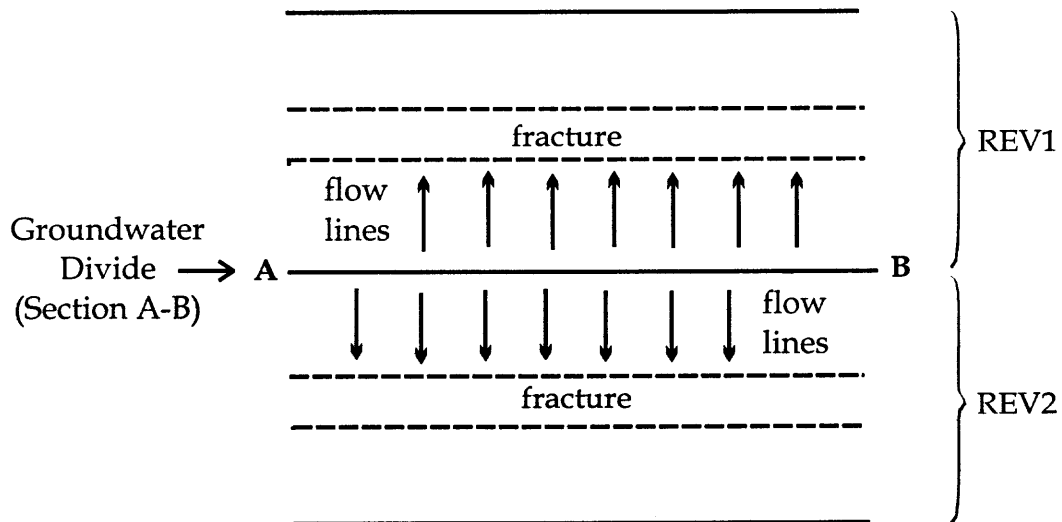


**Figure 4.10** Groundwater Divide Present Between Adjacent REV's

**Initial Condition [IC].** The specific initial condition used for this study solution is  $w_i(z,0) = w_i$  for  $0 \leq z \leq L$ , which is the case where the moisture content along the entire length of the REV half-space is constant.

#### 4.2.2 Mathematical Solutions

The solution of the 'Fracture Volume Change Model' is developed in this section, along with a method for computing aerodynamic evaporation in the fracture.

The general problem developed in the previous sections will now be summarized. Recall the governing equation,

$$\boxed{\frac{\partial w}{\partial t} = c_v \frac{\partial^2 w}{\partial z^2}} \quad (\text{Eq. 4.2})$$

where  $w$  is the gravimetric moisture content, and  $c_v$  is a constant coefficient of consolidation. Two basic cases within the framework of this equation have been formulated, which differ only in the description of the first boundary condition. Each case is described as follows, where  $w$  is a function of the vertical space coordinate,  $z$ , and time,  $t$ :

$$\text{Case 1:} \quad w(0,t) = w_e, \quad 0 < t < \infty \quad (\text{Eq. 4.14})$$

$$\frac{\partial w}{\partial z}(L,t) = 0, \quad 0 < t < \infty \quad (\text{Eq. 4.15})$$

$$w(z,0) = w_i, \quad 0 \leq z \leq L \quad (\text{Eq. 4.16})$$

<p>Case 2: <math>w(0,t) = mt + w_i, \quad 0 &lt; t &lt; \infty</math></p> <p style="text-align: center;"><math>\frac{\partial w}{\partial z}(L,t) = 0, \quad 0 &lt; t &lt; \infty</math></p> <p style="text-align: center;"><math>w(z,0) = w_i, \quad 0 \leq z \leq L</math></p>	<p>(Eq. 4.17)</p> <p>(Eq. 4.15)</p> <p>(Eq. 4.16)</p>
--	---

**4.2.2.1 Fracture Volume Change (FVC) Model Solution.** The FVC Model solution is generated as a single analytical expression from which both Case 1 and Case 2 initial-boundary-value problems may be evaluated. The boundary condition at the fracture (i.e., BC1) for the generalized case may be defined as,

$$w(0,t) = c + mt \quad (\text{Eq. 4.18})$$

Transforming the problem with nonhomogeneous boundary conditions to a problem with homogeneous boundary conditions results in the following new problem:

$$\frac{\partial v}{\partial t} = \frac{\partial w}{\partial t} = c_v \frac{\partial^2 w}{\partial z^2} - m \quad (\text{Eq. 4.19})$$

where, 
$$v(z,t) = w(z,t) - (c + mt) \quad (\text{Eq. 4.20})$$

and the new boundary and initial conditions are:

$$v(0,t) = 0 \quad 0 < t < \infty \quad (\text{Eq. 4.21})$$

$$\frac{\partial v(L,t)}{\partial z} = 0 \quad 0 < t < \infty \quad (\text{Eq. 4.22})$$

$$v(z,0) = w_i - c \quad 0 < z < L \quad (\text{Eq. 4.23})$$

The transformed nonhomogeneous equation (Eq. 4.19) is solved by the method of eigenfunction expansion under the constraints of the boundary and initial conditions (Eqs. 4.21 through 4.23). The final solution is derived, as,

$$w(z,t) = mt + c + \sum_{n=1}^{\infty} \left\{ \left[ \frac{2(w_i - c)}{L\lambda_n} + \frac{2m}{c_v\lambda_n^2 L} \right] \exp(-c_v\lambda_n^2 t) - \frac{2m}{c_v\lambda_n^2 L} \right\} \sin \lambda_n z \quad (\text{Eq. 4.24})$$

$$\lambda_n = \frac{(2n-1)\pi}{2L} \quad (\text{Eq. 4.25})$$

where  $w$  is the gravimetric moisture content (M/M),  $z$  is the vertical coordinate (L),  $t$  is time (T),  $m$  is the moisture flux (L/T),  $c$  is a constant moisture content (M/M),  $c_v$  is the coefficient of consolidation (L<sup>2</sup>/T),  $L$  is the length of the REV half-space (L), and  $n$  is the number of intervals. Case 1 is solved by setting  $m$  equal to zero and  $c$  equal to  $w_e$ . Case 2 is solved by setting  $m$  equal to an evaporation rate [ $m$  is negative] or an infiltration rate [ $m$  is positive], and  $c$  is equal to  $w_i$ . A full derivation of the solution is presented in Appendix F.

The case of drying is now used to illustrate the general forms of the Case 1 and Case 2 solutions. Figure 4.11 shows the solutions for increasing time

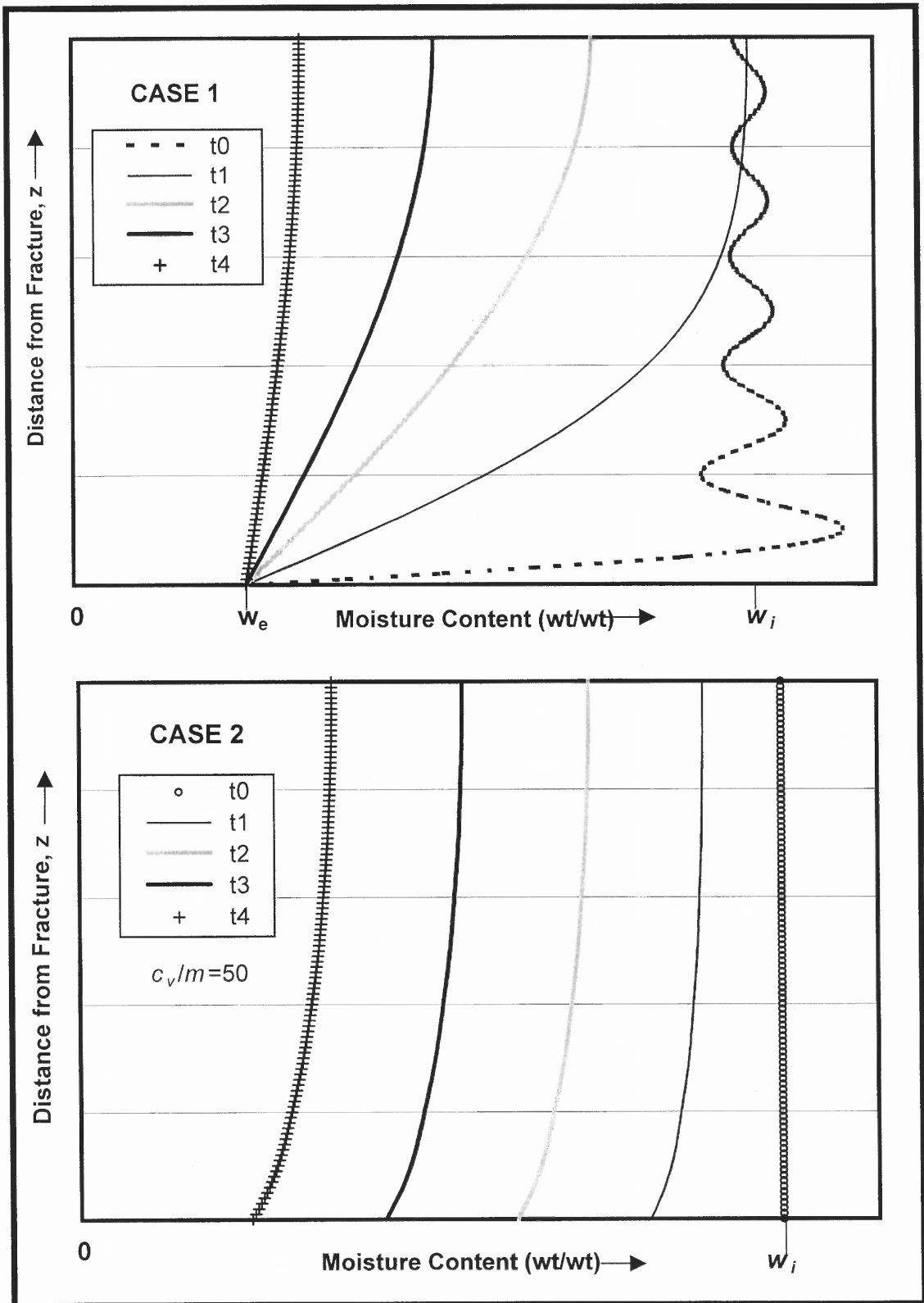


Figure 4.11 General Form of the Case 1 and Case 2 FVC Model Functions (Case of Desiccation)



durations. As expected, the functions are differentiated by the form at the fracture boundary. For Case 1, the boundary is instantaneously brought to a constant equilibrium moisture content, while the boundary in Case 2 continues on a path of drying at a constant rate. Case 1 also shows a stronger drying front emanating outward from the fracture. The Case 2 form is similar to that of drainage where there is a simultaneous decrease in moisture throughout the entire length of the REV. Note that the initial Case 1 moisture content is approximated by a sinusoidal function which is purely a mathematical phenomenon specific to the particular solution.

It is noted that the Case 2 solution is sensitive to the ratio of the coefficient of consolidation,  $c_v$ , to the constant moisture flux,  $m$ . This suggests that there is an important relationship between the rate of moisture flow through the soil and the rate of evaporation at the boundary. When the ratio of  $c_v / m$  is low, the soil fails to provide the moisture needed to meet the demands of the flux and the function becomes unstable. This instability generally occurs at a  $c_v / m$  ratio of less than thirty. The Case 2 function shown in Figure 4.11 has a  $c_v / m$  ratio of fifty. It is also noted that the rate of change in moisture content for a particular soil type reduces with increasing  $c_v / m$  ratios owing to the relatively lower flux.

**4.2.2.2 Supporting Evaporation Rate Calculations.** The Case 2 FVC Model requires the input of an evaporation rate in the drying mode. This section presents a method for determining this rate from conditions in the fracture.

An expression can be derived by assuming that the air velocity through the fracture is the major evaporative force. This is probably true in most cases, with the exception of soils exposed to a heat source. An expression for the aerodynamic evaporation rate in a fracture,  $E_{af}$ , can be derived by adapting an existing semi-empirical expression for aerodynamic evaporation at ground surface (Penman, 1956), as,

$$E_{af} = 0.35 \cdot \left[ e_2^0 - \left( \frac{\bar{h}_r}{100} \cdot e_2^0 \right) \right] \cdot \left[ 0.5 + \frac{\bar{V}}{100} \right] \quad (\text{Eq. 4.26})$$

where  $e_2^0$  is the saturation vapor pressure at mean temperature in the fracture, in mm Hg (see Table J.1);  $\bar{h}_r$  is the relative humidity of the air in the fracture; and  $\bar{V}$  is the average velocity at standard temperature and pressure (STP) (mi./day). The final unit of  $E_{af}$  is mm/day. Note that in addition to velocity, the rate is controlled by the amount of moisture in the air as a function of temperature and humidity. A full derivation of Eq. 4.26 is provided in Appendix F. The method for determining the average velocity in the fracture based on Nautiyal (1993) and Hall (1995) is shown in sample calculations in Appendix H.

### 4.3 Model Suggestions for Other Conditions

This section suggests a general procedure for modeling unsaturated soils and soils in the first stage of evaporative drying. Both procedures follow the general approach established in Sections 4.1 and 4.2.

#### 4.3.1 Unsaturated Conditions

Unsaturated conditions are important for modeling volume changes in subsurface expansive clays at low moisture contents, or for soil of relatively high permeability, such as mixtures of clay, silt, and sand. While the magnitude of volume change is significantly less than the saturated case, analysis of unsaturated soil is of interest in some applications.

Unsaturated conditions may be modeled using the Richards' (1931) equation that describes changes in matric suction,  $\mu$ , in space (i.e.,  $z$ , the vertical direction) and time,  $t$ , expressed as,

$$K(\theta) \frac{\partial^2 \mu}{\partial z^2} + \frac{\partial K(\theta)}{\partial z} = \frac{\partial \theta}{\partial \mu} \frac{\partial \mu}{\partial t} \quad (\text{Eq. 4.27})$$

where  $K$  is the hydraulic conductivity and  $\theta$  is the volumetric moisture content. The values of  $K(\theta)$  and  $\partial \theta / \partial \mu$  are experimentally or theoretically determined parameters, which are specific to a particular soil type.

In addition to the assumptions previously identified for the saturated case, it is assumed that the air phase is continuous and at atmospheric pressure. This condition ensures that excess pore-air pressure throughout the soil mass will be either negligible or rapidly dissipated. The presence of occluded air, common to unsaturated soils at higher moisture contents, is thus neglected. This is a necessary simplifying assumption to reduce the number of variables in the description of state.

The specific boundary and initial conditions defined for saturated conditions are also valid for the unsaturated domain, with the exception of the assumed equilibrium moisture content. For drying, the moisture content of unsaturated soil will tend towards zero, so the drying equilibrium moisture content can be assumed to be  $w_e = 0$ . The equilibrium moisture content for the wetting mode is assumed to be the field capacity (as in the saturated case) since unsaturated soils upon wetting will transition from an unsaturated to a saturated state. Since the Richards' equation defaults to Terzaghi's equation under saturated conditions, it appears suitable for modeling this condition.

The unsaturated FVC Model will almost certainly require a numerical solution since the Richards' equation is highly non-linear owing to the dependence of  $K$  on  $\theta$ . The reader is referred to the following studies for suggested solution approaches: Gottardi and Venutelli (1993), Thomas and Rees (1991), Lam and Fredlund (1984), Celia et al. (1990), Ross (1990), and Islam (1996).

The predicted change in matric suction may be translated to soil volume and fracture aperture changes using the approach presented in Section 4.2 with one modification. The unsaturated coefficient of volume change,  $m_{uv}$ , should be substituted for the saturated version of this coefficient ( $m_{sv}$ ) in Eq. 4.12. Alternately, the change in height of the REV half-space may be determined using the ratio of the change in moisture volume to the change in soil volume, using a method similar that outlined for the saturated case. The moisture ratio may be determined from the residual (and zero) shrinkage zones of the soil-specific water retention curve.

#### 4.3.2 First Stage Evaporative Conditions

This section offers a simplified solution of the FVC Model under the assumption of first stage evaporation. The solution would be of interest in the modeling of very wet soils at early drying times, particularly soil of higher permeability, such as clay, silt, and sand mixtures.

The simplified solution was originally derived by Ghildyal and Tripathi (1987) using the assumption that the soil provides no resistance to flow (i.e., the soil surface approximates a free water surface). By adapting the expression to the FVC Model framework, the solution is defined as,

$$\boxed{c_v \frac{\partial w}{\partial z} = E \left( 1 - \frac{z}{L} \right)} \quad (\text{Eq. 4.28})$$

where  $c_v$  is the coefficient of consolidation ( $L^2/T$ ),  $w$  is the gravimetric moisture content (M/M),  $L$  is the length of the REV half-space (L), and  $z$  is the vertical coordinate (L) .

Equation 4.28 may be used to determine a rate of change in water content with depth (i.e.,  $\partial w / \partial z$ ) as a direct function of evaporation rate. The method is limited in that the magnitude of the moisture content change cannot be predicted. The final moistures contents must be extrapolated from one or more known moisture contents using the relationship  $\partial w / \partial z$  . The associated fracture volume change may be calculated using the method for the saturated state.

## **CHAPTER 5**

### **MODEL VALIDATION AND CALIBRATION**

#### **5.1 Objective**

In order to evaluate the predictive capabilities of the mathematical model, it is necessary to validate and calibrate the model to ensure that the theory provides an acceptable description of reality. The purpose of model validation is to assure that the model adequately represents the actual physical phenomena. Calibration establishes the necessary coefficients for proper functioning of the model. Two sets of data were used for this phase of the study. The first data set was taken from the laboratory horizontal infiltrometer tests. The second was taken from an environmental remediation field project performed on a fractured clay formation in Santa Clara, California.

#### **5.2 Laboratory Horizontal Infiltration Study**

This section presents validation and calibration of the FVC Model using the drying stage horizontal infiltrometer (HI) test data. The wetting data were not used for this purpose because the moisture effects in the fracture were localized and the initial moisture content was not at equilibrium. The section begins with a discussion of the validity of model assumptions (Section 5.2.1), and follows with the model predictions (Section 5.2.2).

### 5.2.1 Validity of Model Assumptions

In order to confirm that the HI test data are appropriate for calibrating and validating the FVC Model, it is necessary to compare the test conditions to the model assumptions. This includes both the general model assumptions and the assumptions used to derive the governing equation, specifically the use of pore-water pressure as the solitary descriptor of soil water potential.

The validity of each general assumption is now reviewed:

1. *The soil is assumed to be homogenous and isotropic.* The assumption is satisfied because the soil was relatively uniform and was prepared in a manner that approached full homogenization.
2. *The REV is structured with outer rigid, no-flow boundaries, inner flexible, yielding boundaries at the fracture, and infinite lateral boundaries.* This assumption was satisfied with the following exceptions: (1) the upper outer boundary was only semi-rigid; (2) the inner boundaries were restrained at the fracture edge; and (3) the lateral boundaries were not infinite.
3. *Flow is assumed to occur in one-dimension in the direction normal to the fracture plane.* The experimental data generally support this assumption since moisture flowed predominantly in the vertical direction away from the fracture. A component of lateral flow likely also occurred in the vicinity of the vertical shrinkage cracks, but the contribution is considered minor.



4. *The total (normal) stress is assumed to remain constant.* This assumption was satisfied since no surcharge pressure was added to the HI test soil, and excess pore-water pressures resulting from compaction were allowed to dissipate prior to testing.
5. *Soil conditions are assumed to be isothermal.* The HI tests were performed in an environmental chamber maintained at relatively constant temperatures. The soil was also temperature-equilibrated prior to testing.
6. *The pore fluid is assumed to be isohaline and have constant dielectric properties.* The properties of the pore fluid were initially constant and did not change over the course of the HI tests, with the exception of an insignificant increase in salt concentration as water was removed.
7. *The moisture-transfer properties of the soil are assumed to be non-hysteretic.* This assumption is not relevant since the model was only applied for a single cycle of drying.

With the FVC Model assumptions generally satisfied, the last step is to confirm that the pore-water pressure potential for the HI tests dominates the soil water potential. This was accomplished by performing an analysis of the significance of each soil water potential component, including pore-water pressure, overburden, osmotic, and gravitational potentials. The reader is referred to Appendix G for a full presentation of the analysis.

The results show that the pore-water pressure potential greatly exceeds the other potentials. The overburden, osmotic, and gravitational potentials together, at 0.02 bars (2 kPa), represented only 0.03% of the pore-water pressure potential, which ranged from 33 to 85 bars (3300 to 8500 kPa). Thus, the use of pore-water pressure in the governing equation is considered valid.

In summary, it is concluded that the HI drying stage test data are appropriate for calibrating and validating the FVC Model, since both the general assumptions and the soil water potential assumptions are generally satisfied.

## 5.2.2 FVC Model Predictions for HI Drying Tests

This section reviews the FVC model predictions for the HI drying tests and is divided into five parts: (1) model input parameters; (2) Case 1 model predictions; (3) Case 2 model predictions; (4) implications of Case 1 and Case 2 model results; and (5) aperture predictions.

**5.2.2.1 Model Input Parameters.** The input parameters used for the FVC Model, shown in Table 5.1, were taken primarily from the HI test conditions. A constant, average value of the coefficient of consolidation,  $c_v$ , was determined from HI void ratio data. The equilibrium moisture content,  $w_e$ , was chosen to be 0.14 from a best fit that ranged from 0.10 to 0.17. This correlates well with the shrinkage limit for the Potomac Formation, which ranges from 11 to 16.

**Table 5.1** Model Input Parameters for HI Tests

Indicator	Input Value
<i>Test Conditions</i>	
Height of the REV Half-Space ( $H$ )	2.5 in.
Initial Moisture Content ( $w_i$ )	0.317
Drying Time Duration ( $t$ )	
Test 5C	420 min
Test 8C	462 min
Test 9C	741 min
Coefficient of Consolidation ( $c_v$ )	0.0003 in <sup>2</sup> /min
<i>Calibrated and Calculated Values</i>	
Equilibrium Moisture Content ( $w_e$ )	0.14
Aerodynamic Evaporation Rate in Fracture ( $E_{af}$ )	
Test 5C	$1.2 \times 10^{-4}$ in/min
Test 8C	$7.2 \times 10^{-4}$ in/min
Test 9C	$8.5 \times 10^{-4}$ in/min

The aerodynamic evaporation rates in the fracture,  $E_{af}$ , were calculated using computed average velocities, average relative humidities, and saturation vapor pressures in the fracture based on mean temperatures.

**5.2.2.2 Case 1 Predictions.** The Case 1 moisture content predictions are shown in Figure 5.1, along with the actual HI moisture data. The model predictions show excellent agreement with the experimental data, which deviate by an average of only 6%. The predictions approximated the actual moisture content well throughout the entire REV half-space over a range of 0.2% to 20%, with the

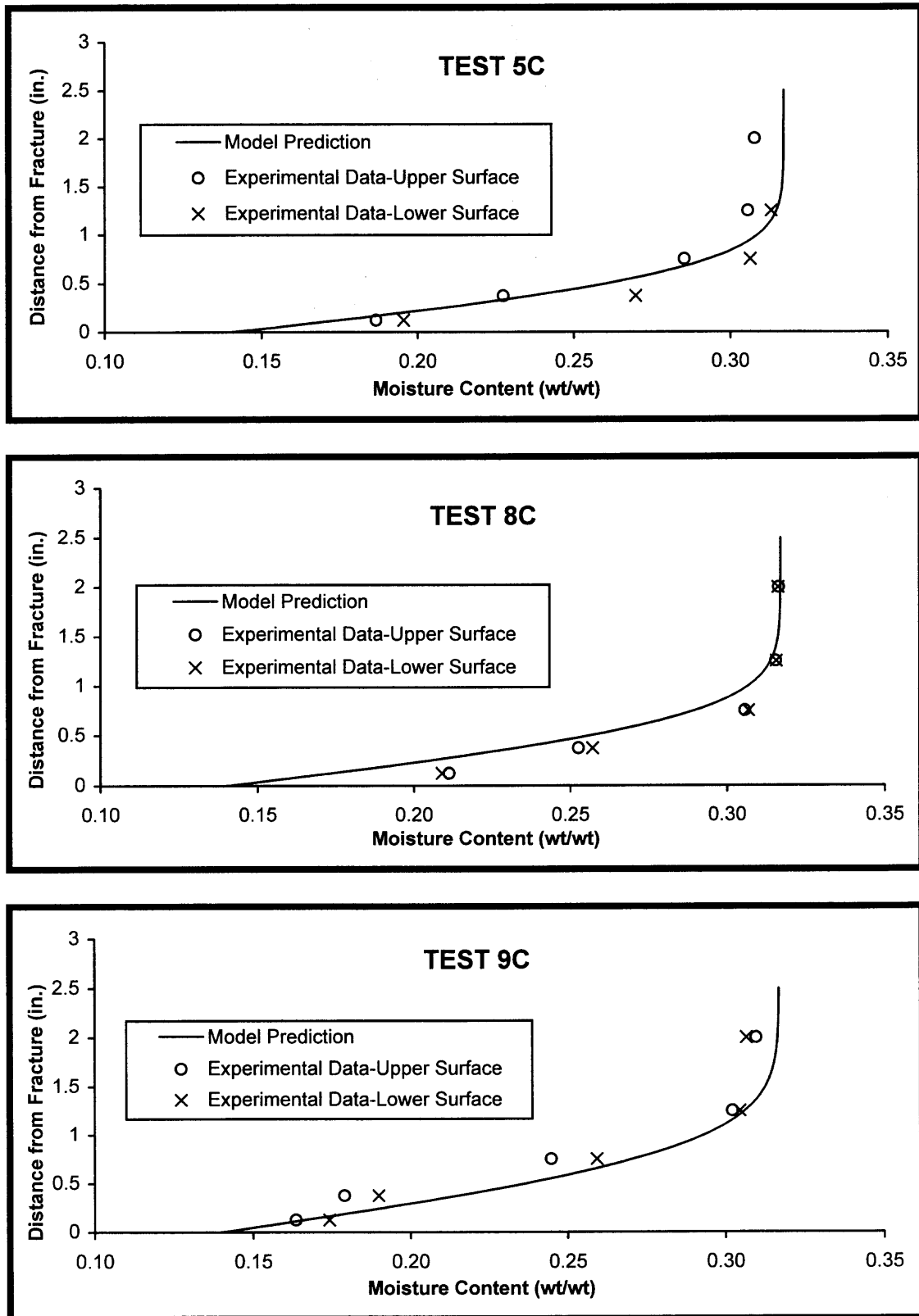


Figure 5.1 Comparison of HI Experimental Data with Case 1 Moisture Predictions

largest deviations tending to occur closest to the fracture level. Note also that the prediction tends towards slight underestimation for the wettest soil (Test 8C) and slight overestimation for the driest soil (Test 9C). The model results suggest that the second stage of evaporation likely predominated, since the moisture contents showed good agreement without considering the evaporative conditions in the fracture.

**5.2.2.3 Case 2 Predictions.** The predicted moisture contents for Case 2 are shown in Figure 5.2 in comparison with the actual moisture content data. The flux for these predictions was set equal to the evaporative demand of the fracture ( $E_{af}$ ). The figure shows that the model becomes unstable at these conditions, due to the low  $c_v/m$  ratios, which vary from 0.35 to 2.5. This behavior is attributed to the fact that the soil cannot support the evaporative demand, again suggesting that evaporation is occurring in the second stage.

Figure 5.3 shows model predictions with three reduced evaporation rates representing  $c_v/m$  ratios of 3, 30, and 300. Note that the stability of the function increases as the  $c_v/m$  ratio increases (i.e., the evaporative demand decreases). While the model is predictive at these low evaporation rates, very little drying occurs rendering this case of little interest in most circumstances.

The predictive capability of the Case 2 model may be evaluated in further detail by examining the  $1 \times 10^{-5}$  in/min ( $2.5 \times 10^{-5}$  cm/min) evaporation rate prediction. This is estimated to be the actual evaporation rate for the HI test

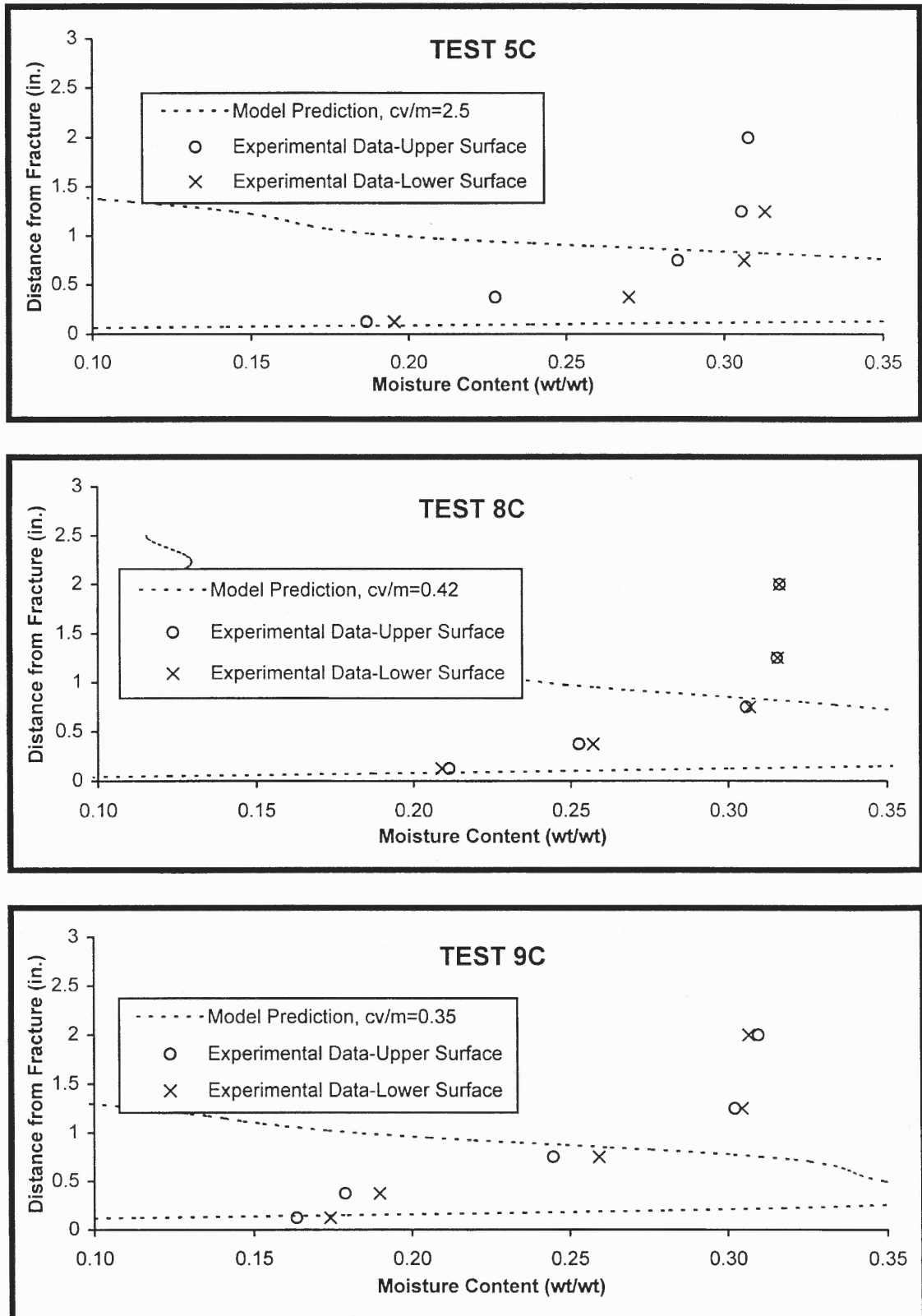
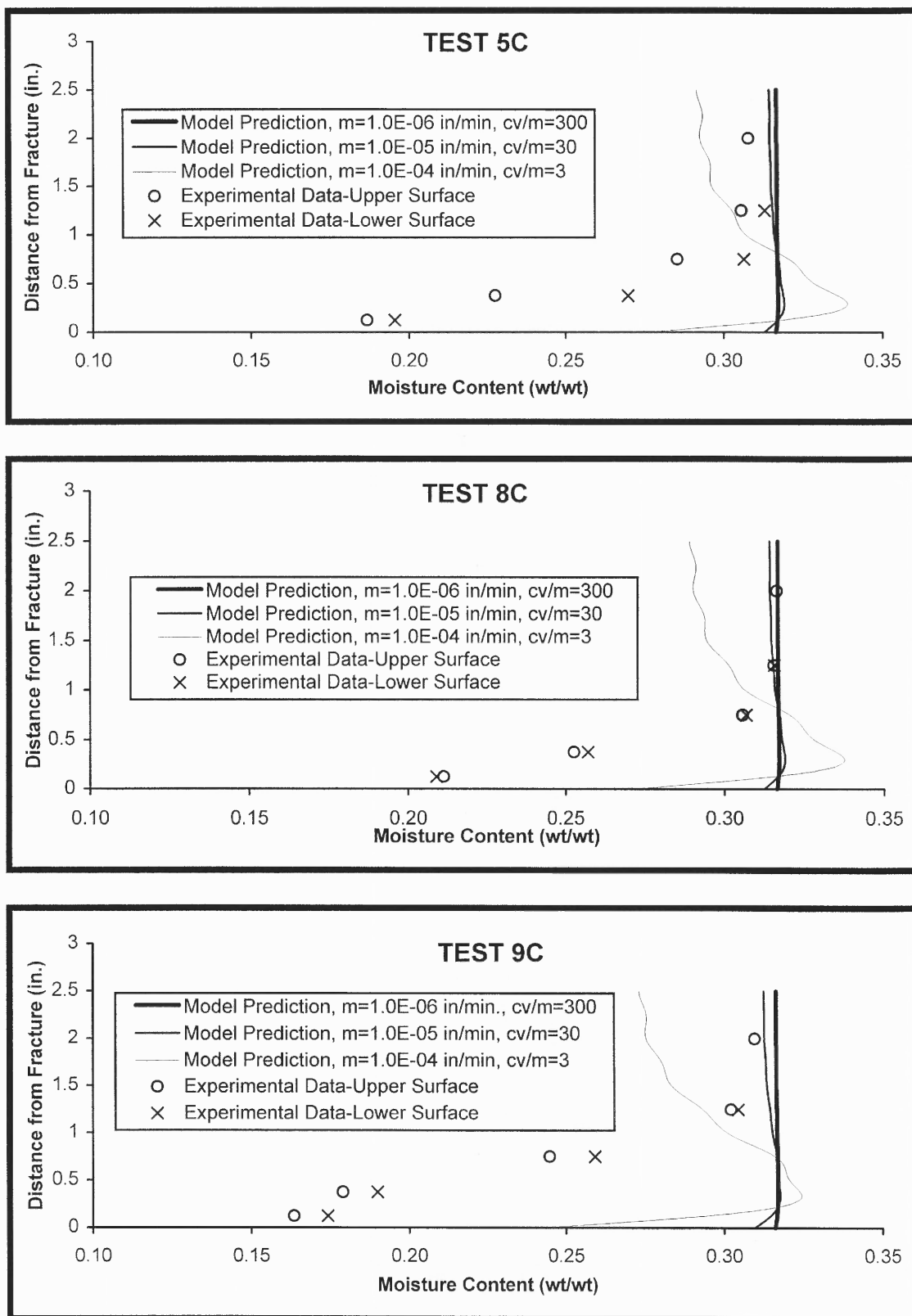


Figure 5.2 Comparison of HI Experimental Data with Case 2 Moisture Predictions Using  $E_{af}$  Evaporation Rates



**Figure 5.3** Comparison of HI Experimental Data with Case 2 Moisture Predictions Using Various Evaporation Rates

soils, which was determined from the slope of the aperture-time plots. Under these conditions, the model also showed poor agreement with the measured moisture content data, particularly at the fracture boundary.

**5.2.2.4 Implications of Case 1 and Case 2 Model Results.** The Case 1 model clearly demonstrates superior predictive ability as compared to the Case 2 model under the given set of HI test conditions. Not only are the predictions more accurate, but the model is convenient as it requires only an easily estimated equilibrium moisture content. The Case 1 model is thus recommended for the majority of field applications in expansive soils.

The Case 2 model is more complex, as it requires input of a fracture boundary flux which is difficult to determine. The use of the evaporative demand from the fracture as an estimate of the flux has shown to be inappropriate in expansive clay unless the rate is very small (i.e.,  $c_v/m$  ratio greater than 30). The results imply that the Case 2 model might be preferred over the Case 1 model in situations where evaporation is in the first stage (i.e., wet soils in early drying times). Soils of higher permeability would therefore be the focus of the Case 2 application in this context.

The Case 1 and Case 2 model results also have important implications for remedial extraction technology design in expansive soils. The study suggests that these systems should not necessarily be designed to maximize evaporation rates in the fracture. Rather, moisture flow is a function of the hydraulic



properties of the formation, so the expenditure of additional energy to attain higher flow velocities in the fracture may be unproductive.

**5.2.2.5 Fracture Aperture Predictions.** The final component of the model is the prediction of changes in fracture aperture. Predictions were made using two sets of moisture data (Table 5.2). Purely theoretical predictions were made using moisture data from the Case 1 predictions (Column 1) and semi-theoretical predictions were made using the HI experimental moisture data (Column 2). Finally, these were compared to the final fracture apertures calculated using the Cubic Law (Column 3).

The results in Table 5.2 show that the FVC Model tends to overpredict the actual final fracture aperture computed with the Cubic Law. There are two factors believed to contribute to this phenomenon. First, the Cubic Law is derived assuming the upper and lower fracture surfaces are parallel (i.e., parallel plate analogy). Because fractures in soil are not truly parallel, but contain surface variation and pinch off laterally, the Cubic Law provides only an approximation of fracture aperture. Secondly, it is possible that the soil immediately adjacent to the fracture is unsaturated, thus reducing the volume change per unit moisture change.

Note that several corrections were made to the data to obtain these results which accounted for scaling effects, since the HI tests did not fully approximate a fracture in a field scenario. One correction accounted for the reduced width of

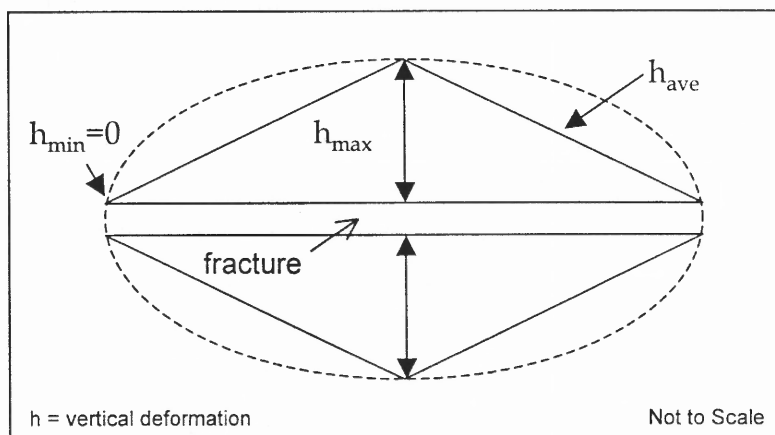
**Table 5.2** Comparison of Predicted and Actual Final Fracture Apertures for HI Drying Tests

Test No.	(1) Theoretical Prediction*	(2) Semi-Theoretical Prediction*	(3) Actual
	<i>Case 1 Moisture Predictions (in.)</i>	<i>HI Experimental Moisture Data (in.)</i>	<i>HI Data with Cubic Law (in.)</i>
Test 5C	0.037 (0.101)	0.036 (0.100)	0.025
Test 8C	0.038 (0.106)	0.029 (0.077)	0.025
Test 9C	0.046 (0.132)	0.059 (0.154)	0.031

\* Values in parentheses represent raw data prior to the application of scaling corrections.

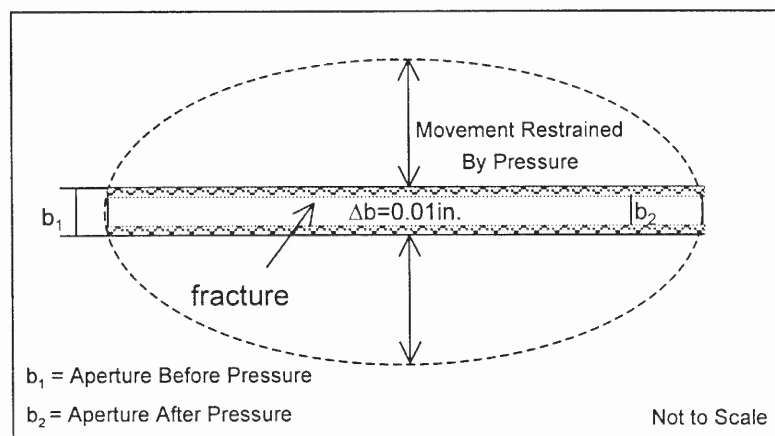
the fracture, since constraint at the fracture edges prevented full dilation of the fracture (Figure 5.4a). Data were corrected by averaging the volume change over the entire width of the fracture. A second correction involved the high vacuum pressures, which inhibited the fracture from opening fully (Figure 5.4b). A correction of 0.01 in. (0.25 mm) was applied to the data, which represents the measured HI aperture constriction upon pressurization. The third correction is related to the long and thin geometry of the fracture (Figure 5.4c). To account for this condition, the vertical and lateral unit strains,  $\varepsilon_z$  and  $\varepsilon_x$ , respectively, were reduced by Poisson's ratio, which was taken as 0.4 for clay. Raw aperture predictions without adjustment are also presented in Table 5.2 in parentheses.

Vertical  
Cross  
Section  
Along  
Width of  
Fracture



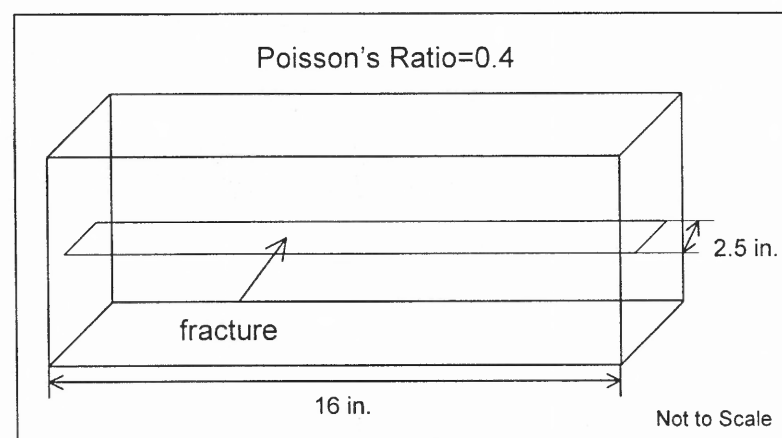
a. Physical Restraint at Fracture Edges

Vertical  
Cross  
Section  
Along  
Width of  
Fracture



b. Pressure Constriction

Soil  
Block  
With  
Discrete  
Fracture



c. Axial Unit Strain Expected to Exceed Lateral Unit Strain due to Fracture Geometry

Figure 5.4 Aperture Corrections for Experimental Scaling Effects

### 5.3 Field Case Study

The final phase of the study involves validation of the FVC Model using field data. The project selected for the validation is an environmental remediation performed in an expansive clay at a site in Santa Clara, CA. At this site, a pneumatic fracturing pilot scale test was coupled with soil vapor extraction (SVE) and hot air injection (HAI). This section begins with a brief description of the pneumatic fracturing process for the convenience of the reader. An overview of the project follows, which includes a review of site background, soil properties, and applicable test data. The section concludes with a comparison of the field results with predictions of the model.

#### 5.3.1 Overview of the Pneumatic Fracturing Process

The pneumatic fracturing (PF) process is a remediation enhancement technology patented by New Jersey Institute of Technology (NJIT). The technology is used to create artificial fractures in a geologic formation by injecting gas into the subsurface at pressures and flow rates that exceed the natural *in situ* stress. This causes failure of the geologic medium resulting in propagation of horizontal fractures in overconsolidated formations. The fractures serve to increase the permeability of fine-grained formations as shown in Figure 5.5. The increased flow rates and diffusion of vapors and liquids from the matrix into the fracture allow for more efficient contaminant removal or treatment by other remedial techniques such as SVE, groundwater pump and treat, and bioremediation.

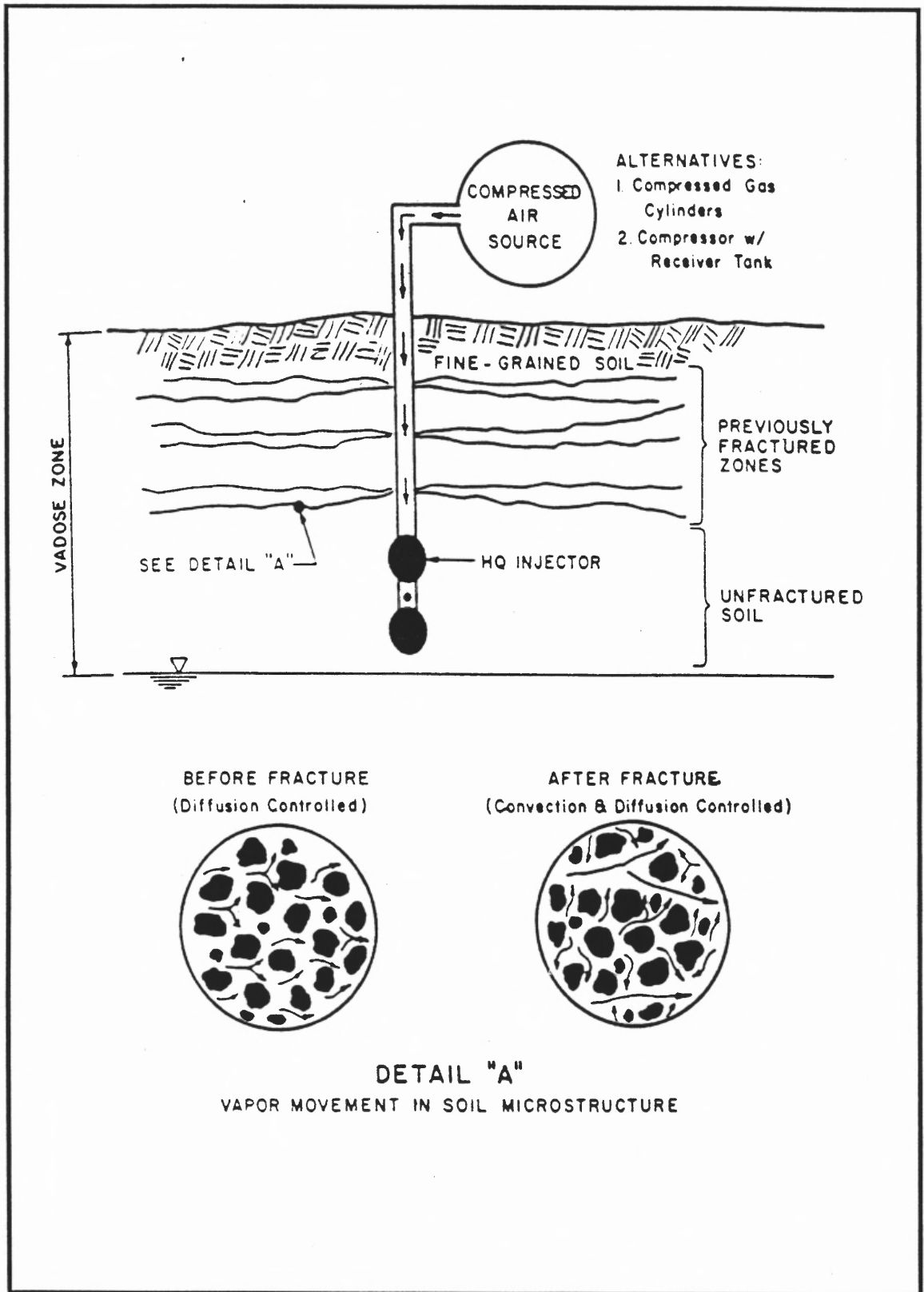


Figure 5.5 Permeability Enhancement by Pneumatic Fracturing (Schuring and Chan, 1992)

### 5.3.2 Santa Clara Site Description

This section presents a description of the case study site, which is based primarily on McLaren/Hart (1993).

Vehicle manufacturing operations at the Santa Clara site resulted in a discharge of solvents at the former waste storage area. The underlying clay soils were found to contain volatile organic compounds (VOCs) at concentrations up to 46 parts per million (ppm). These soils have acted as a source of contamination to the underlying aquifer, where groundwater concentrations of trichloroethylene (TCE) have reached 22 ppm in a plume measuring 2000 ft (610 m) long and 650 ft (200 m) wide.

Conventional soil vapor extraction (SVE) was used as a first attempt to remediate the clay unit, but the results were limited due to the low permeability and high moisture content of the formation. A pilot scale study was performed to investigate the use of pneumatic fracturing and hot air injection (HAI) to enhance SVE. These enhancement technologies served to increase soil permeability through the creation of artificial fractures and clay desiccation, which promotes contaminant volatilization.

The geologic unit of interest to the pilot scale study is a brown to black stiff, silty marine clay of medium to high plasticity that contains thin, laterally discontinuous interbeds of silt and silty sand. The unit extends from zero to twenty feet below ground surface (bgs). A series of physical tests including grain size, Atterberg limits, moisture content and triaxial testing were performed on a

soil sample collected at 10.5 ft (3.2 m) bgs. The test results are shown in Table 5.3.

**Table 5.3** Santa Clara Site Soil Properties at 10.5 ft bgs

Test Parameter	Santa Clara Marine Clay
Grain Size (%)	
Sand (fine)	5
Fines	95
Silt	40
Clay (<2 $\mu$ m)	55
Atterberg Limits	
Liquid Limit ( <i>LL</i> )	81
Plastic Limit ( <i>PL</i> )	28
Plasticity Index ( <i>PI</i> )	53
Miscellaneous	
Natural Moisture Content (wt%)	40
Shear Strength (psf)	2,674
Dry Density (pcf)	77
Porosity (%)	54
USCS Classification	<i>CH</i>

The high liquid limit (*LL*) and plasticity index (*PI*) of 81 and 53, respectively, and the high water content (40 wt%) suggest the presence of the clay mineral montmorillonite. This is also substantiated by the Unified Soil Classification System (USCS) designation of *CH*. In addition, the sample contained a high quantity of clay-size particles, with 55% of the sample measuring less than 2  $\mu$ m in diameter. The data also show that the natural moisture content lies closest to the plastic limit (*PL*). Overconsolidation of the clay formation was confirmed by a comparison of the shear strength, 2,674 lb/ft<sup>2</sup> ( 0.01 kg/km<sup>2</sup>), to the calculated vertical stress at 10.5 ft (3.2 m) bgs. The dry density and porosity of the soil were

calculated from triaxial data to be 77 lb/ft<sup>3</sup> (1.23 g/cm<sup>3</sup>) and 54%, respectively. Based on all of these data, the soil is considered moderately to highly expansive, which is consistent with the findings of Olive et al. (1989) for the soils of this region. The formation is considered suitable for validation of the FVC Model.

### 5.3.3 Pilot Study Test Data

A total of ten wells were installed for the pilot scale study including a fracture well, three hot air injection wells, and six observation wells. The locations of the wells, designated by FW, H, and O, are shown on the site layout plan in Figure 5.6. Fracturing was performed by isolating a 2 ft (0.6 m) interval with a system of packers at depths ranging from 3.5 to 13.5 ft (1.0 to 4.1 m) bgs. The water table was detected at 16.5 ft (5 m) bgs. Sufficient data for model validation were available only for the interval from 9.5 to 11.5 ft (2.9 to 3.5 m) bgs, and thus the remaining analysis focuses on this interval.

Two pneumatic injections, lasting twenty seconds each, were performed in the 9.5 to 11.5 ft (2.9 to 3.5 m) interval. Pressures and flowrates ranged from 275 to 325 lb/in<sup>2</sup> (19 to 23 kg/cm<sup>2</sup>) and 1845 to 2102 ft/min (562 to 640 m/min), respectively. Maximum observed ground surface heave during fracturing was 0.34 in. (8.6 mm) with 0.02 in. (0.5 mm) residual. Vacuum extraction tests performed on the interval showed a substantial increase in flow: 0.03 ft<sup>3</sup>/min (850 cm<sup>3</sup>/min) during pre-fracture to 15.3 ft<sup>3</sup>/min (0.4 m<sup>3</sup>/min) following fracturing at a vacuum pressure of 10 in. Hg (25.4 cm Hg). After adjusting for



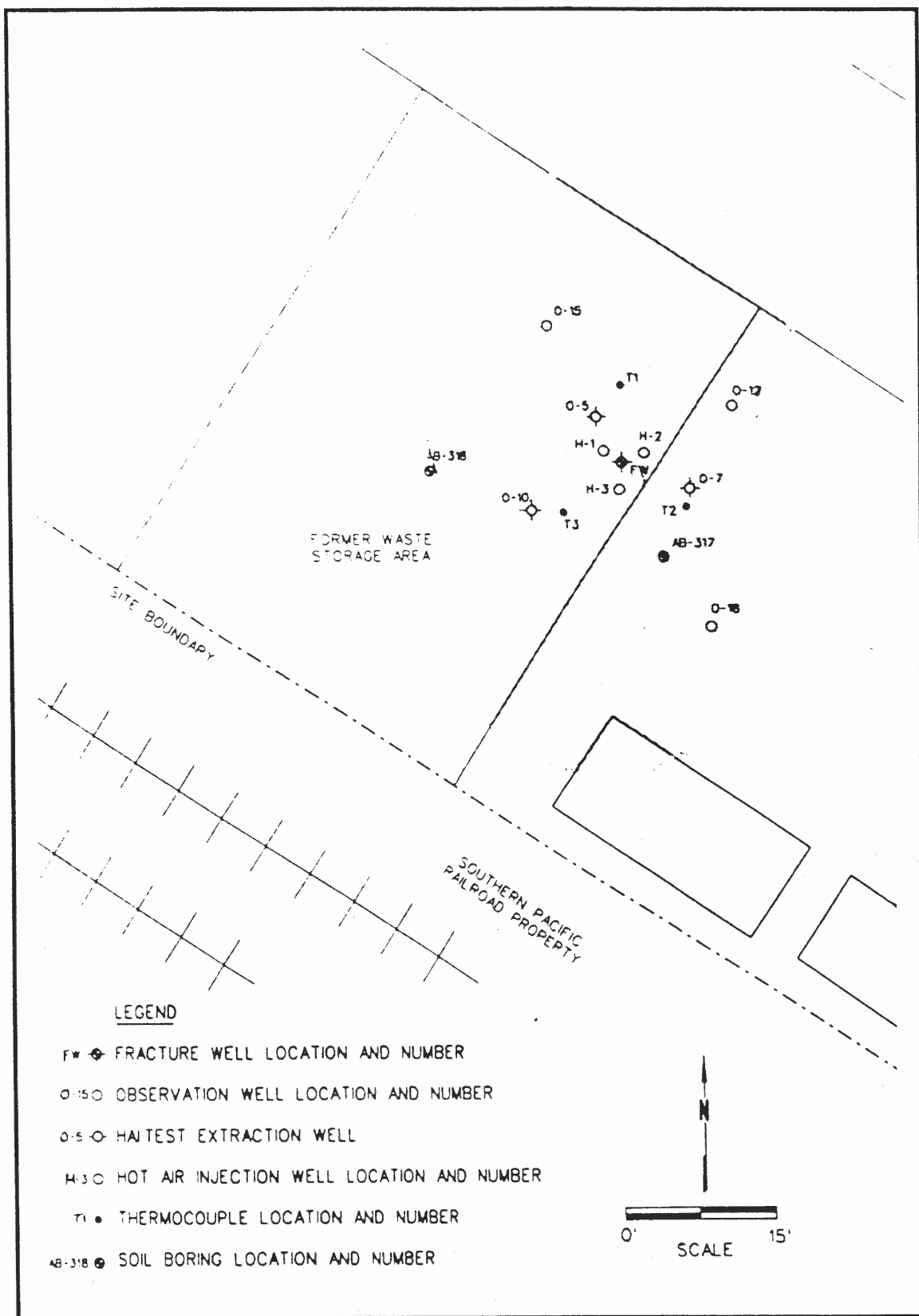


Figure 5.6 Santa Clara Site Plan Layout (Modified from McLaren/Hart, 1993)

the influence of other intervals on the measured flow, the actual post-fracture flow from this interval was estimated to be 6.7 ft<sup>3</sup>/min (0.19 m<sup>3</sup>/min). Total well flows from the 3.5 to 15.5 ft (1.0 to 4.7 m) interval bgs increased from 30.5 to 96 ft<sup>3</sup>/min (0.86 to 2.7 m<sup>3</sup>/min) as a result of fracturing. Overall, the test results showed that the pneumatic fracturing technology successfully created a network of subsurface horizontal fractures. Pressure measurements at outlying observation wells suggest an average radius of influence of 15 ft (4.6 m).

Following the pneumatic fracturing event, the fracture well was subjected to various phases of soil vapor extraction and hot air injection tests. The application of pneumatic fracturing along with these phases resulted in 87% to 96% reductions in soil TCE concentrations. A summary of the test phases is provided as Table 5.4.

At the completion of pilot scale testing, a final moisture content sample was collected one foot from the fracture well at 10.5 ft (3.2 m) bgs. The moisture content at this depth reduced from 40% to 31 wt% over the course of the pilot scale tests.

#### **5.3.4 FVC Model Predictions**

This section presents the moisture content predictions generated with the FVC Model for the Santa Clara pilot scale study. Changes in fracture aperture could not be determined since interval testing was not performed at the completion of the study.

**Table 5.4** Summary of Post-Fracture SVE and HAI Testing

Post-Fracture Testing	Time (min)	Average Vacuum Pressure (in. Hg)	Average Extraction Flow Rate (ft <sup>3</sup> /min)
Soil Vapor Extraction			
Test 1: Total Well, Unplugged	20	7.5	53
Test 2: Total Well, Plugged	240	8.8	62
Test 3: Total Well, Plugged	4,320	5.9	67
Hot Air Injection			
Phase I Hot Air Injection	480	7.7	89
Phase II Hot Air Injection	4,320	7.7	89
Total Well Extraction, Plugged	180	6.5	95
<i>Total and Weighted Averages</i>	<i>Total: 9,560</i>	<i>Weighted Average: 6.9</i>	<i>Weighted Average: 78</i>

Table 5.5 shows the model input parameters for the field study. The assumptions used to apply the FVC Model are now described.

**Table 5.5** Model Input Parameters for Field Case Study

Parameter	Value
Coefficient of Consolidation ( $c_v$ )	0.0003 in <sup>2</sup> /min
Height of the REV Half-Space ( $H$ )	12 in.
Initial Moisture Content ( $w_i$ )	0.40
Total Drying Time ( $t$ )	9,560 min
Equilibrium Moisture Content	0.14
Aerodynamic Evaporation Rate in Fracture ( $E_{af}$ )	$2.0 \times 10^{-4}$ in/min

1. *The soil at the 9.5 to 11.5 ft (2.9 to 3.5 m) interval bgs is assumed to be saturated.*

Although groundwater was at 16.5 ft (5.0 m) bgs, it is well known that capillary rise in clays can extend 5 to 10 ft (1.5 to 3.0 m) above the water table (Tolman, 1937). Thus, the test interval was initially at or near saturation. In addition, the relatively high moisture content is suggestive of saturated conditions.

2. *The soil is considered to exhibit normal shrinkage over the moisture content range of the pilot scale test.* The properties of the site soils clearly suggest that the soil is moderately to highly expansive.

3. *The extraction time is assumed to be 9,260 minutes.* Since the field case study was performed in various phases, drying was not continuous and the vacuum pressures, flows, and evaporation rates were varied. The drying time of 9,260 minutes was chosen as the sum of all of the individual test times.

4. *The coefficient of consolidation,  $c_v$ , is assumed to be 0.0003 in<sup>2</sup>/min (0.002 cm<sup>2</sup>/min).*

Since the properties of the soils at the Santa Clara site are very similar to the Potomac Formation, the same  $c_v$  value was chosen.

5. *The REV half-space is assumed to be 12 in. (0.3 m).* Fracturing was conducted at intervals of 2 ft (0.6 m). Therefore, the REV half-space is estimated to be half of the interval or 1 ft (0.3 m).

6. *Effects of temperature changes in the test soil are neglected.* Although the pilot scale study involved the injection of hot air into the soil at 230°F (110°C), the injection occurred in wells several feet from the test location. It also appears that the heat dissipated quickly, as the temperature of the soils in the observation wells only increased by 1.4°F (0.8°C) on average.

7. *The osmotic potential is assumed to be insignificant in comparison to the moisture potential.* Although there were slight changes in the contaminant level as the TCE volatilized during extraction, the osmotic potential is considered insignificant as compared with the pore-water pressure potential.

8. *The aerodynamic evaporation rate,  $E_{af}$ , is assumed to be  $6.8 \times 10^{-5}$  in./min ( $1.7 \times 10^{-4}$  cm/min).* This  $E_{af}$  value was calculated using the method described in Section 4.2.2.2 as shown in Appendix H.

Since the  $c_v / m$  ratio, at 4.4, is less than 5, the Case 2 FVC Model does not apply. The Case 1 moisture content predictions are shown in Figure 5.7. Since the exact interval of soil moisture content testing is unknown, testing intervals of 0.5, 1.0, and 2.0 ft (0.15, 0.30, and 0.61 m) were considered. The final moisture content measured in the field was 31%. The final moisture content predicted by the model ranges from 25.5% to 35.8%, depending on the assumed sampling interval. If the moisture content over the three intervals is averaged, then the model prediction becomes 30.7% (versus 31% actual field moisture). These

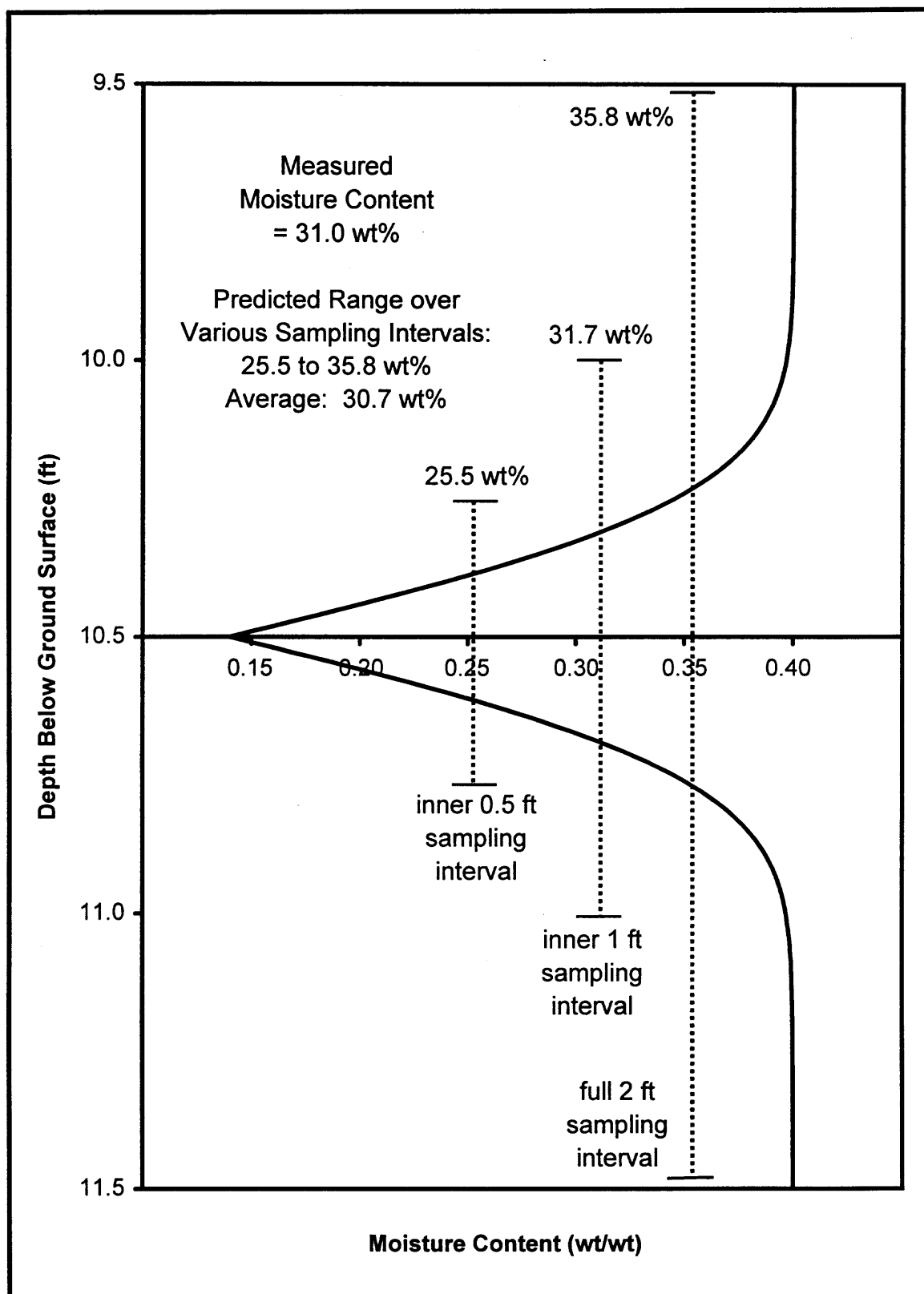


Figure 5.7 Comparison of Field Case Study Data with Case 1 FVC Model Moisture Predictions

favorable results suggest that the FVC model adequately represents the observed moisture loss at the Santa Clara site, and they provide a first field validation of the model.

## CHAPTER 6

### FVC MODEL APPLICATION PROCEDURES

#### 6.1 Introduction

This section presents explicit procedures for running and applying the Fracture Volume Change Model (FVC Model). It is written as a guidance document for the consultant or modeler to aid in extending the FVC model to actual industrial applications. The FVC model can be used to solve problems as a single, stand-alone component or it may be incorporated as a subroutine in an existing model. The chapter begins with an overview followed by a detailed procedural guide to applying the FVC Model (Section 6.2). General functional relationships are established in Section 6.3, and an example application of the model is presented in Section 6.4. The chapter concludes with a review of data requirements for continued model calibration and validation (Section 6.5).

#### 6.2 Procedural Guide to FVC Model

This section presents step-by-step procedures for applying the FVC Model. It is assumed that the model is being applied to a field site underlain by clay soil containing natural or artificial horizontal fractures.

Step 1: Obtain a soil sample(s) at the depth(s) of interest and perform an **expansivity characterization** (Hall, 1995, e.g., Figure 2.1). Proceed if the soil is moderately to highly expansive.



Step 2: Determine the **homogeneity** of the soil body of interest. This may be accomplished by collecting continuous split spoon, core barrel, or Shelby tube samples in the depths of interest. The FVC Model should be applied if the soil body is generally homogeneous.

Step 3: Ensure that the expected moisture content change is within the **normal shrinkage range**. When high accuracy modeling is required, a shrinkage curve may be created from laboratory analysis (e.g., Figure 3.17). In most applications, it is sufficient to confirm that the moisture content does not fall significantly below the Atterberg *PL*. For highly expansive soils, the moisture content may approach the Atterberg *SL*. Proceed if this condition is satisfied.

Note: The FVC Model can be used to approximate soil behavior in the residual shrinkage phase (i.e., unsaturated condition), although such results must be considered a maximum. Better results can be obtained by incorporating the unsaturated component into the model.

Step 4: Ensure that there is a **constant initial moisture profile** within each half-REV. This is usually determined by professional judgement. If questionable, sampling and moisture content testing may be performed. Proceed if this condition is satisfied.

Step 5: Estimate the **vertical distance between adjacent fractures**. This may be determined by borehole video analysis, identified from previous investigations, or determined from field fracturing depths if artificial fractures are created. Half the distance of the fracture spacing represents the thickness of the REV half-space.

Step 6: Determine the **initial moisture content(s)**,  $w_i$ , of the soil at the depth(s) of interest. This may be determined by sampling and testing or *in situ* measurements, where appropriate.

Step 7: Estimate a **coefficient of consolidation**,  $c_v$ , for the field soil at the depth(s) of interest. This may entail running a consolidation test and/or obtaining literature values.

Step 8: Determine the **equilibrium moisture content**,  $w_e$ . The  $w_e$  for drying may be estimated by the Atterberg *SL* for most expansive soils. In a wetting mode, the equilibrium moisture content may be approximated as the field capacity. Both the *SL* and the field capacity are determined in the laboratory.

Step 9: Determine the **duration of drying or wetting**, defined as time  $t$ . This may be the estimated duration of an extraction system, for example. Natural desiccation or infiltration effects may be computed from local or regional rainfall and evapotranspiration data combined with an analysis of hydrogeologic soil properties.

Step 10: **Calculate the moisture content change** with space and time using Eq. 6.1, which is the reduced form of Eqs. 4.25 and 4.26 for Case 1 modeling.

$$w(z,t) = w_e + \sum_{n=1}^{\infty} \left\{ \left[ \frac{4(w_i - w_e)}{(2n-1)\pi} \right] \exp \left[ -c_v \left( \frac{(2n-1)\pi}{2L} \right)^2 t \right] \right\} \sin \left( \frac{(2n-1)\pi}{2L} z \right) \quad (\text{Eq. 6.1})$$

where  $w$  is the gravimetric moisture content,  $z$  is the vertical coordinate,  $t$  is time,  $w_e$  is the equilibrium moisture content,  $c_v$  is the coefficient of consolidation,  $L$  is the length of the REV half-space, and  $n$  is the number of intervals (Suggest use of  $n=100$ ).

Step 11: Determine if **one-dimensional or three-dimensional volumetric change** is appropriate for the site conditions. In most cases, the volumetric change may be considered three-dimensional. One-dimensional strain may be considered for swelling soils under lateral constraint.

Step 12: Relate the change in moisture content to **vertical soil deformation**. First, determine the amount of water lost in the REV half-space (Figure 4.8, Eqs. 4.3 and 4.4). Convert this to the volume of water lost over the REV half-space (Eq. 4.5). The vertical soil deformation is then computed for one- and three-dimensional strain by Eq. 4.6 and Eqs. 4.7 through 4.11, respectively.

Step 13: Compute the **change in aperture** from the vertical soil deformation in each REV half-space using Eq. 4.13. Where appropriate, the volume

change may be converted to a final aperture by addition of the positive (i.e., swelling) or negative (i.e., desiccation) deformation to the initial aperture. Initial apertures may be back-calculated from flow tests using the Cubic Law (Appendix F), or determined from borehole video analysis, for example.

**Step 14:** The **cumulative effect on a soil body from multiple fractures** may be determined by summing the vertical strains of each individual fracture to examine the effect on the overall soil body.

Use of these procedures are illustrated in an example application contained in Section 6.4.

### 6.3 Functional Relationships

This section presents three functional relationships that can be generated using the FVC Model. These relationships are useful for analyzing fractured clays, and they include: (1) moisture content-time, (2) fracture aperture-moisture content, and (3) fluid flow-moisture content. Each of these will now be described.

#### 6.3.1 Moisture Content-Time Relationship

The FVC Model can be used to generate a general relationship between moisture variation and time for various fracture spacings. Moisture reduction may be a useful indicator, for example, of the mass removal rate of certain solutes. Conversely, moisture increase in a clay is of interest when assessing water

availability of crops. The rate of moisture change is primarily dependent on soil hydraulic properties, so the coefficient of consolidation,  $c_v$ , is used as a range variable. Fracture spacing is the other key range variable in this relationship.

The generalized functional relationship between moisture content and time is presented in Figure 6.1 for a range of typical  $c_v$  values and fracture spacings. Note that the moisture factor ( $MF$ ) represents the percent of the total potential moisture change, and is computed as:

$$MF = \frac{w_i - w_f}{w_i - w_e} \cdot 100 \quad (\text{Eq. 6.2})$$

where  $w_i$ ,  $w_f$ , and  $w_e$  are the initial, final, and equilibrium moisture contents. The use of this moisture factor is illustrated in Section 6.4.

It is important to note that the relationship depicted in Figure 6.1 represents an average moisture content over the REV half-space. In actuality, the moisture change is greatest near the fracture and least at the boundary between adjacent REV's. The FVC Model may be directly applied to obtain moisture content variations within the REV half-space, where necessary.

It is additionally noted that the moisture-time relationship was developed assuming a moisture content change within the normal shrinkage range. Thus, use of Figure 6.1 should be limited to this condition. Expansion of the analysis to other shrinkage ranges will be possible in the future when the unsaturated model component is incorporated.

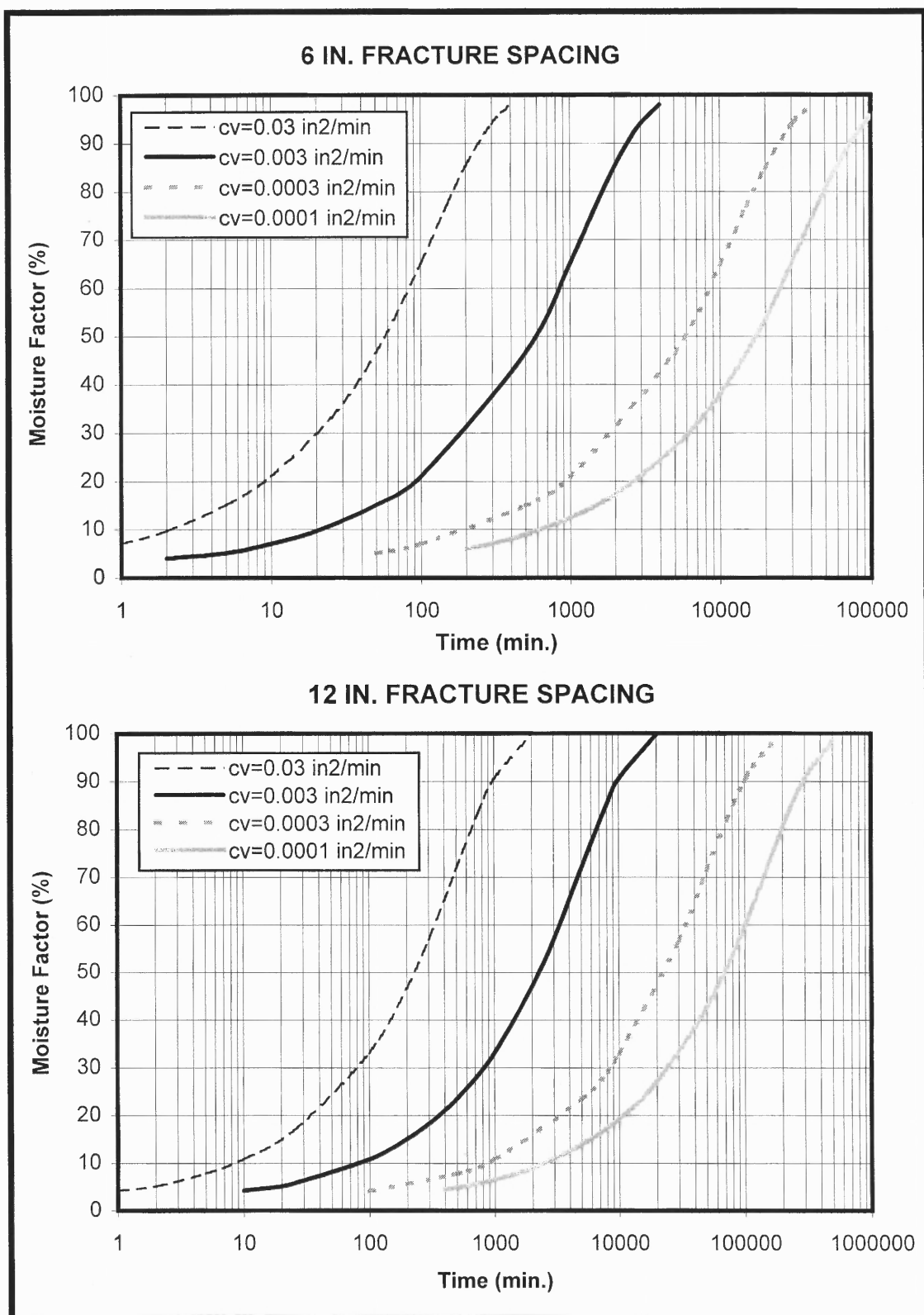


Figure 6.1 Theoretical Moisture Content-Time Relationship

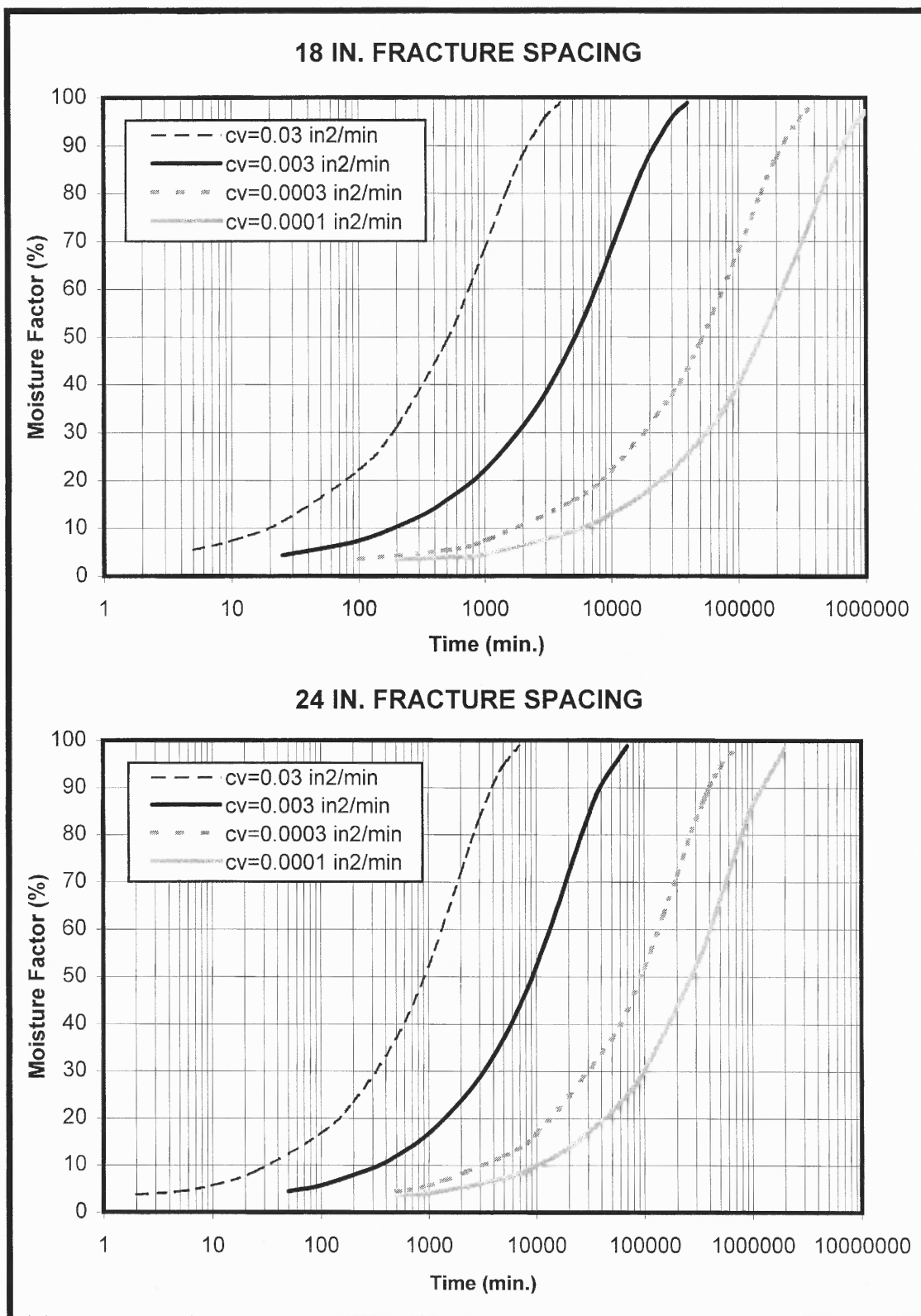


Figure 6.1 (cont'd.) Theoretical Moisture Content-Time Relationship

### 6.3.2 Fracture Aperture-Moisture Content Relationship

The FVC Model can also be used to generate a general relationship between moisture content variation and changes in fracture aperture. The functional relationship between moisture content and fracture aperture is presented in Figure 6.2, where fracture spacing and soil dry density are the major range variables. The graphs were developed by assuming three-dimensional shrinkage, an average moisture content change over the entire fracture interval, and normal shrinkage.

To use Figure 6.2, it is first necessary to input a moisture content change. This may be determined from Figure 6.1, or it may be obtained in the field. If the latter is used, it is critical that the formation be sampled over the entire REV half-space to maintain consistency with the general assumptions. Moisture contents should also be within the normal shrinkage range. Figure 6.2 shows that in expansive soil, large changes in fracture aperture can occur for relatively small moisture content changes in the normal shrinkage range.

### 6.3.3 Fluid Flow-Moisture Content Relationship

The third functional relationship predicted by the FVC Model is the effect of moisture content changes on fluid flow. Fluid flow through an expansive clay is directly related to the fracture aperture (i.e., there is little influence of flow through the matrix). Since the FVC Model can quantify the interaction between moisture and fracture aperture, it can also be used to predict changes in fluid



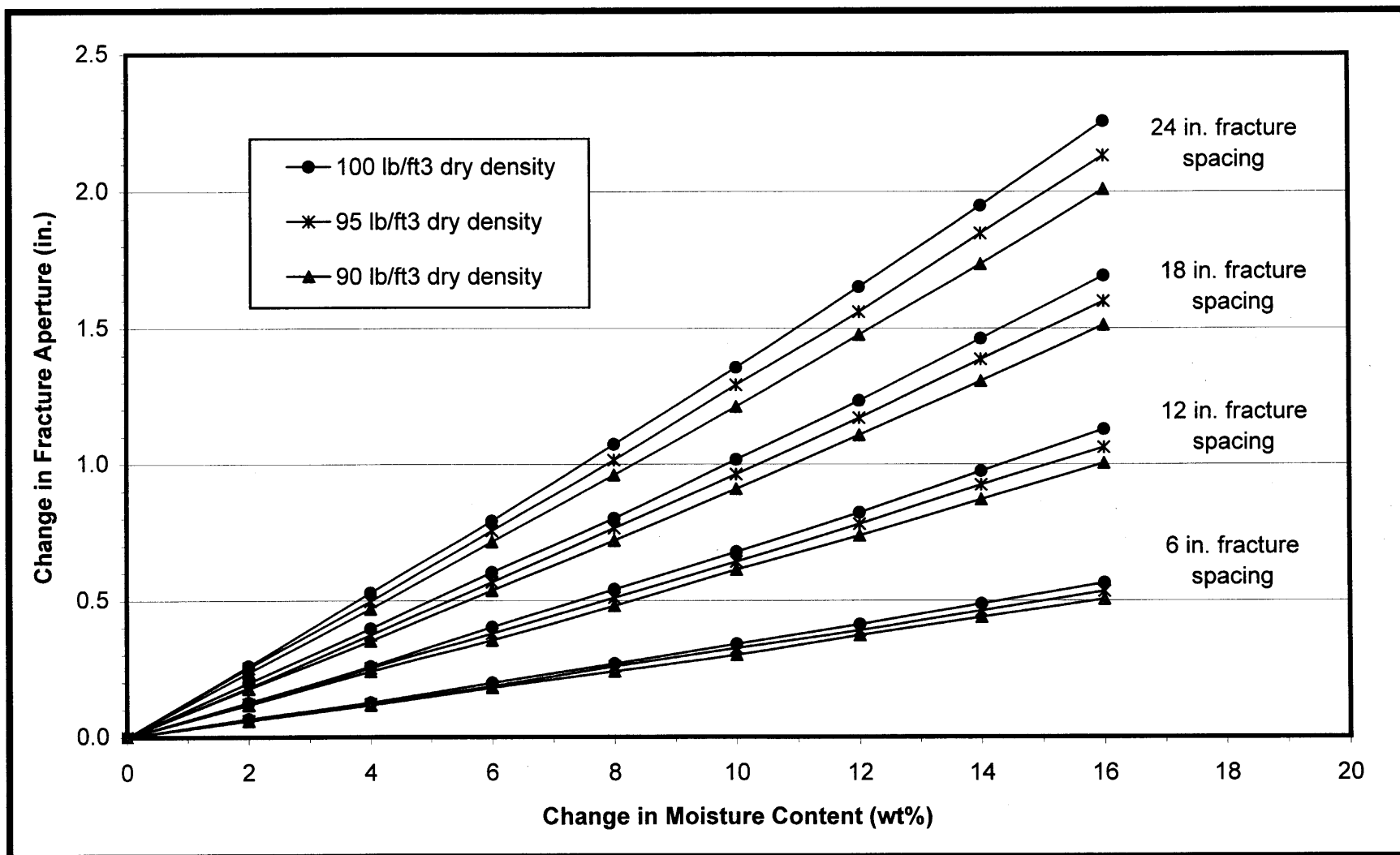
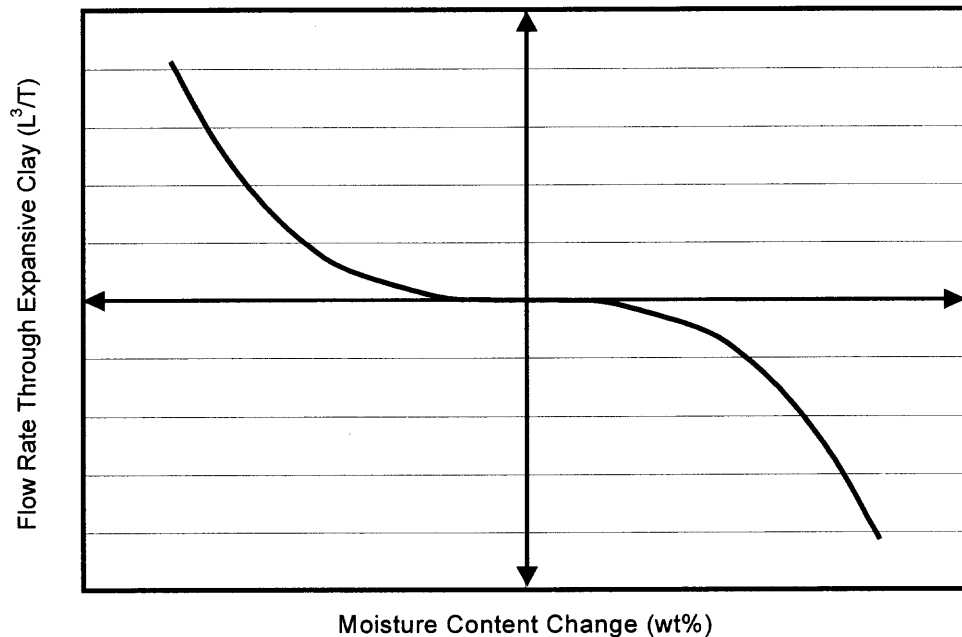


Figure 6.2 Theoretical Moisture Content-Fracture Aperture Relationship

flow. The primary range variables in this case are fracture aperture, radial extent of the fracture, and pressure differential across the fracture. Figure 6.3 presents the general form of the fluid flow-moisture content relationship which is developed on a site-specific basis. The relation can also be used to predict changes in the bulk hydraulic conductivity,  $K$ , since this is also controlled by fracture aperture size.



**Figure 6.3** Relationship between Fluid Flow and Moisture Content

#### 6.4 Example Application

It will be assumed that surface spills at an industrial site in Southeastern Fairfax County, VA have contaminated the overburden. Collection and analysis of subsurface soil samples show that the contamination has migrated into a clay

layer, which is serving as a slow, yet continuing source of contamination to underlying groundwater. Based on results of the risk assessment, the responsible party has decided to treat the source area.

The contaminated source area belongs to the southern facies of the Potomac Formation, which carries the clay mineral montmorillonite. The clay is homogeneous, overconsolidated, moderately to highly expansive, and contains natural fractures. The natural moisture content of 40% falls between the Atterberg Plastic Limit (45%) and Shrinkage Limit (15%). The moisture content is constant throughout the 10 ft (3.1 m) layer, which lies from 5 to 15 ft (1.5 to 4.6 m) below ground surface. The coefficient of consolidation,  $c_v$ , was determined in the laboratory to be 0.0003 in<sup>2</sup>/min (0.002 cm<sup>2</sup>/min), and the average dry density is 95 lb/ft<sup>3</sup> (1.52 g/cm<sup>3</sup>).

Soil vapor extraction (SVE) was chosen as the treatment technique to remove volatile contamination. The SVE will also serve to desiccate the clay, thus opening the existing fractures, improving connectivity, and increasing access to the contaminants. The system was run for approximately 2 weeks with no infiltration events occurring during this time. Borehole video analysis confirmed the presence of five main horizontal fractures at intervals of approximately 2 ft (0.6 m).

The FVC Model will now be used to predict the final moisture content and change in aperture using the previously described procedural guide (Section 6.2) and functional relationships (Section 6.3).

1. The soil is identified as moderately to highly expansive using the literature and/or expansivity characterization. Field sampling confirmed that the soil is homogeneous and of uniform moisture. Normal shrinkage is expected because of the large shrinkage index ( $SI$ ) and a natural moisture content near the plastic limit ( $PL$ ). The conditions at the site satisfy the requirements of the FVC Model (Steps 1 to 4).
2. The distance between adjacent fractures is determined by borehole video analysis to be 2 ft (0.6 m). Thus, the REV half-space thickness is 12 in. (0.3 m) (Step 5).
3. The initial moisture content and coefficient of consolidation are determined by laboratory analysis of extracted soil samples to be 40 wt % and  $0.0003 \text{ in}^2/\text{min.}$ , respectively (Steps 6 and 7).
4. The equilibrium moisture content for drying is estimated by the Atterberg Shrinkage Limit ( $SL$ ) test to be 14% (Step 8).
5. The duration of drying is dictated by the length of treatment, which in this case, is 2 weeks, or 20,160 min. (Step 9).
6. The FVC Model Eq. 6.1 is now applied to compute the moisture content profile shown in Figure 6.4, upper graph (Step 10). It is necessary to determine the average final moisture content over the interval for 2 weeks

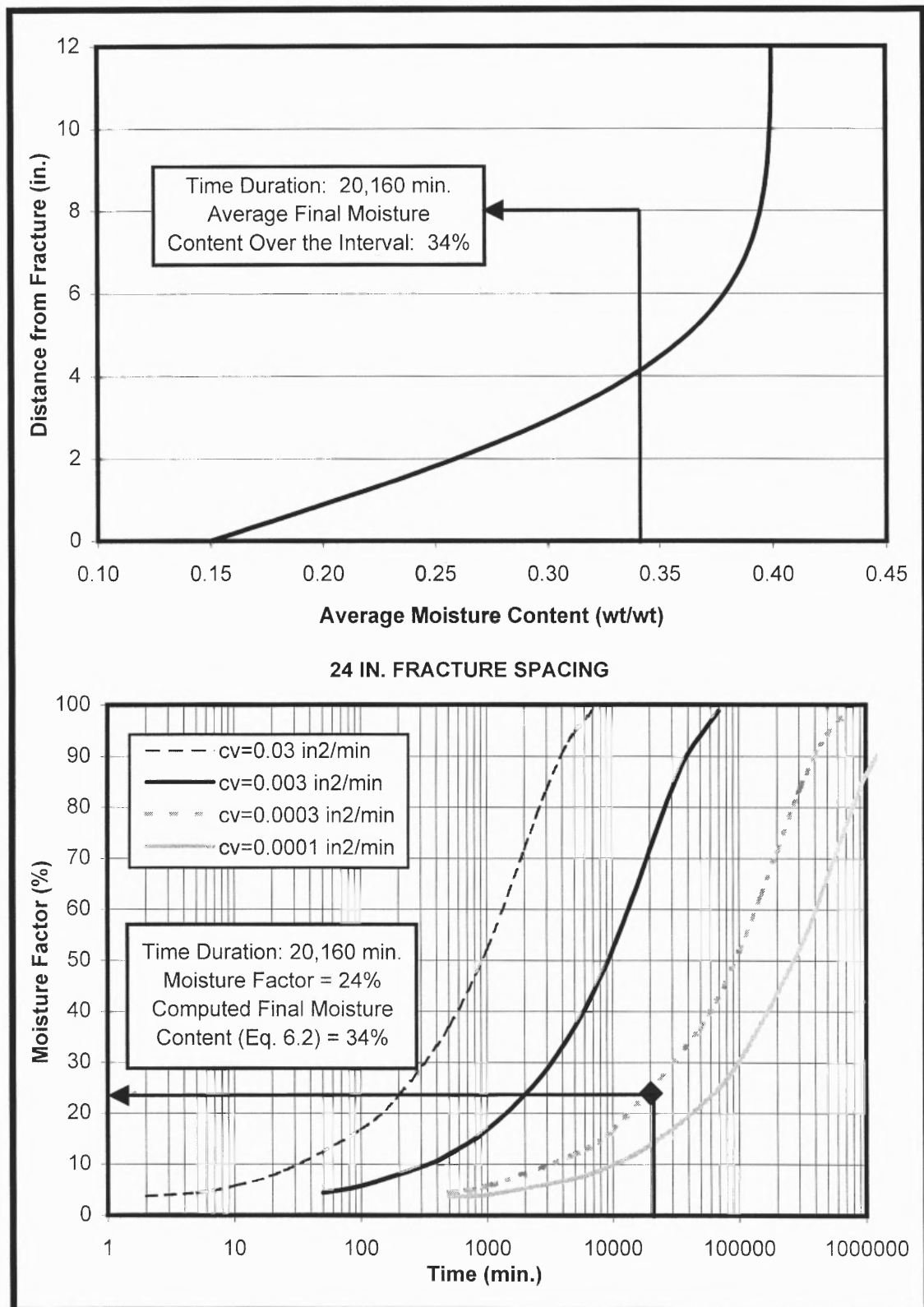


Figure 6.4 Example Determination of Change in Moisture Content

of drying. One method is to calculate the average moisture content from the curve in Figure 6.4 (upper graph), which yields a value of 34%. Alternatively, the final average moisture content may be determined using Figure 6.1 and the Moisture Factor ( $MF$ ) Eq. 6.2. This procedure is illustrated in Figure 6.4, lower graph, where a duration of 20,160 min. and a  $c_v$  of 0.0003 in<sup>2</sup>/min. yields a  $MF$  of 24%. The moisture factor relation, Eq. 6.2, is then solved for final average moisture content,  $w_f$ , which yields 34%, as before.

Note: The target endpoint in most applications is the average moisture content over the entire interval, in which case either method is appropriate. Where specific moisture contents within the interval are needed, then the former method must be used.

7. Assuming three-dimensional shrinkage, vertical soil deformation is now determined using Eqs. 4.3 to 4.5 and Eqs. 4.7 to 4.11, which is then converted into aperture change using Eq. 4.13. Figure 6.2, which summarizes this functional relationship, can be used in lieu of calculations. Application to the current example is illustrated in Figure 6.5. Here, a moisture content change of 6 wt% (i.e., 40 wt% - 34 wt%) at an average dry density of 95 lb/ft<sup>3</sup> (1.52 g/cm<sup>3</sup>) translates into a change in aperture of 0.76 in. (1.9 cm), as shown in Figure 6.5 (Steps 11 to 13).

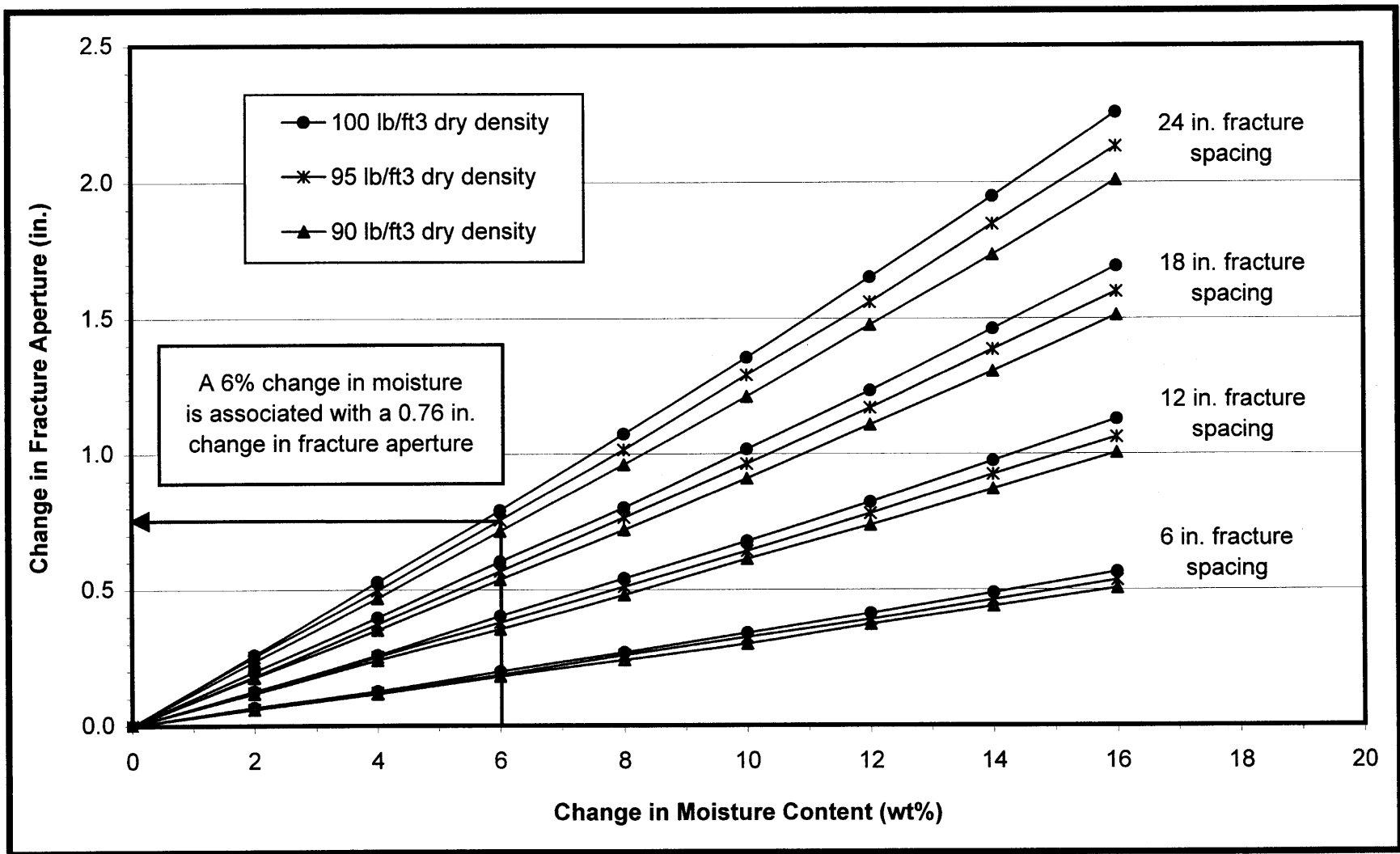


Figure 6.5 Example Determination of Change in Fracture Aperture

Note: When available, a shrinkage curve should be used to define dry density changes associated with soil volume fluctuations since it will improve model accuracy.

Finally, the final fracture aperture is computed by adding the change in aperture to the actual initial aperture. The initial aperture is best determined by extracting air, measuring flows and pressures and applying the Cubic Law. For the present example, field extraction from the 4 in. borehole yielded a flow of 0.16 ft<sup>3</sup>/min (4,500 cm<sup>3</sup>/min) under a vacuum pressure of 10 in. Hg (254 mm Hg). Assuming for simplification purposes that the five discrete fractures are of equal size, flow through each is 0.032 ft<sup>3</sup>/min (900 cm<sup>3</sup>/min). The initial aperture is calculated using the Cubic Law to be 0.0051 in. (0.13 mm) (Appendix H), assuming a fracture radius of 15 ft (4.6 m). The final aperture is thus estimated as the sum of 0.0051 in. (0.13 mm) and 0.76 in. (19.3 mm), or 0.7651 in. (19.4 mm).

The effect of this aperture increase on fluid transfer is illustrated by calculating the associated flow using the Cubic Law (Appendix H). Under similar conditions, the flow from each fracture would theoretically increase to  $1.2 \times 10^8$  ft<sup>3</sup>/min ( $3.4 \times 10^6$  m<sup>3</sup>/min). While this figure is clearly exaggerated, it does show that volume change in expansive clay can significantly affect apertures, which profoundly influences flow.

In reality, pressures drop sharply as the aperture increases, so the formation would not exhibit changes in flow of such magnitude. Also, the



fractures are not truly planar, but rather contain asperities and discontinuities, particularly at the fracture intersection where localized swelling causes differential volume change. These areas act as dead zones, reducing the overall conductivity of the fracture network. By reopening these areas, the connectivity and efficiency of network fluid transfer is improved. Additionally, some formation collapse can be expected as a result of multiple stacked fractures. Finally, shrinkage cracks develop vertically from the fracture as the soil desiccates, which reduces the diffusive distance contaminants must travel before contacting the fracture.

### 6.5 Data Requirements for Continued Model Calibration

To increase the accuracy and reliability of the FVC Model, it is imperative that the calibration process be continued. Certain field data beyond that required to run the model are required to perform calibration, and are described in this section. The principal objectives are to: (1) improve selection of equilibrium moisture content; (2) confirm final moisture content predictions; and (3) verify final fracture aperture predictions.

To calibrate the equilibrium moisture content,  $w_e$ , collect multiple measurements of moisture content within the REV half-space after the drying or wetting event. For a fracture spacing of 24 in. (61 cm), for example, obtain a field soil core which spans the upper and/or lower REV half-space of 12 in. (31 cm). The soil should then be separated into increments of 1 or 2 in. (2.5 or 5 cm), and

moisture content testing performed on each. Calibration is executed by varying the  $w_e$  in the FVC Model until the model predictions correlate most closely with the field data. This  $w_e$  should then be used for all future model predictions in similar soils and conditions.

Moisture content predictions are confirmed by collecting initial and final field moisture data within the REV. For high accuracy verification, moisture content samples should be collected in small increments within the REV half-space as described above. Alternately, one moisture content sample can be collected which represents an average over the entire REV half-space. Use the field moisture data to substantiate the FVC Model predictions.

To verify the FVC Model fracture aperture predictions, it is necessary to obtain initial and final fracture aperture data from field sites. This is normally accomplished by packing off and isolating a discrete fracture and performing an interval extraction test. Fracture aperture is then computed by measuring flow and pressure at radial distances from the extraction point and applying the Cubic Law (Appendix H). Compare the final fracture aperture predictions to those computed with the Cubic Law.

Users of the FVC Model are encouraged to maintain a database of equilibrium moisture contents for various soil types and conditions, as well as accuracies of moisture content and fracture aperture predictions. This is especially important for the wetting mode since current data are most limited in this area.

## CHAPTER 7

### CONCLUSIONS AND RECOMMENDATIONS

#### 7.1 Conclusions

Clay soils are unique in that they are prone to volume change from moisture fluctuation. When fractures are present in these soils, volume change induces a change in fracture geometry. Since the fracture is the principal conduit for environmental fluctuations that trigger volume change, an important interrelationship exists. Tools are needed to define this interaction since it is the source of adverse behavior in variety of fields including environmental remediation, agriculture, civil engineering, and resource geology.

The current study has focused on the mechanisms of volume change and its effect on fracture geometry with the goal of developing a model that predicts these changes. The approach is unique in that it examines effects of volume change on discrete fractures. The work considers horizontal fractures since these are expected to predominate at most overburden depths. An overview of the study and the general conclusions are now presented:

1. The basic premise of the study was verified experimentally using horizontal infiltrometer tests. In these tests, changes in aperture of an artificial discrete fracture were successfully induced in an expansive clay by controlling the environmental conditions in the fracture. Drying of the fracture boundary soils caused fracture dilation, while wetting caused fracture constriction.

2. A new model, termed the 'Fracture Volume Change Model,' or FVC Model, was developed to predict soil volume change and associated changes in fracture aperture from moisture fluctuations in the fracture. The representative elemental volume (REV) is assumed to be a discrete horizontal fracture in an expansive clay with rigid, outer no-flow boundaries and an inner flexible yielding boundary along the fracture. The moisture prediction component of the FVC Model is based on a particular solution of the one-dimensional diffusion equation. Two model variations were considered, differing only in the boundary condition at the fracture. Case 1 considers a constant equilibrium moisture content, while Case 2 uses a constant flux. Changes in fracture geometry (i.e., aperture) are predicted directly from the change in water volume considering either one-dimensional or three-dimensional volume change. The model allows for analysis at both the discrete and bulk scales.

3. Validation and calibration of the FVC Model was performed using drying stage horizontal infiltrometer test data. Moisture values predicted with the Case 1 FVC Model demonstrated reasonable agreement with the laboratory data, deviating 6% on average. Predictions of fracture aperture were generally overestimated. Case 2 was shown to be less predictive of the experimental data, and the function appears to mimic first stage evaporation and drainage. Therefore, the Case 2 solution may have some application in soils of higher permeability.

4. A field validation of the model was performed using data from an environmental remediation project in an expansive clay formation located in Santa Clara, California. Artificial discrete fractures, created using the pneumatic fracturing process, were subjected to soil vapor extraction and hot gas injection to remove chlorinated solvent contamination. The FVC Model was used to predict moisture loss at depth in the clay following desiccation by extraction testing. Model predictions showed good agreement with field moisture measurements.

5. The modeling results indicated that the test soil was dominated primarily by second stage evaporation (i.e., the water transmission properties of the soil control the flux at the fracture boundary). The results have important implications for extraction technology design. The study suggests that field extraction systems designed to maximize evaporation rates in the fractures of expansive soil may not be cost-effective.

6. The Case 2 FVC Model was shown to be sensitive to the ratio between the coefficient of consolidation,  $c_v$ , and the flux at the fracture boundary,  $m$ . It is predictive only when the  $c_v / m$  ratio exceeds approximately thirty. The model is also limited by the difficulty of identifying the fracture boundary flux in a field situation. The Case 2 model may have application for modeling soil behavior in the first stage of evaporative drying (i.e., where evaporation rate controls the

moisture flow). Such conditions are usually present in soils of moderate to high permeability.

7. The horizontal infiltrometer tests also provided important insight about fracture permanence and closure. Differential volume change was observed to be the major mechanism of fracture closure, although full closure was not observed under the experimental conditions. As moisture entered the fracture, the high soil suction caused the water to partition immediately to the soil matrix, resulting in a localized constriction of aperture. The fracture was shown to completely recover on redrying, and occurred at an accelerated rate compared with initial drying.

8. The current study has provided the impetus for an improved understanding of saturation conditions in expansive soils, which has implications for modeling of soil behavior. The literature generally considers expansive clays to be unsaturated, in part because the saturation domain has recently been extended to include soils with negative pore-water pressures. In many soils with negative pressures, pores desaturate quickly so the two conditions (i.e., negative pore-water pressure and air entry into the pore space) are often coupled. In expansive clays, however, the clay structure has the capacity to collapse to accommodate the loss in moisture. The matrix thus remains saturated over a wide range of

moisture contents. Thus, air enters the formation only in the form of shrinkage cracks except at very low moisture contents.

The current trend for modeling expansive soils is unsaturated soil mechanics. While it is not disputed that this method provides an accurate model of expansive soil behavior, it is computationally intensive and requires numerical processing of a large number of specialized input parameters. Recognizing that expansive soils exhibit normal shrinkage in the range of typical field moisture contents, saturated domain modeling serves the same purpose but in a more simplified fashion, using closed-form solutions that require only a small number of industrially available input parameters. This is significant since the industrial utility of a mathematical model is typically proportional to its simplicity.

## **7.2 Recommendations for Future Work**

The results of the current study have provided a template for additional investigation into the interrelationship between fractures and volume change. The following are recommended topics for future study:

*Continued Model Validation and Calibration:* It is recommended that additional horizontal infiltrometer tests be performed on soils of differing expansivities and moisture regimes. A controlled field case study, designed specifically for the purposes of validation and calibration, is also recommended.

*Expand Model to Other Initial Conditions:* The current study focused on soils with an initially constant moisture profile. It is recommended that the model be solved for other initial conditions, which would allow predictions of cyclic moisture changes.

*Consider Alternate Means of Identifying the Fracture Boundary Flux:* The Case 2 Model may be rendered more useful if a means of identifying the fracture boundary flux can be determined for field soils. Use of the aerodynamic evaporation rate in the fracture is expected to result in low  $c_v/m$  values in most cases, which causes instability of the Case 2 Model function.

*Further Define Limits of Applicability:* There are two critical application limits that warrant further investigation. The first is the critical moisture content that defines the transition from the first to second stage evaporation. This would be useful in determining the limits of applicability for the Case 1 and Case 2 model forms. The second is the point at which the evaporative driving force equals the soil moisture holding force (i.e., suction). At evaporation rates below this critical level for a particular soil type, no-flow conditions will prevail, and the Case 1 model becomes obsolete.

*Integrate the Unsaturated Domain into the FVC Model:* It is recommended that the FVC Model be developed to include both saturated and unsaturated domains. Model validation and calibration would require additional laboratory HI testing.



**APPENDIX A**  
**PHOTOGRAPHS**



Photograph A-1. Gullies formed by erosion of weathered, unvegetated Potomac Formation clay, Rainwater Landfill, Lorton, VA.



Photograph A-2. Shrinkage cracks in Potomac Formations clay, Rainwater Landfill, Lorton, VA. The end of the mattock is 15 in. long.





**Photograph A-3.** The Potomac Formation clays required excavation by a bulldozer. The blue and red clays are shown to the left and right, respectively.



**Photograph A-4.** The clay maintained itself as large blocks and was difficult to breakdown.





Photograph A-5. This photograph shows the form of the soil clods prior to compaction. The diameter of the bowl is approximately 10 inches.



Photograph A-6. The clay was compacted using a series of blows from a Proctor rammer.



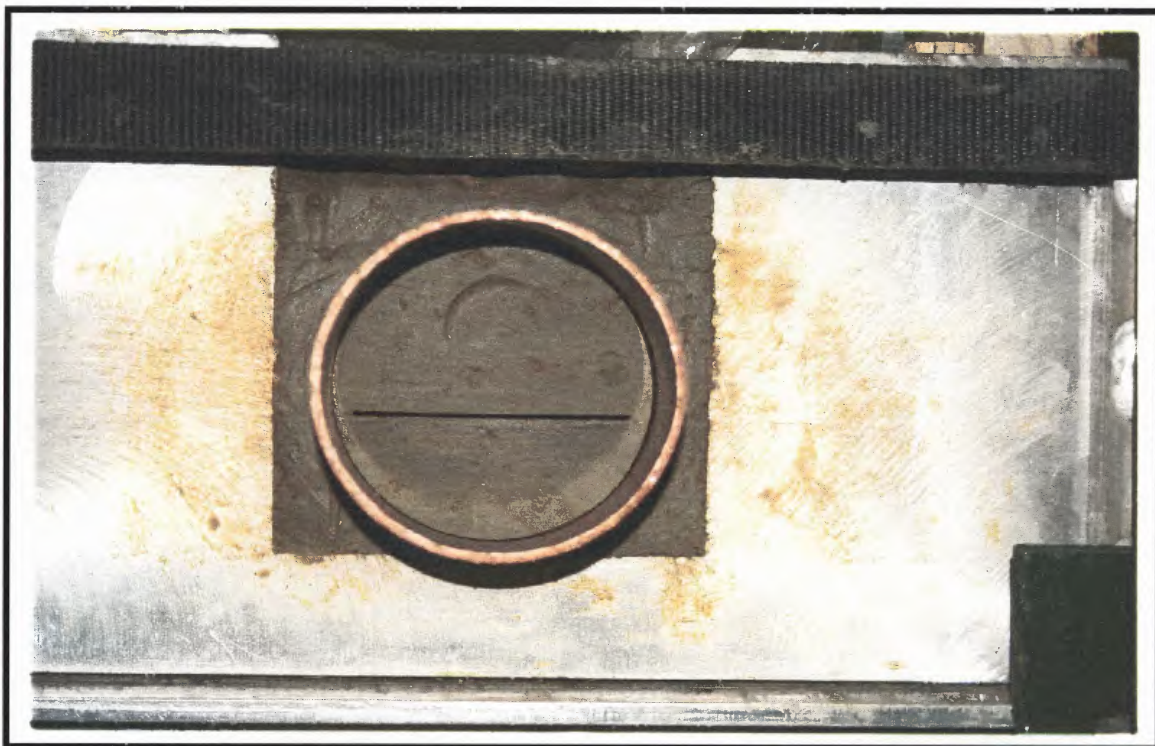


Photograph A-7. The sheet metal spacer is placed on top of the compacted soils. Note the slightly slickensided surface.

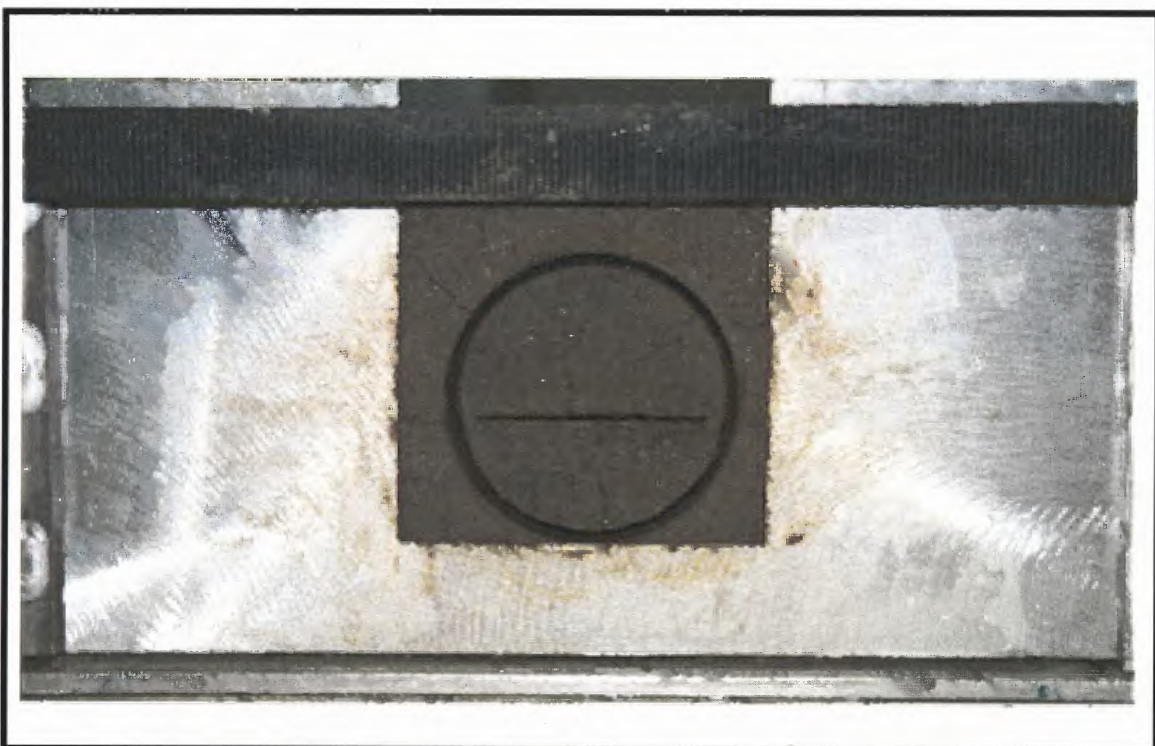


Photograph A-8. The sheet metal spacer was pulled from the soil using a modified sample ejector leaving an open discrete fracture.





Photograph A-9. This is a view of the discrete fracture that was created by removing the sheet metal spacer. Note the uniformity of the aperture.



Photograph A-10. The fracture showed a slight increase in aperture at the completion of the horizontal infiltrometer test. Note the shrinkage cracks.



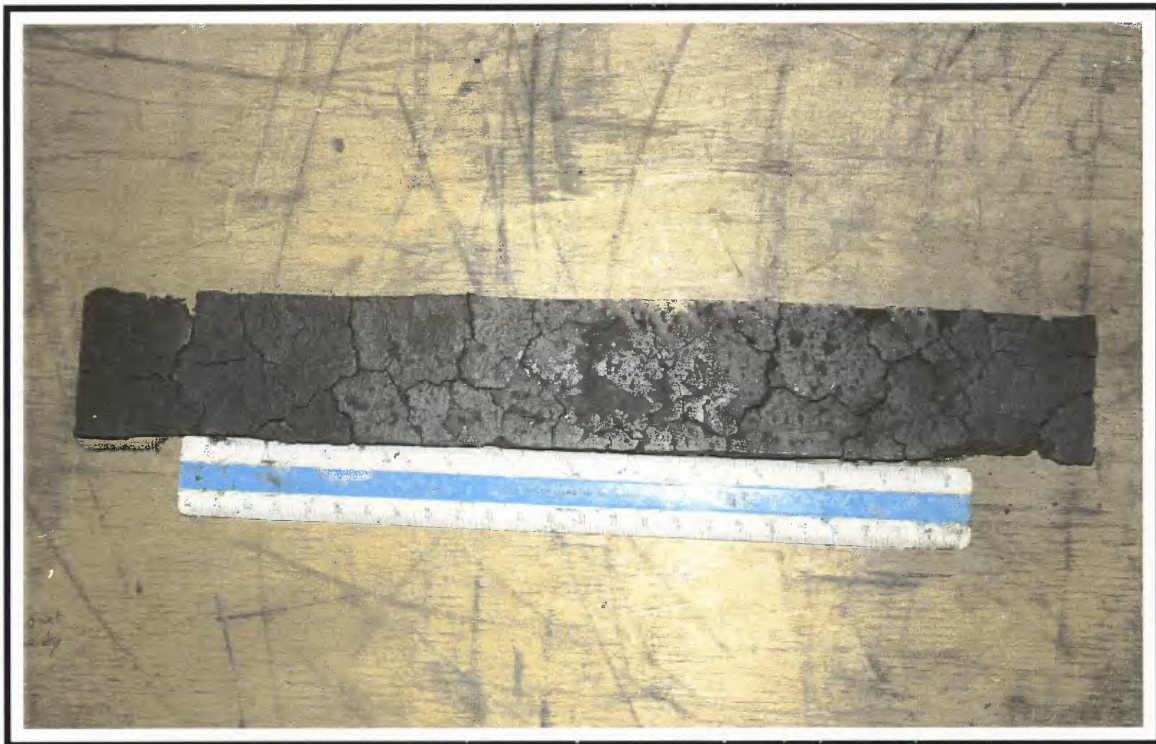


Photograph A-11. The soil block was excavated and sampled in vertical and horizontal layers to obtain moisture data.



Photograph A-12. Shrinkages cracks were apparent in the soils 1 in. above the fracture. The cracks are approximately 1 to 2 mm wide.





**Photograph A-13.** A higher density of shrinkage cracking occurred in the soils at the fracture. This is a photograph of the upper surface of the fracture.



**Photograph A-14.** A similar form of shrinkage cracking occurred on the lower surface of the fracture.



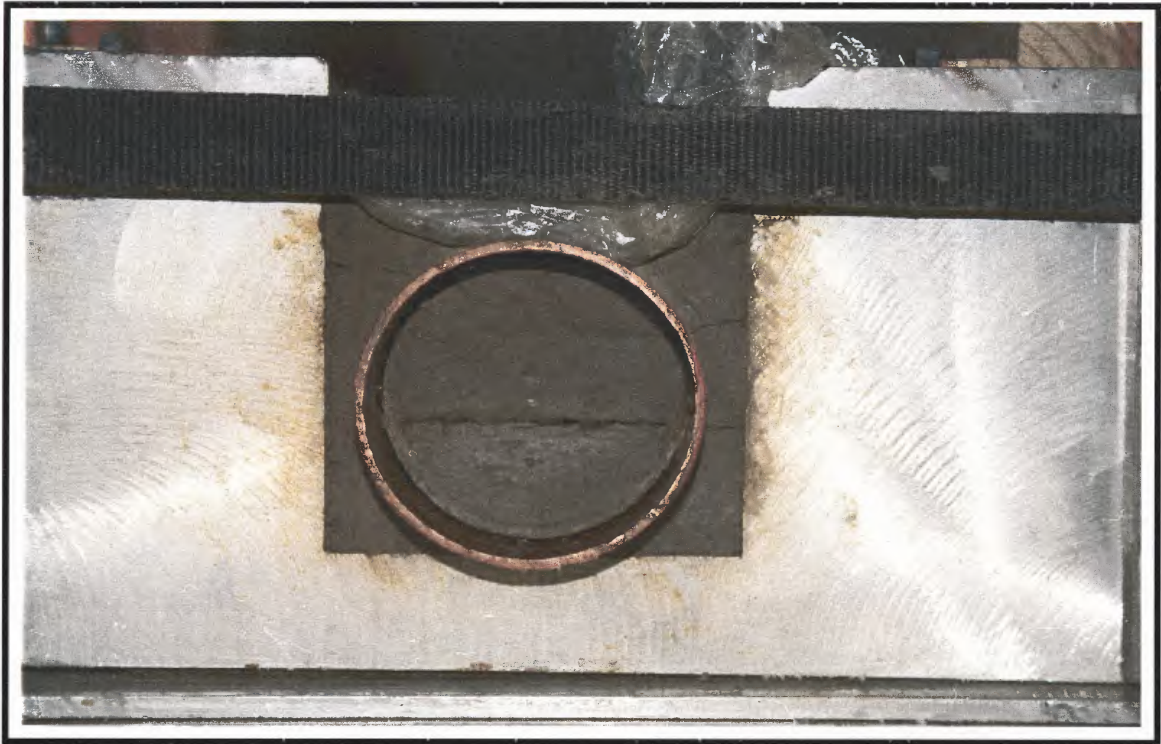


Photograph A-15. Wetting caused preferential swelling at the inlet end (on right). Others parts of the fracture were representative of drying conditions.

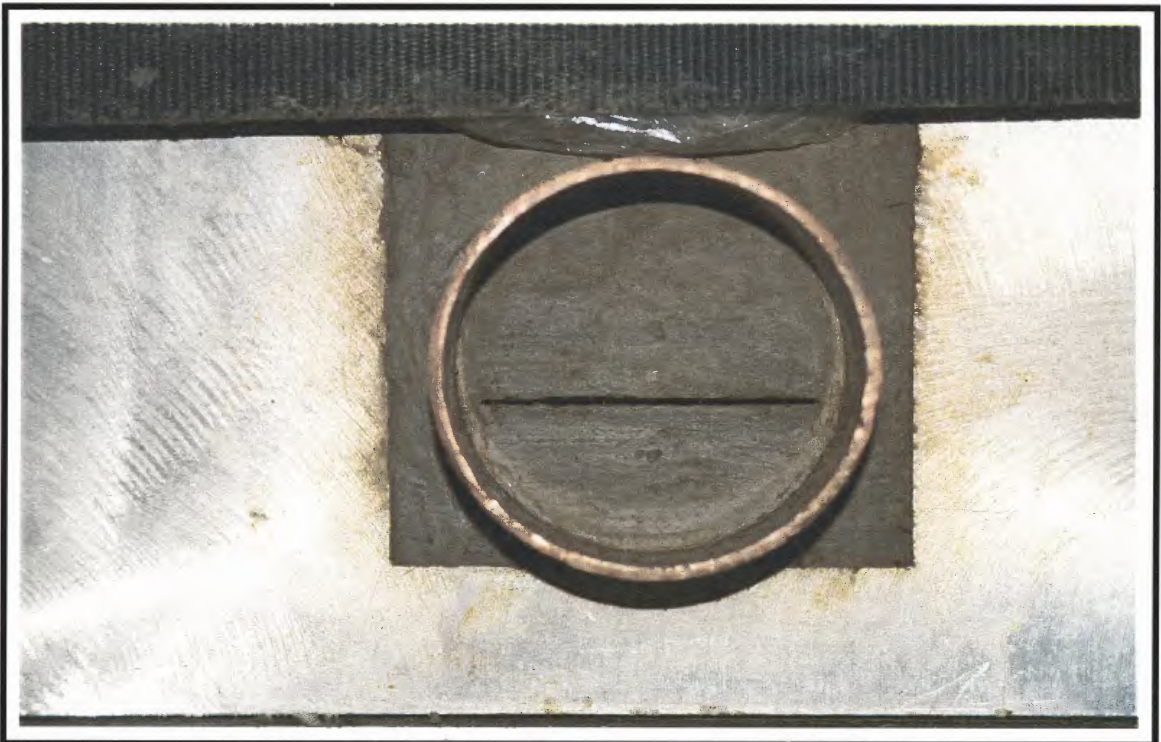


Photograph A-16. Note that the wetting also caused the vertical shrinkage cracks to seal at the fracture level.





Photograph A-17. This photograph shows the inlet end after wetting. The boundary soils had swollen and almost completely sealed the fracture.



Photograph A-18. The entrance of the fracture shown in Photograph A-17 was cleared with a feeler gauge showing the constriction was superficial.

**APPENDIX B**

**HORIZONTAL INFILTROMETER FLOW DATA**

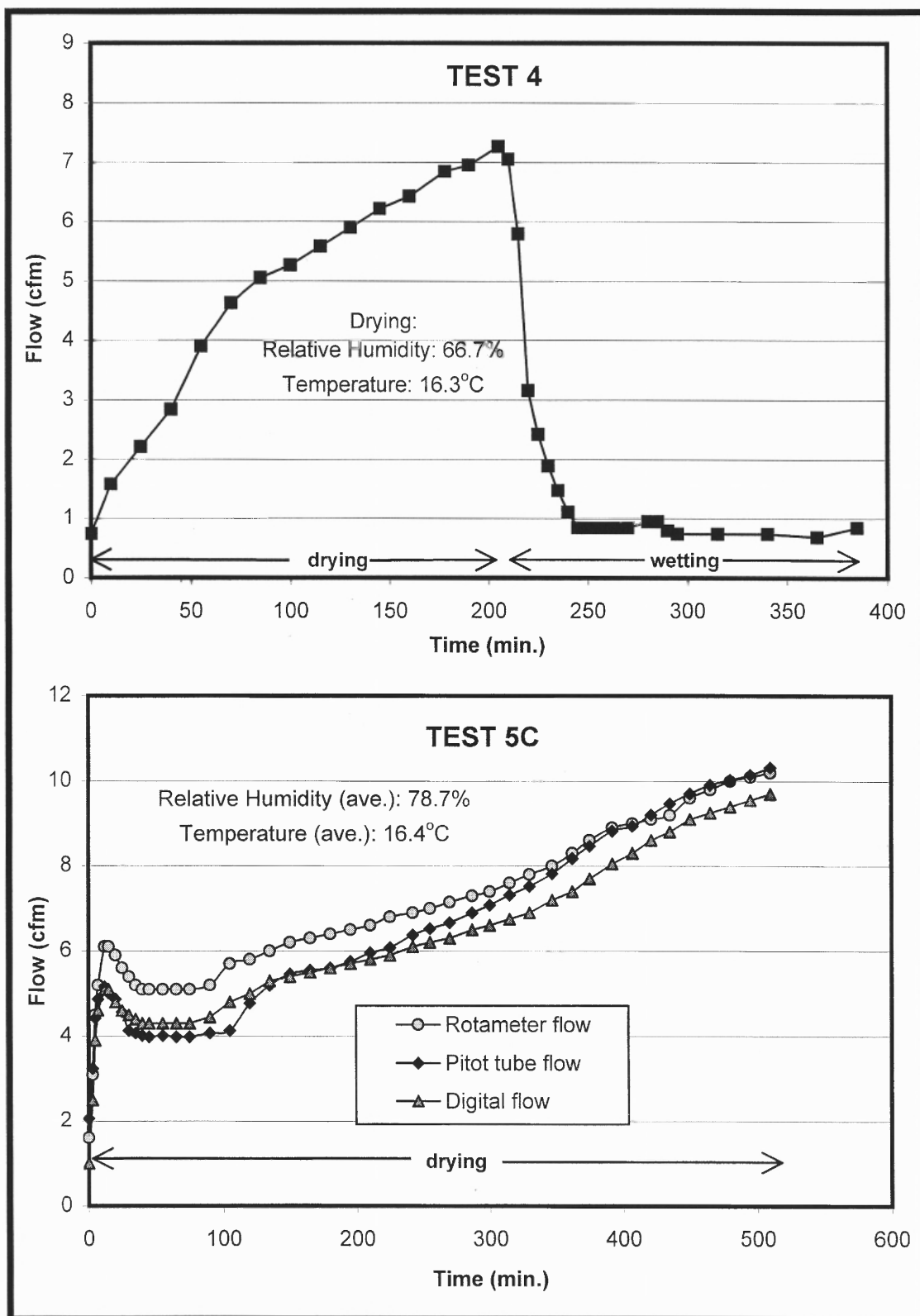


Figure B.1 Raw Flow-Time Data for Various HI Tests

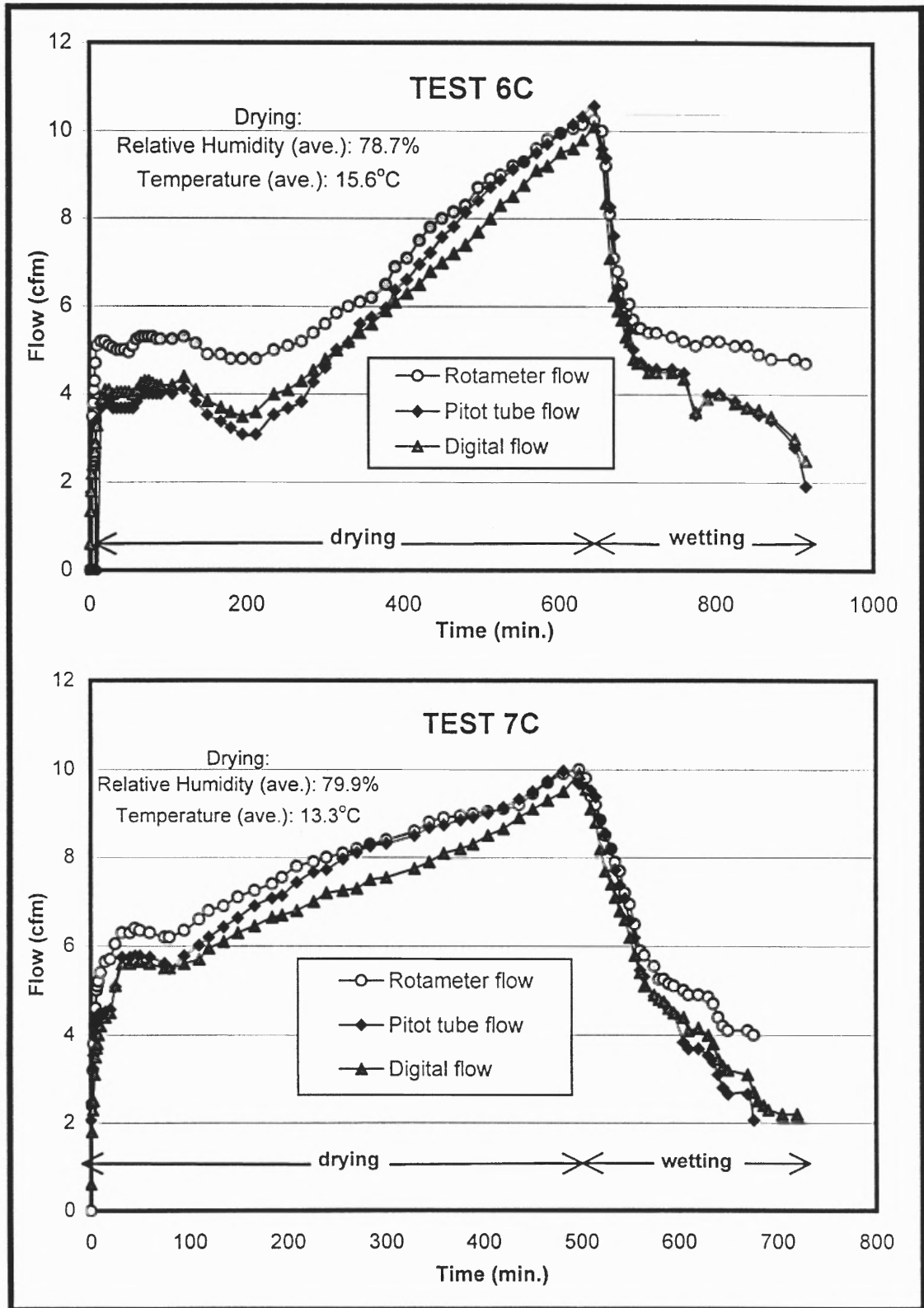


Figure B.1 (cont'd.) Raw Flow-Time Data for Various HI Tests

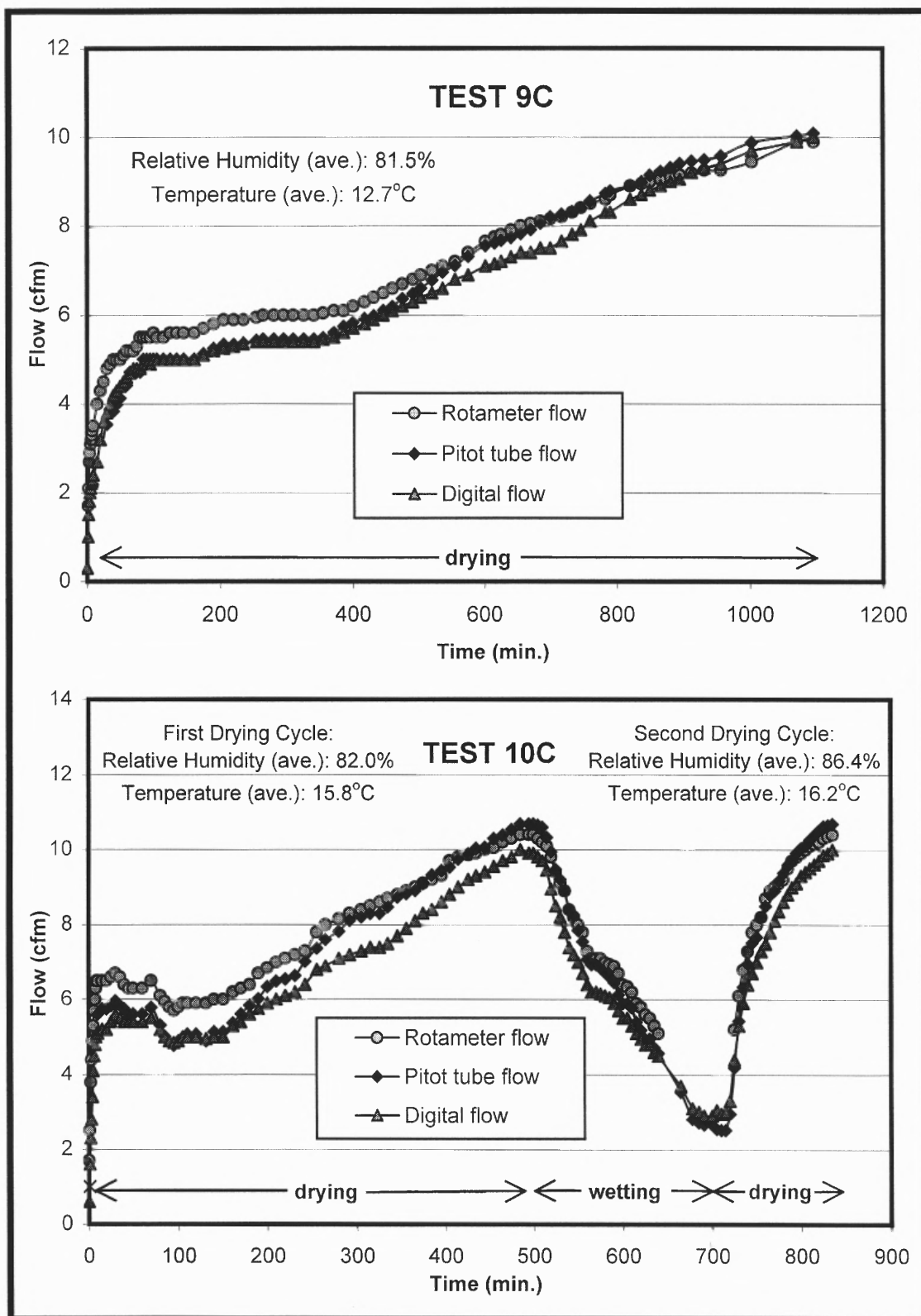


Figure B.1 (cont'd.) Raw Flow-Time Data for Various HI Tests

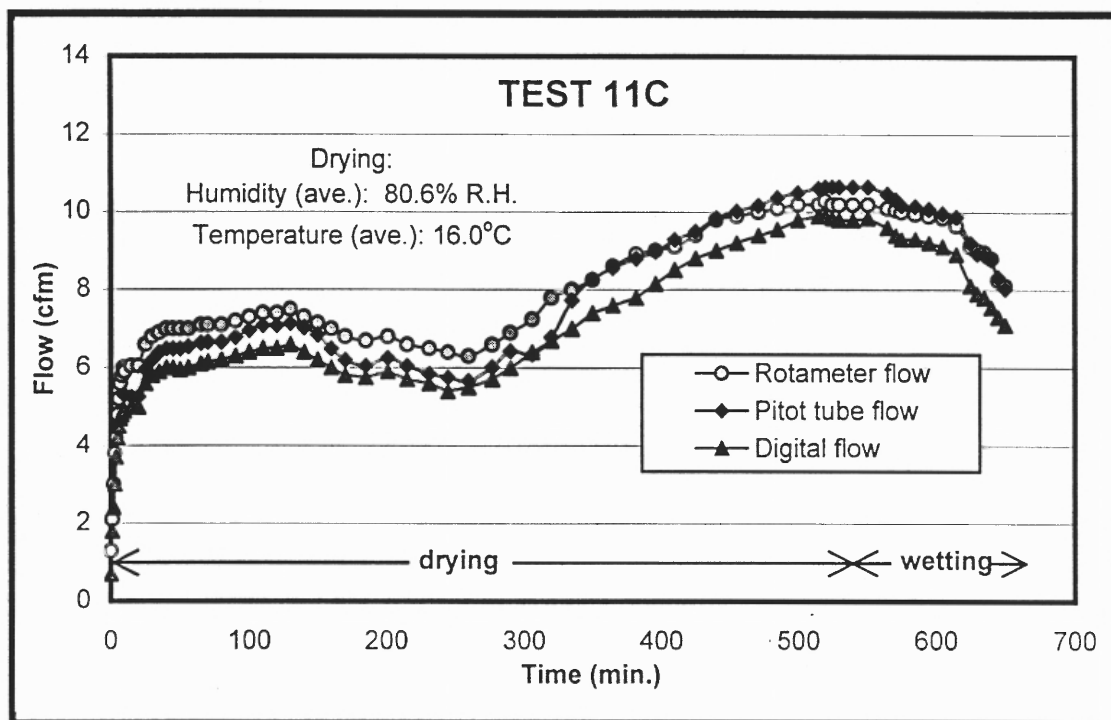


Figure B.1 (cont'd.) Raw Flow-Time Data for Various HI Tests

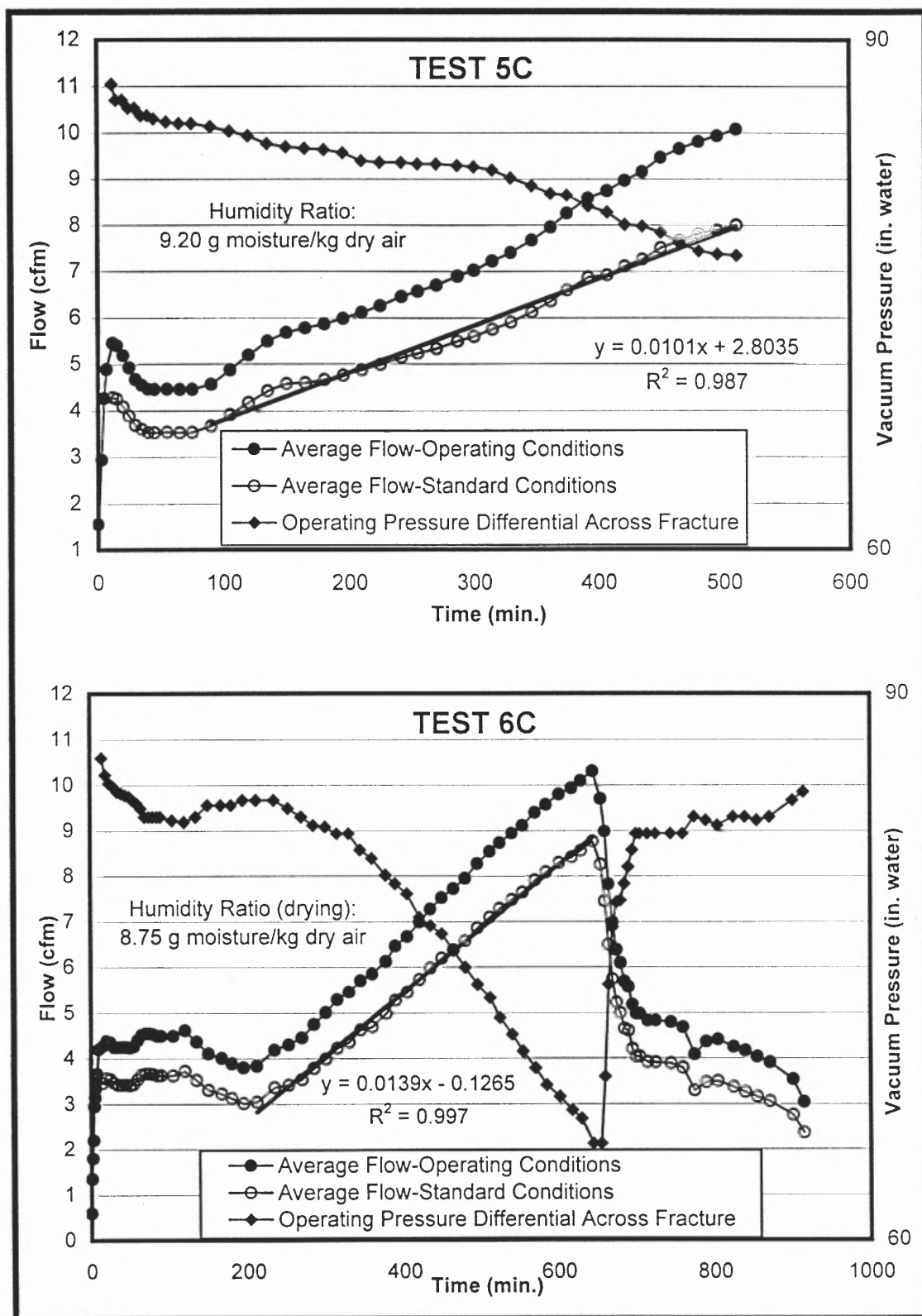


Figure B.2 Average Flow-Time-Pressure Data for Various HI Tests



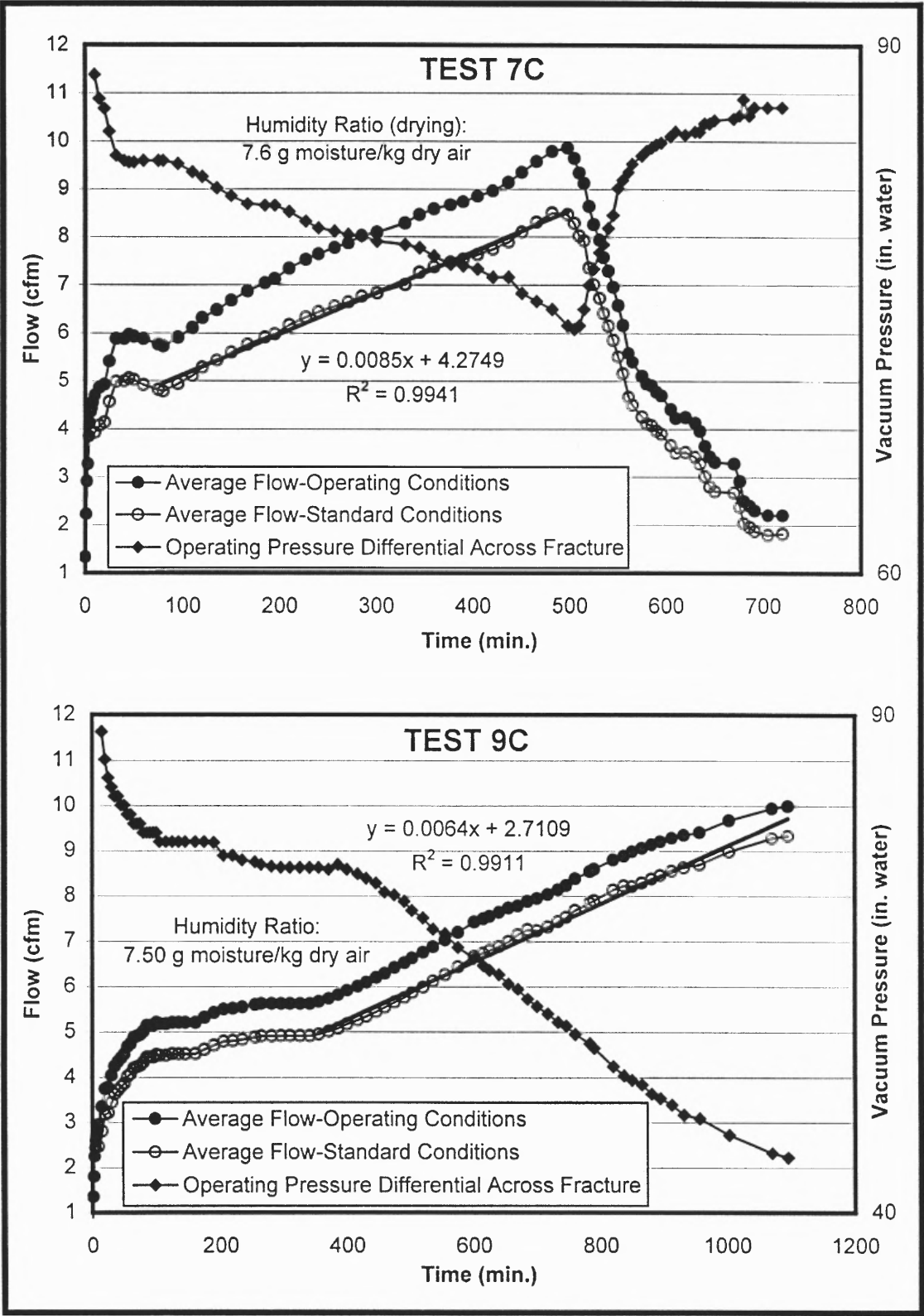


Figure B.2 (cont'd.) Average Flow-Time-Pressure Data for Various HI Tests

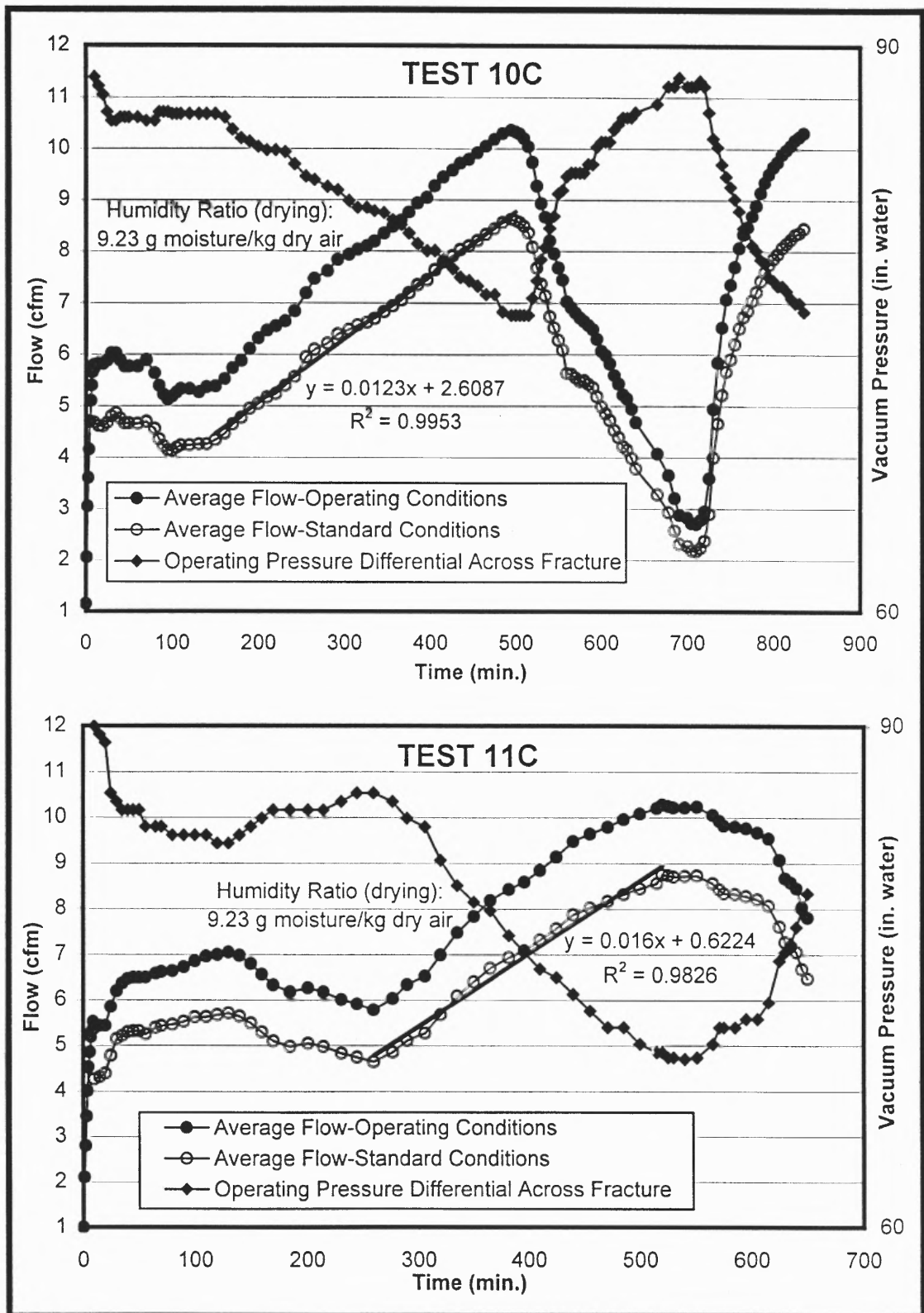


Figure B.2 (cont'd.) Average Flow-Time-Pressure Data for Various HI Tests

## **APPENDIX C**

### **RAW HORIZONTAL INFILTROMETER MOISTURE DATA**

Table C.1 Raw Moisture Data for Horizontal Infiltrometer Tests

TEST 5C							
X (in.)	Y (in.)	Z (in.)	Moisture (wt%)	X (in.)	Y (in.)	Z (in.)	Moisture (wt%)
5.875	9	4.5	31.03	5.875	1	2.25	30.87
3.5	1	4.5	31.10	5.875	9	2.25	30.55
3.5	7	4.5	30.78	3.5	0.5	2.375	19.64
3.5	15	4.5	31.14	3.5	1.5	2.375	19.42
1.125	5	4.5	31.44	3.5	3	2.375	20.33
1.125	13	4.5	31.44	3.5	5	2.375	20.21
5.875	7	3.75	30.90	3.5	7	2.375	20.25
3.5	0.5	3.75	27.79	3.5	9	2.375	19.13
3.5	1.5	3.75	31.17	3.5	11	2.375	18.59
3.5	5	3.75	30.33	3.5	13	2.375	20.39
3.5	9	3.75	30.79	3.5	14.5	2.375	20.31
3.5	14.5	3.75	30.92	3.5	15.5	2.375	18.13
3.5	15.5	3.75	28.80	3.5	0.5	2.125	24.42
1.125	11	3.75	31.05	3.5	1.5	2.125	25.58
5.875	5	3.25	30.78	3.5	3	2.125	27.55
5.875	13	3.25	30.98	3.5	5	2.125	27.99
3.5	0.5	3.25	27.73	3.5	7	2.125	27.35
3.5	1.5	3.25	29.41	3.5	9	2.125	27.01
3.5	3	3.25	27.28	3.5	11	2.125	25.56
3.5	7	3.25	30.19	3.5	13	2.125	27.84
3.5	11	3.25	26.88	3.5	14.5	2.125	27.71
3.5	14.5	3.25	30.36	3.5	15.5	2.125	21.51
3.5	15.5	3.25	26.73	1.125	5	2.25	30.71
1.125	1	3.25	31.28	1.125	13	2.25	30.80
1.125	9	3.25	30.93	5.875	7	1.75	30.76
5.875	3	2.75	30.45	5.875	15	1.75	30.96
5.875	11	2.75	30.81	3.5	0.5	1.75	26.94
3.5	0.5	2.625	18.81	3.5	1.5	1.75	30.33
3.5	1.5	2.625	17.82	3.5	5	1.75	30.56
3.5	3	2.625	18.31	3.5	9	1.75	30.72
3.5	5	2.625	19.05	3.5	13	1.75	30.83
3.5	7	2.625	19.36	3.5	14.5	1.75	30.66
3.5	9	2.625	18.33	3.5	15.5	1.75	25.63
3.5	11	2.625	17.92	1.125	3	1.75	31.00
3.5	13	2.625	19.36	1.125	11	1.75	31.23
3.5	14.5	2.625	19.21	5.875	9	1.25	31.75
3.5	15.5	2.625	17.83	3.5	0.5	1.25	28.03
3.5	0.5	2.875	23.63	3.5	1.5	1.25	30.80
3.5	1.5	2.875	22.38	3.5	7	1.25	31.54
3.5	3	2.875	19.25	3.5	11	1.25	31.06
3.5	5	2.875	22.77	3.5	14.5	1.25	31.14
3.5	7	2.875	24.22	3.5	15.5	1.25	30.80
3.5	9	2.875	23.83	1.125	5	1.25	30.86
3.5	11	2.875	20.15	5.875	7	0.5	31.22
3.5	13	2.875	25.55	3.5	1	0.5	30.66
3.5	14.5	2.875	25.43	3.5	13	0.5	30.88
3.5	15.5	2.875	21.82	3.5	15	0.5	30.93
1.125	15	2.75	31.13	1.125	3	0.5	30.35
1.125	7	2.75	30.99	1.125	11	0.5	30.97

Table C.1 (cont'd.) Raw Moisture Data for Horizontal Infiltrometer Tests

TEST 6C							
X (in.)	Y (in.)	Z (in.)	Moisture (wt%)	X (in.)	Y (in.)	Z (in.)	Moisture (wt%)
5.875	9	4.5	31.10	5.875	1	2.25	30.36
3.5	1	4.5	30.97	5.875	9	2.25	30.38
3.5	7	4.5	30.82	3.5	0.5	2.375	18.42
3.5	15	4.5	30.45	3.5	1.5	2.375	19.10
1.125	5	4.5	31.33	3.5	3	2.375	20.65
1.125	13	4.5	31.10	3.5	5	2.375	20.51
5.875	7	3.75	31.28	3.5	7	2.375	19.90
3.5	0.5	3.75	26.54	3.5	9	2.375	19.84
3.5	1.5	3.75	30.71	3.5	11	2.375	21.14
3.5	5	3.75	30.58	3.5	13	2.375	29.78
3.5	9	3.75	30.90	3.5	14.5	2.375	27.27
3.5	14.5	3.75	30.87	3.5	15.5	2.375	25.85
3.5	15.5	3.75	27.76	3.5	0.5	2.125	20.72
1.125	11	3.75	31.53	3.5	1.5	2.125	21.89
5.875	5	3.25	31.40	3.5	3	2.125	25.03
5.875	13	3.25	31.23	3.5	5	2.125	24.02
3.5	0.5	3.25	24.06	3.5	7	2.125	21.76
3.5	1.5	3.25	26.00	3.5	9	2.125	22.07
3.5	3	3.25	24.00	3.5	11	2.125	22.33
3.5	7	3.25	25.43	3.5	13	2.125	26.33
3.5	11	3.25	26.00	3.5	14.5	2.125	26.09
3.5	14.5	3.25	28.89	3.5	15.5	2.125	27.27
3.5	15.5	3.25	25.77	1.125	5	2.25	30.60
1.125	1	3.25	30.81	1.125	13	2.25	31.28
1.125	9	3.25	31.47	5.875	7	1.75	31.12
5.875	3	2.75	31.07	5.875	15	1.75	31.32
5.875	11	2.75	30.66	3.5	0.5	1.75	24.69
3.5	0.5	2.625	18.75	3.5	1.5	1.75	27.57
3.5	1.5	2.625	18.13	3.5	5	1.75	29.23
3.5	3	2.625	18.61	3.5	9	1.75	27.25
3.5	5	2.625	18.90	3.5	13	1.75	28.33
3.5	7	2.625	18.11	3.5	14.5	1.75	29.94
3.5	9	2.625	17.83	3.5	15.5	1.75	31.86
3.5	11	2.625	18.21	1.125	3	1.75	31.32
3.5	13	2.625	27.18	1.125	11	1.75	31.34
3.5	14.5	2.625	28.36	5.875	9	1.25	31.07
3.5	15.5	2.625	25.21	3.5	0.5	1.25	27.17
3.5	0.5	2.875	20.53	3.5	1.5	1.25	30.89
3.5	1.5	2.875	18.98	3.5	7	1.25	30.24
3.5	3	2.875	19.49	3.5	11	1.25	30.48
3.5	5	2.875	20.77	3.5	14.5	1.25	31.28
3.5	7	2.875	18.70	3.5	15.5	1.25	32.49
3.5	9	2.875	18.12	1.125	5	1.25	31.48
3.5	11	2.875	19.09	5.875	7	0.5	30.65
3.5	13	2.875	25.82	3.5	1	0.5	31.21
3.5	14.5	2.875	23.90	3.5	9	0.5	30.82
3.5	15.5	2.875	22.25	3.5	15	0.5	31.67
1.125	15	2.75	30.97	2.3	3	0.5	30.92
1.125	7	2.75	31.02	1.125	11	0.5	31.05

Table C.1 (cont'd.) Raw Moisture Data for Horizontal Infiltrometer Tests

TEST 7C							
X (in.)	Y (in.)	Z (in.)	Moisture (wt%)	X (in.)	Y (in.)	Z (in.)	Moisture (wt%)
5.875	9	4.5	31.16	5.875	1	2.25	30.91
3.5	1	4.5	30.55	5.875	9	2.25	30.84
3.5	7	4.5	31.25	3.5	0.5	2.375	19.15
3.5	15	4.5	30.58	3.5	1.5	2.375	20.56
1.125	5	4.5	31.51	3.5	3	2.375	18.64
1.125	13	4.5	31.02	3.5	5	2.375	18.31
5.875	7	3.75	31.33	3.5	7	2.375	18.73
3.5	0.5	3.75	28.35	3.5	9	2.375	19.50
3.5	1.5	3.75	31.25	3.5	11	2.375	18.56
3.5	5	3.75	30.41	3.5	13	2.375	19.46
3.5	9	3.75	30.54	3.5	14.5	2.375	19.72
3.5	14.5	3.75	31.37	3.5	15.5	2.375	20.60
3.5	15.5	3.75	29.93	3.5	0.5	2.125	21.66
1.125	11	3.75	31.42	3.5	1.5	2.125	24.55
5.875	5	3.25	31.43	3.5	3	2.125	21.12
5.875	13	3.25	31.02	3.5	5	2.125	19.51
3.5	0.5	3.25	27.01	3.5	7	2.125	21.68
3.5	1.5	3.25	29.75	3.5	9	2.125	23.44
3.5	3	3.25	29.28	3.5	11	2.125	23.54
3.5	7	3.25	28.58	3.5	13	2.125	25.98
3.5	11	3.25	29.66	3.5	14.5	2.125	25.07
3.5	14.5	3.25	29.98	3.5	15.5	2.125	23.24
3.5	15.5	3.25	28.13	1.125	5	2.25	31.17
1.125	1	3.25	31.54	1.125	13	2.25	31.24
1.125	9	3.25	31.07	5.875	7	1.75	31.24
5.875	3	2.75	31.24	5.875	15	1.75	31.44
5.875	11	2.75	31.30	3.5	0.5	1.75	25.72
3.5	0.5	2.625	18.72	3.5	1.5	1.75	28.77
3.5	1.5	2.625	19.24	3.5	5	1.75	26.95
3.5	3	2.625	19.27	3.5	9	1.75	28.89
3.5	5	2.625	19.97	3.5	13	1.75	30.35
3.5	7	2.625	19.01	3.5	14.5	1.75	30.48
3.5	9	2.625	18.83	3.5	15.5	1.75	27.21
3.5	11	2.625	19.18	1.125	3	1.75	31.68
3.5	13	2.625	19.68	1.125	11	1.75	31.47
3.5	14.5	2.625	18.48	5.875	9	1.25	31.34
3.5	15.5	2.625	18.81	3.5	0.5	1.25	27.43
3.5	0.5	2.875	22.90	3.5	1.5	1.25	31.44
3.5	1.5	2.875	25.38	3.5	7	1.25	31.28
3.5	3	2.875	23.31	3.5	11	1.25	31.51
3.5	5	2.875	24.51	3.5	14.5	1.25	31.55
3.5	7	2.875	22.33	3.5	15.5	1.25	31.47
3.5	9	2.875	22.88	1.125	5	1.25	31.90
3.5	11	2.875	24.31	5.875	7	0.5	31.54
3.5	13	2.875	25.15	3.5	1	0.5	31.57
3.5	14.5	2.875	24.07	3.5	9	0.5	31.00
3.5	15.5	2.875	23.02	3.5	15	0.5	31.27
1.125	15	2.75	30.75	1.125	3	0.5	31.52
1.125	7	2.75	31.21	1.125	11	0.5	31.13

Table C.1 (cont'd.) Raw Moisture Data for Horizontal Infiltrometer Tests

TEST 8C							
X (in.)	Y (in.)	Z (in.)	Moisture (wt%)	X (in.)	Y (in.)	Z (in.)	Moisture (wt%)
5.875	9	4.5	31.37	5.875	9	2.25	31.33
3.5	1	4.5	31.68	3.5	0.5	2.375	21.77
3.5	7	4.5	31.64	3.5	1.5	2.375	21.25
3.5	15	4.5	31.72	3.5	3	2.375	21.64
1.125	5	4.5	31.72	3.5	5	2.375	20.91
1.125	13	4.5	32.08	3.5	7	2.375	21.93
5.875	7	3.75	31.73	3.5	9	2.375	21.60
3.5	0.5	3.75	28.95	3.5	11	2.375	19.15
3.5	1.5	3.75	31.70	3.5	13	2.375	20.39
3.5	5	3.75	31.73	3.5	14.5	2.375	19.54
3.5	9	3.75	31.37	3.5	15.5	2.375	18.66
3.5	14.5	3.75	31.50	3.5	0.5	2.125	27.04
3.5	15.5	3.75	28.99	3.5	1.5	2.125	28.11
1.125	11	3.75	32.02	3.5	3	2.125	27.25
5.875	13	3.25	31.66	3.5	5	2.125	26.53
3.5	0.5	3.25	28.91	3.5	7	2.125	26.32
3.5	1.5	3.25	31.31	3.5	9	2.125	26.50
3.5	3	3.25	30.26	3.5	11	2.125	23.48
3.5	7	3.25	30.86	3.5	13	2.125	26.52
3.5	11	3.25	30.28	3.5	14.5	2.125	25.81
3.5	14.5	3.25	30.99	3.5	15.5	2.125	25.25
3.5	15.5	3.25	28.35	1.125	5	2.25	32.37
1.125	1	3.25	31.79	1.125	13	2.25	31.34
1.125	9	3.25	32.10	5.875	7	1.75	31.73
5.875	3	2.75	31.86	5.875	15	1.75	31.55
5.875	11	2.75	31.57	3.5	0.5	1.75	28.42
3.5	0.5	2.625	21.39	3.5	1.5	1.75	31.30
3.5	1.5	2.625	22.46	3.5	5	1.75	30.76
3.5	3	2.625	22.23	3.5	9	1.75	30.61
3.5	5	2.625	21.60	3.5	13	1.75	30.65
3.5	7	2.625	21.29	3.5	14.5	1.75	30.69
3.5	9	2.625	21.35	3.5	15.5	1.75	27.11
3.5	11	2.625	20.26	1.125	3	1.75	31.87
3.5	13	2.625	19.23	1.125	11	1.75	31.67
3.5	14.5	2.625	18.50	5.875	9	1.25	32.01
3.5	15.5	2.625	17.65	3.5	0.5	1.25	29.17
3.5	0.5	2.875	26.70	3.5	1.5	1.25	31.78
3.5	1.5	2.875	28.10	3.5	7	1.25	31.46
3.5	3	2.875	26.43	3.5	11	1.25	31.68
3.5	5	2.875	25.02	3.5	14.5	1.25	31.45
3.5	7	2.875	25.37	3.5	15.5	1.25	30.19
3.5	9	2.875	25.61	1.125	5	1.25	32.08
3.5	11	2.875	25.04	5.875	7	0.5	31.83
3.5	13	2.875	23.27	3.5	1	0.5	31.77
3.5	14.5	2.875	24.47	3.5	9	0.5	31.63
3.5	15.5	2.875	23.07	3.5	15	0.5	31.62
1.125	15	2.75	31.97	1.125	3	0.5	32.11
1.125	7	2.75	31.95	1.125	11	0.5	31.94
5.875	1	2.25	31.86				

Table C.1 (cont'd.) Raw Moisture Data for Horizontal Infiltrometer Tests

TEST 9C							
X (in.)	Y (in.)	Z (in.)	Moisture (wt%)	X (in.)	Y (in.)	Z (in.)	Moisture (wt%)
5.875	9	4.5	30.88	5.875	1	2.25	30.26
3.5	1	4.5	30.75	5.875	9	2.25	30.55
3.5	7	4.5	30.98	3.5	0.5	2.375	19.21
3.5	15	4.5	31.15	3.5	1.5	2.375	20.38
1.125	5	4.5	31.32	3.5	3	2.375	19.25
1.125	13	4.5	31.38	3.5	5	2.375	18.27
5.875	7	3.75	30.92	3.5	7	2.375	17.77
3.5	0.5	3.75	26.89	3.5	9	2.375	16.92
3.5	1.5	3.75	30.22	3.5	11	2.375	16.71
3.5	5	3.75	30.01	3.5	13	2.375	17.22
3.5	9	3.75	30.44	3.5	14.5	2.375	17.33
3.5	14.5	3.75	30.49	3.5	15.5	2.375	15.86
3.5	15.5	3.75	25.11	3.5	0.5	2.125	22.85
1.125	11	3.75	31.25	3.5	1.5	2.125	25.47
5.875	5	3.25	30.70	3.5	3	2.125	23.04
5.875	13	3.25	30.70	3.5	5	2.125	20.49
3.5	0.5	3.25	24.31	3.5	7	2.125	19.92
3.5	1.5	3.25	24.73	3.5	9	2.125	18.21
3.5	3	3.25	23.99	3.5	11	2.125	17.35
3.5	7	3.25	25.02	3.5	13	2.125	21.03
3.5	9	3.25	24.09	3.5	14.5	2.125	22.15
3.5	11	3.25	24.33	3.5	15.5	2.125	18.36
3.5	14.5	3.25	27.94	1.125	5	2.25	31.06
3.5	15.5	3.25	24.15	1.125	13	2.25	28.31
1.125	1	3.25	31.32	5.875	7	1.75	30.66
5.875	3	2.75	30.39	5.875	15	1.75	31.07
5.875	11	2.75	30.78	3.5	0.5	1.75	25.24
3.5	0.5	2.625	18.11	3.5	1.5	1.75	29.34
3.5	1.5	2.625	17.19	3.5	5	1.75	27.02
3.5	3	2.625	17.64	3.5	9	1.75	24.83
3.5	5	2.625	16.84	3.5	13	1.75	27.36
3.5	7	2.625	15.66	3.5	14.5	1.75	26.87
3.5	9	2.625	17.02	3.5	15.5	1.75	22.33
3.5	11	2.625	15.90	1.125	3	1.75	31.33
3.5	13	2.625	16.18	1.125	11	1.75	31.15
3.5	14.5	2.625	18.15	5.875	9	1.25	31.22
3.5	15.5	2.625	15.87	3.5	0.5	1.25	27.48
3.5	0.5	2.875	19.76	3.5	1.5	1.25	30.88
3.5	1.5	2.875	17.71	3.5	7	1.25	30.63
3.5	3	2.875	18.57	3.5	11	1.25	30.29
3.5	5	2.875	18.33	3.5	14.5	1.25	30.77
3.5	7	2.875	18.17	3.5	15.5	1.25	30.38
3.5	9	2.875	18.15	1.125	5	1.25	31.25
3.5	11	2.875	16.94	5.875	7	0.5	30.98
3.5	13	2.875	17.91	3.5	1	0.5	31.01
3.5	14.5	2.875	20.71	3.5	9	0.5	30.67
3.5	15.5	2.875	18.83	3.5	15	0.5	31.14
1.125	15	2.75	30.74	1.125	3	0.5	31.26
1.125	7	2.75	30.97	1.125	11	0.5	31.01



Table C.1 (cont'd.) Raw Moisture Data for Horizontal Infiltrometer Tests

TEST 10C							
X (in.)	Y (in.)	Z (in.)	Moisture (wt%)	X (in.)	Y (in.)	Z (in.)	Moisture (wt%)
5.875	9	4.5	30.85	5.875	1	2.25	30.16
3.5	1	4.5	30.70	5.875	9	2.25	30.20
3.5	7	4.5	30.79	3.5	0.5	2.375	18.96
3.5	15	4.5	30.64	3.5	1.5	2.375	18.63
1.125	5	4.5	31.43	3.5	3	2.375	19.92
1.125	13	4.5	31.33	3.5	5	2.375	19.47
5.875	7	3.75	30.95	3.5	7	2.375	19.44
3.5	0.5	3.75	26.70	3.5	9	2.375	18.96
3.5	1.5	3.75	30.03	3.5	11	2.375	19.36
3.5	5	3.75	30.24	3.5	13	2.375	18.67
3.5	9	3.75	30.51	3.5	14.5	2.375	18.01
3.5	14.5	3.75	30.03	3.5	15.5	2.375	17.80
3.5	15.5	3.75	27.83	3.5	0.5	2.125	22.34
1.125	11	3.75	31.05	3.5	1.5	2.125	22.96
5.875	5	3.25	31.04	3.5	3	2.125	23.39
5.875	13	3.25	30.54	3.5	5	2.125	22.07
3.5	0.5	3.25	26.26	3.5	7	2.125	21.92
3.5	1.5	3.25	27.48	3.5	9	2.125	22.19
3.5	3	3.25	24.93	3.5	11	2.125	23.21
3.5	7	3.25	28.02	3.5	13	2.125	21.96
3.5	11	3.25	24.31	3.5	14.5	2.125	20.80
3.5	14.5	3.25	28.70	3.5	15.5	2.125	21.80
3.5	15.5	3.25	26.27	1.125	5	2.25	30.23
1.125	1	3.25	31.05	1.125	13	2.25	30.80
1.125	9	3.25	30.71	5.875	7	1.75	31.14
5.875	3	2.75	30.27	5.875	15	1.75	30.85
5.875	11	2.75	30.30	3.5	0.5	1.75	25.50
3.5	0.5	2.625	18.78	3.5	1.5	1.75	28.90
3.5	1.5	2.625	18.71	3.5	5	1.75	27.31
3.5	3	2.625	18.67	3.5	9	1.75	27.07
3.5	5	2.625	19.13	3.5	13	1.75	27.80
3.5	7	2.625	20.18	3.5	14.5	1.75	27.58
3.5	9	2.625	20.47	3.5	15.5	1.75	24.30
3.5	11	2.625	19.31	1.125	3	1.75	31.23
3.5	13	2.625	19.40	1.125	11	1.75	31.27
3.5	14.5	2.625	18.08	5.875	9	1.25	30.97
3.5	15.5	2.625	18.15	3.5	0.5	1.25	28.17
3.5	0.5	2.875	22.17	3.5	1.5	1.25	30.80
3.5	1.5	2.875	20.05	3.5	7	1.25	30.58
3.5	3	2.875	19.62	3.5	11	1.25	30.69
3.5	5	2.875	20.95	3.5	14.5	1.25	30.70
3.5	7	2.875	23.83	3.5	15.5	1.25	29.54
3.5	9	2.875	23.44	1.125	5	1.25	31.48
3.5	11	2.875	21.03	5.875	7	0.5	31.06
3.5	13	2.875	22.97	3.5	1	0.5	31.41
3.5	14.5	2.875	22.68	3.5	9	0.5	30.88
3.5	15.5	2.875	21.85	3.5	15	0.5	31.40
1.125	15	2.75	30.91	1.125	3	0.5	31.37
1.125	7	2.75	30.85	1.125	11	0.5	31.14

Table C.1 (cont'd.) Raw Moisture Data for Horizontal Infiltrometer Tests

TEST 11C							
X (in.)	Y (in.)	Z (in.)	Moisture (wt%)	X (in.)	Y (in.)	Z (in.)	Moisture (wt%)
5.875	9	4.5	31.66	5.875	9	2.25	31.08
3.5	1	4.5	31.19	3.5	0.5	2.375	20.79
3.5	7	4.5	31.61	3.5	1.5	2.375	21.41
3.5	15	4.5	31.50	3.5	3	2.375	19.89
1.125	5	4.5	31.93	3.5	5	2.375	18.94
1.125	13	4.5	31.82	3.5	7	2.375	20.86
5.875	7	3.75	31.49	3.5	9	2.375	21.21
3.5	0.5	3.75	27.89	3.5	11	2.375	20.68
3.5	1.5	3.75	31.23	3.5	13	2.375	19.70
3.5	5	3.75	30.93	3.5	14.5	2.375	20.46
3.5	9	3.75	31.14	3.5	15.5	2.375	19.54
3.5	14.5	3.75	31.16	3.5	0.5	2.125	25.75
3.5	15.5	3.75	28.39	3.5	1.5	2.125	28.19
1.125	11	3.75	31.50	3.5	3	2.125	26.49
5.875	5	3.25	31.60	3.5	5	2.125	23.51
5.875	13	3.25	31.40	3.5	7	2.125	24.22
3.5	0.5	3.25	27.17	3.5	9	2.125	25.96
3.5	1.5	3.25	30.48	3.5	11	2.125	24.81
3.5	3	3.25	27.47	3.5	13	2.125	24.88
3.5	7	3.25	25.61	3.5	14.5	2.125	25.89
3.5	11	3.25	25.46	3.5	15.5	2.125	23.15
3.5	14.5	3.25	30.08	1.125	5	2.25	31.73
3.5	15.5	3.25	27.06	1.125	13	2.25	31.38
1.125	1	3.25	31.92	5.875	7	1.75	31.65
1.125	9	3.25	31.43	5.875	15	1.75	31.26
5.875	3	2.75	31.11	3.5	0.5	1.75	27.46
5.875	11	2.75	31.10	3.5	1.5	1.75	30.92
3.5	0.5	2.625	18.87	3.5	5	1.75	30.00
3.5	1.5	2.625	20.31	3.5	9	1.75	30.89
3.5	3	2.625	18.75	3.5	13	1.75	30.06
3.5	5	2.625	18.99	3.5	14.5	1.75	29.86
3.5	7	2.625	19.20	3.5	15.5	1.75	25.73
3.5	9	2.625	18.63	1.125	3	1.75	31.85
3.5	11	2.625	18.96	1.125	11	1.75	31.75
3.5	13	2.625	18.17	5.875	9	1.25	31.54
3.5	14.5	2.625	19.89	3.5	0.5	1.25	28.40
3.5	15.5	2.625	19.00	3.5	1.5	1.25	31.36
3.5	0.5	2.875	23.76	3.5	7	1.25	31.72
3.5	1.5	2.875	25.80	3.5	11	1.25	31.87
3.5	3	2.875	20.98	3.5	14.5	1.25	31.39
3.5	5	2.875	20.27	3.5	15.5	1.25	29.10
3.5	7	2.875	20.02	1.125	5	1.25	31.75
3.5	9	2.875	19.27	5.875	7	0.5	31.39
3.5	11	2.875	19.33	3.5	1	0.5	31.58
3.5	13	2.875	19.62	3.5	9	0.5	31.57
3.5	14.5	2.875	24.61	3.5	15	0.5	31.56
3.5	15.5	2.875	22.67	1.125	3	0.5	31.47
1.125	15	2.75	31.28	1.125	11	0.5	31.95
1.125	7	2.75	31.33				

Distance  
From  
Fracture  
(in.)

## TEST 5C

Outlet

Inlet

1½-2½	31.10		--	--	30.78	--	--	--	30.14	
1-1½	27.79	31.17	--	30.33	--	30.79	--	--	30.92	28.80
½-1	27.73	29.41	27.28	--	30.19	--	26.88	--	30.36	26.73
¼-½	23.63	22.38	19.25	22.77	24.22	23.83	20.15	25.55	25.43	21.82
0-¼	18.81	17.82	18.31	19.05	19.36	18.33	17.92	19.36	19.21	17.83
0-¼	19.64	19.42	20.33	20.21	20.25	19.13	18.59	20.39	20.31	18.13
¼-½	24.42	25.58	27.55	27.99	27.35	27.02	25.56	27.84	27.71	21.51
½-1	26.94	30.33	--	30.56	--	30.72	--	30.83	30.66	25.63
1-1½	28.03	30.80	--	--	31.54	--	31.06	--	31.14	30.80
1½-2½	30.66		--	--	--	--	--	30.88	30.93	

Moisture contents are in wt%; -- Not applicable, no data collected at this location

**Figure C.1** Vertical Cross-Sections of the Soil Block at the Fracture Showing Moisture Data

Distance  
From  
Fracture  
(in.)

## TEST 6C

Outlet

Inlet

1½-2½	30.97		--	--	30.82	--	--	--	30.45	
1-1½	26.54	30.71	--	30.58	--	30.90	--	--	30.87	27.76
½-1	24.06	26.00	24.00	--	25.43	--	26.00	--	28.89	25.77
¼-½	20.53	18.98	19.49	20.77	18.70	18.12	19.09	25.82	23.90	22.25
0-¼	18.75	18.13	18.61	18.90	18.11	17.83	18.21	27.18	28.36	25.21
0-¼	18.42	19.10	20.65	20.51	19.90	19.84	21.14	29.78	27.27	25.85
¼-½	20.72	21.89	25.03	24.02	21.76	22.07	22.33	26.33	26.09	27.27
½-1	24.69	27.57	--	29.23	--	27.25	--	28.33	29.94	31.86
1-1½	27.17	30.89	--	--	30.24	--	30.48	--	31.28	32.24
1½-2½	31.21		--	--	--	30.82	--	--	31.67	

Moisture contents are in wt%; -- Not applicable, no data collected at this location

**Figure C.1** Vertical Cross-Sections of the Soil Block at the Fracture Showing Moisture Data

Distance  
From  
Fracture  
(in.)

## TEST 7C

Outlet

Inlet

1½-2½	30.55		--	--	31.25	--	--	--	30.58	
1-1½	28.35	31.25	--	30.41	--	30.54	--	--	31.37	29.93
½-1	27.01	29.75	29.28	--	28.58	--	29.66	--	29.98	28.13
¼-½	22.90	25.38	23.31	24.51	22.33	22.88	24.31	25.15	24.07	23.02
0-¼	18.72	19.24	19.27	19.97	19.01	18.83	19.18	19.68	18.48	18.81
0-¼	19.15	20.56	18.64	18.31	18.73	19.50	18.56	19.46	19.72	20.60
¼-½	21.66	24.55	21.12	19.51	21.68	23.44	23.54	25.98	25.07	23.24
½-1	25.72	28.77	--	26.95	--	28.89	--	30.35	30.48	27.21
1-1½	27.43	31.44	--	--	31.28	--	31.51	--	31.55	31.47
1½-2½	31.57		--	--	--	31.00	--	--	31.27	

Moisture contents are in wt%; -- Not applicable, no data collected at this location

**Figure C.1** Vertical Cross-Sections of the Soil Block at the Fracture Showing Moisture Data

Distance  
From  
Fracture  
(in.)

## TEST 8C

Outlet

Inlet

1½-2½	31.68		--	--	31.64	--	--	--	31.72	
1-1½	28.95	31.70	--	31.73	--	31.37	--	--	31.50	28.99
½-1	28.91	31.31	30.26	--	30.86	--	30.28	--	30.99	28.35
¼-½	26.70	28.10	26.43	25.02	25.37	25.61	25.04	23.27	24.47	23.07
0-¼	21.39	22.46	22.23	21.60	21.29	21.35	20.26	19.23	18.50	17.65
0-¼	21.77	21.25	21.64	20.91	21.93	21.60	19.15	20.39	19.54	18.66
¼-½	27.04	28.11	27.25	26.53	26.32	26.50	23.48	26.52	25.81	25.25
½-1	28.42	31.30	--	30.76	--	30.61	--	30.65	30.69	27.11
1-1½	29.17	31.78	--	--	31.46	--	31.68	--	31.45	30.19
1½-2½	31.77		--	--	--	31.63	--	--	31.62	

Moisture contents are in wt%; -- Not applicable, no data collected at this location

**Figure C.1** Vertical Cross-Sections of the Soil Block at the Fracture Showing Moisture Data

Distance  
From  
Fracture  
(in.)

## TEST 9C

Outlet

Inlet

1½-2½	30.75		--	--	30.98	--	--	--	31.15	
1-1½	26.89	30.22	--	30.01	--	30.44	--	--	30.49	25.11
½-1	24.31	24.73	23.99	--	25.02	24.09	24.33	--	27.94	24.15
¼-½	19.76	17.71	18.57	18.33	18.17	18.15	16.94	17.91	20.71	18.83
0-¼	18.11	17.19	17.64	16.84	15.66	17.02	15.90	16.18	18.15	15.87
0-¼	19.21	20.38	19.25	18.27	17.77	16.92	16.71	17.22	17.33	15.86
¼-½	22.85	25.47	23.04	20.49	19.92	18.21	17.35	21.03	22.15	18.36
½-1	25.24	29.34	--	27.02	--	24.83	--	27.36	26.87	22.33
1-1½	27.48	30.88	--	--	30.63	--	30.29	--	30.77	30.38
1½-2½	31.01		--	--	--	30.67	--	--	31.14	

Moisture contents are in wt%; -- Not applicable, no data collected at this location

**Figure C.1** Vertical Cross-Sections of the Soil Block at the Fracture Showing Moisture Data

Distance  
From  
Fracture  
(in.)

## TEST 10C

Outlet

Inlet

1½-2½	30.70		--	--	30.79	--	--	--	30.64	
1-1½	26.70	30.03	--	30.24	--	30.51	--	--	30.03	27.83
½-1	26.26	27.48	24.93	--	28.02	--	24.31	--	28.70	26.27
¼-½	22.17	20.05	19.62	20.95	23.83	23.44	21.03	22.97	22.68	21.85
0-¼	18.78	18.71	18.67	19.13	20.18	20.47	19.31	19.40	18.08	18.15
0-¼	18.96	18.63	19.92	19.47	19.44	18.96	19.36	18.67	18.01	17.80
¼-½	22.34	22.96	23.39	22.07	21.92	22.19	23.21	21.96	20.80	21.80
½-1	25.50	28.90	--	27.31	--	27.07	--	27.80	27.58	24.30
1-1½	28.17	30.80	--	--	30.58	--	30.69	--	30.70	29.54
1½-2½	31.41		--	--	--	30.88	--	--	31.40	

Moisture contents are in wt%; -- Not applicable, no data collected at this location

**Figure C.1** Vertical Cross-Sections of the Soil Block at the Fracture Showing Moisture Data



Distance  
From  
Fracture  
(in.)

## TEST 11C

Outlet

Inlet

1½-2½	31.19		--	--	31.61	--	--	--	31.50	
1-1½	27.89	31.23	--	30.93	--	31.14	--	--	31.16	28.39
½-1	27.17	30.48	27.47	--	25.61	--	25.46	--	30.08	27.06
¼-½	23.76	25.80	20.98	20.27	20.02	19.27	19.33	19.62	24.61	22.67
0-¼	18.87	20.31	18.75	18.99	19.20	18.63	18.96	18.17	19.89	19.00
0-¼	20.79	21.41	19.89	18.94	20.86	21.21	20.68	19.70	20.46	19.54
¼-½	25.75	28.19	26.49	23.51	24.22	25.96	24.81	24.88	25.89	23.15
½-1	27.46	30.92	--	30.00	--	30.89	--	30.06	29.86	25.73
1-1½	28.40	31.36	--	--	31.72	--	31.87	--	31.39	29.10
1½-2½	31.58		--	--	--	31.57	--	--	31.56	

Moisture contents are in wt%; -- Not applicable, no data collected at this location

**Figure C.1** Vertical Cross-Sections of the Soil Block at the Fracture Showing Moisture Data

**APPENDIX D**  
**CONSOLIDATION TEST DATA**

Table D.1 Summary of Consolidation Test Data

Remolded soil mixed to initial moisture content, compacted, cut into ring; ASTM Method D-2435 (B),  
24 hr. load increment duration except final unloading cycle-122 kPa to 0 kPa (121 hr.), 71 mm cell

Coefficient of Consolidation				Other Consolidation Test Data	
Load (kPa)	$c_v$ (in <sup>2</sup> /min)	$c_v$ (cm <sup>2</sup> /sec)	$c_v$ (ft <sup>2</sup> /day)	Parameter	Value
122	1.1E-03	1.2E-04	1.1E-02	Compression Index (Cc)	0.137
244	6.3E-04	6.8E-05	6.3E-03	Swell Index (Cs)	0.042
488	5.7E-04	6.1E-05	5.7E-03	Recompression Index (Cr)	0.042
977	3.6E-04	3.9E-05	3.6E-03	Initial Water Content	47.3 wt%
1956*	2.2E-04	2.4E-05	2.2E-03	Final Water Content	39.9 wt%
977	3.6E-04	3.9E-05	3.6E-03	Initial Dry Unit Weight	73.1 lb/ft <sup>3</sup>
488	2.0E-04	2.2E-05	2.0E-03	Final Dry Unit Weight	81.2 lb/ft <sup>3</sup>
244	1.3E-04	1.3E-05	1.3E-03	Initial Void Ratio	1.36
122	7.4E-05	7.9E-06	7.4E-04	Final Void Ratio	1.03
244	4.4E-04	4.7E-05	4.4E-03	Initial Saturation	96.4 %
488	2.3E-04	2.5E-05	2.3E-03	Final Saturation	99.0 %
977	2.5E-04	2.7E-05	2.5E-03	Preconsolidation Pressure	Could not be determined
1956	2.2E-04	2.4E-05	2.2E-03		
977	2.9E-04	3.1E-05	2.9E-03		
488	1.9E-04	2.1E-05	1.9E-03		
244	1.3E-04	1.4E-05	1.3E-03		
122	8.9E-05	9.6E-06	8.9E-04		
0	3.8E-05	4.1E-06	3.8E-04		

\* Correction applied for meter disfunction.

Pressure Increment (kPa)	Average Void Ratio e	Coefficient of Compressibility		Coefficient of Volume Change		Hydraulic Conductivity	
		$a_v$ (kPa <sup>-1</sup> )	$a_v$ (ft <sup>2</sup> /lb)	$m_v$ (m <sup>2</sup> /MN)	$m_v$ (ft <sup>2</sup> /lb)	Vertical K (cm/sec)	Vertical K (ft/min)
0-122	1.26	1.7E-03	7.9E-05	0.70	3.4E-05	8.9E-09	1.7E-08
122-244	1.07	1.4E-03	6.8E-05	0.68	3.3E-05	4.8E-09	9.4E-09
244-488	0.93	4.6E-04	2.2E-05	0.23	1.1E-05	1.5E-09	2.9E-09
488-977	0.82	2.1E-04	9.9E-06	0.11	5.3E-06	4.5E-10	8.8E-10
977-1956	0.73	9.1E-05	4.4E-06	0.05	2.5E-06	1.3E-10	2.5E-10
1956-977	0.69	1.9E-05	9.2E-07	0.01	5.4E-07	4.3E-11	8.5E-11
977-488	0.71	5.4E-05	2.6E-06	0.03	1.5E-06	6.7E-11	1.3E-10
488-244	0.74	1.3E-04	6.2E-06	0.08	3.6E-06	9.8E-11	1.9E-10
244-122	0.77	2.3E-04	1.1E-05	0.13	6.2E-06	9.9E-11	2.0E-10
122-244	0.78	7.7E-05	3.7E-06	0.04	2.1E-06	2.0E-10	3.9E-10
244-488	0.77	9.8E-05	4.7E-06	0.05	2.6E-06	1.4E-10	2.7E-10
488-977	0.74	7.1E-05	3.4E-06	0.04	1.9E-06	1.1E-10	2.2E-10
977-1956	0.70	4.7E-05	2.2E-06	0.03	1.3E-06	6.6E-11	1.3E-10
1956-977	0.68	1.8E-05	8.7E-07	0.01	5.2E-07	3.3E-11	6.4E-11
977-488	0.70	5.6E-05	2.7E-06	0.03	1.6E-06	6.6E-11	1.3E-10
488-244	0.73	1.2E-04	5.9E-06	0.07	3.4E-06	9.6E-11	1.9E-10
244-122	0.76	2.4E-04	1.2E-05	0.14	6.7E-06	1.3E-10	2.5E-10
122-0	0.90	2.0E-03	9.8E-05	1.15	5.5E-05	4.1E-10	8.0E-10

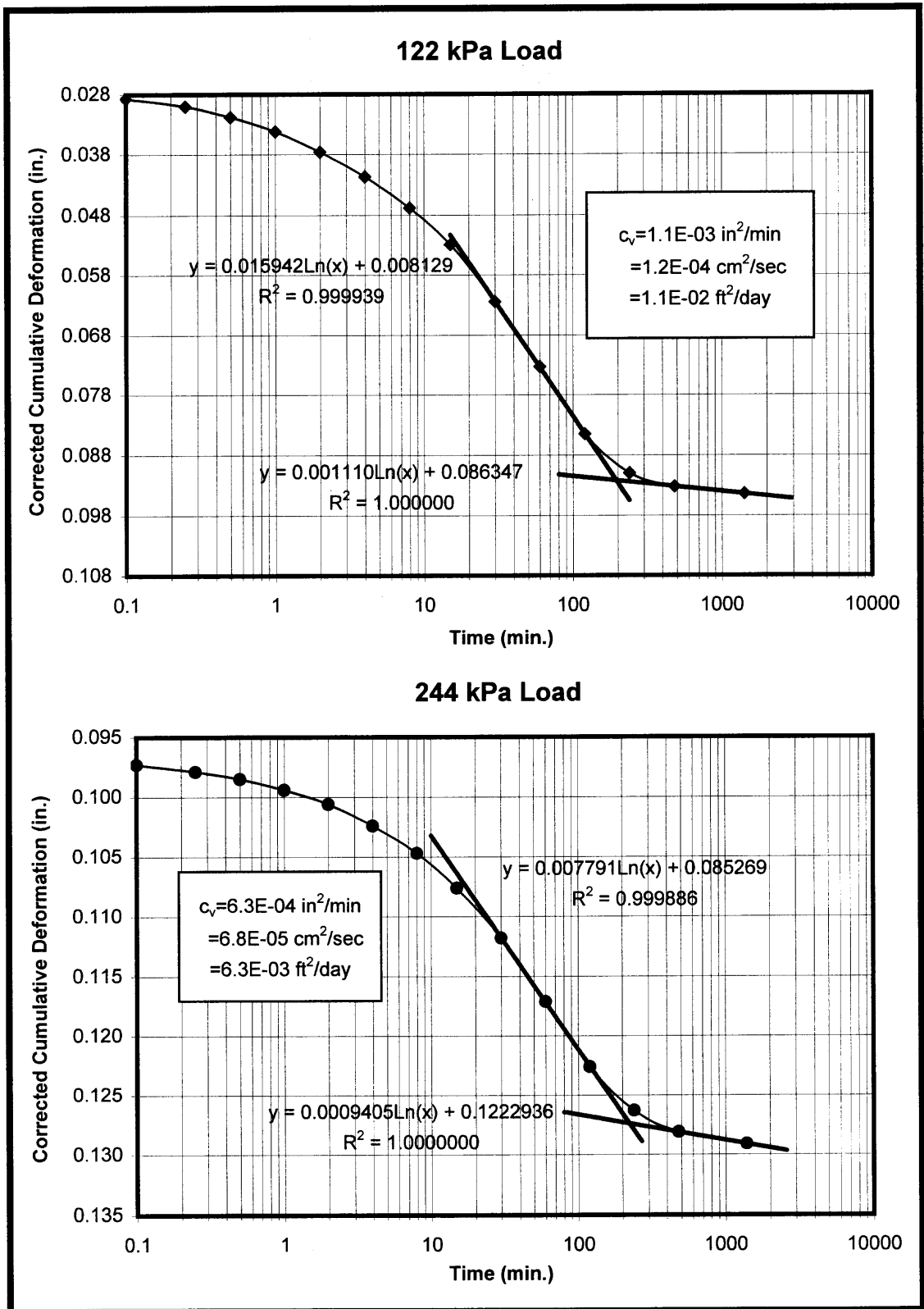


Figure D.1 Consolidation Time-Deformation Plots for Potomac Clay

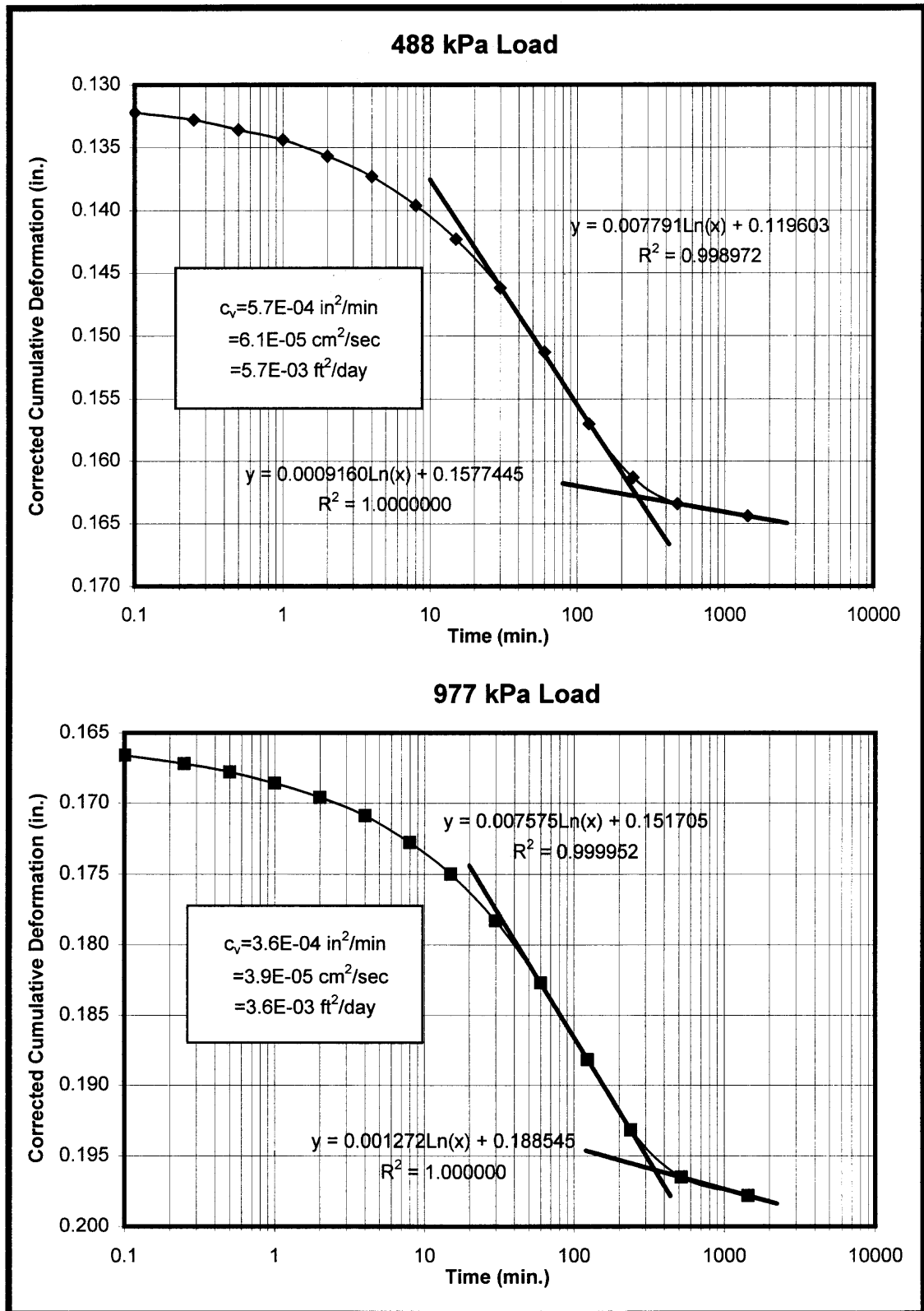


Figure D.1 (cont'd.) Consolidation Time-Deformation Plots for Potomac Clay

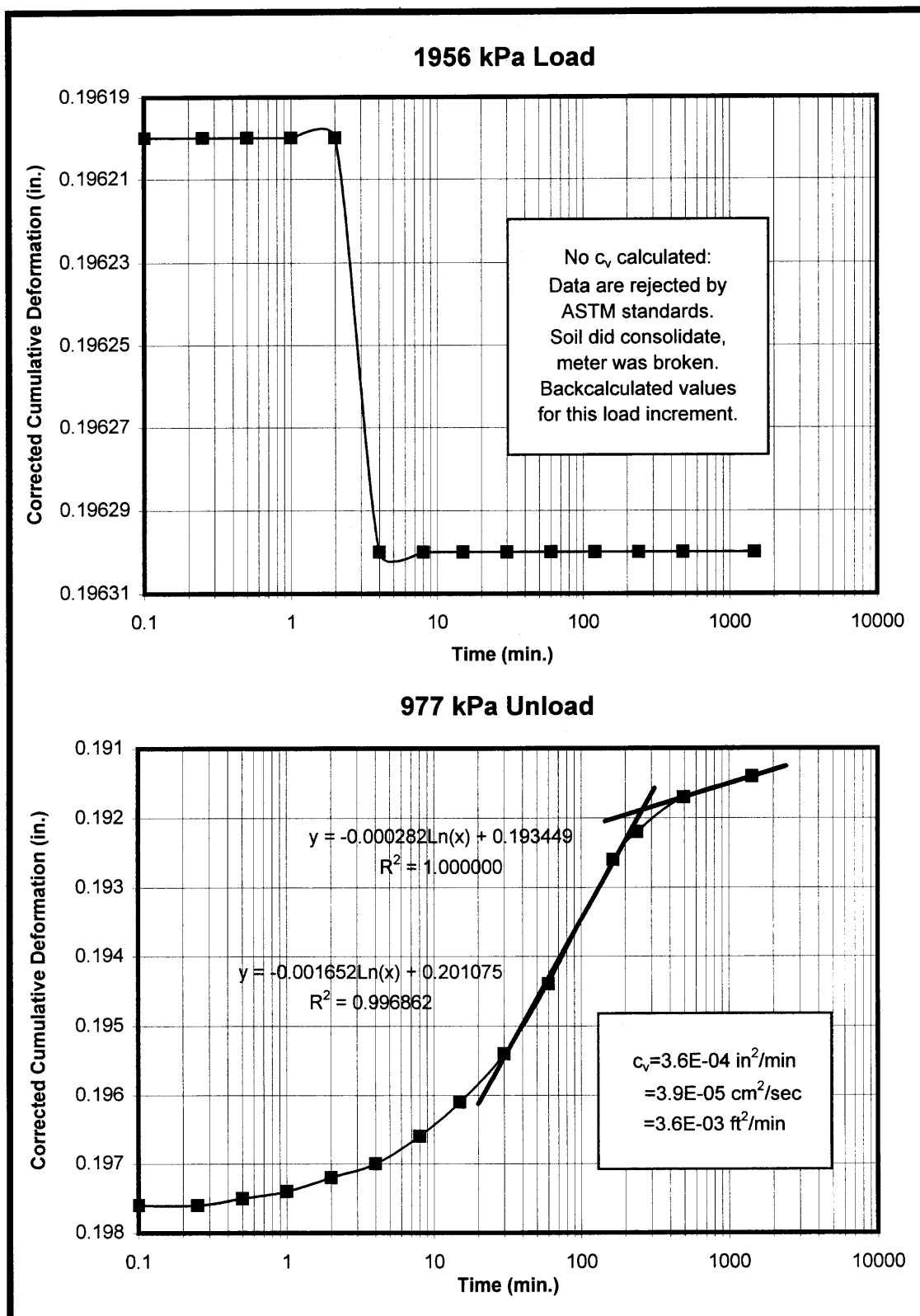


Figure D.1 (cont'd.) Consolidation Time-Deformation Plots for Potomac Clay

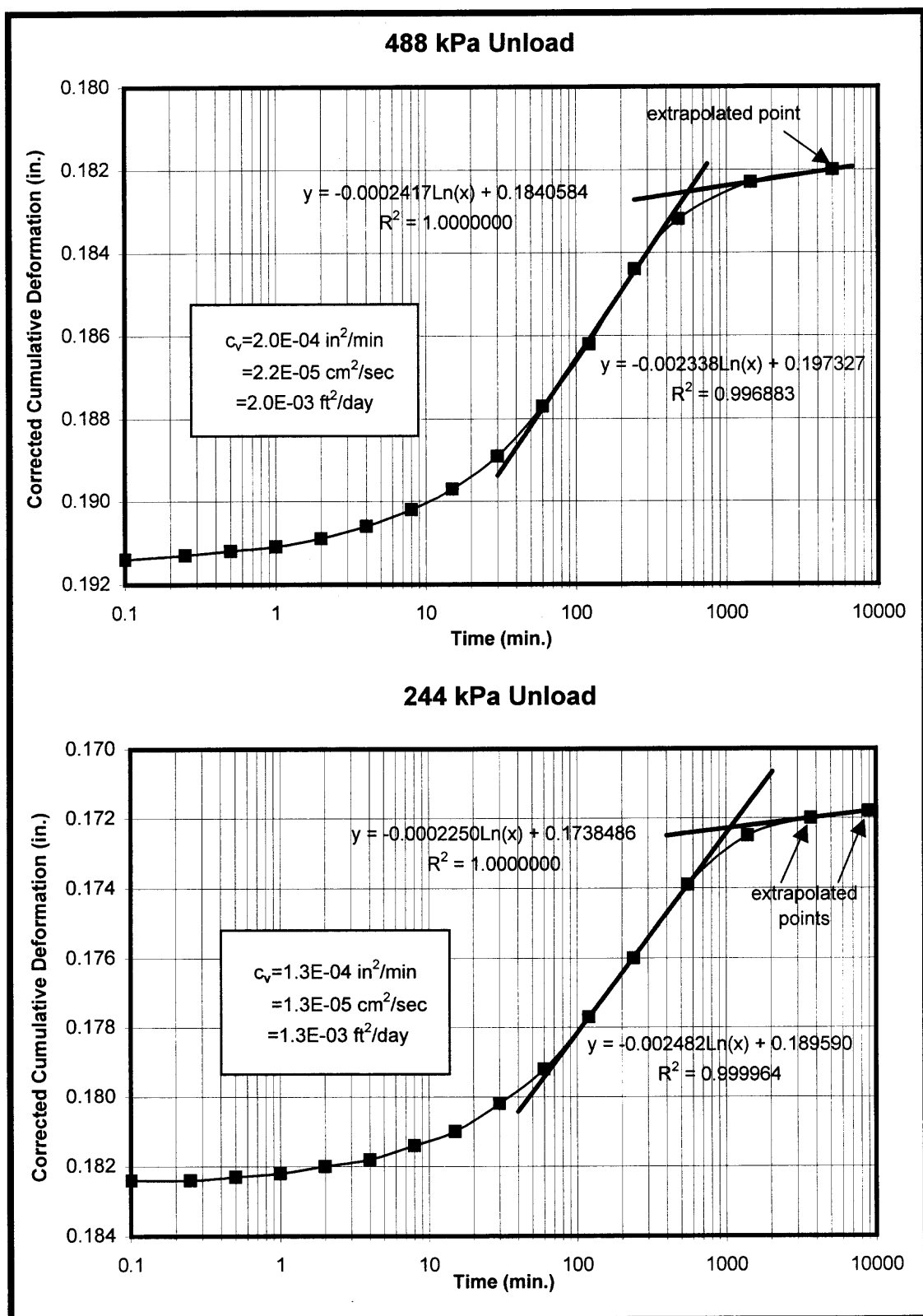


Figure D.1 (cont'd.) Consolidation Time-Deformation Plots for Potomac Clay

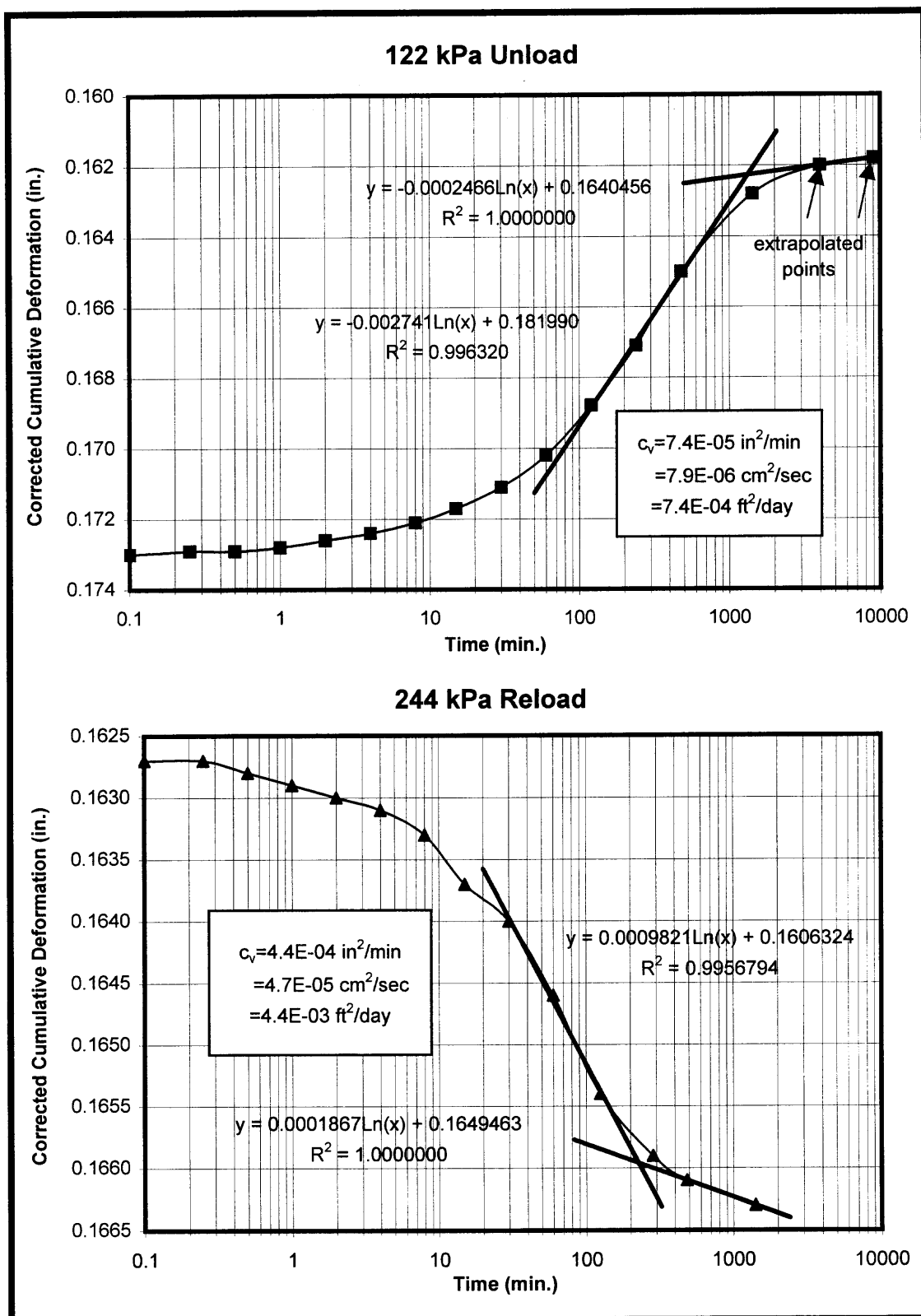


Figure D.1 (cont'd.) Consolidation Time-Deformation Plots for Potomac Clay



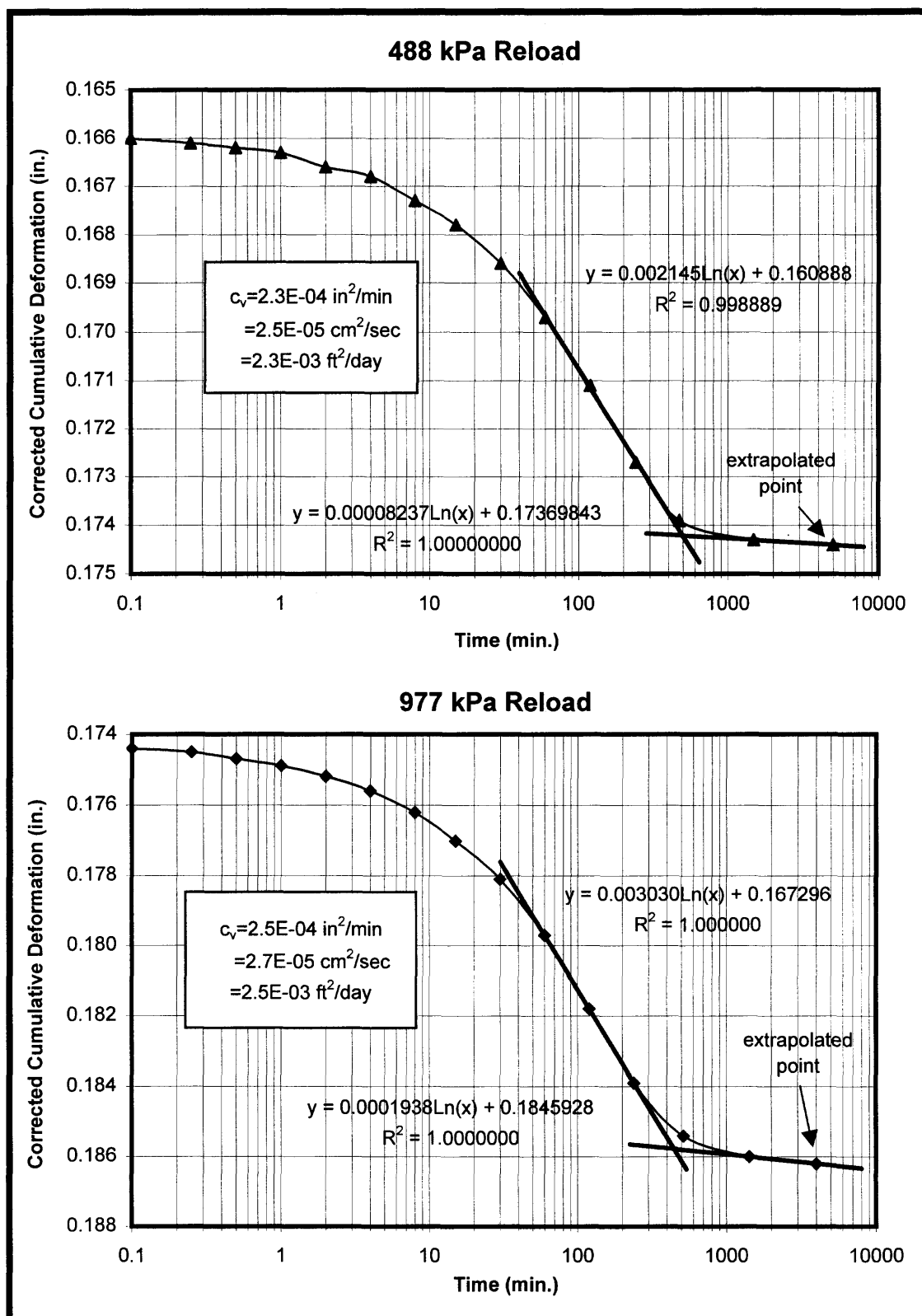


Figure D.1 (cont'd.) Consolidation Time-Deformation Plots for Potomac Clay

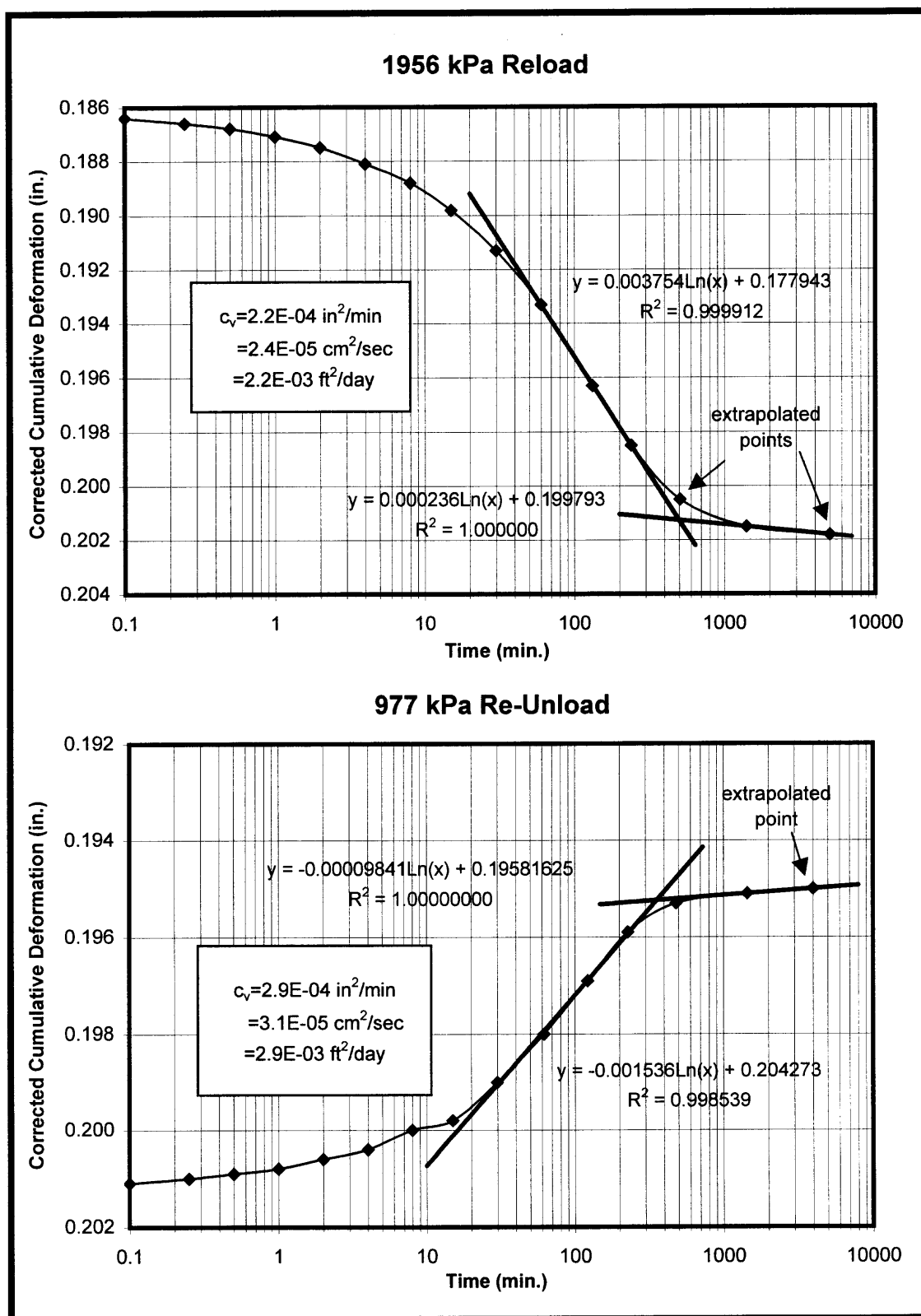


Figure D.1 (cont'd.) Consolidation Time-Deformation Plots for Potomac Clay

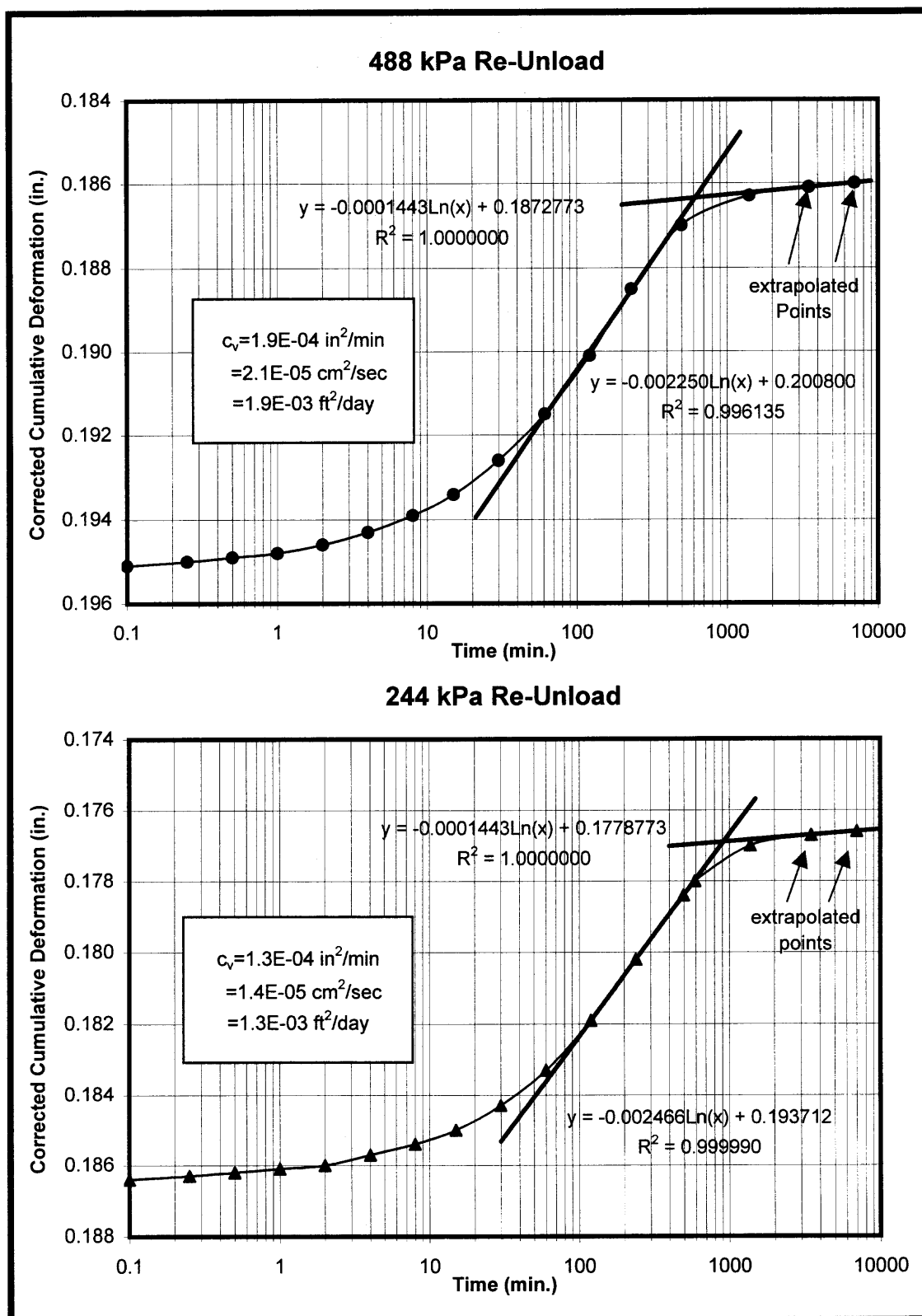


Figure D.1 (cont'd.) Consolidation Time-Deformation Plots for Potomac Clay

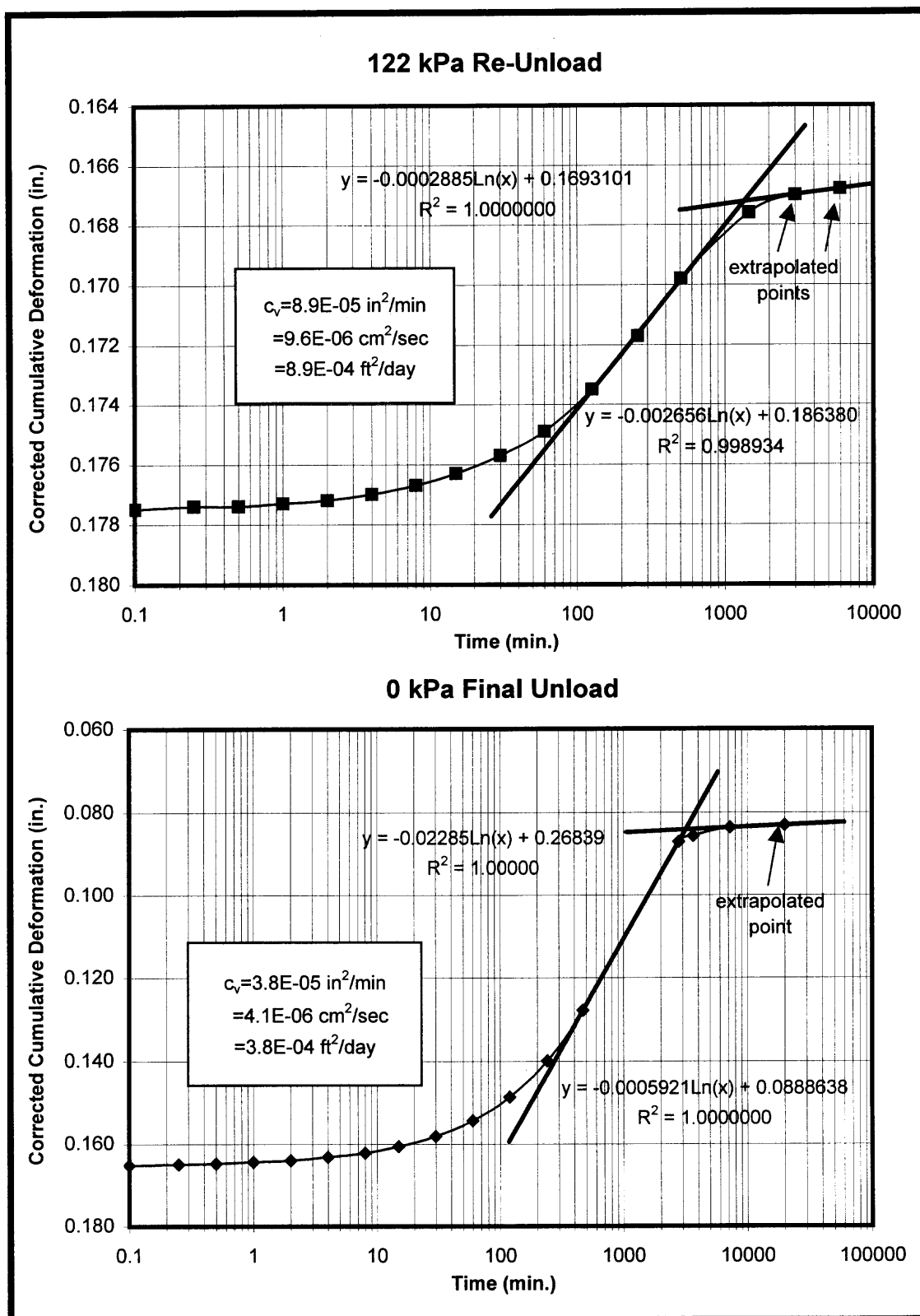


Figure D.1 (cont'd.) Consolidation Time-Deformation Plots for Potomac Clay

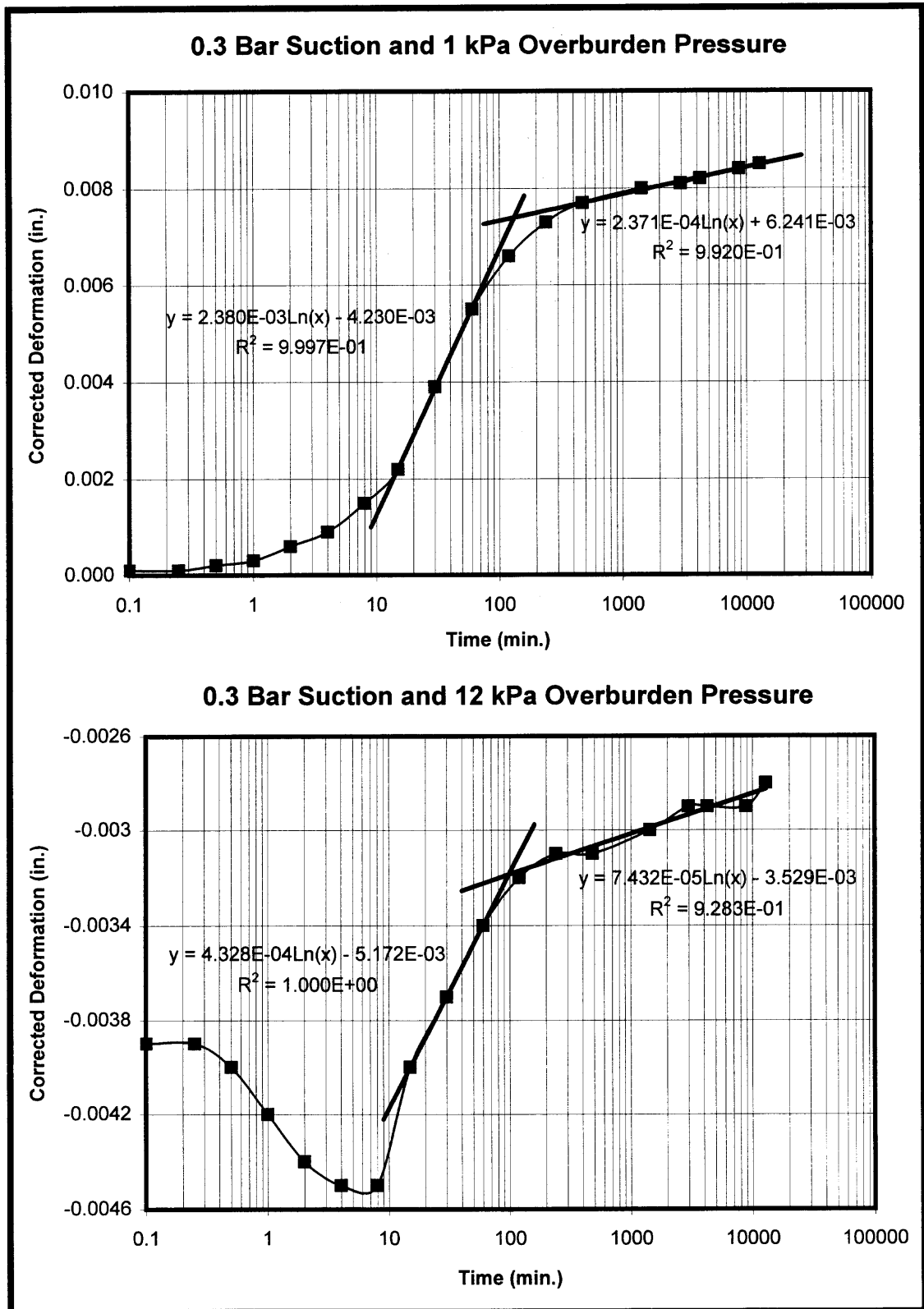
**APPENDIX E**  
**SWELL TEST DATA**

Table E.1 Summary of Swell Test Data

Test Parameter	0.3 bar Suction				1.5 bar suction			
	1 kPa	12 kPa	49 kPa	125 kPa	1 kPa	12 kPa	49 kPa	125 kPa
Initial Water Content (wt%)	42.36	42.25	-	-	31.96	32.05	32.34	32.39
Final Water Content (wt%)	44.23	44.28	-	-	40.21	39.29	37.99	35.82
Initial Dry Density (g/cm <sup>3</sup> )	1.28	1.24	-	-	1.4	1.37	1.37	1.41
Final Dry Density (g/cm <sup>3</sup> )	1.25	1.23	-	-	1.32	1.33	1.36	1.4
Initial Dry Unit Weight (lb/ft <sup>3</sup> )	79.9	77.4	-	-	87.4	85.5	85.5	88
Final Dry Unit Weight (lb/ft <sup>3</sup> )	78	76.8	-	-	82.4	83	84.9	87.4
Initial Wet Unit Weight (lb/ft <sup>3</sup> )	114	111	-	-	115	113	1.82	1.87
Final Wet Unit Weight (lb/ft <sup>3</sup> )	113	111	-	-	116	116	1.88	1.91
Equivalent Height of Solids (cm)	0.654	0.638	-	-	0.715	0.696	0.679	0.728
Initial Void Ratio	1.16	1.23	-	-	0.972	1.01	1	0.95
Final Void Ratio	1.2	1.23	-	-	1.08	1.07	1.02	0.96
Initial Saturation (%)	101	95.1	-	-	90.6	87.4	88.7	93.9
Final Saturation (%)	102	99.6	-	-	102	101	103	103
Percent Heave (%)	1.5	0.2	-	-	5.65	2.78	0.86	0.52

- Not Tested

Test Parameter	2.9 bar Suction				6.0 bar suction			
	1 kPa	12 kPa	49 kPa	125 kPa	1 kPa	12 kPa	49 kPa	125 kPa
Initial Water Content (wt%)	30.52	30.57	30.5	30.33	30.03	30.4	30.21	30.45
Final Water Content (wt%)	40.01	36.86	35.91	33.8	39.53	38.53	35.43	34.44
Initial Dry Density (g/cm <sup>3</sup> )	1.49	1.45	1.45	1.47	1.48	1.48	1.2	1.48
Final Dry Density (g/cm <sup>3</sup> )	1.43	1.39	1.42	1.46	1.4	1.39	1.18	1.46
Initial Dry Unit Weight (lb/ft <sup>3</sup> )	93	90.5	90.5	91.8	92.4	92.4	72.9	92.4
Final Dry Unit Weight (lb/ft <sup>3</sup> )	89.3	86.8	88.7	91.1	87.4	86.8	73.7	91.1
Initial Wet Unit Weight (lb/ft <sup>3</sup> )	121	118	119	119	120	120	97.4	120
Final Wet Unit Weight (lb/ft <sup>3</sup> )	125	119	120	122	122	120	99.9	122
Equivalent Height of Solids (cm)	0.75	0.771	0.773	0.836	0.699	0.708	0.648	0.712
Initial Void Ratio	0.853	0.907	0.902	0.878	0.86	0.864	1.3	0.868
Final Void Ratio	0.933	0.984	0.94	0.89	0.974	0.992	1.35	0.896
Initial Saturation (%)	98.5	93	93.5	95.2	96.4	97.1	64.1	96.8
Final Saturation (%)	119	103	105	105	119	107	72.6	106
Percent Heave (%)	4.39	4.27	1.87	0.68	6.69	6.47	2.28	1.48



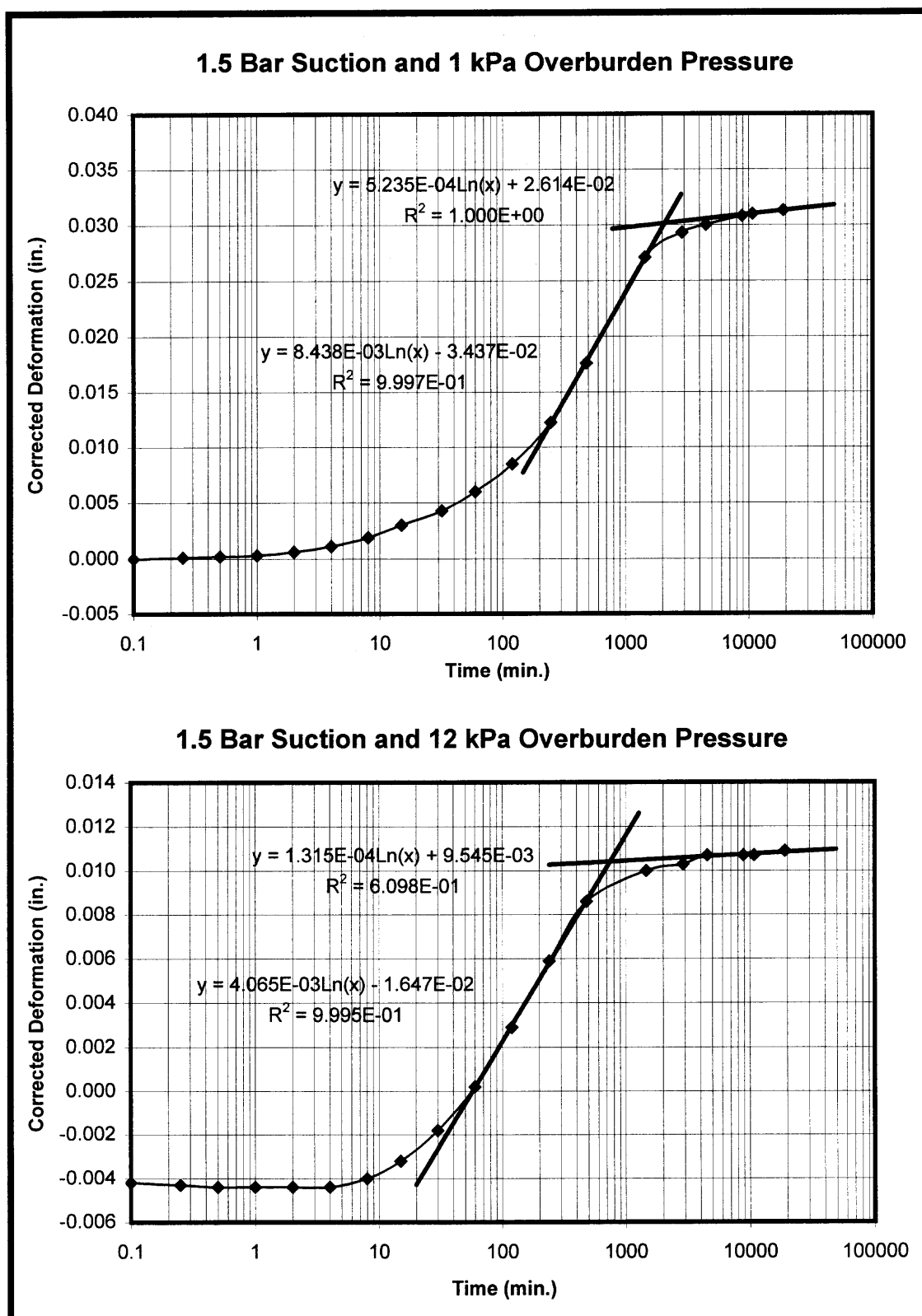


Figure E.1 (cont'd.) Swell Test Time-Deformation Plots for Potomac Clay



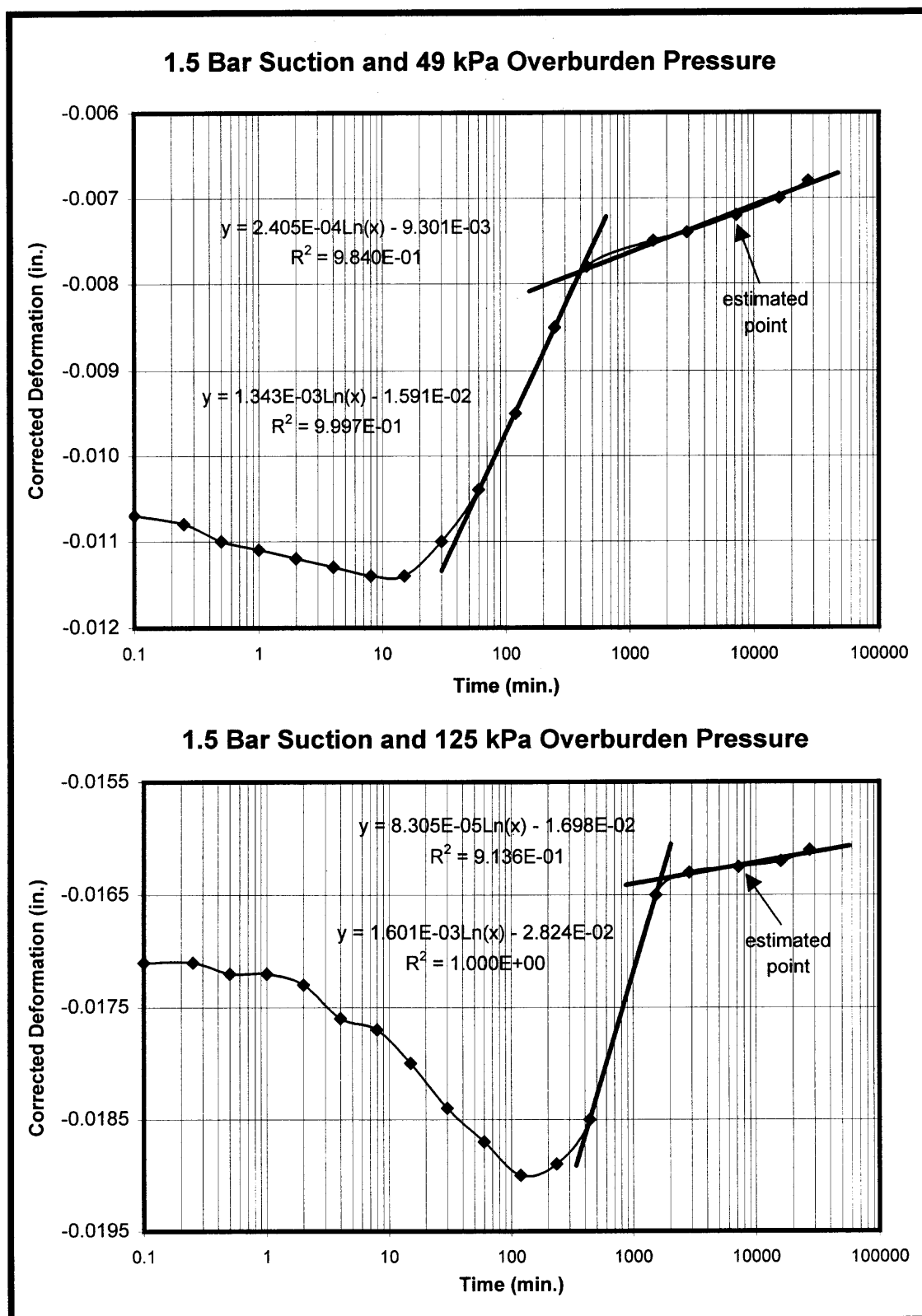
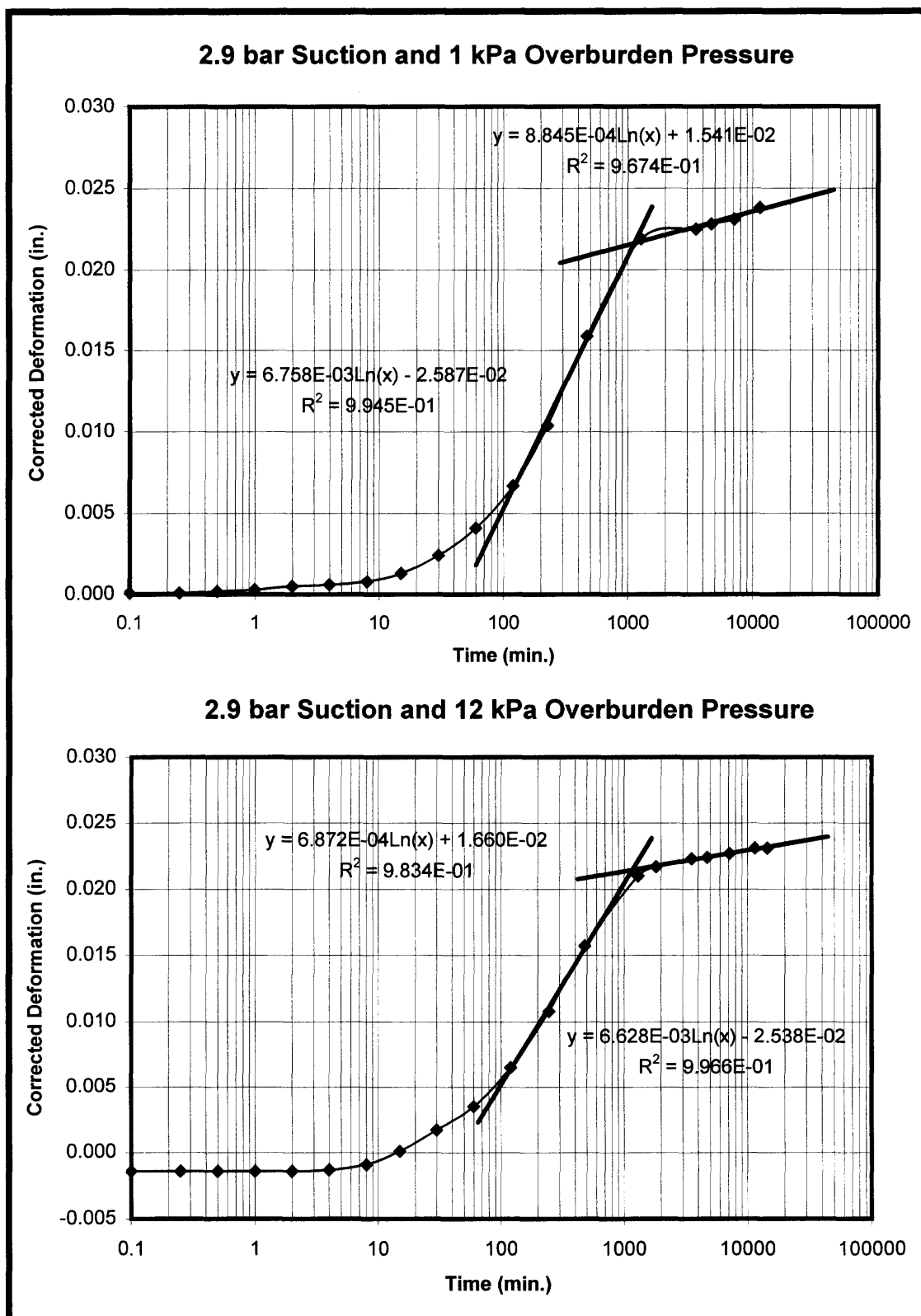


Figure E.1 (cont'd.) Swell Test Time-Deformation Plots for Potomac Clay



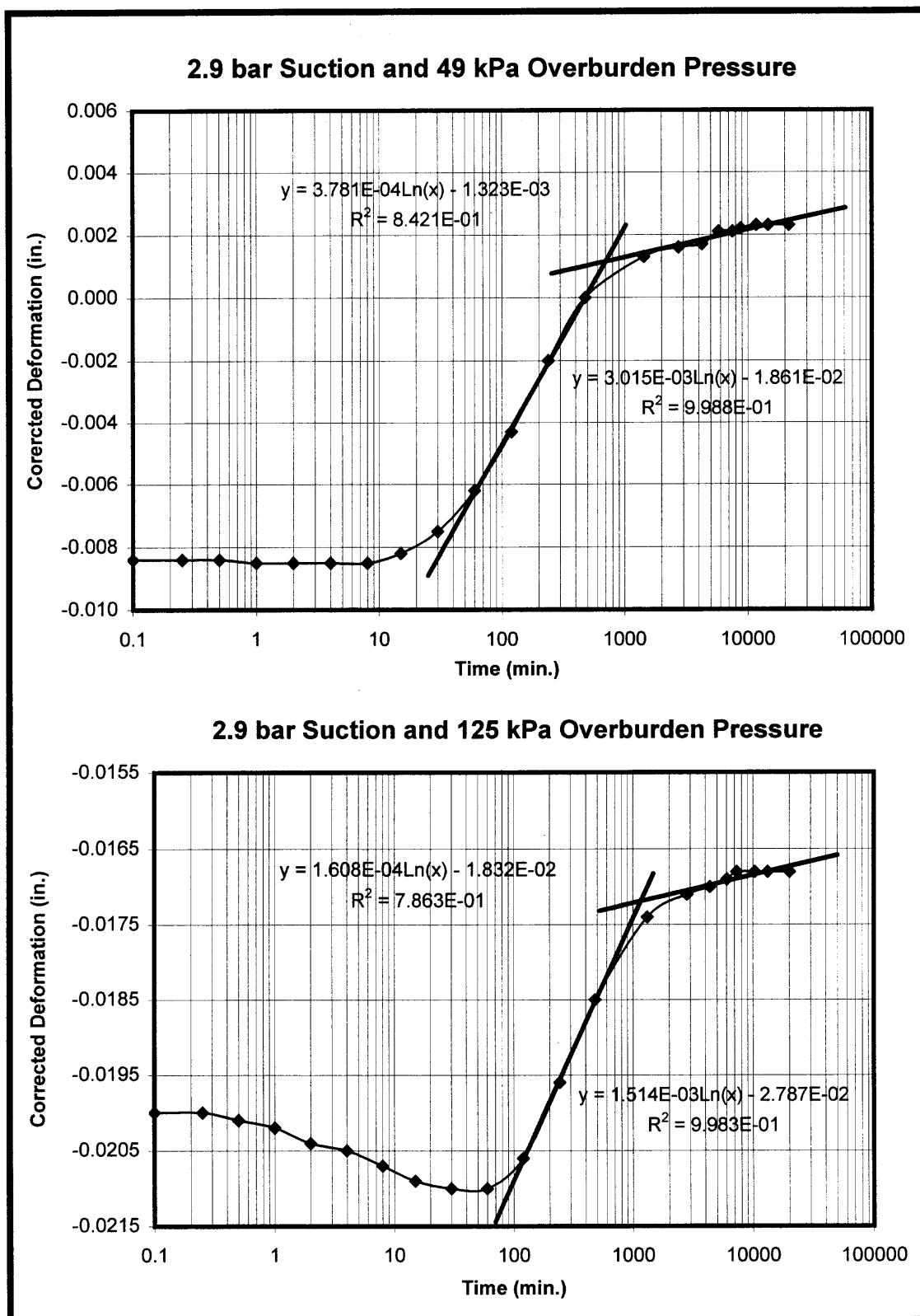


Figure E.1 (cont'd.) Swell Test Time-Deformation Plots for Potomac Clay

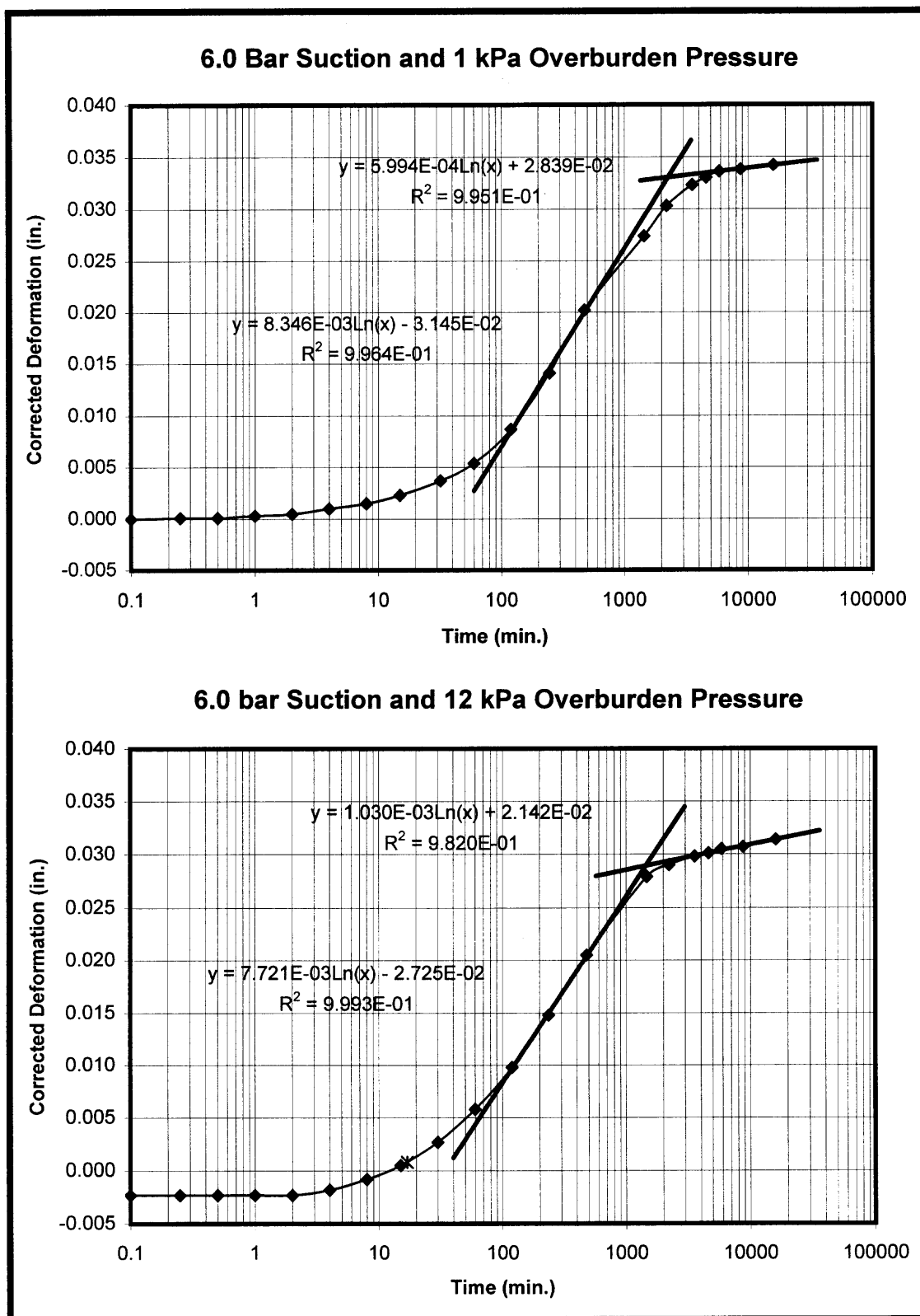


Figure E.1 (cont'd.) Swell Test Time-Deformation Plots for Potomac Clay

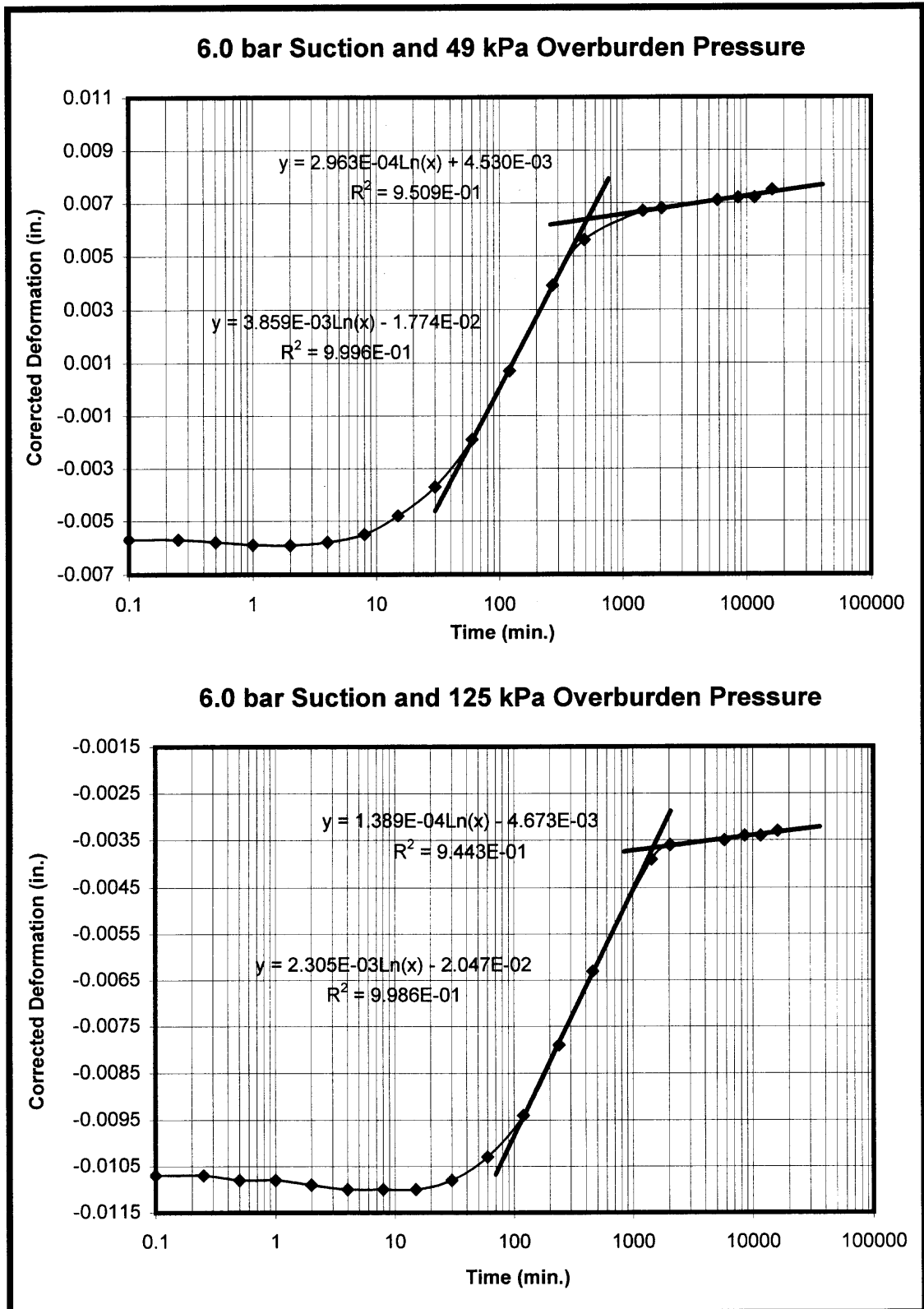


Figure E.1 (cont'd.) Swell Test Time-Deformation Plots for Potomac Clay

**APPENDIX F**  
**SOLUTION DERIVATIONS**

## SOLUTION OF THE GOVERNING EQUATION OF THE FVC MODEL

This section presents the derivation of the solution of the governing equation for the 'Fracture Volume Change Model.' The solution is formulated for a generalized case that allows for both Case 1 and Case 2 solutions from a single expression. In addition, the boundary condition at the fracture has been expanded to a third order polynomial, which will allow for potential future analysis of alternate forms. For simplicity of presentation, this boundary condition is also written with constants in the form of  $\beta_n$ , where  $n=0$  to 3. The governing equation and boundary conditions under this framework are given as,

$$w_t = c_v w_{zz}$$

$$w(0,t) = \beta_0 + \beta_1 t + \beta_2 t^2 + \beta_3 t^3 = f(t)$$

$$\frac{\partial w}{\partial z}(L,t) = 0$$

$$w(z,0) = w_i$$

where  $z \in [0, L]$  at  $0 < t < \infty$ . Look for a solution,

$$w(z,t) = A(t) \left( 1 - \frac{z}{L} \right) + B(t) \left( \frac{z}{L} \right) + v(z,t)$$

$$\sigma(z,t) = A(t) \left( 1 - \frac{z}{L} \right) + B(t) \left( \frac{z}{L} \right)$$

It is required that  $\sigma(z,t)$  satisfy the boundary conditions:

$$\left. \frac{\partial \sigma}{\partial z} \right|_{z=L} = 0 = -\frac{A}{L} + \frac{B}{L} \quad \text{Therefore, } \boxed{A = B}$$

$$\sigma(0,t) = f(t) = A(1-0) + B(0) \quad \text{Therefore, } \boxed{A = f(t)}$$

$$\sigma(z,t) = f(t) \left(1 - \frac{z}{L}\right) + f(t) \left(\frac{z}{L}\right) \quad \text{Therefore, } \boxed{f(t) = \sigma(z,t)}$$

$$w(z,t) = f(t) + v(z,t) = \beta_0 + \beta_1 t + \beta_2 t^2 + \beta_3 t^3 + v(z,t)$$

$$w_t = \beta_1 + 2\beta_2 t + 3\beta_3 t^2 + v_t$$

$$w(z,0) = w_i = \beta_0 + \beta_1 0 + \beta_2 0 + \beta_3 0 + v(z,0), \quad v(z,0) = w_i - \beta_0,$$

$$w_{zz} = v_{zz}$$

Substituting into the PDE,

$$\beta_1 + 2\beta_2 + 3\beta_3 t^2 + v_t = c_v v_{zz}$$

$$v_t = c_v v_{zz} - (\beta_1 + 2\beta_2 t + 3\beta_3 t^2) \quad \text{with } v(0,t) = 0 \quad \left. \frac{\partial v}{\partial z} \right|_{z=L} = 0 \quad v(z,0) = w_i - \beta_0$$

Solving the homogeneous problem :

$$v_t = c_v v_{zz} \quad v(0,t) = \left. \frac{\partial v}{\partial z} \right|_{z=L} = 0,$$

Separation of variables leads to the following problem in space :

$$\text{BCs: } S(0) = 0, \quad S'(L) = 0$$

$$S'' + \lambda^2 S = 0, \quad S = c_1 \cos \lambda z + c_2 \sin \lambda z \quad \text{for } \lambda > 0$$

( $\lambda \leq 0$  leads to trivial solutions)



From BCs :  $S(0) = 0 = c_1 \cos(0) + c_2 \sin(0)$  Therefore  $c_1 = 0$

$S(z) = c_2 \sin \lambda z$ ,  $S'(L) = 0 = c_2 \lambda \cos \lambda L$  since  $\lambda_1 c_2 \neq 0$ , then  $\cos \lambda L = 0$

$\cos \lambda L = 0$  when  $\lambda L = \frac{n\pi}{2}$   $n = 1, 3, 5, \dots$

$$= \frac{(2n-1)\pi}{2} \quad n = 1, 2, \dots, \text{ Therefore, } \lambda_n = \frac{(2n-1)\pi}{2L} \quad n = 1, 2, \dots,$$

The homogeneous problem has the following eigenfunctions:

$$S_n(z) = \sin \lambda_n z \quad \text{where, } \lambda_n = \frac{(2n-1) \cdot \pi}{2L}, \quad n = 1, 2, 3, \dots$$

For this problem, let  $v(z, t) = \sum_{n=1}^{\infty} v_n(z, t) = \sum_{n=1}^{\infty} T_n(t) S_n(z)$

$$v_t = \sum_{n=1}^{\infty} T_n'(t) S_n(z) = \sum_{n=1}^{\infty} T_n' \sin \lambda_n z$$

$$v_{zz} = \sum_{n=1}^{\infty} T_n S_n'' = \sum_{n=1}^{\infty} -\lambda_n^2 T_n S_n = -\sum_{n=1}^{\infty} \lambda_n^2 T_n \sin \lambda_n z$$

Plugging into the nonhomogeneous PDE,

$$\sum_{n=1}^{\infty} T_n' \sin \lambda_n z = -c_v \sum_{n=1}^{\infty} \lambda_n^2 T_n \sin \lambda_n z - (\beta_1 + 2\beta_2 t + 3\beta_3 t^2)$$

Multiplying both sides by  $\sin \lambda_m z$  and integrating over the space, utilizing orthogonality :

$$\sum_{n=1}^{\infty} T_n' \int_0^L \sin \lambda_n z \sin \lambda_m z dz = -c_v \sum_{n=1}^{\infty} \lambda_n^2 T_n \int_0^L \sin \lambda_n z \sin \lambda_m z dz - \int_0^L (\beta_1 + 2\beta_2 t + 3\beta_3 t^2) \sin \lambda_m z dz$$

$$\frac{L}{2} T_m' = -\frac{c_v \lambda_m^2 L}{2} T_m - (\beta_1 + 2\beta_2 t + 3\beta_3 t^2) \left( \frac{1}{\lambda_m} \right)$$

$$\boxed{T_m' + c_v \lambda_m^2 T_m = -\frac{2}{\lambda_m L} (\beta_1 + 2\beta_2 t + 3\beta_3 t^2)} \quad \text{ODE in time}$$

$T_m = T_{m,n}, T_{m,p}$  where  $T_{m,n} = A_m \exp(-c_v \lambda_m^2 t)$  The Homogeneous Solution

Guess,  $T_{m,p} = \alpha_0 + \alpha_1 t + \alpha_2 t^2$

$$T_{m,p}' = \alpha_1 + 2\alpha_2 t$$

$$\alpha_1 + 2\alpha_2 t + c_v \lambda_m^2 (\alpha_0 + \alpha_1 t + \alpha_2 t^2) = -\frac{2}{\lambda_m L} (\beta_1 + 2\beta_2 t + 3\beta_3 t^2)$$

$$0(t^0) \quad \alpha_1 + c_v \lambda_m^2 \alpha_0 = -\frac{2\beta_1}{\lambda_m L}$$

$$0(t^1) \quad 2\alpha_2 + c_v \lambda_m^2 \alpha_1 = -\frac{4\beta_2}{\lambda_m L}$$

$$0(t^2) \quad c_v \lambda_m^2 \alpha_2 = -\frac{6\beta_3}{\lambda_m L}$$

$$\boxed{\alpha_2 = -\frac{6\beta_3}{c_v \lambda_m^3 L}}$$

$$2\alpha_2 + c_v \lambda_m^2 \alpha_1 = -\frac{4\beta_2}{\lambda_m L} \rightarrow \alpha_1 = -\frac{2\alpha_2}{\lambda_m^2 c_v} - \frac{4\beta_2}{c_v \lambda_m^3 L} = \frac{12\beta_3}{c_v^2 \lambda_m^5 L} - \frac{4\beta_2}{c_v \lambda_m^3 L}$$

$$\boxed{\alpha_1 = -\frac{4}{c_v \lambda_m^3 L} \left( \frac{3\beta_3}{c_v \lambda_m^2} - \beta_2 \right)}$$

$$\alpha_1 + c_v \lambda_m^2 \alpha_o = -\frac{2\beta_1}{\lambda_m L} \rightarrow \alpha_o = \frac{-\alpha_1}{c_v \lambda_m^2} - \frac{2\beta_1}{c_v \lambda_m^3 L}$$

$$= \frac{4\beta_2}{c_v^2 \lambda_m^5 L} - \frac{12\beta_3}{c_v^3 \lambda_m^7 L} - \frac{2\beta_1}{c_v \lambda_m^3 L}$$

$$\alpha_o = \frac{2}{c_v \lambda_m^3 L} \left( -\beta_1 + \frac{2\beta_2}{c_v \lambda_m^2} - \frac{6\beta_3}{c_v^2 \lambda_m^4} \right)$$

$$T_m = A_m \exp(-c_v \lambda_m^2 t) + \alpha_o + \alpha_1 t + \alpha_2 t^2$$

$$v(z, t) = \sum_{n=1}^{\infty} T_n S_n = \sum_{n=1}^{\infty} [A_n \exp(-c_v \lambda_n^2 t) + \alpha_o + \alpha_1 t + \alpha_2 t^2] \sin \lambda_n z$$

$$v(z, 0) = w_i - \beta_o = \sum_{n=1}^{\infty} [(A_n + \alpha_o) \sin \lambda_n z]$$

$$\text{Let } B_n = (A_n + \alpha_o), \quad w_i - \beta_o = \sum_{n=1}^{\infty} B_n \sin \lambda_n z$$

$$\text{Recall } B_n = \frac{2(w_i - \beta_o)}{L \lambda_n} = A_n + \alpha_o, \quad A_n = \frac{2(w_i - \beta_o)}{L \lambda_n} - \alpha_o$$

$$w(z, t) = \sigma(z, t) + v(z, t)$$

$$= \beta_o + \beta_1 t + \beta_2 t^2 + \beta_3 t^3 + \sum_{n=1}^{\infty} \{A_n \exp(-c_v \lambda_n^2 t) + \alpha_{0n} + \alpha_{1n} t + \alpha_{2n} t^2\} \sin \lambda_n z$$

$$w(z, t) = \beta_o + \beta_1 t + \beta_2 t^2 + \beta_3 t^3 + \sum_{n=1}^{\infty} \left\{ \left[ \frac{2(w_i - \beta_o)}{L \lambda_n} - \alpha_{0n} \right] \exp(-c_v \lambda_n^2 t) + \alpha_{0n} + \alpha_{1n} t + \alpha_{2n} t^2 \right\} \sin \lambda_n z$$

$$\lambda_n = \frac{(2n-1)\pi}{2L}, \quad \alpha_{0n} = \frac{2}{c_v \lambda_n^3 L} \left( -\beta_1 + \frac{2\beta_2}{c_v \lambda_n^2} - \frac{6\beta_3}{c_v^2 \lambda_n^4} \right), \quad \alpha_{1n} = -\frac{4}{c_v \lambda_n^3 L} \left( \frac{3\beta_3}{c_v \lambda_n^2} - \beta_2 \right), \quad \alpha_{2n} = -\frac{6\beta_3}{c_v \lambda_n^3 L}$$

For the current study,

$$\sigma(z, t) = mt + c \rightarrow \beta_0 = c, \beta_1 = m$$

$$\beta_2 = \beta_3 = 0 \rightarrow \alpha_{0n} = \frac{-2m}{c_v \lambda_n^2 L}, \quad \alpha_{1n} = \alpha_{2n} = 0$$

$$w(z, t) = mt + c + \sum_{n=1}^{\infty} \left\{ \left[ \frac{2(w_i - c)}{L \lambda_n} + \frac{2m}{c_v \lambda_n^2 L} \right] \exp(-c_v \lambda_n^2 t) - \frac{2m}{c_v \lambda_n^2 L} \right\} \sin \lambda_n z, \text{ and } \lambda_n = \frac{(2n-1)\pi}{2L}$$

## DERIVATION OF THE AERODYNAMIC EVAPORATION RATE IN THE FRACTURE

The method for calculating the evaporation rate at ground surface (Section 2.3.4) may be extended to analysis of the evaporation rate in the fracture by viewing the boundary soils adjacent to the fracture as a free water surface. The velocity component of the expression describing aerodynamic evaporation,  $E_a$ , from Eq. 2.12, may be expressed as the mean air velocity in the fracture,  $\bar{V}$ , computed for the linear and radial flow conditions, respectively, as,

$$\bar{V} = \frac{Q_s}{W \cdot b_e}$$

$$\bar{V} = \frac{Q_s}{2\pi r \cdot b_e}$$

where  $Q_s$  is the average flow through the fracture under standard conditions of temperature and pressure ( $L^3/T$ ),  $W$  is the width of the fracture (L),  $r$  is the radius of the fracture (L), and  $b_e$  is the average effective aperture (L). Hall (1995) and Nautiyal (1993) provided definitions for the effective aperture,  $b_e$ , for linear and radial flow conditions (Cubic Law), respectively, with gas compressibility effects, as,

$$b_e = \left( - \frac{(2 \cdot P_1) \cdot 12 \cdot Q_s \cdot \nu \cdot (L_2 - L_1)}{(P_2^2 - P_1^2) \cdot g \cdot W} \right)^{\frac{1}{n}}$$

$$b_e = \left( - \frac{(2 \cdot P_1) \cdot 6 \cdot Q_s \cdot \nu \cdot \ln\left(\frac{R_2}{R_1}\right)}{(P_2^2 - P_1^2) \cdot g \cdot \pi} \right)^{\frac{1}{n}}$$

where  $L_1$  and  $L_2$ , and  $R_1$  and  $R_2$  are linear and radial distances from the extraction point (L), respectively, where  $L_2 > L_1$  and  $R_2 > R_1$ ;  $P_1$  and  $P_2$  are absolute air pressures (L) at either  $L_1$  and  $L_2$ , or  $R_1$  and  $R_2$ , respectively;  $Q_s$  is the volumetric flow rate at standard temperature and pressure (STP) ( $L^3/T$ );  $\nu$  is the kinematic viscosity of air at the operating temperature ( $L^2/T$ );  $g$  is the acceleration due to gravity ( $L/T^2$ );  $W$  is the fracture width (L); and  $n$  is aperture exponent. For laminar flows under parallel plate conditions,  $n$  is equal to 3, and may decrease to 1.2 for fully turbulent flow within a rough discontinuity (Sharp and Maini, 1972).

Importing the velocity component into Eq. 2.12 yields a generalized equation for the evaporation rate in the fracture,  $E_{af}$ , as,

$$E_{af} = 0.35 \cdot \left[ e_2^0 - \left( \frac{\bar{h}_r}{100} \cdot e_0^0 \right) \right] \cdot \left[ 0.5 + \frac{\bar{V}}{100} \right]$$

The saturation vapor pressure at the surface of the fracture,  $e_0^0$ , may be approximated by the saturation vapor pressure at the fracture temperature,  $e_2^0$ . The two are differentiated by the fact that the saturation vapor pressure at the fracture surface considers the effects of relative humidity while that in the

fracture does not. It should be noted that the vapor pressure components are insignificant as compared to the velocity (wind) components. As such, the vapor pressure approximations are considered acceptable.

Thus, the final expression for the aerodynamic evaporation rate in the fracture,  $E_{af}$ , is,

$$E_{af} = 0.35 \cdot \left[ e_2^0 - \left( \frac{\bar{h}_r}{100} \cdot e_2^0 \right) \right] \cdot \left[ 0.5 + \frac{\bar{V}}{100} \right]$$

where  $e_2^0$  is the saturation vapor pressure at mean temperature in the fracture (in mm Hg);  $\bar{h}_r$  is the relative humidity of the air in the fracture; and  $\bar{V}$  is the average velocity at standard temperature and pressure (STP) (mi./day). The final unit of  $E_{af}$  is mm/day. A table of saturation vapor pressures,  $e_2^0$ , at various temperatures is provided in Appendix J for convenience.

## SIMPLIFIED SOLUTION FOR FIRST STAGE EVAPORATION

The discipline of soil physics offers a manipulation of the governing equation of the FVC Model (Eq. 4.2) using the principles of evaporation theory. The simplification is now reviewed, using an approach that has been modified from Ghildyal and Tripathi (1987).

The simplification is based on the assumption that the soil is in the first stage evaporation (Section 2.3.4). By letting  $A$  be the cross-sectional area of the REV half-space, the volumetric evaporation loss per unit volume of soil can be given by,

$$\frac{AE}{AL} = \frac{E}{L}$$

where  $E$  is the evaporation rate (L/T). Under the premises of first stage drying, the change in moisture content with time is proportional to the evaporation rate, or,

$$\frac{\partial(Aw\Delta z / A\Delta z)}{\partial t} = \frac{\partial w}{\partial t} = -\frac{E}{L}$$

The negative sign represents the rate of decrease in water content with time in the REV half-space. Substituting this equation into Eq. 4.2, the following equation is derived,

$$\frac{\partial}{\partial z} \left( c_v \frac{\partial w}{\partial z} \right) = -\frac{E}{L}$$



which on integration yields,

$$c_v \frac{\partial w}{\partial z} = -\frac{Ez}{L} + f(t)$$

where  $f(t)$  is an arbitrary function of  $t$ . Applying the zero flux boundary condition at the outer edges of the REV (Eq. 4.15) into the equation above,

$$f(t) = E$$

Substituting this into the previous equation yields,

$$c_v \frac{\partial w}{\partial z} = E \left( 1 - \frac{z}{L} \right)$$

where  $c_v$  is the coefficient of consolidation ( $L^2/T$ ),  $w$  is the gravimetric moisture content ( $M/M$ ),  $L$  is the length of the REV half-space ( $L$ ), and  $z$  is the vertical coordinate ( $L$ ).

This equation is the final simplified solution derived from first stage evaporation theory. The manipulation served to decrease the order of the equation, and allow determination of the change in water content with depth as a direct function of evaporation rate.

## APPENDIX G

### SIGNIFICANCE OF THE COMPONENTS OF TOTAL SOIL WATER POTENTIAL

The governing equation for the FVC Model considers only the pore-water pressure potential, which is one of four components of the total soil water potential in expansive clays. This appendix presents an analysis of the significance of each component including pore-water pressure, overburden, osmotic, and gravitational potentials. Sample calculations are performed using data from the drying stage horizontal infiltrometer test 5C. The reader is referred to Section 2.3 for a more detailed discussion of the stress state variables.

The overburden potential is the pressure imposed on the soil water by the weight of the overburden, and may be described as,

$$\Omega = \left( P_0 + \int_0^z \frac{\theta \cdot (1 + e) + G_s}{1 + e} dz \right) \frac{de}{dv} \quad (\text{Eq. G.1})$$

where  $z$  is the depth to the point of interest,  $P_0$  is the external load at ground surface (i.e.,  $z=0$ ),  $\theta$  is the volumetric water content, and  $e$  is the void ratio (Philip, 1969). Since the Potomac clay exhibits normal shrinkage over the HI test moisture content range, the shrinkage characteristic term,  $\partial e / \partial v$ , is equal to one. It should be noted that for soils with residual shrinkage  $0 < \partial e / \partial v < 1$ . The HI

tests also imposed no external load on the soil, and thus  $P_o$  is equal to zero. Incorporating these HI test conditions, Equation G.1 reduces to,

$$\Omega = \int_0^z \frac{\theta \cdot (1 + e) + Gs}{1 + e} dz \quad (\text{Eq. G.2})$$

The void ratio and volumetric moisture content differences over the REV half-space for Test 5C were 0.669 and 0.3945, respectively. The  $G_s$  for the Potomac clay is 2.76. Incorporating these values and calculating the integral over the REV half-space thickness of 2.5 in. (6.4 cm), the overburden potential difference is computed to be 5.12 in. water, or 0.013 bars (1.3 kPa). The equivalent values for Tests 8C and 9C are also 0.013 bars (1.3 kPa). The overburden potential would tend to draw water towards the fracture on the upper boundary and away from the fracture on the lower boundary.

The osmotic potential is a consequence of the diffuse double layer, and may be computed using the approximate relationship between osmotic potential,  $\pi$ , and electrical conductivity,  $EC$ , at 77°F (25°C),

$$\pi = 40 \cdot EC \quad (\text{Eq. G.3})$$

where the units of  $\pi$  and  $EC$  are kPa and dS/m, respectively (Tanji, 1990). For osmotic potential data obtained at 0°C, the proportionality constant decreases to 36 (U.S. Salinity Laboratory, 1954). The electrical conductivity of the pore fluid in the Potomac deposit is 0.4 mmho/cm, or 0.4 dS/m. The osmotic potential is

thus computed to be 16 kPa, or 0.16 bars. Since the cation type, temperature and relative permittivity (dielectric constant) of the pore fluid were constant during the HI tests, the only change affecting the osmotic potential is the cation concentration. The concentration of salt in the pore water is expected to have increased slightly as water was removed from the soil, but in such a minor quantity that the difference is considered negligible.

The gravitational potential,  $\psi_g$ , is the amount of energy required to move water across the REV half-space, i.e., from some reference elevation,  $z_0$ , to the soil water elevation,  $z_{soil}$ . It is defined as,

$$\psi_g = \rho_w \cdot g \cdot (z_{soil} - z_0) \quad (\text{Eq. G.4})$$

where  $\rho_w$  is the density of water and  $g$  is the gravitational acceleration (Jury et al., 1991). Since the density of water and gravitational acceleration do not appreciably change over the REV half-thickness, the gravitational potential difference is simply proportional to the height of the REV half-space, and computes to 2.5 in. water, or 0.0062 bars (0.62 kPa). Gravity would tend to draw the moisture towards the fracture on the upper boundary surface and away from the fracture on the lower boundary surface.

The pore-water pressure potential may be determined using the desorption water retention curve (Figure 3.19). The suction potential difference over the REV half-space is approximately 52 bars (5200 kPa), which was computed using measured moisture contents of 45.92 and 31.14 vol% from the

outer and inner boundaries, respectively. Equivalent values for Tests 8C and 9C are 33 and 85 bars (3300 and 8500 kPa), respectively. The pore-water pressure potential draws moisture towards the fracture.

In summary, the pore-water pressure potential difference of 52 bars (5200 kPa) is clearly dominant to the other potentials. The computed overburden and gravitational potential differences were 0.013 bars (1.3 kPa) and 0.0062 bars (0.62 kPa), respectively. The osmotic potential difference over the REV half-space is considered negligible. The inclusion of stress state variables other than pore-water pressure would be important only when modeling very small changes in moisture content.

## APPENDIX H

### SAMPLE CALCULATIONS

This appendix presents sample calculations that support the application of the theoretical model to the horizontal infiltrometer and field case study data. Specifically, calculations are provided for: (1) applying aperture corrections to HI data; and (2) calculating the aerodynamic evaporation rate in the fracture.

**Aperture Corrections to HI Data:** The results of HI Test 5C will be used to illustrate the corrections.

#### **STEP 1: Apply Poisson's Ratio to Determine Change in Vertical Thickness**

The total amount of volume change for Test 5C, computed with the FVC Model, was  $0.244 \text{ in}^3$ . From an original volume of  $5.0 \text{ in}^3$ , the new volume is computed as,

$$5.0 \text{ in}^3 - 0.244 \text{ in}^3 = 4.756 \text{ in}^3$$

The volumetric strain,  $\varepsilon$ , is computed by matching the new volume considering three-dimensional volume change and Poisson's ratio,  $\mu$ , which has been chosen to be 0.4. In this case, the volume change represents a strain of 2.75%, or

$$\begin{array}{ccc} \underline{X} & \underline{Y} & \underline{Z} \\ \% \varepsilon = 2.75\% & 0.989 \text{ in} \cdot 0.9725 \text{ in} \cdot 4.945 \text{ in} = 4.756 \text{ in}^3 \end{array}$$

The new thicknesses of the REV in the X, Y, and Z directions were computed as,

$$X : 1 \text{ in.} - (0.0275 \cdot 1 \text{ in.} \cdot 0.4) = 0.989 \text{ in.}$$

$$Y : 1 \text{ in.} - (0.0275 \cdot 1 \text{ in.}) = 0.9725 \text{ in.}$$

$$Z : 5.0 \text{ in.} - (0.0275 \cdot 5.0 \text{ in.} \cdot 0.4) = 4.945 \text{ in.}$$

The change of thickness of the REV in the vertical direction is thus,

$$\Delta H = 5.0 \text{ in.} - 4.945 \text{ in.} = 0.055 \text{ in.}$$

### **STEP 2: Apply Ends Constriction Correction**

The change of thickness of the REV in the vertical direction calculated in Step 1 is the maximum amount of volume change. Because the ends were constricted in the HI tests, an average volume change is taken across the width of the fracture. Assuming no volume change at the ends, the new change in thickness of the REV in the vertical direction is,

$$\Delta H = \left( \frac{0 \text{ in.} + 0.055 \text{ in.}}{2} \right) = 0.0275 \text{ in.}$$

### **STEP 3: Apply Pressure Constriction Correction**

Since the vacuum pressure caused a constriction of 0.01 in. of fracture aperture, the final  $\Delta H$  is computed as,

$$\Delta H = 0.0275 \text{ in.} - 0.01 \text{ in.} = 0.0175 \text{ in.}$$

The final aperture,  $b_{ef}$ , is then computed by adding the initial aperture, calculated from the HI tests using the Cubic Law, to the change of thickness of the REV in the vertical direction, or,

$$b_{ef} = 0.019 \text{ in.} + 0.0175 \text{ in.} = 0.037 \text{ in.}$$

### **Field Study Calculation of Aerodynamic Evaporation Rate in the Fracture ( $E_{af}$ ):**

**STEP 1:** Calculate Average Effective Aperture,  $b_e$

Since extraction occurred under radial flow conditions, the effective aperture,  $b_e$ , may be computed from the Cubic Law (Appendix F) as,

$$b_e = \left( - \frac{(2 \cdot P_1) \cdot 6 \cdot Q_s \cdot \nu \cdot \ln\left(\frac{R_2}{R_1}\right)}{(P_2^2 - P_1^2) \cdot g \cdot \pi} \right)^{\frac{1}{n}}$$

For the field case study, the first radial distance from the extraction point,  $R_1$ , is given as 0.17 ft, which is the radius of the 4 in. diameter fracture well.  $R_2$  is taken as 15 ft, which is the estimated radius of influence. The vacuum pressure at  $R_1$ ,  $P_1$ , is -6.9 in. Hg, which is weighted average of the average gauge pressures measured during extraction (Table 4.3). The associated pressure at  $R_2$ ,  $P_2$ , is assumed to be atmospheric pressure generally taken as 1 atm or 29.92 in. Hg. Converting  $P_1$  and  $P_2$  to absolute air pressures,  $P_{abs}$ , at standard conditions,



$$P_{abs} = (P_{atm} + P_g) \cdot \frac{\gamma_w}{\gamma_a}$$

where  $P_{atm}$  is atmospheric pressure (L),  $P_g$  is the gauge pressure (L), and  $\gamma_w$  and  $\gamma_a$  are the unit weights of water and air (M/L<sup>3</sup>), respectively. For an average soil temperature of 77°F (25°C), the absolute pressures  $P_1$  and  $P_2$  are,

$$P_1 = (29.92 \text{ in. Hg} - 6.9 \text{ in. Hg}) \cdot \frac{13.596 \text{ in. H}_2\text{O}}{\text{in. Hg}} \cdot \frac{62.24 \frac{\text{lb}}{\text{ft}^3}}{0.074 \frac{\text{lb}}{\text{ft}^3}} \cdot \frac{\text{ft}}{12 \text{ in}} = 21,940 \text{ ft air absolute}$$

$$P_2 = (29.92 \text{ in. Hg}) \cdot \frac{13.596 \text{ in. H}_2\text{O}}{\text{in. Hg}} \cdot \frac{62.24 \text{ lb/ft}^3}{0.074 \text{ lb/ft}^3} \cdot \frac{\text{ft}}{12 \text{ in}} = 28,510 \text{ ft air absolute}$$

The volumetric flow rate at STP,  $Q_s$ , is estimated using the operating volumetric flow rate,  $Q_o$ ,

$$Q_s = Q_o \cdot \left( \frac{P_o}{P_s} \right) \cdot \left( \frac{T_s}{T_o} \right)$$

where  $P_o$  and  $T_o$  are the absolute operating pressure and temperature, and  $P_s$  and  $T_s$  are the pressure and temperature at standard conditions (i.e., 1 atm and 70°F).

$P_s$ ,  $T_s$  and  $T_o$  are computed as follows:

$$P_s = (29.92 \text{ in. Hg}) \cdot \frac{13.596 \text{ in. H}_2\text{O}}{\text{in. Hg}} \cdot \frac{62.30 \text{ lb/ft}^3}{0.075 \text{ lb/ft}^3} \cdot \frac{\text{ft}}{12 \text{ in}} = 28,160 \text{ ft air absolute}$$

$$T_s = 70^\circ\text{F} + 459.67 = 529.67\text{R}$$

$$T_o = 77^\circ\text{F} + 459.67 = 536.67\text{R}$$

By taking a weighted average of the average flows measured during testing,  $Q_o$  at the extraction well is estimated to be 78 acfm (Table 4.3). This may be converted to  $Q_s$  as follows,

$$Q_s = 78 \frac{ft^3}{min} \cdot \left( \frac{21,940 \text{ ft air absolute}}{28,160 \text{ ft air absolute}} \right) \cdot \left( \frac{529.67 R}{536.67 R} \right) = 60 \frac{ft^3}{min}$$

The kinematic viscosity of air,  $\nu$ , at the average soil temperature of 77°F is 0.000166 ft<sup>2</sup>/sec. It is also assumed that the aperture exponent,  $n$ , is equal to 3. The effective aperture is thus calculated as,

$$b_e = \left( - \frac{(2 \cdot 21,940 \text{ ft air}) \cdot 6 \cdot -60 \frac{ft^3}{min} \cdot 0.000166 \frac{ft^2}{sec} \cdot \ln \left( \frac{15 \text{ ft}}{0.17 \text{ ft}} \right)}{[(28,510 \text{ ft air})^2 - (21,940 \text{ ft air})^2] \cdot 32.2 \frac{ft}{sec^2} \cdot \pi} \right)^{\frac{1}{3}}$$

$$= 0.0071 \text{ ft} = 0.085 \text{ in.}$$

**STEP 2:** Calculate the average air velocity in the fracture,  $\bar{V}$ , at the radius of interest.

The mean air velocity in the fracture,  $\bar{V}$ , as,

$$\bar{V} = \frac{Q_s}{A}$$

where  $Q_s$  ( $L^3/T$ ) and  $A$  ( $L^2$ ) are the flow and area, respectively, at the radius of interest. Incorporating the radial area of the fracture,

$$\bar{V} = \frac{Q_s}{2 \cdot \pi \cdot r \cdot b_e}$$

where  $r$  is the radius of interest ( $L$ ). In this case,  $r = 1$  ft since the model validation is performed on conditions one foot from the fracture well.

It is now necessary to determine the amount of flow attributed to the interval of interest. The post-fracture flow at the interval of 9.5 to 11.5 ft bgs was shown to be 7.0% of the total flow (i.e.,  $(6.7 \text{ acfm}/96 \text{ acfm}) \times 100$ ). Thus, the average flow over the course of the extraction and HAI tests at this level is adjusted to 7.0% of 60 acfm, or 4.2 acfm. Plugging in the associated values,

$$\bar{V} = \frac{4.2 \text{ ft}^3/\text{min}}{2 \cdot \pi \cdot 1 \text{ ft} \cdot 0.0071 \text{ ft}} = 94 \frac{\text{ft}}{\text{min}} \cdot \frac{60 \text{ min}}{\text{hr}} \cdot \frac{24 \text{ hr}}{\text{day}} \cdot \frac{\text{mi}}{5280} = 26 \frac{\text{mi}}{\text{day}}$$

**STEP 3:** Compute the aerodynamic evaporation rate in the fracture,  $E_{af}$

The aerodynamic evaporation rate in the fracture,  $E_{af}$ , may be computed in mm/day as,

$$E_{af} = 0.35 \cdot \left[ e_2^0 - \left( \frac{\bar{h}_r}{100} \cdot e_2^0 \right) \right] \cdot \left[ 0.5 + \frac{\bar{V}}{100} \right]$$

**Table H.1 Saturated Vapor Pressures of Water for Various Temperatures**  
(Ghildyal and Tripathi, 1987)

Temperature (°F)	Saturated Vapor Pressure (mm Hg)	Temperature (°F)	Saturated Vapor Pressure (mm Hg)	Temperature (°F)	Saturated Vapor Pressure (mm Hg)
36	5.378	61	13.730	86	31.824
37	5.597	62	14.229	87	32.859
38	5.819	63	14.734	88	33.908
39	6.054	64	15.267	89	35.002
40	6.292	65	15.802	90	36.109
41	6.543	66	16.363	91	37.266
42	6.803	67	16.936	92	38.434
43	7.067	68	17.535	93	39.655
44	7.345	69	18.152	94	40.887
45	7.628	70	18.776	95	42.175
46	7.925	71	19.432	96	43.499
47	8.228	72	20.095	97	44.833
48	8.546	73	20.790	98	46.227
49	8.869	74	21.492	99	47.634
50	9.209	75	22.230	100	49.104
51	9.560	76	22.977	101	50.584
52	9.917	77	23.756	102	52.132
53	10.292	78	24.559	103	53.695
54	10.676	79	25.374	104	55.324
55	11.071	80	26.225	105	56.990
56	11.476	81	27.087	106	58.680
57	11.902	82	27.988	107	60.440
58	12.334	83	28.898	108	62.210
59	12.778	84	29.853	109	64.050
60	13.256	85	30.816	110	65.920

The saturation vapor pressure at mean temperature in the fracture,  $e_2^0$ , determined from Table H.1, is 23.756 in mm Hg, and the average relative humidity of the airstream,  $\bar{h}_r$ , is estimated to be 60% for summer conditions in the Santa Clara, CA region. The  $E_{af}$  is calculated as,

$$E_{af} = 0.35 \cdot \left[ 23.765 \text{ mm Hg} - \left( \frac{60}{100} \cdot 23.765 \text{ mm Hg} \right) \right] \cdot \left[ 0.5 + \frac{26 \text{ mi/day}}{100} \right]$$

$$E_{af} = 2.5 \frac{\text{mm}}{\text{day}} \cdot \frac{\text{in.}}{25.4 \text{ mm}} \cdot \frac{\text{day}}{24 \text{ hr}} \cdot \frac{\text{hr}}{60 \text{ min}} = 6.8 \times 10^{-5} \frac{\text{in.}}{\text{min}}$$

#### Example Application Calculations:

Field extraction from the borehole in the Potomac Formation clay at the example site yielded a flow of 0.16 ft<sup>3</sup>/min under a vacuum pressure of 10 in. Hg. Assuming, for simplification purposes, that the five discrete fractures are of equal size, flow through each is 0.032 ft<sup>3</sup>/min. (i.e., 0.16 ft<sup>3</sup>/min ÷ 5). The effective aperture,  $b_e$ , may be computed from the Cubic Law (Appendix F) as,

$$b_e = \left( - \frac{(2 \cdot P_1) \cdot 6 \cdot Q_s \cdot \nu \cdot \ln \left( \frac{R_2}{R_1} \right)}{(P_2^2 - P_1^2) \cdot g \cdot \pi} \right)^{\frac{1}{n}}$$

Since the extraction well is 4 in. in diameter, the first radial distance from the extraction point,  $R_1$ , is 2 in., or 0.17 ft.  $R_2$  is taken as 15 ft, which is the estimated

radial distance of fracturing. The vacuum pressure at  $R_1$ ,  $P_1$ , is -10 in. Hg, and the associated pressure at  $R_2$ ,  $P_2$ , is atmospheric pressure, or 29.92 in. Hg. Converting  $P_1$  and  $P_2$  to absolute air pressures,  $P_{abs}$ , at standard conditions,

$$P_{abs} = (P_{atm} + P_g) \cdot \frac{\gamma_w}{\gamma_a}$$

where  $P_{atm}$  is atmospheric pressure (L),  $P_g$  is the gauge pressure (L), and  $\gamma_w$  and  $\gamma_a$  are the unit weights of water and air (M/L<sup>3</sup>), respectively. For an average soil temperature of 77°F (25°C), the absolute pressures  $P_1$  and  $P_2$  are,

$$P_1 = (29.92 \text{ in. Hg} - 10 \text{ in. Hg}) \cdot \frac{13.596 \text{ in. H}_2\text{O}}{\text{in. Hg}} \cdot \frac{62.24 \frac{\text{lb}}{\text{ft}^3}}{0.074 \frac{\text{lb}}{\text{ft}^3}} \cdot \frac{\text{ft}}{12 \text{ in}} = 18,980 \text{ ft air absolute}$$

$$P_2 = (29.92 \text{ in. Hg}) \cdot \frac{13.596 \text{ in. H}_2\text{O}}{\text{in. Hg}} \cdot \frac{62.24 \text{ lb/ft}^3}{0.074 \text{ lb/ft}^3} \cdot \frac{\text{ft}}{12 \text{ in}} = 28,510 \text{ ft air absolute}$$

The volumetric flow rate at STP,  $Q_s$ , is estimated using the operating volumetric flow rate,  $Q_o$ ,

$$Q_s = Q_o \cdot \left( \frac{P_o}{P_s} \right) \cdot \left( \frac{T_s}{T_o} \right)$$

where  $P_o$  and  $T_o$  are the absolute operating pressure and temperature, and  $P_s$  and  $T_s$  are the pressure and temperature at standard conditions (i.e., 1 atm and 70°F).  $P_s$ ,  $T_s$  and  $T_o$  are computed as follows:

$$P_s = (29.92 \text{ in. Hg}) \cdot \frac{13.596 \text{ in. H}_2\text{O}}{\text{in. Hg}} \cdot \frac{62.30 \text{ lb/ft}^3}{0.075 \text{ lb/ft}^3} \cdot \frac{\text{ft}}{12 \text{ in}} = 28,160 \text{ ft air absolute}$$

$$T_s = 70^\circ\text{F} + 459.67 = 529.67\text{R}$$

$$T_o = 77^\circ\text{F} + 459.67 = 536.67\text{R}$$

The flow under standard conditions,  $Q_s$ , is computed as,

$$Q_s = 0.032 \frac{\text{ft}^3}{\text{min}} \cdot \left( \frac{18,980 \text{ ft air absolute}}{28,160 \text{ ft air absolute}} \right) \cdot \left( \frac{529.67\text{R}}{536.67\text{R}} \right) = 0.021 \frac{\text{ft}^3}{\text{min}}$$

The kinematic viscosity of air,  $v$ , at the average soil temperature of  $77^\circ\text{F}$  is  $0.000166 \text{ ft}^2/\text{sec}$ . It is also assumed that the aperture exponent,  $n$ , is equal to 3.

The effective aperture is thus calculated as,

$$b_e = \left( - \frac{(2 \cdot 18,980 \text{ ft air}) \cdot 6 \cdot -0.021 \frac{\text{ft}^3}{\text{min}} \cdot 0.000166 \frac{\text{ft}^2}{\text{sec}} \cdot \ln\left(\frac{15 \text{ ft}}{0.17 \text{ ft}}\right)}{[(28,510 \text{ ft air})^2 - (18,980 \text{ ft air})^2] \cdot 32.2 \frac{\text{ft}}{\text{sec}^2} \cdot \pi} \right)^{\frac{1}{3}}$$

$$= 0.00043 \text{ ft} = 0.0051 \text{ in.}$$

The FVC Model was used to determine there was a 6 wt% change in moisture content (Figure 6.4) for the 2 week period of extraction, and an aperture increase of 0.76 in. (Figure 6.5). The final aperture for each fracture is thus,

$$0.0051 \text{ in.} + 0.76 \text{ in.} = 0.7651 \text{ in.}$$

The new flow rate from the extraction well under similar conditions is,

$$Q = \frac{\left[ (28,510 \text{ ft air})^2 - (18,980 \text{ ft air})^2 \right] \cdot \pi \cdot 32.2 \frac{\text{ft}}{\text{sec}^2} \cdot (0.7651 \text{ in.})^3}{(2 \cdot 18,980) \cdot 6 \cdot 0.000166 \frac{\text{ft}^2}{\text{sec}} \cdot \ln \left( \frac{15 \text{ ft}}{0.17 \text{ ft}} \right)} = 1.2 \times 10^8 \frac{\text{ft}^3}{\text{min}}$$



## REFERENCES

- Aitchison, G.D. and J.W. Holmes. 1953. "Aspects of Swelling in the Soil Profile," *Australian Journal of Applied Science*, 4: 244-259.
- Altmeyer, W.T. 1955. "Discussion of the Engineering Properties of Expansive Clays," *Proceedings of the American Society of Civil Engineers* 81 (Separate No. 658): 17-19.
- ASTM. 1970. Special Procedures for Testing Soil and Rock for Engineering Purposes, Special Technical Publication 479, 5<sup>th</sup> edition, American Society for Testing and Materials, Philadelphia, PA.
- ASTM. 2000a. "Method D 422-63: Standard Test Method for Particle Size Analysis of Soils," Annual Book of ASTM Standards, Volume 4.08, American Society of Testing and Materials, Philadelphia, PA.
- ASTM. 2000b. "Method D 698-91: Standard Test Method for Laboratory Compaction Characteristics of Soil Using Standard Effort (12,400 ft-lbf/ft<sup>3</sup> (600 kN-m/m<sup>3</sup>))." Annual Book of ASTM Standards, Volume 4.08, American Society of Testing and Materials, Philadelphia, PA.
- ASTM. 2000c. "Method D 854-98: Standard Test Method for Specific Gravity of Soils," Annual Book of ASTM Standards, Volume 4.08, American Society of Testing and Materials, Philadelphia, PA.
- ASTM. 2000d. "Method D 1140-97: Standard Test Method for Amount of Material in Soils Finer Than the No. 200 (75  $\mu$ m) Sieve," Annual Book of ASTM Standards, Volume 4.08, American Society of Testing and Materials, Philadelphia, PA.
- ASTM. 2000e. "Method D 2216-98: Standard Test Method for Laboratory Determination of Water (Moisture) Content of Soil and Rock," Annual Book of ASTM Standards, Volume 4.08, American Society of Testing and Materials, Philadelphia, PA.
- ASTM. 2000f. "Method D 2217-85: Standard Practice for Wet Preparation of Soil Samples for Particle-Size Analysis and Determination of Soil Constants," Annual Book of ASTM Standards, Volume 4.08, American Society of Testing and Materials, Philadelphia, PA.

- ASTM. 2000h. Method D 2435-96: "Standard Test Method for One-Dimensional Consolidation Properties of Soils," Annual Book of ASTM Standards, Volume 4.08, American Society of Testing and Materials, Philadelphia, PA.
- ASTM. 2000i. "Method D 2487-98: Standard Practice for Classification of Soils for Engineering Purposes (Unified Soil Classification System)," Annual Book of ASTM Standards, Volume 4.08, American Society of Testing and Materials, Philadelphia, PA.
- ASTM. 2000j. "Method D 2974-87: Standard Test Methods for Moisture, Ash, and Organic Matter of Peat and Other Organic Soils," Annual Book of ASTM Standards, Volume 4.08, American Society of Testing and Materials, Philadelphia, PA.
- ASTM. 2000k. "Method D 4318-98: Standard Test Methods for Liquid Limit, Plastic Limit, and Plasticity Index of Soils," Annual Book of ASTM Standards, Volume 4.08, American Society of Testing and Materials, Philadelphia, PA.
- ASTM. 2000l. "Method D 4546-96: Standard Test Methods for One-Dimensional Swell or Settlement Potential of Cohesive Soils," Annual Book of ASTM Standards, Volume 4.08, American Society of Testing and Materials, Philadelphia, PA.
- ASTM. 2000m. "Method D 4943-95: Standard Test Method for Shrinkage Factors of Soils by the Wax Method," Annual Book of ASTM Standards, Volume 4.09, American Society of Testing and Materials, Philadelphia, PA.
- ASTM. 2000n. "Method D 5298-94: Standard Test Method for Measurement of Soil Potential (Suction) Using Filter Paper," Annual Book of ASTM Standards, Volume 4.09, American Society of Testing and Materials, Philadelphia, PA.
- Barenblatt, G.I. and I.P. Zheltov. 1960. "Fundamental Equations of Filtration of Homogeneous Liquids in Fissured Rocks," *Soviet Dokl. Akad. Nauk.*, 132: 545-548.
- Barenblatt, G.I., Zheltov, I.P. and I.N. Kochina. 1960. "Basic Concepts in the Theory of Seepage of Homogenous Liquids in Fissured Rocks," *Soviet Appl. Math. Mech. (P.M.M.)*, 24(5): 852-864.
- Barton, N. 1987. "Discontinuities," Chapter 5 in Ground Engineer's Reference Book, F.O. Bell, ed., Butterworths, London.

- Bates, R.L. and J.A. Jackson. 1984. Dictionary of Geological Terms. American Geological Institute, New York, NY.
- Blackwell, P.S., Ringrose-Voase, A.J., Jayawardane, N.S., Olsson, K.A., McKenzie, D.C., and W.K. Mason. 1990. "The Use of Air Filled Porosity and Intrinsic Permeability to Air to Characterize Structure of Macropore Space and Saturated Hydraulic Conductivity of Clay Soils," *Journal of Soil Science*, 41: 215-228.
- Bouma, J. and J. Loveday. 1988. "Characterizing Soil Water Regimes in Swelling Clay Soils," In Vertisols: Their Distribution, Properties, Classification, and Management, L.P. Wilding and R. Puentes, eds., pp. 83-96, Technical Monograph No. 18, Texas A&M Printing Center, College Station, TX.
- Bronswijk, J.J.B. 1986. "Evaporation and Cracking of a Heavy Clay Soil," *Twelfth Conference of the Romanian National Society of Soil Science*, Report 14, Institute for Land and Water Management Research, Wageningen, Netherlands.
- Bronswijk, J.J.B. 1988. "Modeling of Water Balance, Cracking and Subsidence of Clay Soils," *Journal of Hydrology*, 97: 199-212.
- Bronswijk, J.J.B. 1989. "Prediction of Actual Cracking and Subsidence in Clay Soils," *Soil Science*, 148 (2): 87-93.
- Bronswijk, J.J.B. 1991. "Relation between Vertical Soil Movements and Water-Content Changes in Cracking Clays," *Soil Science Society of America Journal*, 55: 1220-1226.
- Brown, K.W. and D.C. Anderson. 1983. "Effects of Organic Solvents on the Permeability of Clay Liners," U.S. Environmental Protection Agency Report EPA 600/2-83-016.
- Buckingham, E. 1907. "Studies on the Movement of Soil Moisture," Bulletin 38, U.S. Department of Agriculture, Bureau of Soils, Washington, DC.
- Bui, E.N. and A.R. Mermut. 1988. "Orientation of Planar Voids in Vertisols and Soils with Vertic Properties," *Soil Science Society of America Journal*, 52: 171-178.
- Buitenkijk, J. 1984. "FLOWEX: A Numerical Model for Simulation of Vertical Flow of Water Through Unsaturated Layered Soil," Report No. 1494, Institute for Land and Water Management Research (ICW), Wageningen, The Netherlands (in Dutch).

- Cameron, R.E. 1991. "Guide to Site and Soil Description for Hazardous Waste Site Characterization, Vol. 1, Metals," EPA 600/4-91-029 (NTIS PB92-146158).
- Celia, M.A., Bouloutas, E.T., and R.L. Zarba. 1990. "A General Mass-Conservative Numerical Solution for the Unsaturated Flow Equation," *Water Resources Research*, 26(7): 1483-1496.
- Chapman, D.L. 1913. "A Contribution to the Theory of Electrocapillarity," *Philosophical Magazine*, 25(6): 475-481.
- Chen, F.H. 1965. "The Use of Piers to Prevent the Uplifting of Lightly Loaded Structures Founded on Expansive Soils," Supplementing the Symposium in Print, Texas A&M Press, pp. 152-171.
- Chen, F.H. 1988. Foundations on Expansive Soils, American Elsevier Science Publishers, New York, NY.
- Childs, E.C. and G.N. Collis-George. 1950. "The Permeability of Porous Materials," *Proceedings of the Royal Society of London, Series A*, 201: 392-405.
- Cokca, E. and A. Birand. 1993. "Determination of Cation Exchange Capacity of Clayey Soils by the Methylene Blue Test," *Geotechnical Testing Journal*, 16(4): 518-524.
- Coulombe, C.E., Wilding, L.P., and J.B. Dixon. 1996. "Overview of Vertisols: Characteristics and Impacts on Society," *Advances in Agronomy*, 57: 289-375.
- Darcy, H. 1856. Les Fontaines Publiques de la Ville de Dijon, Dalmont, Paris.
- Das, B.M. 1983. Advanced Soil Mechanics, McGraw-Hill Book Company, New York, NY.
- Das, B.M. 1994. Principles of Geotechnical Engineering, PWS Publishing Company, Boston, MA.
- Dasog, G.S. and G.B. Shashidhara. 1993. "Dimension and Volume of Cracks in a Vertisol under Different Crop Covers," *Soil Science*, 156 (6): 424-428.
- Dawson, K.J. and J.D. Istok. 1991. Aquifer Testing: Design and Analysis of Pumping and Slug Tests. Lewis Publishers, Inc., Chelsea, MI.
- Dexter, A.R. 1988. "Advances in Characterization of Soil Structure," *Soil Tillage Research*, 11: 199-238.

- Domenico, P.A. and F.W. Schwartz. 1990. Physical and Chemical Hydrogeology. John Wiley and Sons, Inc., New York, NY.
- Dudal, R. and H. Eswaran. 1988. "Distribution, Properties, and Classification," *In Vertisols: Their Distribution, Properties, Classification, and Management*, L.P. Wilding and R. Puentes, eds., pp. 1-22, Technical Monograph No. 18, Texas A&M Printing Center, College Station, TX.
- Elsbury, B.R. et al. 1988. "Field and Laboratory Testing of a Compacted Soil Liner," Report to USEPA for Contract No. 68-03-3250, Cincinnati, OH.
- ENR. 1992. Shrink-swell soils plaque Virginia homes," *Engineering News Record* (ENR), January 27, 1992.
- Fairfax County Soil Science Office. 1993. General Ratings for Urban Development for Fairfax County. Fairfax County Soil Science Office, Fairfax, VA.
- Fickies, R.H., Fakundiny, R.H., and E.T. Mosley. 1979. "Geotechnical Analysis of Soil Samples from Test Trench at Western New York Nuclear Service Center," Report to the U.S. Nuclear Regulatory Commission, West Valley, NY.
- Force, L.M. and G.K. Moncure. 1978. "Origin of Two Clay Mineral Facies of the Potomac Group (Cretaceous) in the Middle Atlantic States," *U.S. Geological Survey Journal of Research*, 6(2): 203-214.
- Fox, W.E. 1964. "A Study of Bulk Density and Water in A Swelling Soil," *Soil Science*, 98: 307-316.
- Fredlund, D.G. and N.R. Morgenstern. 1977. "Stress State Variables for Unsaturated Soils," *ASCE Journal of Geotechnical Engineering*, Division GT5, 103: 447-466.
- Fredlund, D.G. and H. Rahardjo. 1993. Soil Mechanics for Unsaturated Soils. John Wiley and Sons, Inc., New York, NY.
- Froelich, A.J. 1985. "Folio of Geologic and Hydrologic Maps for Land-Use Planning in the Coastal Plain of Fairfax County and Vicinity, Virginia," Miscellaneous Investigations Map I-1423, U.S. Geological Survey, Reston, VA.
- Ghildyal, B.P. and R.P. Tripathi. 1987. Soil Physics. Wiley Eastern Limited, New Delhi, India.

- Gillott, J.E. 1986. "Some Clay-Related Problems in Engineering Geology in North America," *Clay Minerals*, 21: 261-278.
- Giraldez, J.V., Sposito, G., and C. Delgado. 1983. "A General Soil Volume Change Equation: I. The Two Parameter Model," *Soil Science Society of America Journal*, 47: 419-422.
- Glaser, J.D. 1969. "Petrology and origin of Potomac and Magothy (Cretaceous) sediments, Middle Atlantic Coastal Plain," Maryland Geological Survey Report of Investigations No. 11, Baltimore, MD.
- Gottardi, G. and M. Venutelli. 1993. "Richards: Computer Program for the Numerical Simulation of One-Dimensional Infiltration into Unsaturated Soil," *Computers and Geosciences*, 19 (9): 1239-1266.
- Gouy, G. 1910. "Sur la Constitution de la Charge Electrique a la Surface d'un Electrolyte," *Annuie Physique*, 4 (9): 457-468.
- Grant, C.D., Dexter, A.R., and C. Huang. 1990. "Roughness of Soil Fracture Surfaces as a Measure of Soil Microstructure," *Journal of Soil Science*, 41: 95-110.
- Groenendijk, P. and J.G. Kroes. 1997. "Modelling the Nitrogen and Phosphorus Leaching to Groundwater and Surface Water: ANIMO 3.5," Report 144, DLO Wining Staring Centre, Wageningen, The Netherlands (In Dutch).
- Hall, H.A. 1995. "Investigation into Fracture Behavior and Longevity of Pneumatically Fractured Fine-Grained Formations," M.S. Thesis, New Jersey Institute of Technology, Newark, NJ.
- Hamburg, D.J. 1985. "A Simplified Method for Predicting Heave in Expansive Soils," M.S. Thesis, Colorado State University, Fort Collins, CO.
- Head, K.H. 1994. Manual of Soil Laboratory Testing, Volume 2: Permeability, Shear Strength and Compressibility Tests, 2<sup>nd</sup> Edition, Pentech Press, London.
- Hendriks, R. F.A., Oostindie, K., and P. Hamminga. 1999. "Simulation of Bromide Tracer and Nitrogen Transport in a Cracked Clay Soil with the FLOCR/ANIMO model combination," *Journal of Hydrology*, 215(1-4): 94-115.

- Hilf, J.W. 1956. "An Investigation of Pore-Water Pressure in Compacted Cohesive Soils," Ph.D. thesis, Technical Memorandum No. 654, U.S. Department of the Interior, Bureau of Reclamation, Design and Construction Division, Denver, CO.
- HSMRC (Hazardous Substance Management Research Center), Accutech Remedial Systems, Inc., Battelle Memorial Institute, and Battelle Pacific Northwest National Laboratory. 1994. "Pneumatic Fracturing Demonstration, Tinker Air Force Base, Oklahoma City, Oklahoma," Prepared for U.S. Department of Energy, U.S. Environmental Protection Agency, and U.S. Air Force.
- Hubbert, M.K. and G. Willis. 1957. "Mechanics of Hydraulic Fracturing," *Trans. AIME*, 210: 153-166.
- Idso, S.B., Reginato, R.J., Jackson, B.A., Kimball, B.A., and F.S. Nakayama. 1974. "The Three Stages of Drying of a Field Soil," *Soil Society of America Proceedings*, 38: 831-837.
- Islam, M.R. 1996. "A Comparative Study of the Transformed Methods for Solving Richards' Equation," North American Water and Environment Congress, American Society of Civil Engineers, New York, NY.
- Iwata, S., Tabuchi, T., and B.P. Warkentin. 1988. Soil-Water Interactions: Mechanisms and Applications, Marcel Dekker, Inc., New York, NY.
- Jarvis, N.J. and P.B. Leeds-Harrison. 1987. "Modelling Water Movement in Drained Clay Soil. I Description of the Model, Sample Output and Sensitivity Analysis," *Journal of Soil Science*, 38:487-498.
- Jarvis, N.J. and P.B. Leeds-Harrison. 1990. "Field Test of a Water Balance Model of Cracking Clay Soils," *Journal of Hydrology*, 112: 203-218.
- Johnson, L.K. 1990. "Homeowner's Guide to Overcoming Problems with Marine Clay in Fairfax County," Soil Science Office, Department of Environmental Management, Fairfax, VA.
- Jones, D.E., Jr. and W.G. Holtz. 1973. "Expansive Soils: The Hidden Disaster," *Civil Engineering*, 43(8): 49-51.
- Jones, M.J. and K.K. Watson. 1987. "Effect of Soil Hysteresis on Solute Movement During Intermittent Leaching," *Water Resources Research*, 23: 1251-1256.

- Jury, W.A., Gardner, W.R., and W.H. Gardner. 1991. Soil Physics. John Wiley and Sons, Inc., New York, NY.
- Kays, W.B. 1977. Construction of Lining for Reservoirs, Tanks, and Pollution Control Facilities. John Wiley and Sons, Inc., New York, NY.
- Krohn, J.P. and J.E. Slosson. 1980. "Assessment of Expansive Clay Soils in the United States," *Proceedings of the Fourth International Conference on Expansive Soils, June 16-18, Denver, CO*. American Society of Civil Engineers, New York, NY.
- Krueger, R.F. 1986. "An Overview of Formation Damage and Well Productivity in Oilfield Operations," *Journal of Petroleum Technology*, February: 131-152.
- Kuipers, H. 1984. "The Challenge of Soil Cultivations and Soil Water Problems," *Journal of Agricultural Engineering Research*, 29: 177-190.
- Kulhawy, F.H. and P.W. Mayne. 1990. "Manual on Estimating Soil Properties for Foundation Design," Final Report, Project 1493-6, EL-6800, Electric Power Research Institute, Palo Alto, CA.
- Lam, L. and D.G. Fredlund. 1984. "Saturated-Unsaturated Transient Finite Element Seepage Model for Geotechnical Engineering," *Advanced Water Resources*, 7: 132-136.
- Lambe, T.W. and R.V. Whitman. 1969. Soil Mechanics. John Wiley and Sons, New York, NY.
- Liu, X. and F. Civan. 1995. "Formation Damage by Fines Migration Including Effects of Filter Cake, Pore Compressibility, and Non-Darcy Flow—A Modeling Approach to Scaling from Core to Field," SPE 28980, Society of Petroleum Engineers, Richardson, TX.
- McBride, M.B. 1994. Environmental Chemistry of Soils, Oxford University Press, New York, NY.
- McGarry, D. and K.W.J. Malafant. 1987. The Analysis of Volume Change in Unconfined Units of Soil," *Soil Science Society of America Journal*, 51: 290-297.
- McKay, L.D., Cherry, J.A., and R.W. Gillham. 1993. "Field Experiments in a Fractured Clay Till. 1. Hydraulic Conductivity and Fracture Aperture," *Water Resources Research*, 29(4): 1149-1162.



- McKeen, R.G. and D.J. Hamburg. 1981. "Characterization of Expansive Soils," Trans. Res. Rec. 790, Trans. Res. Board 73-78.
- McLaren/Hart (McLaren/Hart Environmental Engineering Corporation). 1993. "Pneumatic Fracturing, Soil Vapor Extraction and Hot Air Injection Pilot Test at the FMC Facility, Santa Clara, California," Prepared for FMC Corporation, Santa Clara, CA.
- Mitchell, J.D. 1993. Fundamentals of Soil Behavior. John Wiley and Sons, Inc., New York, NY.
- Murray, R.S. and J.P. Quirk. 1990. "Intrinsic Failure and Cracking of Clay," *Soil Science Society of America Journal*, 54: 1179-1184.
- Nagaraj, T. and B.R.S. Murty. 1985. "Prediction of the Preconsolidation Pressure and Recompression Index of Soils," *Geotechnical Testing Journal*, 8(4): 199-202.
- Nautiyal, D. 1994. "Fluid Flow Modeling for Pneumatically Fractured Formations," M.S. Thesis, Department of Civil and Environmental Engineering, New Jersey Institute of Technology, Newark, NJ.
- Nelson, J.D. and D.J. Miller. 1992. Expansive Soils: Problems and Practice in Foundation and Pavement Engineering. John Wiley and Sons, Inc., New York, NY.
- NFEC (Naval Facilities Engineering Command). 1986. "Soil Mechanics Design Manual 7.01," Naval Facilities Engineering Command, Alexandria, VA.
- Obermeier, S.F. 1979. "Slope Stability Map of Fairfax County, Virginia," U.S. Geological Survey Miscellaneous Field Studies Map MF-1072, scale 1:48,000, USGS, Reston, VA.
- Obermeier, S.F., Swanson, P.G., Jones, J.S. Jr., and J.J. Schnabel. 1984. "Engineering Geology and Design of Slopes for Cretaceous Potomac Deposits in Fairfax County, Virginia, and Vicinity," Geological Survey Bulletin 1556, U.S. Government Printing Office, Washington, D.C.
- Obermeier, S.F. and W.H. Langer. 1986. "Relationships Between Geology and Engineering Characteristics of Soils and Weathered Rocks of Fairfax County and Vicinity, Virginia." U.S. Geological Survey Professional Paper 1344, U.S. Government Printing Office, Washington, D.C.

- Olive, W.W., Chleborad, A.F., Frahme, C.W., Shlocker, J., Schneider, R.R., and R.L. Schuster. 1989. "Swelling Clays Map of the Conterminous United States," Miscellaneous Investigation Series, Map I-1940, U.S. Geological Survey, Reston, VA.
- Oostindie, K. and J.J.B. Bronswijk. 1992. "FLOCR - A Simulation Model for Calculation of Water Balance, Cracking, and Surface Subsidence of Clay Soils," Report No. 47, Agricultural Research Department, The Winand Staring Centre for Integrated Land, Soil, and Water Research, Wageningen, The Netherlands.
- Penman, H.L. 1948. "Natural Evaporation from Open Water, Bare Soil, and Grass," *Proc. Roy. Soc. A* 190: 120-145.
- Penman, H.L. 1956. "Evaporation: An Introductory Survey," *Netherlands Journal of Agricultural Science*, 4: 9-29.
- Philip, J.R. 1969. "Moisture Equilibrium in the Vertical in Swelling Soils: I. Basic Theory," *Australian Journal of Soil Research*, 7: 99-120.
- Raman, V. 1967. "Identification of Expansive Soils from the Plasticity Index and the Shrinkage Index Data," *Indian Engineering*, 11(1): 17-22.
- Ranganatham, B.V. and B. Satyanarayana. 1965. "A Rational Method of Predicting Swelling Potential for Compacted Expansive Clays," *Proceedings of the 6<sup>th</sup> International Conference of Soil Mechanics Foundation Engineering*, 1: 92-96.
- Rees, S.W. and H.R. Thomas. 1993. "Simulating Seasonal Ground Movement in Unsaturated Clay," *Journal of Geotechnical Engineering*, 119 (7): 1127-1143.
- Rendon-Herrero, O. 1983. "Universal Compression Index Equation," *Discussion, Journal of Geotechnical Engineering*, ASCE, 109 (10): 1349.
- Rhoades, J.D. 1982. "Soluble Salts," in Methods of Soil Analysis, Agronomy No. 9, Chapter 10, Part 2, 2<sup>nd</sup> edition, American Society of Agronomy, Soil Science Society of America, Madison, WI.
- Richards, L.A. 1931. "Capillary Conduction of Liquids through Porous Media," *Physics*, 1: 318-333.

- Roseberg, R.J. and E.L. McCoy. 1992. "Tillage and Traffic-Induced Changes in Macroporosity and Macropore Continuity: Air Permeability Assessment," *Soil Science Society of America Journal*, 56: 1261-1267.
- Ross, P.J. 1990. "Efficient Numerical Method for Infiltration Using Richards' Equation," *Water Resources Research*, 26(2): 279-290.
- Rowe, R.K. and J.R. Booker. 1991. "Pollutant Migration Through Liner Underlain by Fractured Soil," *Journal of Geotechnical Engineering*, 117 (12): 1902-1919.
- Russo, D., Jury, W.A., and G.L. Butters. 1989. "Numerical Analysis of Solute Transport during Transient Irrigation. I. Effect of Hysteresis and Profile Heterogeneity," *Water Resources Research*, 25: 2109-2118.
- Saada, A.S., Bianchini, G.F., and L. Liang. 1994. "Cracks, Bifurcation and Shear Bands Propagation in Saturated Clays," *Géotechnique*, 44(1): 35-64.
- Schuring, J.R. and P.C. Chan. 1992. "Removal of Contaminants from the Vadose Zone by Pneumatic Fracturing," USGS Award 14-08-0001-G1739, U.S. Geological Survey, Reston, VA.
- Scott, G.J.T., Webster, R., and S. Nortcliff. 1988. "The Topology of Pore Structure in Cracking Clay Soil. I. The Estimation of Numerical Density," *Journal of Soil Science*, 39: 303-314.
- SCS (Soil Conservation Service). 1971. "Handbook of Soil Survey Investigations Procedures," SCS, Washington, DC.
- Seiders, V.M. and R.B. Mixon. 1981. "Geologic Map of the Occoquan Quadrangle and Part of the Fort Belvoir Quadrangle, Prince William and Fairfax Counties, Virginia," Miscellaneous Investigations Map I-1175, U.S. Geological Survey, Reston, VA.
- Sharp, J.S. and Y.N.T. Maini. 1972. "Fundamental consideration on the Hydraulic Characteristics of Joints in Rocks," *Proceedings on the Symposium on Percolation Through Fissured Rock*, Int. Soc. For Rock Mech. and Int. Ass. of Eng. Geology, T1-F.
- Shouse, P., Jury, W.A., and L.A. Stolzy. 1982. "Field Measurement and Modeling of Cowpea Water Use and Yield under Stressed and Well-Watered Growth Conditions," *Hilgardia*, 50: 1-25.

- Skempton, A.W. 1953. "The Colloidal Activity of Clay," *Foundation Engineering*, 1: 57-61.
- Soil Survey Staff. 1993. "Examination and Description of Soils," *In Soil Survey Manual, Agricultural Handbook No. 18, Soil Conservation Service, Washington, DC.*
- Sowers, G.F. 1962. Shallow Foundations, Foundation Engineering, ed. G.A. Leonards, McGraw-Hill Book Co., New York, NY.
- Suter, G.W. II, Luxmoore, R.J., and E.D. Smith. 1993. "Compacted Soil Barriers at Abandoned Landfill Sites are Likely to Fail in Long Term," *Journal of Environmental Quality*, 22: 217-226.
- Tan, K.H. 1996. Soil Sampling, Preparation, and Analysis, Marcel Dekker, Inc., NY, NY.
- Tanji, K.K., ed. 1990. Agricultural Salinity Assessment and Management, ASCE Manual and Reports on Engineering Practice No. 71, American Society of Civil Engineers, New York, NY.
- Tariq, A. and D.S. Durnford. 1993. "Analytical Volume Change Model for Swelling Clay Soils," *Soil Science Society of America Journal*, 57: 1183-1187.
- Terzaghi, K. 1925. "Principles of Soil Mechanics. A Summary of Experimental Results of Clay and Sand," *Engineering News Record*, 3-98.
- Terzaghi, K. 1943. Theoretical Soil Mechanics. John Wiley and Sons, Inc., New York, NY.
- Terzaghi, K. and R.B. Peck. 1948. Soil Mechanics in Engineering Practice, John Wiley and Sons, New York, NY.
- Thomas, H.R. and S.W. Rees. 1991. "A Comparison of Field-Monitored and Numerically Predicted Moisture Movement in Unsaturated Soil," *International Journal for Numerical and Analytical Methods in Geomechanics*, 15: 417-431.
- Tolman, C.F. 1937. Ground Water. McGraw-Hill Book Company, New York, NY.

- USDA-SCS (U.S. Department of Agriculture-Soil Conservation Service). 1994. "Global Soil Regions," World Soil Resources, Soil Survey Division of the Soil Conservation Service, U.S. Department of Agriculture.
- U.S. Salinity Laboratory Staff. 1954. "Diagnosis and Improvement of Saline and Alkali Soils," U.S. Department of Agriculture Handbook No. 60, U.S. Printing Office, Washington, D.C.
- Venkatraman, S.N., Bossert, I.D., Kosson, D.S., Puppala, S., Boland, T.M., and J.R. Schuring. 1995. "Integrated Pneumatic Fracturing and Bioremediation for the In-Situ Treatment of Contaminated Soil," U.S. Environmental Protection Agency, Office of Research and Development, Releases Control Branch, Edison, NJ.
- Voltz, M. and Y.-M. Cabidoche. 1995. "Non-Uniform Volume and Water Content Changes in Swelling Clay Soil: I. Theoretical Analysis," *European Journal of Soil Science*, 46: 333-343.
- Vukovic, M. and A. Soro. 1992. Determination of Hydraulic Conductivity of Porous Media From Grain-Size Composition. Water Resources Publications, Littleton, CO.
- Wilding, L.P. and C.E. Coulombe. 1996. "Expansive Soils: Distribution, Morphology and Genesis," *Proceedings of NATO-ARW on Clay Swelling and Expansive Soils*, P. Baveye and M.B. McBride, eds., Kluwer Academic, Dordrecht, Netherlands.
- Wind, G.P. , and W. Van Doorne. 1975. "A Numerical Model for the Simulation of Unsaturated Vertical Flow of Moisture in Soils," *Journal of Hydrology*, 24: 1-20.